# Scaling-Up Eutectic Freeze Crystallization

Fatma Elif Genceli



#### Propositions accompanying the thesis of F. Elif Genceli

### **Scaling-Up Eutectic Freeze Crystallization**

- 1. In heat flow calculations of crystallization on a cold surface [*Pronk*, *P. et al.*; *Chemical Engineering Science*, 2006, 61, p.4354-4362; *Mershmann*, A.; *Crystallization Technology Handbook*, 2001], it is frequently assumed that all heat of crystallization is transferred to the cold side which is not necessarily true (Chapter 7).
- 2. The Raman spectra presented in the work of Freeman et al. [Freeman J.J.; Wang, A.; Jolliff B.L.; 38th Lunar and Planetary Science Conference, 2007, No. 1338, p.1197] are not those of MgSO<sub>4</sub>.11H<sub>2</sub>O (Meridianiite) as they claim, but are spectra of crystal samples which have already been dehydrated into a magnesium sulfate with a lower hydrate content (Chapter 5-6).
- 3. It is surprising that no care was ever given since 1837 [Fritzsche, C.J.; Poggendorff's Annalen, 1837, 42, 577-580] to determine the exact phase diagram of MgSO<sub>4</sub> aqueous solution nor to determining the crystal structure of the magnesium sulfate phase formed at lower temperatures, despite the fact that the solution has been used in many crystallization applications as the model solution. [e.g.: Hogenboom, D.L.; Kargel, J.S.; Ganasan, J.P.; Lee, L.; Icarus. 1995, 115, 258-277] (Chapter 5).
- 4. It is easier to make nano-crystals from supercritical CO<sub>2</sub> [Jung, J.; Perrut, M.; J. Supercrit. Fluids, 2001, 20, 3, 179-219] than by arrested precipitation from solution.
- 5. Putting CO<sub>2</sub> underground is not a sustainable solution to our energy problem.
- 6. It is surprising, even paradoxical, that results in highly prestigious journals are not necessarily more reliable than those in second-tier journals.
- 7. The Turkish saying 'the mirror of a person is his work, not his word' is not true when working in a group! 'Talking skills' mostly overcome the 'working skills'.
- 8. In modern world more intelligent women dedicate themselves to their career rather than to having more children. Due to the changing priorities of women, our society is under the threat of a decrease in the number of intelligent people.
- 9. Effective valorization and high level scientific research can reinforce each other.
- 10. The moneys spent on subsidies for "biofuels" would better be spent on purchasing and preserving rain forests.

These propositions are considered opposable and defendable as such have been approved by the supervisor, Prof. Dr. G. J. Witkamp.

#### Stellingen behorende bij het proefschrift van F. Elif Genceli

### **Eutectische Vrieskristallisatie Opschalen**

- 1. Bij berekeningen van warmtestromen van kristallisatie op een koud oppervlak [*Pronk, P. et al.; Chemical Engineering Science, 2006, 61, p.4354-4362; Mershmann, A.; Crystallization Technology Handbook, 2001*], wordt het regelmatig aangenomen dat alle kristallisatiewarmte overgedragen wordt naar de koude zijde wat niet noodzakelijkerwijs waar is (Hoofdstuk 7).
- 2. De Raman spectra uit het werk van Freeman et al. [Freeman J.J.; Wang, A.; Jolliff B.L.; 38th Lunar and Planetary Science Conference, 2007, No. 1338, p.1197] zijn niet die van MgSO<sub>4</sub>.11H<sub>2</sub>O (Meridianiite) zoals zij claimen, maar zijn de spectra van kristalmonsters welke al zijn gedehydrateerd tot een magnesiumsulfaat met een lager watergehalte (Hoofdstuk 5-6).
- 3. Het is verrassend dat er sinds 1837 geen aandacht is geschonken [Fritzsche, C.J.; Poggendorff's Annalen, 1837, 42, 577-580] aan het bepalen van het exacte fasediagram van waterige MgSO<sub>4</sub> oplossing noch aan het bepalen van de kristalstructuur van de magnesiumsulfaatfase gevormd bij lagere temperaturen, ondanks het feit dat de oplossing in veel kristallisatietoepassingen is gebruikt als modelstof [bijv.: Hogenboom, D.L.; Kargel, J.S.; Ganasan, J.P.; Lee, L.; Icarus. 1995, 115, 258-277] (Hoofdstuk 5).
- 4. Het is gemakkelijker om nanokristallen te maken vanuit superkritisch CO<sub>2</sub> [Jung, J.; Perrut, M.; J. Supercrit. Fluids, 2001, 20, 3, 179-219] dan door middel van arrested precipitatie vanuit oplossing.
- 5. CO<sub>2</sub> onder de grond stoppen is geen duurzame oplossing voor ons energieprobleem.
- 6. Het is verrassend, zelfs paradoxaal, dat resultaten uit zeer prestigieuze journals niet noodzakelijkerwijs betrouwbaarder zijn dan die uit tweederangs journals.
- 7. Het Turkse gezegde "de spiegel van een persoon is zijn werk, niet zijn woord" is niet waar wanneer er in een groep gewerkt wordt! 'spreekvaardigheden' overtreffen grotendeels de 'werkvaardigheden'.
- 8. In de moderne wereld wijden intelligentere vrouwen zichzelf aan hun carrière in plaats van aan het krijgen van kinderen. Door de veranderende prioriteiten van vrouwen, is onze maatschappij onder bedreiging van een afname van het aantal intelligente mensen.
- 9. Effectieve valorisatie en wetenschappelijk onderzoek op hoog niveau kunnen elkaar versterken.
- 10. Het geld gespendeerd aan subsidies voor biobrandstoffen zou beter besteed kunnen worden aan het aanschaffen en behouden van tropisch regenwoud.

Deze stellingen worden opponeerbaar en verdedigbaar geacht en zijn als zodanig goedgekeurd door de promotor, Prof. Dr. G. J. Witkamp.

# Scaling-Up **Eutectic Freeze Crystallization**

Fatma Elif GENCELİ

# Scaling-Up **Eutectic Freeze Crystallization**

#### Proefschrift

ter verkrijging van de graad van doctor
aan de Technische Universiteit Delft,
op gezag van de Rector Magnificus prof. dr. J.T. Fokkema,
voorzitter van het College voor Promoties,
in het openbaar te verdedigen op maandag 21 januari 2008 om 12:30 uur

door

### Fatma Elif GENCELİ

Master of Science in Chemical Engineering, İstanbul Technical University geboren te Üsküdar/ İstanbul/ Turkije

Dit proefschrift is goedgekeurd door de promotor:

Prof. dr. G.J. Witkamp

Samenstelling promotiecommissie:

Rector Magnificus Voorzitter

Prof. dr. G.J. Witkamp Technische Universiteit Delft, promotor

Prof. dr. S. Kjelstrup Norwegian University of Science and Technology

Prof. dr. T. Hondoh

Prof. dr. ir. A.J. Berkhout

Prof. dr. W. Buijs

Hokkaido University of Japan

Technische Universiteit Delft

Technische Universiteit Delft

Ir. H. Vrijenhoef Proton Ventures B.V.

Prof. dr. ir. G.M. van Rosmalen reservelid, emeritus Technische Universiteit Delft

This research was financially supported by the Ministry of Economic Affairs, the Ministry of Housing, Spatial Planning, and Environment, the Ministry of Education and Science of the Netherlands through the EET program, and Kemira Agro Ventures. The supports from Larox-Pannevis B.V., Nedmag Industries Mining & Manufacturing B.V., TNO, AVR B.V. and DSM Research are acknowledged.

Cover design & layout by: Jelan Kuhn & F. Elif Genceli

Crystal picture by Prof. dr. G.J. Witkamp

ISBN: 978-90-9022729-0

Copyright © 2008 by F.E. Genceli

Printed by Sieca Repro, Delft

All rights reserved. No part of the material protected by this copyright notice may be reproduced or utilized in any form or by any means, electronic or mechanical, including photocopy, recording or by any information storage and retrieval system, without written permission from the publisher.

To my dear mom, dad and sister Her zaman fedakar ve sonsuz sevgi dolu anneme Desteğini ve sevgisini hep kalbimde taşıyacağım babama En güzel yıllarımı beraber geçirdiğim, arkadaşım, dostum, canım ablama

# Table of Contents

Chapter 1.	Introduction	1
Chapter 2.	Development and Performance	
	of EFC Cooled Disk Column Crystallizer (CDCC)	19
Chapter 3.	Inline Determination of Supersaturation and	
	Metastable Zone Width of MgSO <sub>4</sub> ·11H <sub>2</sub> O	
	with Conductivity and Refractive Index	
	Measurement Techniques	29
Chapter 4.	Scaling-up Eutectic Freeze Crystallization	45
Chapter 5.	Crystallization and characterization of a	
	new Magnesium Sulfate Hydrate -MgSO <sub>4</sub> ·11H <sub>2</sub> O-	65
Chapter 6.	Meridianiite: Detected In Ice	91
Chapter 7.	Coupled heat and mass transfer during	
	crystallization of MgSO <sub>4</sub> ·7H <sub>2</sub> O on a cooled surface	119
Chapter 8.	Cyclic Innovation Model Application:	
	Eutectic Freeze Crystallization	153
Appendix		191
	Status of Eutectic Freeze Crystallization	193
	English summary	197
	Nederlandse samenvatting	203
	Özet (Turkish summary)	209
	Acknowledgments	215
	Curriculum vitae	221
	List of publications	222

# Chapter 1

## Introduction

### **Eutectic Freeze Crystallization**

#### F. Elif Genceli<sup>a</sup>

<sup>a</sup> Process Equipment, Process & Energy Department TUDelft, Delft-The Netherlands *Contains parts of NPT Processtechnologie, Augustus 2005, No.4, 19-20* 



#### INTRODUCTION

The world total energy consumption, global and industrial water usage-withdrawal are increasing very steep (see Figure 1.1) [Energy 2004, United Nations 2007]. It is estimated that without taking precautions and innovative changes, these rises will be even steeper due to multiplication by the increase in the world population [Energy 2004]. Related to this are environmental issues and the water problem. 88.7% of water on the Earth is salty water, and over two thirds of fresh water is frozen in glaciers and polar ice caps, leaving only 0.9% available for human use. Fresh water is a renewable resource, yet the world's supply of clean, fresh water is steadily decreasing. Water demand already exceeds supply in many parts of the world, and as world population continues to rise at an unprecedented rate, many more areas are expected to experience this imbalance in the near future. It is estimated that 15-20 % of world-wide water use is industrial (4% of world-wide water consumption). In general 52% of the world-wide water use is consumed [United Nations 2007, Wikipedia 2007, Coleridge 2006]. The prices of nonrenewable energy sources of petroleum, coal and gas are increasing dramatically. Therefore it is essential to develop true renewable sources such as solar energy, and to use exergy\* more efficiently. This also counts for the process industry, which currently uses approximately 155 EJ per year [Energy 2004].

In the process industry, separation technology is a key enabler in medical, mining, food, paper, chemical, pharmaceutical and biotechnological processes, since only very rarely a process is 100% selective. Separations, however, are costly in terms of equipment and energy. In the process industry more than half of the costs in equipment and in energy are due to separations. Economical issues, global competition and changing stricter environmental regulations force the new equipment and technology developers to reduce the exergy use, waste production, size of the production equipment and investment costs resulting in more sustainable and safer technologies.

<sup>\*</sup> In the thesis, sometimes instead of correct scientific word *exergy* (the useful portion of energy that allows us to do work and perform energy services) *energy* is used when colloquial expressions of 'saving energy' or 'energy use' terms are used.

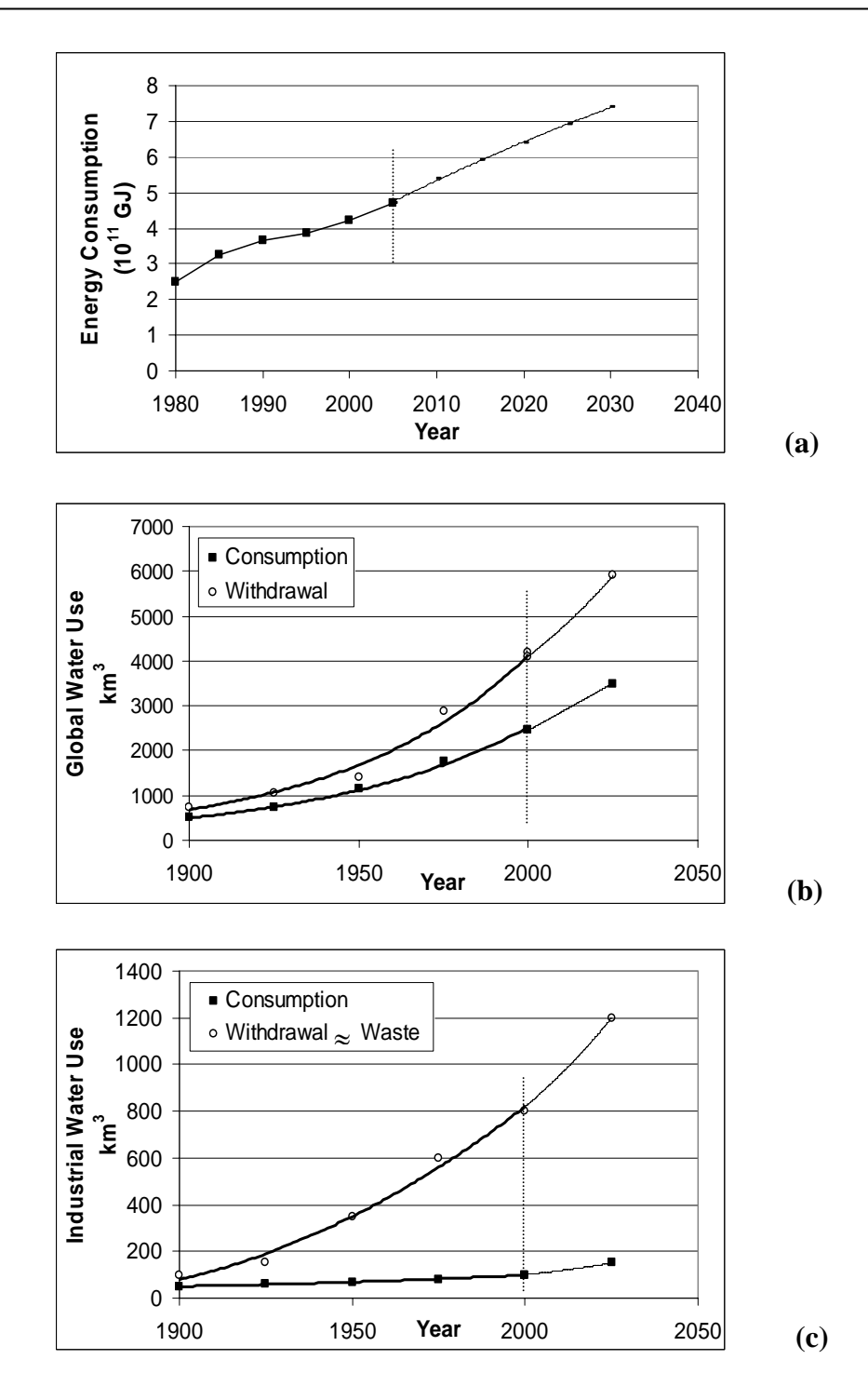


Figure 1.1: (a) World energy consumption 1980-2030 [Energy 2004]

- **(b)** Global fresh water use [United Nations 2007]
- (c) Global industrial water use[United Nations 2007]

**Withdrawal** is the removal of freshwater from water resources or reservoirs. **Consumption** is the use of water by humans from natural water resources or reservoirs.

A tremendous amount of exergy could be saved by more efficient separations. Moreover, huge amounts of valuable industrial aqueous streams that are currently too energy intensive to be treated and are disposed of, could be used as raw material for those valuable materials instead, if only the technology to do so were available, turning a burden into a blessing.

For certain types of aqueous process streams and processes, new technologies such as reverse osmosis, multiple stage evaporation with mechanical vapor recompression, combined heat-power generation, have come a long way to enhance the efficiency dramatically. For systems containing higher salt or acid concentrations, however, and where conditions for building a power plant at a matching scale is not feasible (in other words, where heat is not for free), there is no efficient technology yet.

The type of the process applied in separation of water from mixtures depends on the type of the mixture. The most commonly used technologies for separation of aqueous electrolyte solutions, their separation principle and the disadvantages are listed in Table 1.1.

The subject of this thesis is the novel crystallization technology of Eutectic Freeze Crystallization (EFC) for recovery of (valuable) dissolved salts (or acids) and water from aqueous streams. Using EFC, process streams currently producing large quantities of saline waste could be treated in an ecologically and economically sustainable way. It offers extremely high levels of purity of the end products, and avoids undesirable side effects such as poisonous fumes or extra chemicals added for waste water treatment. It can also be applied to food or pharmaceutical industry where high temperature operating conditions have to be avoided to preserve product quality. EFC changes the focus from cost to value by introducing a new separation process which converts waste into raw materials by a low-energy manner (energy efficient process) in accordance with physical calculations.

**Table 1.1**: Commonly used conventional separation technologies

[Mullin 2001, Myerson 2002, Kentish et al. 2001, Chowdhury 1988, Zijlema 1999, Oostherhof 1999, Sluys et al. 1996, Curcio et al. 2001, Drioli et al. 2004]

#### Removal of low solute concentrations

Technology Solvent extraction	Separation principle Selective solvents are applied allowing the separation of specific molecules from the aqueous phase selectively	<b>Disadvantage</b> Additional chemicals and re-separations required
Reverse osmosis	Solution is pumped against a membrane that selectively allows passage of the solvent. A pure solvent stream is obtained at the permeate side, whereas more concentrate salt at the retentate side.	Doesn't work for mixtures with high concentrations  Sensitive to fouling and
Freeze concentration	Remove water by crystallization of ice	Not suitable for eutectic systems

#### Removal of high solute concentrations

<b>Technology</b> Evaporative	Separation principle The crystals are grown from a solution by separating the	<b>Disadvantage</b> High exergy consumption	
crystallization	solvent via evaporation. In industrial scale processes, the vapor is reused to reduce energy consumption.	Works at high temperature (unsafe)	
Cooling crystallization	Crystallization is obtained by cooling a solution below its saturation temperature.	The yield is limited by the solubility of the crystallization substance	
Anti-solvent (AS) crystallization	Combines extraction and crystallization. An AS is introduced into the mixture that shows selective affinity with only the water molecules in the mixture and causes components to crystallize.	AS has to be recovered form the spent mother liquor after crystallization. Extra chemicals necessary.	
Membrane crystallization	Integrates membrane separation and crystallization. The membrane is used to remove the solvent from the solution to create or to enhance the generation of the crystallization driving force.	Scale formation on the membrane surface	

Eutectic freeze crystallization not only can replace existing technologies but enables completely new processes to be designed as it constitutes a new unit operation. For instance, a new type of process where reverse osmosis does the first concentration step up to 5 wt% salt while an EFC stage produces crystalline product and more clean water combines the two technologies both at their strongest points. In the past, a combination of lacking equipment, prejudices ("cooling is always too expensive", the crystals will never be pure") has hampered development and implementation of EFC. Providing safer,

sustainable, economical and ecological requirements for aqueous stream treatment, Eutectic Freeze Crystallization is a leading technology candidate for the coming decade.

#### **EUTECTIC FREEZE CRYSTALLIZATION**

The term crystallization, as known in the chemical industry, refers to the formation of a dispersed solid phase from a fluid that is either a solution or an impure melt. Phase diagrams represent the ranges of temperature, pressure and composition at which the solid and fluid phases are thermodynamically stable. Most of the inorganic compounds and many organics from solutions crystallize from solution in the eutectic system. Figure 1.2 shows for a binary eutectic system the regions of stability of one phase (liquid), two phases (solid consisting of pure I (ice- for our case) in equilibrium with the liquid; pure solid S (salt) with liquid; pure I and S) and three phases (solids I, S and liquid in equilibrium at the eutectic point C). Besides, when the components in the mixture fit into each others lattice, a rather common behavior of solid-solution system form and both components are deposited simultaneously. This type of systems, when submitted to a cooling operation, at any stage one of the components deposit in the pure state [Mullin 2001]. During developing Eutectic Freeze Crystallization technology, aqueous solutions with eutectic phase diagram were chosen as model solutions.

#### Separation principle

EFC operates around the eutectic temperature and composition of aqueous solutions and can treat a wide variety of feed solutions without adding any further solvents or chemicals. EFC can be considered as a combination of cooling and freeze crystallization. 100% theoretical yield and up to 90% exergy cost saving make EFC technology attractive. The principle of EFC can be described using a phase diagram of a binary saltwater mixture, shown in Figure 1.2. If a solution in unsaturated area with a concentration lower than eutectic composition (A) is cooled down below its freezing point, ice crystals start to form (B). Further cooling decreases the temperature, and increases the concentration with the formation of ice crystals along the ice line B to C. At point C

(eutectic point: the intersection of the ice and salt solubility lines), the liquid concentration reaches saturation and further cooling will result the formation of ice and salt crystals simultaneously. Similarly, starting with a solution having higher concentration than eutectic composition will result in the formation of first salt and reach to the eutectic point by following the salt solubility line.

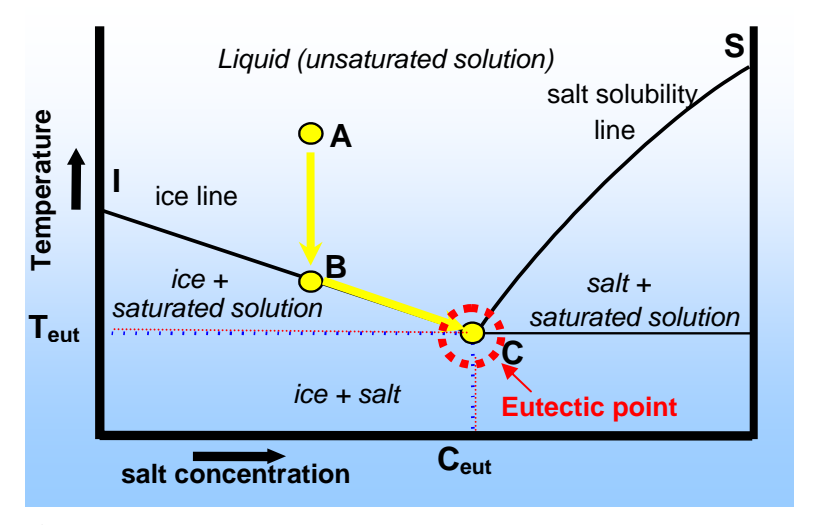


Figure 1.2: Eutectic phase diagram of an aqueous solution

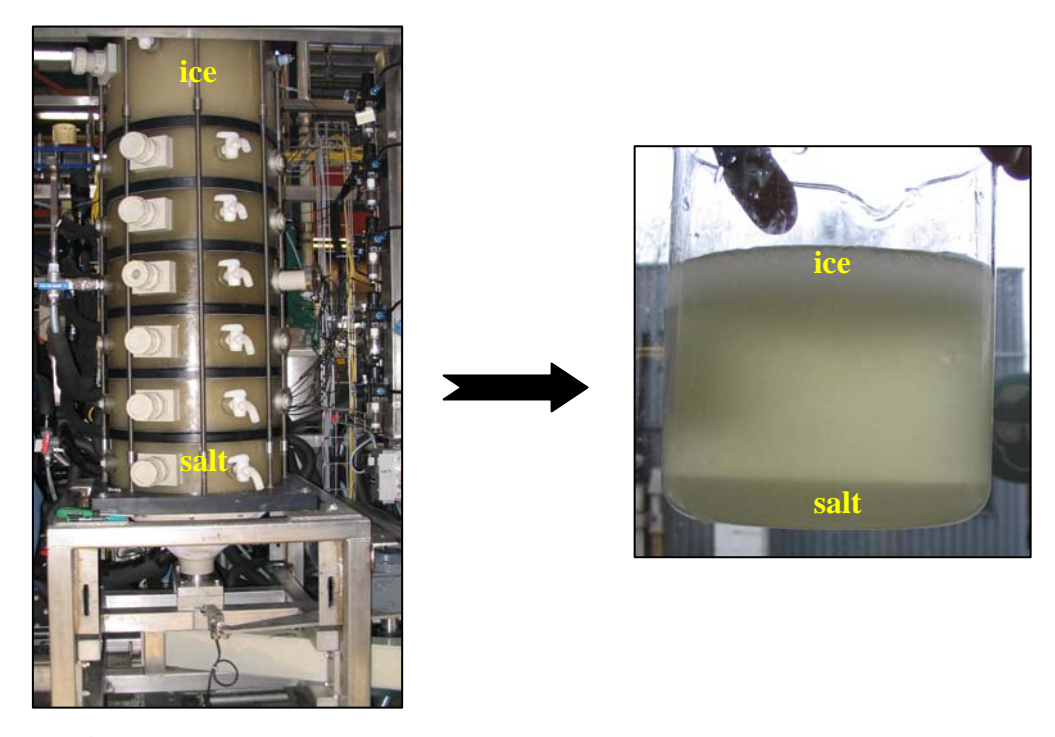


Figure 1.3: Gravitational separation of ice and salt crystals formed by EFC

The two solid products (ice and salt) are separated gravitationally based on their density difference. Salt crystals sink to the bottom of a solution while the ice crystals rise to the surface as shown in Figure 1.3.

#### State of the art of Eutectic Freeze Crystallization

Stepakoff [Stepakoff et al. 1974], Barduhn [Barduhn 1979], Swenne and Thoenes [Swenne 1983, Swenne et al. 1985] made the first studies on a eutectic freeze crystallization process for brine disposal and concentration of industrial wastewater, of natural waters and of sodium chloride production from solution mining. In the late 1990's Van der Ham and Witkamp started to develop eutectic freeze crystallization process, with the concept of indirect cooling. He proved the feasibility of EFC technology for the waste water treatment of aqueous systems like NaNO<sub>3</sub>, CuSO<sub>4</sub>, NH<sub>4</sub>H<sub>2</sub>PO<sub>4</sub> and an industrial case for a KNO<sub>3</sub>-HNO<sub>3</sub>-H<sub>2</sub>O process stream [Van de Ham 1999a, Van de Ham et al. 1998, 1999b, 2003]. Following the work of Van der Ham, in 1998 Vaessen designed and constructed two types of 100-liter eutectic freeze crystallizers: The cooled disc column crystallizer (CDCC) and the scraped cooled wall crystallizer (SCWC). He evaluated their technical performance based on the treatment of ternary aqueous KNO<sub>3</sub>–HNO<sub>3</sub> solutions [Vaessen 2003a, Vaessen et al. 2003b, 2003c]. Besides indirect cooling, Vaessen did also some direct cooling studies with the help of CO<sub>2</sub> clathrates by changing the eutectic temperature by crystallizing CO<sub>2</sub> clathrates instead of normal ice [Vaessen et al. 1999]. In 2002, Himawan applied EFC technology for the recovery of magnesium sulphate and ice from an industrial magnesium sulphate stream from ex-flue gas desulphurization and developed a general model for continuous eutectic freeze crystallization in a scraped surface crystallizer based on population balances (crystal size distributions during the simultaneous solute and solvent crystallization into ice and salt crystals) [Himawan et al. 2002, 2006, Himawan 2004].

#### Scope of the research and outline of the thesis

The aim of the thesis work has been to investigate some unexplored fundamental aspects of EFC and to develop eutectic freeze crystallization equipment and the technology for industrial scale. As a model system MgSO<sub>4</sub> was used, because of its industrial relevance as product from flue gas desulphurisation and because it is scientifically interesting.

Chapter 2 focuses on the experimental study on the continuous operation EFC in a 150 liter pilot scale CDCC crystallizer. The performance of the crystallizer was evaluated according to its heat transfer and the production rate, the product size and the growth rates comparing to the previous designs [Genceli et al. 2005a].

Chapter 3 covers the investigation on inline determination of the MgSO<sub>4</sub> solution concentration and supersaturation using conductivity and refractive index measurement techniques [Genceli et al. 2005b].

Chapter 4 reports the design, scale-up and construction of a complete mobile skid mounted unit for 130 ton/year  $MgSO_4\cdot 7H_2O$  and water production capacities. The experiments for technical evaluation and consequently determination of the optimum operation parameters were performed for the  $3^{rd}$  generation CDCC and for the skid mounted unit [Genceli et al. 2005c, 2005d]. The nucleation and growth rate kinetic parameters of ice and  $MgSO_4\cdot 11H_2O$  salt crystallization were estimated.

The MgSO<sub>4</sub> salt crystal structure at eutectic conditions was also investigated during this research. According to the phase diagram of MgSO<sub>4</sub>-H<sub>2</sub>O system in literature, MgSO<sub>4</sub>·12H<sub>2</sub>O is the stable salt form around the eutectic point (concentration 17.3-21.4 %-w MgSO<sub>4</sub> and temperature between -3.9 to 1.8 °C) [Chernogorenko 1956, Gmelin 1958, Marion 1999]. MgSO<sub>4</sub> salt water content in that area was first defined by Fritzsche in 1837 as MgSO<sub>4</sub>·12H<sub>2</sub>O via dehydration by weight loss of the salt [Fritzche 1837]. Considering the lack of crystal structure data for the related salt, single-crystal X-Ray Diffraction measurement of the salt was performed [Genceli et al. 2007]. A newly discovered magnesium sulfate-hydrate crystal structure is reported in Chapter 5.

The natural occurrence of MgSO<sub>4</sub>·11H<sub>2</sub>O crystals in sea ice inclusions from Saroma Lake-Japan and their likely existence in Antarctic ice inclusions were discovered using Micro Raman Spectroscopy technique. MgSO<sub>4</sub>·11H<sub>2</sub>O named Meridianiite, deposited and recognized as a valid mineral by the Commission on New Mineral Names and Mineral Nomenclature of the International Mineralogical Association (2007-11, Peterson and Genceli). In Chapter 6, the discovery of this new mineral –Meridianiite- is presented.

In order to lower operational costs in industrial crystallizers and to achieve crystallization process intensification, scale prevention on cooled surfaces is extremely important. Prevention of scaling may be possible by understanding its mechanism better and developing more knowledge about the nucleation and growth conditions on the cooled wall. Therefore, growth of MgSO<sub>4</sub> aqueous solution on a cooled surface has been studied theoretically and experimentally. The excess entropy production rate for heat and mass transport into, out of and across the interface was derived using thermodynamic excess densities as proposed by Gibbs [Gibbs 1961]. These variables describe the interface as a separate (two-dimensional) system in local equilibrium. Coupled heat and mass flux equations from non-equilibrium thermodynamics [Kjelstrup et al. 2008] describing the crystal growth and the temperature jump at the interface of the growing crystal and the distribution ratio of heat of crystallization between the salt and liquid phases are presented in Chapter 7.

A consortium including knowledge institutes, the users (process industries) and a equipment manufacturer has effectively developed EFC during the last ten years to the state of pilot scale. Now it is time to accelerate the translation of this scientific-technological knowledge into business. Fast implementation of EFC technology to the market is desired both for economical and environmental reasons. Traditionally, innovations are considered as linear chains of independent actions, where each stage requires a considerable amount of time, holding up the next stage. This is one important reason for the traditional long implementation trajectory. The time between invention and successful implementation can be reduced by simultaneous actions using the Cyclic

Innovation Model which considers the innovation process as couples 'cycles of change', where developments take place in all cycles simultaneously [Berkhout 2000, Berkhout et al. 2006]. This helpful innovation model tool is described and subsequently applied to set out a path for commercialization of the eutectic freeze crystallization technology in Chapter 8.

#### REFERENCES

- Barduhn et al. 1979 Barduhn, A. J.; Manudhane, A.; Temperatures Required for Eutectic Freezing of Natural Waters, *Desalination*. 1979, 28, 233-241.
- Berkhout 2000 Berkhout, A. J.; The Dynamic Role of Knowledge in Innovation. An Integrated Framework of Cyclic Networks for the Assessment of Technological Change and Sustainable Growth. Delft University Press, Delft, 2000.
- Berkhout et al. 2006 Berkhout, A. J.; Hartmann, D.; Duin, P. van der; Ortt, R.; Innovating the Innovation Process, *Int. J. Technol. Management*. 2006, 34, Nos. 3/4, 390-404.
- Chernogorenko 1956 Chernogorenko, V. B.; *Zhurnal Neorganicheskoi Khimii.* 1956, Vol. I, No.2, 317-322.
- Chowdhury 1988 Chowdhury, J.; CPI warm up to freeze concentration, *Chem. Eng.* April 1988, 24.
- Coleridge 2006 Coleridge; Rhyme of the Ancient Mariner; Human Appropriation of the World's Fresh Water Supply: "Water, water, everywhere, nor any drop to drink", 01/04/2006.

  http://www.globalchange.umich.edu/globalchange2/current/lectures/freshwater\_s upply/freshwater.html
- Curcio et al. 2001 Curcio, E.; Criscuoli, A.; Drioli, E.; Membrane crystallizers, *Ind. Eng. Chem. Res.* 2001, 40, 2679.
- Drioli et al. 2004 Drioli, E.; Curcio, E.; Criscuoli, A.; Di Profio, G.; Integrated system for recovery of CaCO<sub>3</sub>, NaCl, and MgSO<sub>4</sub>·7H<sub>2</sub>O from nonofiltration retentate, *J. Membrane Sci.* 2004, 239, 27.
- Energy 2004 Energy Information Administration, International Energy Annual 2004, http://www.eia.doe.gov, 2004.
- Fritzche 1837 Fritzche, C.J.; Ueber eine neue Verbindung der schwefelsauren Talkerde mit wasser. Annalen der Physik und Chemie, *Poggendorff's Annalen*. 1837, 42, 577-580.

- Genceli et al. 2005a Genceli, F. E.; Gärtner, R.; Witkamp, G. J.; Eutectic Freeze Crystallization in a 2<sup>nd</sup> Generation Cooled Disk Column Crystallizer for MgSO<sub>4</sub>-H<sub>2</sub>O System, *Journal of Crystal Growth*. 2005, 275(1-2), e1369-e1372.
- Genceli et al. 2005b Genceli, F. E.; Himawan, C.; Witkamp, G. J.; Inline Determination of Supersaturation and Metastable Zone Width of MgSO<sub>4</sub>·12H<sub>2</sub>O with Conductivity and Refractive Index Measurement Techniques, *Journal of Crystal Growth.* 2005, 275(1-2), e1757-e1762.
- Genceli et al. 2005c Genceli, F. E.; Trambitas, D. O.; Gärtner, R. S.; Rodriguez, M.; Witkamp, G. J.; 3<sup>rd</sup> Generation Cooled Disk Column Crystallizer and Skid Mounted Unit for Eutectic Freeze Crystallization, *VDI Berichte (1901 II)*. 2005, 855-860.
- Genceli et al. 2005d Genceli, F. E.; Gärtner, R. S.; Trambitas, D.; Rodriguez, M.; Witkamp, G. J.; A sustainable technology: Eutectic freeze crystallization-From batch laboratory to continuous industry applications, *Sustainable (Bio)Chemical Process Technology-Incorporating the 6th International Conference on Process Intensification.* pp. 235-242, 27-29 September 2005, Delft, The Netherlands.
- Genceli et al. 2007 Genceli, F. E.; Lutz, M.; Spek, A. L.; Witkamp, G. J.; Crystallization and Characterization of a New Magnesium Sulfate Hydrate -MgSO<sub>4</sub>·11H<sub>2</sub>O-, *Crystal Growth & Design*. 2007, 7(12), 2460-2466.
- Gibbs, J. W.; *The Scientific Papers of J.W. Gibbs*. Dover, New York, 1961.
- Gmelin 1958 Gmelin; *Gmelins Handbuch der Anorganischen Chemie*. Verlag Chemie, Weinheim, 1958.
- Himawan et al. 2002 Himawan, C.; Vaessen, R. J. C.; Seckler, M. M.; Witkamp,
   G. J.; Recovery of Magnesium Sulfate and Ice from Magnesium Sulfate Industrial
   Solution by Eutectic Freezing, *Proceeding of the 15<sup>th</sup> International Symp. on Industrial Crystallization*. Sorrento-Italy 2002, 951-955.
- Himawan 2005 Himawan, C.; Characterization and Population Balance Modelling of Eutectic Freeze Crystallization. PhD dissertation, Delft, 2005.

- Himawan et al. 2006 Himawan, C.; Witkamp, G. J.; Crystallization Kinetics of MgSO<sub>4</sub>·12H<sub>2</sub>O from different scales of batch cooling scraped crystallizers, *Crystal Research and Technology*. 2006, 41(9), 865-873.
- Kentish et al. 2001 Kentish, S. E.; Stevens, G. W.; Innovations in separations technology for the recycling and re-use of liquid waste streams, *Chem. Eng. Journal*. 2001, 84. 149.
- Kjelstrup et al. 2008 Kjelstrup, S.; Bedeaux, D.; *Non-equilibrium thermodynamic* of heterogeneous systems. Series on Advances in Statistical Mechanics, Vol. 16, World Scientific, Singapore, 2008.
- Marion 1999 Marion, G. M.; Farren, R. E.; *Geochim. Cosmochim. Acta* 1999, 63(9), 1305-1318.
- Mullin 2001 Mullin, J. W.; *Crystallization*. 4<sup>th</sup> ed. Butterworth-Heinemann, Boston, 2001.
- Myerson 2002 Myerson, A. S.; *Handbook of Industrial Crystallization*, 2<sup>nd</sup> ed., Butterworth-Heinemann, 2002.
- Oostherhof 1999 Oostherhof, H.; *The Anti-solvent Crystallization of Sodium Carbonate*. PhD Dissertation, Delft, 1999.
- Sluys et al. 1996 Sluys, J. T. M.; Verdoes, D.; Hanemaaijer, J. H.; Water treatment in a membrane –assisted crystallizer (MAC). *Desalination*. 1996, 104, 135.
- Stepakoff et al. 1974 Stepakoff G. L.; Siegelman, D.; Johnson, R.; Gibson, W.; Development of a Eutectic Freezing Process for Brine Disposal, *Desalination*. 1974, 15, 25-38.
- Swenne 1983 Swenne, D. A.; *The Eutectic Crystallization of NaCl-2H<sub>2</sub>O and Ice*. PhD dissertation, Eindhoven, 1983.
- Swenne et al. 1985 Swenne D. A.; Thoenes, D.; The eutectic crystallization of sodium chloride dihydrate and ice, *Journal of Separation Process Technology*. 1985, 6, 17-25.
- United Nations 2007 United Nations Environment Programme/Grid-Arendal.

  Maps and Graphics, http://maps.grida.no, 2007.

- Vaessen et al. 1999 Vaessen, R. J. C.; Van der Ham, F.; Witkamp, G. J.; Shifting Eutectic Conditions by Use of CO<sub>2</sub> Clathrates in Eutectic Freeze Crystallization, *Ann. N. Y. Acad. Sci.* 1999, 912, 483-495.
- Vaessen 2003a Vaessen, R. J. C.; Development of Scraped Eutectic Freeze Crystallizers. PhD dissertation, Delft, 2003.
- Vaessen et al. 2003b Vaessen, R. J. C.; Seckler, M. M.; Witkamp, G. J.; Eutectic Freeze Crystallization with an Aqueous KNO<sub>3</sub>-HNO<sub>3</sub> Solution in a 100-liter Cooled Disc Column Crystallizer, *Industrial Engineering and Chemistry Research*. 2003, 42(20), 4874-4880.
- Vaessen et al. 2003c
  Vaessen, R. J. C.; Janse, B. J. H.; Seckler, M. M.; Witkamp,
  G. J.; Evaluation of the Performance of a Newly Developed Eutectic Freeze
  Crystallizer Scraped Cooled Wall Crystallizer, *Chemical Engineering Research*and Design. 2003, 81(A10), 1363-1372.
- Van der Ham et al. 1998 Van der Ham, F.; Witkamp, G. J.; De Graauw, J.; Van Rosmalen, G. M.; Eutectic Freeze Crystallization: Application to Process Streams and Waste Water Purification, *Chem. Eng. Proc.* 1998, *37*(2), 207.
- Van der Ham 1999a Van der Ham, F.; *Eutectic Freeze Crystallization*. PhD dissertation, Delft, 1999.
- Van der Ham et al. 1999b Van der Ham, F.; Witkamp, G. J.; De Graauw, J.; Rosmalen, G. M.; Eutectic Freeze Crystallization Simultaneous Formation and Separation of Two Solid Phases, *Journal of Crystal Growth*. 1999, 198/199, 744-748.
- Van der Ham et al. 2003 Van der Ham, F.; Seckler, M. M.; Witkamp, G. J.; Eutectic Freeze Crystallization in a New Apparatus: The Cooled Disk Column Crystallizer, *Chemical Engineering and Processing*. 2003, 43(2), 161-167.
- Wikipedia 2007 Wikipedia The Free Encyclopedia: Water resources, 2007, http://en.wikipedia.org/wiki/Water\_resources
- Zijlema 1999 Zijlema, T.; *The Anti-solvent Crystallization of Sodium Chloride*. PhD Dissertation, Delft, 1999.

# **Chapter**

# Development and Performance of EFC Cooled Disc Column Crystallizer (CDCC2)

Eutectic Freeze Crystallization in a 2<sup>nd</sup> Generation Cooled Disk Column Crystallizer for MgSO<sub>4</sub>-H<sub>2</sub>O System

### F. Elif Genceli<sup>a</sup>, Robert Gärtner<sup>a</sup>, Geert-Jan Witkamp<sup>a</sup>

<sup>a</sup> Process & Energy Department TUDelft, Deft-The Netherlands

Journal of Crystal Growth, Volume 275, Issues 1-2, 2005, pp. e1369-e1372



#### ABSTRACT

Eutectic freeze crystallization is a new separation process to produce pure ice and salt from concentrated salt solutions. For this new process, specialized crystallizers are being developed. A new, 2<sup>nd</sup> generation Cooled Disc Column Crystallizer (CDCC-2) with 150-liter capacity and 5.6 m<sup>2</sup>/m<sup>3</sup> cooling area was designed and tested for MgSO<sub>4</sub> crystallization. A heat flux of 1.1-3.9 kW/m<sup>2</sup> was achieved at a temperature difference between coolant and crystallizer bulk solution of 3-6.5 K and a residence time of 1-3 hours. Crystallization and gravitational separation of ice and salt are discussed.

#### INTRODUCTION

Very pure water and solid salt can be simultaneously recovered from electrolyte solutions by Eutectic Freeze Crystallization (EFC) at low energy costs and very high yields [Van der Ham et al. 1998-1999]. Previous work dealt with the prototypes Cooled Disc Column Crystallizer (CDCC-1) and Scraped Cooled Wall Crystallizer (SCWC-1) [Van der Ham et al. 2003, Vaessen et al. 2002-2003a]. Scaling on the cooling surface was the main problem and was caused by secondary nucleation of ice near the scrapers followed by growth on the cooling surface. This limited the heat transfer to 2.5 kW/m² [Vaessen et al. 2002-2003b, Vaessen 2003a]. A new crystallizer, CDCC-2 was designed with an optimized scraper-plate system and crystallizer geometry for efficient gravitational separation and adequate residence time for nucleation and growth. Heat transfer and crystallization kinetics were investigated for ice and MgSO<sub>4</sub>·11H<sub>2</sub>O.

#### **EXPERIMENTAL**

See Figure 2.1. The feed liquor was pumped (P-01) from T-01 through a plate heat exchanger (H-01) to the CDCC-2 (150 liter capacity). Freezium<sup>TM</sup> solution containing 43%-potassium formate was used as coolant. Ice and salt crystals were formed under near eutectic conditions inside the CDCC-2. The top slurry (mainly ice) was withdrawn by overflow and the bottom flow (mainly salt) was pumped peristaltically (P-02) into a stirred 150-liter tank (T-02). In T-02, the ice and salt crystals dissolved at room temperature and recycled as solution to T-01.

Heraeus Pt-100 Elements (+/- 0.05 °C), Fisher Rosemount Magnetic Flow Meters (+/- 0.25%) with a Fisher Rosemount Delta-V measurement and control system was used.

The CDCC-2 contains 3 compartments separated by 2 cooling plates (SS-316 steel). Orifices are built into the outer rims of the disks allowing vertical transport of fluid, ice and salt through the column. The wall is made of transparent PMMA, 4 rotating scrapers made of HMPE on each cooling plate are mounted on a central axis which is connected to

a motor with variable speed. In the crystallizer main body, the total cooled surface area per crystallizer volume is  $5.6 \text{ m}^2/\text{m}^3$ .

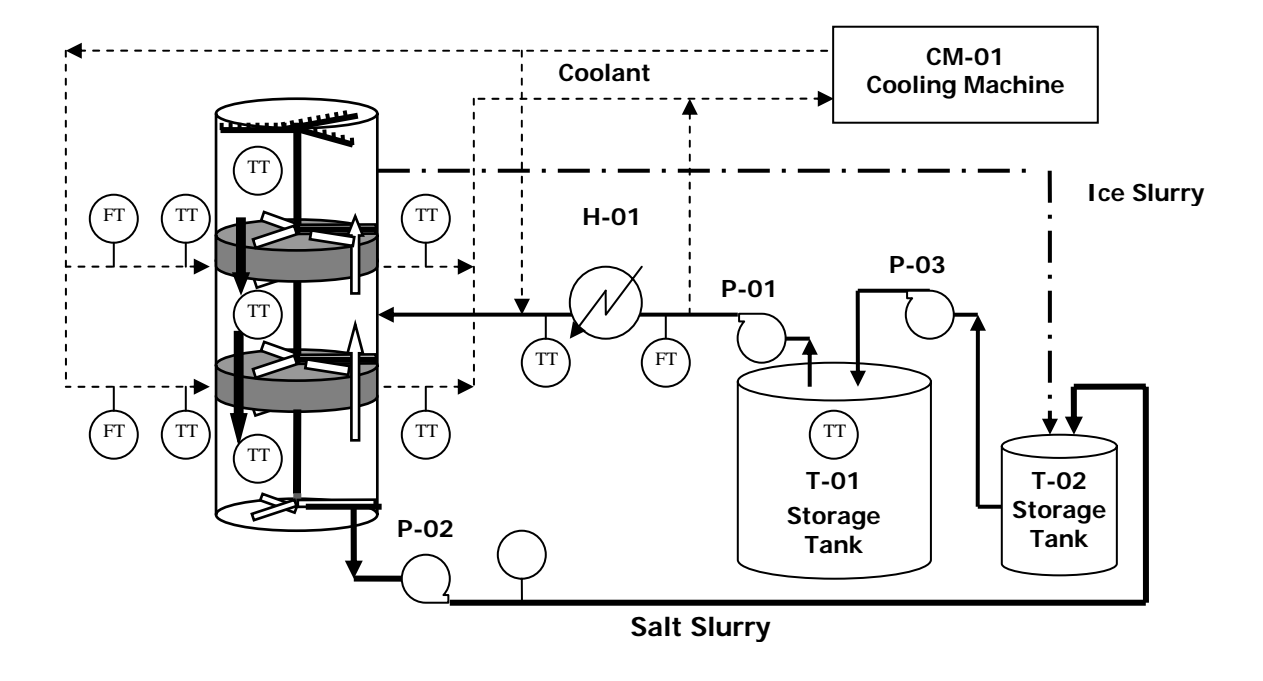


Figure 2.1: Flow sheet of experimental setup

**First,** The CDCC-2 was filled with feed solution at ambient temperature and supercooled in batch mode until sufficient ice and salt were formed. Subsequently the crystallizer was switched to continuous operation. Variables were the feed flow and thereby the residence time and top and bottom product outlet flow rates. The scraping rate was constantly 80 rpm.

At steady state, Ice and salt samples were taken every 30 minutes from top and bottom outlets.

The used industrial magnesium sulfate solution initially contained 17.7 wt% of MgSO<sub>4</sub> and the following impurities in mg/kg level: 40 Mn, 380 Ca, 27 K, 74 Na, 100 Mo, 60 P, 0.9 Al, determined by Inductively Coupled Plasma Atomic Emission Spectrometry (ICP-AES) at  $\pm 2.5\%$ .

MgSO<sub>4</sub>·11H<sub>2</sub>O and ice were crystallized near the eutectic point. The MgSO<sub>4</sub>·11H<sub>2</sub>O was subsequently recrystallized into the final product MgSO<sub>4</sub>·7H<sub>2</sub>O (epsomite).

The heat transfer coefficients in the system were determined from measured flows and temperatures and the heat capacities, using the logarithmic driving temperature difference between coolant and bulk solution as a driving force.

#### **RESULTS AND DICUSSION**

The effects of operating conditions on the heat transfer and the solid production are given in Table 2.1. The temperature of cooling liquid ( $T_{cool}$ ) was varied between -7.6 to -11.7 °C, the residence time ( $\tau$ ) was changed in the range from 1.1 to 3 hours and the ratio of the top outlet flow to the feed flow was varied between 0.67 to 0.95. At eutectic conditions, a vertical temperature profile inside the column was observed: The temperature in the bottom compartment was lower than in the top compartment. The middle compartment temperature value varied with the feed flow rate to the CDCC-2 as warmer MgSO<sub>4</sub> solution was fed to the middle compartment. Increasing the feed rate, i.e. lowering the residence time, increased the temperature in the middle compartment.

**Operating** Heat transfer Solid content **Temperature** conditions distribution Tcool  $\Delta T_{log}^{\ddagger}$ Qtotal/Awall  $T_{top} \\$ Exp  $\mathbf{F}_{top}$ Qtotal  $T_{mid}$  $T_{bot}$ Xice Xsalt  $(kW/m^2)$ . No (h) **(K)** (kW) (wt%) (wt%) (°C) (°C) (°C) (°C) Ftotal 0.96 -7.6 1.1 0.95 3.02 1.14 -4.10 -4.16 -4.297.6% 7.2% A В -4.12 7.9% -7.6 1.5 0.67 3.06 1.04 1.24 -4.00 -4.257.6% C -8.7 4.33 -4.04 -4.11 -4.273 0.95 1.28 1.52 12.0% 9.0% D 3 1.29 -8.7 0.8 4.36 1.54 -4.06 -4.14 -4.2711.4% 8.5% E \_\* -9.8 1.5 0.95 5.06 2.12 2.52 -4.25 -4.18 -4.29F -4.25 \_\* \_\* -9.8 1.3 0.67 5.09 2.06 2.45 -4.16 -4.291.3 6.42 5.7% G -11.7 0.67 3.25 3.87 -4.28 -4.18 -4.34 11.7%

**Table 2.1:** Operating conditions and measurements

$$^{\ddagger} \Delta T_{log} = (T_{cool,in} - T_{cool,out}) / ln \left( \frac{T_{cool,out} - T_{cryst}}{T_{cool,in} - T_{cryst}} \right)$$

<sup>-\*</sup> Solid content not measured

The influence of the heat transfer rate on the formation of ice and salt crystals in CDCC-2 was analyzed. As seen in Table 2.1, lowering the coolant temperature from -7.6 to -11.7 °C, i.e. the logarithmic temperature difference from 3 to 6.4 K, increased the heat flux from 1.1 to 3.9 kW/m². These results indicate a significant improvement compared to those of previous designs. Under the same operation conditions, a heat flux of 0.9-2.5 kW/m² was obtained in the SCWC, while for CDCC-1 it was 2.5 kW/m² in the best case [Vaessen et al. 2002-2003b, Vaessen 2003a].

The gravitational separation of ice and salt occurs inside the crystallizer as a result of the density differences:  $\rho_{MgSO_4 \bullet IIH_2O} \approx 2000 \text{ kg.m}^{-3}$ ,  $\rho_{solution} \approx 1200 \text{ kg.m}^{-3}$  and  $\rho_{ice} \approx 900 \text{ kg.m}^{-3}$ . To prevent ice scaling on the cooling plates and for achieving better heat transfer rate during the experiments, the maximum scraping rate (80 rpm) was used. No scaling was observed nor visually nor indirectly from the heat flux.

The solid content varied between 7.6 to 12 wt% for ice and between 5.7 to 9 wt% for salt as a function of process conditions. The ice crystals (Figure 2.2), had a circular shape with sizes ranging from 100 to 200  $\mu$ m whereas the MgSO<sub>4</sub>·11H<sub>2</sub>O crystals (Fig. 2.3) had prismatic shape with sizes ranging from 100 to 250  $\mu$ m. The average observed crystal growth rates were  $G_{ice} = 9 \times 10^{-9} - 5 \times 10^{-8} \, \text{m/s}$  and  $G_{salt} = 9 \times 10^{-9} - 6 \times 10^{-8} \, \text{m/s}$ .

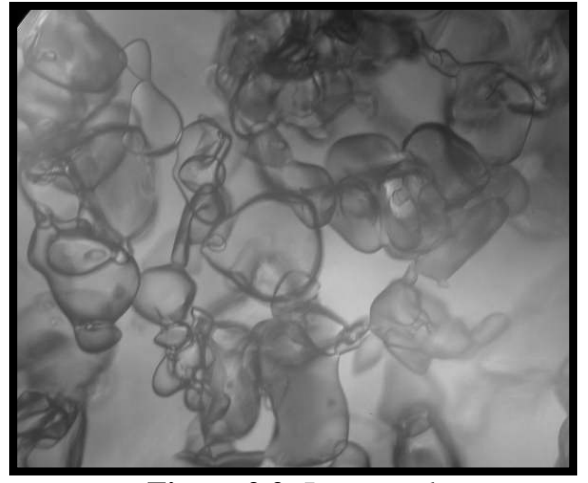


**Figure 2.2:** Ice crystals (Picture width 1000 µm)



**Figure 2.3:** MgSO<sub>4</sub>·11H<sub>2</sub>O salt crystals (Picture width 1000 μm)

#### **CONCLUSION**

- The new crystallizer exhibits a good crystallization performance (i.e. secondary nucleation and growth) and a reduced scaling; allowing a much higher (up to 3.9 kW/ m²) heat flux and thus production rate (in kg per second per cubic meter of the main crystallizer body) of 0.024 kg.s¹.m³ for ice and 0.017 kg.s¹.m³ for MgSO<sub>4</sub>·11H<sub>2</sub>O salt.
- The solid content at steady state was up to 12 wt% with mean average crystal size of  $100\text{-}200~\mu m$  for ice and up to 9 wt% with mean average crystal size of  $100\text{-}250~\mu m$  for MgSO<sub>4</sub>·11H<sub>2</sub>O.
- The growth rates were estimated to be  $G_{ice} = 9 \times 10^{-9} 5 \times 10^{-8} \, \text{m/s}$  and  $G_{salt} = 9 \times 10^{-9} 6 \times 10^{-8} \, \text{m/s} \, .$

#### REFERENCES

- Vaessen et al. 2002 Vaessen, R. J. C.; Himawan, C.; Witkamp, G. J.; Scale formation of ice from electrolyte solutions on a scraped surface heat exchanger plate, *Journal of Crystal Growth*. 2002, 237-239.
- Vaessen 2003a Vaessen, R. J. C.; *Development of Scraped Eutectic Freeze Crystallizers*. PhD dissertation, Delft, 2003.
- Vaessen et al. 2003b
  Vaessen, R. J. C.; Janse, B. J. H.; Seckler, M. M.; Witkamp,
  G. J.; Evaluation of the Performance of a Newly Developed Eutectic Freeze
  Crystallizer Scraped Cooled Wall Crystallizer, *Chemical Engineering Research*and Design. 2003, 81(A10), 1363-1372.
- Van der Ham et al. 1998 Van der Ham, F.; Witkamp, G. J.; de Graauw, J.; Van Rosmalen, G. M.; Eutectic Freeze Crystallization: Application to Process Streams and Waste Water Purification, *Chem. Eng. Proc.* 1998, *37*(2), 207.
- Van der Ham et al. 1999 Van der Ham, F.; Witkamp, G. J.; De Graauw, J.; Rosmalen,
  G. M.; Eutectic Freeze Crystallization Simultaneous Formation and Separation of
  Two Solid Phases, *Journal of Crystal Growth*. 1999, 198/199, 744-748.
- Van der Ham et al. 2003 Van der Ham, F.; Seckler, M. M.; Witkamp, G. J.; Eutectic Freeze Crystallization in a New Apparatus: The Cooled Disk Column Crystallizer, *Chemical Engineering and Processing*. 2003, 43(2), 161-167.

# Chapter 3

Inline Determination of
Supersaturation and Metastable Zone
Width of MgSO<sub>4</sub>·11H<sub>2</sub>O with
Conductivity and Refractive Index
Measurement Techniques

 $F.\ Elif\ Genceli^a,\ Chrismono\ Himawan^a,\ Geert-Jan\ Witkamp^a$ 

<sup>a</sup> Process & Energy Department TUDelft, Deft-The Netherlands

Journal of Crystal Growth, Volume 275, Issues 1-2, 2005, pp. e1757-e1762



#### **ABSTRACT**

Inline measurement of the supersaturation is important to support process control and for evaluation of crystallization experiments. Especially when different hydrates or polymorphs of the crystallized component occur, very precise measurement is required. For example MgSO<sub>4</sub>·7H<sub>2</sub>O - MgSO<sub>4</sub>·11H<sub>2</sub>O lines are quite close, and when operating under Eutectic Freeze Crystallization (EFC) or cooling crystallization both salts might be produced. Therefore conductivity and refractive index inline measurement methods are investigated and compared for MgSO<sub>4</sub> solution having concentration range between 16 to 22 wt% and temperature range between 10 to -5 °C. Conductivity measurements are correlated to concentrations and temperature with the empirical Casteel-Amis equation and refractivity index measurements are correlated to concentrations and temperature with a developed empirical model. The metastable lines for ice and salt of MgSO<sub>4</sub> system is drawn based on the measurements at the onset of crystallization upon cooling of several solution concentrations. In the working range of EFC, the relative supersaturations are calculated to be  $\sigma_{icemax}=0.2$  and  $\sigma_{saltmax}=0.23$ . The accuracy for conductivity measurement in relation to the metastable zone width is roughly calculated to be around 20% and for refractive index measurements 3%.

#### INTRODUCTION

Eutectic Freeze Crystallization (EFC) is a technique to separate aqueous solutions into ice and solidified solutes simultaneously by operating near the eutectic point. The solution concentration and temperature determine the supersaturations with respect to both ice and salt. There is a complex interplay between these supersaturations and the (simultaneous) crystallization of each compound. Therefore, inline determination of the solution concentration in EFC processes is particularly relevant. Inline conductivity and refractive index measurements seem suitable techniques for this purpose.

Conductivity ( $\kappa$ ) is typically expressed as a function of the solute concentration (C) and temperature (T). The literature data of MgSO<sub>4</sub> solutions are limited to high temperature ranges and undersaturated systems [Lobo 1989]. De Diego studied several compounds in a wide range of concentrations and temperatures, to find a model that can fit his ( $\kappa$ , C, T) data [De Diego et al. 1997-2001]. He extended the Casteel-Amis [Casteel et al. 1972] equation to include the effect of the temperature upon the conductivity. For MgSO<sub>4</sub> solutions, the measurements were done between 0-23 %-w and 15-55 °C. Himawan determined the conductivity of the pure MgSO<sub>4</sub> solutions under eutectic conditions with offline measurements and adapted the Casteel-Amis equation with new parameters [Widjaja et al. 2002].

Refractive index (RI) of a solution together with temperature is also one of the common techniques used for to measure the solute concentration. In literature several reports can be found for measuring supersaturation and concentration gradient and observing convective flow in the field of crystal growth by using refractometer techniques [Hirano et al. 1981, Takubo et al. 1989, Takubo 1990, Russo et al. 1993, Fredericks et al. 1994, Rilo et al. 2003]. The refractive index is related to the density and molar electronic polarisability by the Lorentz-Lorenz Equation [Yagi et al. 2003]. It has been found that for some aqueous solutions, the refractive index is a linear function of temperature and density data [Yagi et al. 2003]. In order to confirm such a linear temperature the empirical approximation of Ward and Kurtz was used [Valkai et al. 1998]. The linear

temperature dependence of the refractive index is not a common feature of molecular liquids for example in the case of water the fitted curve is a third order polynomial [Valkai et al. 1998].

In this study, using the Mg-SO<sub>4</sub>-H<sub>2</sub>O system as a model, the potentials of using inline conductivity and refractive index methods to measure supersaturation in EFC are evaluated. Besides, a discussion on the suitability of the Casteel-Amis Equation, using new parameters for low temperatures, an empirical model for representing refractive index data, and determining metastable zone for MgSO<sub>4</sub> system is presented.

## EXPERIMENTAL SETUPS & MEASURING PRINCIPLES FOR CONDUCTOMETER AND REFRACTIVE INDEX MEASUREMENTS

Inline conductometer measurement experiments were performed in a 15-liter, batch type, Scraped Cooled Wall Crystallizer (SCWC) designed for EFC processes. Cooling was achieved by circulating Kyro 85 cooling liquid through a thermostatic unit, Lauda RUK 90 SW. In so doing, the temperature of the cooling liquid was controlled with an accuracy of  $\pm 0.1$ -0.5 °C. Temperature of the MgSO<sub>4</sub> solution was measured using an ASL F250 precision thermometer connected to a PT-100 temperature sensor with an accuracy of  $\pm 0.01$  °C and resolution up to  $\pm 0.001$  °C. Inline conductivity measurements were carried out with an ISC40S inductive conductivity sensor (Yokogawa). The measurement technique is based on the inductive coupling of 2 ring transformers (toroids) by the liquid. The instrument has an accuracy of  $\pm 0.5\%$  of reading and  $\pm 0.5$   $\mu$ S/cm additionally.

Inline refractometer index measurements are performed in a stirred batch type, jacketed glass vessel with an effective volume of 2-liter. A cooling machine, Lauda RK 8 KP, circulated the cooling liquid, ethylene glycol-water, with a well-controlled temperature within ±0.05 °C. Temperature of solution was measured by a precision thermometer ASL F250, connected to a PT-100 sensor, having same accuracy and resolution which is attached to the conductometer setup. Inline refractometer index measurements were carried out with a PR-03-P Sanitary Probe Refractometer sensor (K-Patents). The

instrument determines the refractive index of the process solution by measuring the critical angle of refraction. The instrument has an accuracy of  $\pm 0.0002$  RI (corresponds typically to  $\pm 0.1\%$  by weight).

#### PREPERATION OF SOLUTIONS

16-22 wt% MgSO<sub>4</sub> solutions, prepared from 99 wt% MgSO<sub>4</sub>·7H<sub>2</sub>O (Merck) and ultra pure water of 18.2 m $\Omega$  were used for the conductometer experiments, whereas 16-22 wt% MgSO<sub>4</sub> solutions, prepared from 99.99 wt% MgSO<sub>4</sub>·7H<sub>2</sub>O (J.T. Baker) and ultra pure water of 18.2 m $\Omega$  were used for the refractometer index experiments. The scale used was Mettler type PM30 with accuracy  $\pm 0.2\%$  of reading. The solutions were mixed for a minimum of  $\pm 1$  hour to create a homogeneous solution at around 25 °C inside the crystallizer before starting the experiment. The magnesium sulfate concentrations of the prepared solutions were measured offline with Inductive Coupled Plasma Atomic Emission Spectrometry (ICP-AES) with an accuracy of  $\pm 2.5\%$ . ICP-AES was used to determine the concentration of Mg<sup>2+</sup> cationic contaminant. A 5 ml pycnometer was additionally used to determine the density of the solution with an accuracy of  $\pm 0.15\%$ .

#### EXPERIMENTAL PROCEDURE

In both measuring techniques, the salt solution was put inside the crystallizer and was allowed to stabilize at 10 °C for 1 hour. It was then cooled down following a rate of 4 °C/hour. The data were collected every 20 seconds and were recorded with LabView for conductometer and an acquisition system from K-Patents with software for refractive index measurements. The onset of crystallization was detected from a temperature jump inside the crystallizer. The corresponding conditions of concentration, refractivity index and temperature were used to determine the metastable line.

#### DATA ANALYSIS AND EXPERIMENTAL RESULTS

The conductivity and refractive index data of magnesium sulfate solutions with concentrations between 16 to 22 wt% and temperatures ranging between -5 to 10 °C are given in Figure 3.1 and 3.2. Above 17 wt% the conductivity of magnesium sulfate solution monotonically decreases at all temperatures according to Figure 3.1. This implies the possibility of using conductivity measurements as a method to measure the concentration in the temperature and concentration range of interest for EFC. The sensitivity of the measurement is calculated from the ratio of conductivity difference over concentration difference at constant temperature. From the experimental data recorded, it is found that the sensitivity of the MgSO<sub>4</sub> solution increases with decreasing temperature (0.19mS/cm.wt% at 10 °C and 0.34ms/cm.wt% at -5 °C). The accuracy of the instrument known to be  $\pm 0.5\%$  of the reading and  $\pm 0.5$   $\mu$ S/cm additionally, which is equivalent to 0.1-0.15 mS/cm at low temperatures. This accuracy in conductivity corresponds to a concentration accuracy of about  $\pm 0.25$  wt%. In the case of laboratory scale offline sensor having an accuracy of and  $\pm 0.2\%$ , the accuracy at the same region is about 0.1 wt% [Widiaja et al. 2002].

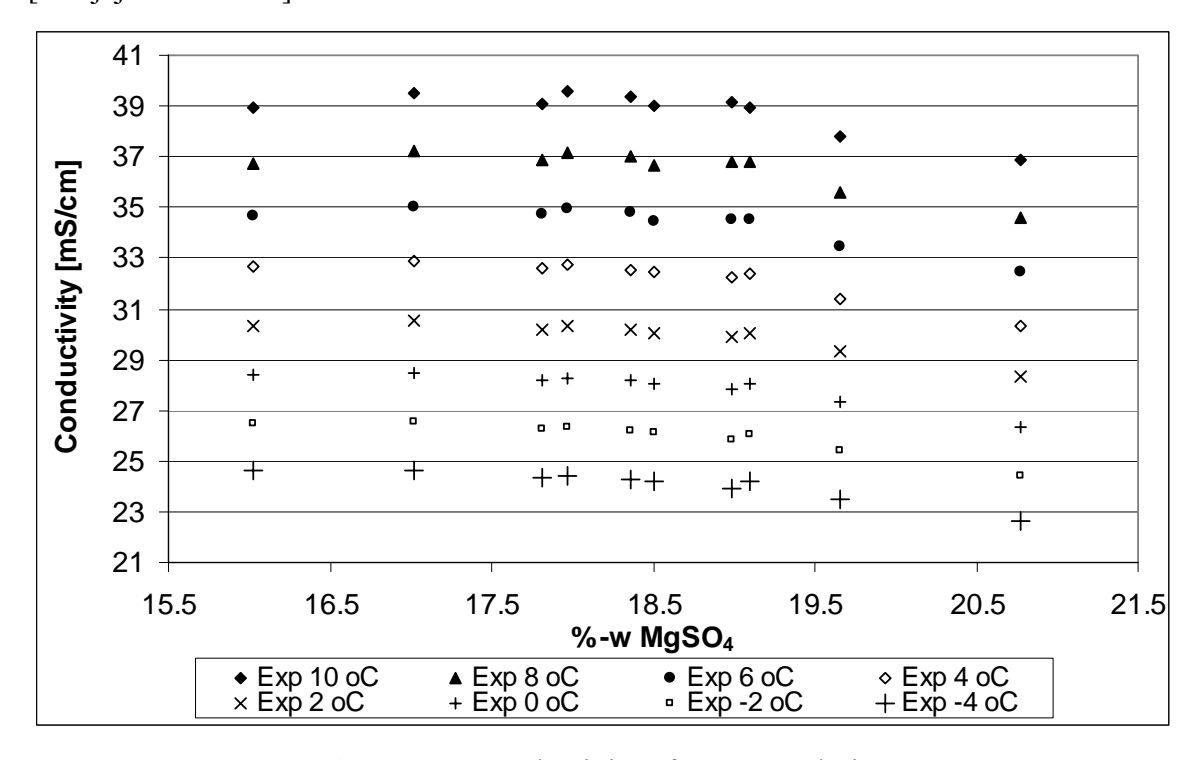


**Figure 3.1:** Conductivity of MgSO<sub>4</sub> solution

The Casteel-Amis equation shown in Equation 3.1 is based on an entirely empirical model [Casteel et al. 1972], derived by the mathematical analysis of the shape of the plots κ vs. C in the whole concentration range, e.g., from infinite dilution to solubility-allowed top concentration, Equation 3.2-3.5. It has been used to for the experimental data of several electrolyte systems [Casteel et al. 1972, Gores et al. 1980, Werblan et al 1993]. De Diego modified Casteel-Amis equation to incorporate the effect of temperature upon conductivity [De Diego et al. 2001],

$$\left(\frac{\kappa}{\kappa_{max}(T)}\right) = \left(\frac{C}{C_{max}(T)}\right)^{x(T)} exp\left[y(T)\left(C - C_{max}(T)\right)^2 - \frac{x(T)}{C_{max}(T)}\left(C - C_{max}(T)\right)\right]$$
(3.1)

where:

$$\kappa_{max}(T) = \kappa_{max}^0 + \kappa_{max}^1 T \tag{3.2}$$

$$C_{max}(T) = C_{max}^{0} + C_{max}^{1}.T$$
(3.3)

$$x(T) = x^0 + x^T T (3.4)$$

$$y(T) = y^0 + y^1 . T (3.5)$$

 $\kappa^0_{max}$  and  $C^0_{max}$  are respectively, the maximum of conductivity (mS/cm) of the chemical system and the concentration (wt%) at which it is attained, both of them at 0 °C.  $\kappa^1_{max}$  and  $C^1_{max}$  represent the shift of the  $\kappa^0_{max}$  and the  $C^0_{max}$  with the temperature-coefficient of the system at the point of maximum conductivity.  $x^0$ ,  $x^1$ ,  $y^0$  and  $y^1$  are adjustable parameters with no physical meaning and temperatures are in °C [De Diego et al. 1997]. Modeling of conductometer data of magnesium sulfate solutions with the help of de Diego parameters are not possible as the relative error between the experimental data and the model is very large (>10%) and increases with decreasing temperature probably as the data for parameterization of de Diego ranges from 15-55 °C. Therefore, it is necessary to determine new parameters for our specific case.

**Table 3.1:** General parameters for MgSO<sub>4</sub> system (2<T<10 °C for High Temperatures and -5<T<2 °C for Low Temperatures)

Par.	High Temperatures		Par.	Low Temp	eratures
	0	1		0	1
K <sub>max</sub>	1.1452	28.1483	K <sub>max</sub>	0.9692	28.7076
C <sub>max</sub>	0.0369	16.6617	$\mathbf{C}_{\max}$	0.0883	14.1650
X	0.3024	0.4696	X	-0.0456	-3.0889
y	0.0004	-0.0058	y	0.0000	-0.0077

An optimization program was used to extract general parameters of the modified Casteel-Amis equation. The adjusted parameters of the modified Casteel-Amis Equation calculated for MgSO<sub>4</sub> solution for concentrations between 16 to 22 w% and temperatures between 10 to -5 °C are as shown in Table 3.1. The relative error of the conductivity data between the model and the measured values are calculated to be 0.5%, which is reasonable. The error decreases even more at lower temperatures (T<2°C). This proves that under EFC conditions, the Casteel-Amis Equation with modified parameters can be used to convert measured conductivities into concentrations successfully.

According to Figure 3.2, the refractive index of magnesium sulfate solution monotonically increases with increasing temperature. This shows the possibility of using refractive index as a method to measure the concentration. The sensitivity of MgSO<sub>4</sub> solution to concentration at constant temperature is  $0.002 \, RI/wt\%$  and to temperature at constant concentration is  $0.0001 \, RI/^{\circ}C$ . This shows that the refractive index data for MgSO<sub>4</sub> solution is more sensitive to concentration change compared to temperature. The accuracy of the measurements is found out to be  $\pm 0.0002 \, R.I.$  corresponding to  $\pm 0.1 \, wt\%$  of solution by weight which suits well with our experimental data. The relationship between refractive index, temperature and concentration for MgSO<sub>4</sub> solution is defined with an empirical model. According to the model, temperature is defined to be a function of  $3^{rd}$  order polynomial equation of concentration, Equation 3.6 and the constants specified in this equation are functions of temperature shown in equations Equation 3.7-3.10.

$$RI = AC_{i}^{3} + BC_{i}^{2} + DC_{i} + E$$
(3.6)

$$A = -1.3984 \times 10^{-9} \,\mathrm{T}^3 - 1.373 \times 10^{-7} \,\mathrm{T}^2 + 1.7063 \times 10^{-6} \,\mathrm{T} - 1.6953 \times 10^{-5} \tag{3.7}$$

$$B = 7.242 \times 10^{-8} \,\mathrm{T}^3 + 7.7232 \times 10^{-6} \,\mathrm{T}^2 - 9.4023 \times 10^{-5} \,\mathrm{T} + 8.7888 \times 10^{-4}$$
 (3.8)

$$D = -1.2342 \times 10^{-6} \,\mathrm{T}^3 - 1.4403 \times 10^{-4} \,\mathrm{T}^2 + 1.7174 \times 10^{-3} \,\mathrm{T} - 1.2913 \times 10^{-2} \tag{3.9}$$

$$E = 6.9203 \times 10^{-6} \,\mathrm{T}^3 + 8.9009 \times 10^{-4} \,\mathrm{T}^2 - 1.0501 \times 10^{-2} \,\mathrm{T} + 1.4181 \tag{3.10}$$

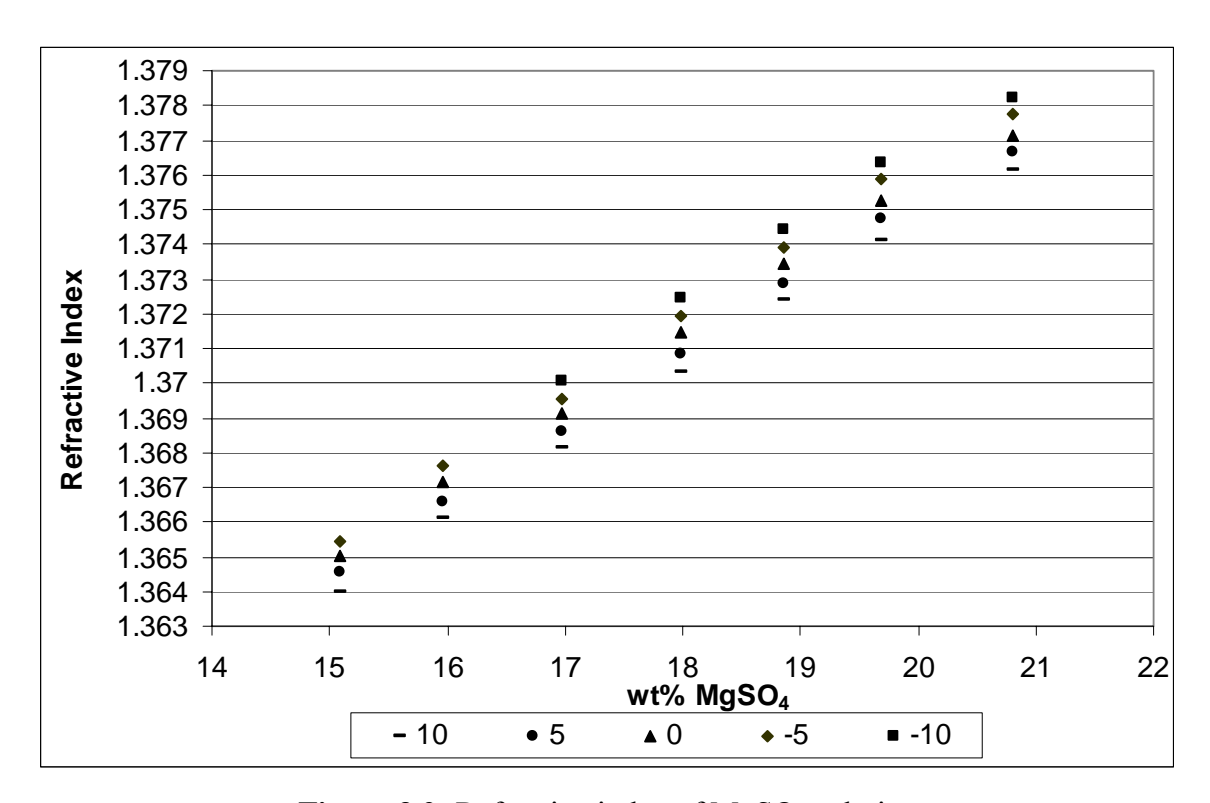
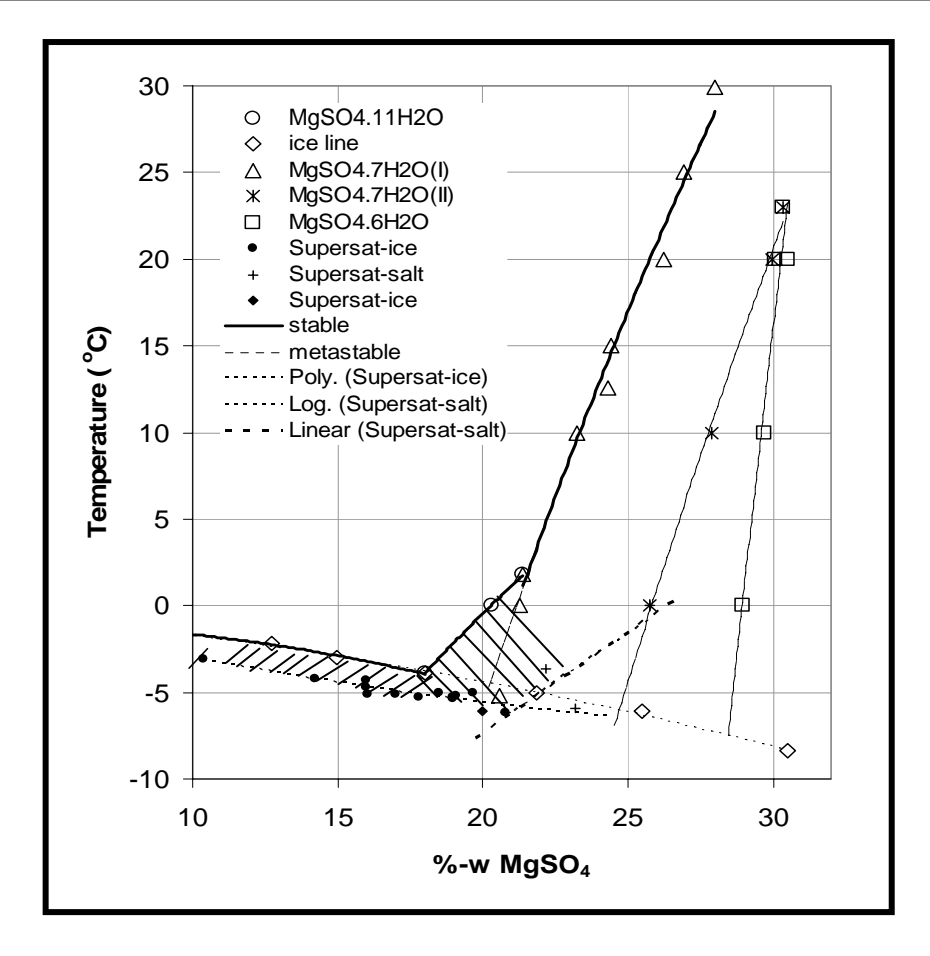


Figure 3.2: Refractive index of MgSO<sub>4</sub> solution

The relative error of the refractive index data between the model and the measured values are calculated to be  $1.7 \times 10^{-3}$  %, which indicates quite high accuracy. The standard deviation of the data obtained from the empirical model and the measured values is found out to be  $1.04 \times 10^{-4}$ . It is clear that very good achievement by using a 3<sup>rd</sup> order polynomial empirical model is obtained for the presentation of MgSO<sub>4</sub> system refractive index data, as a function of temperature and concentration.



**Figure 3.3:** Phase diagram of MgSO<sub>4</sub> system

The phase diagram of the MgSO<sub>4</sub> system is given in Figure 3.3, taken from Gmelin [Gmelin 1958]. The measurements at the onset of crystallization upon cooling for several solution concentrations allowed us to draw the metastable lines for ice and salt. Eutectic freeze crystallization takes place between solubility and metastable lines (hatched area). If we define relative supersaturations as  $\sigma_{ice} = (C_{ice}^* - C)/C_{ice}^*$  and  $\sigma_{salt} = (C - C_{salt}^*)/C_{salt}^*$ , then inspections of Figure 3.3 shows that  $\sigma_{icemax}$ = 0.2 and  $\sigma_{saltmax}$ = 0.23. Comparing the measured concentration (H=C<sub>measured</sub> ± accuracy, considering the error coming from the instruments), with the maximum supersaturation (MZW, metastable zone width), the accuracy ratio (=H/MZW) are for the conductometer measurement calculated to be <20% for ice and about 20% for salt and for refractometer index measurement 3% for both ice and salt which is quite satisfactory.

#### CONCLUSIONS

- The conductivity has been modelled with Casteel-Amis equation whereas the refractive index data has been modelled with an empirical equation with two sets of fit parameters for the ranges of temperature –5 to 10 °C and concentration 16-22 %-w.
- In the EFC working area, the metastable supersaturations for MgSO<sub>4</sub> and ice are about  $\sigma_{\text{saltmax}}$ = 0.23 and  $\sigma_{\text{icemax}}$ = 0.2.
- For eutectic freeze crystallization of  $MgSO_4\cdot 11H_2O$ , the conductivity method has an accuracy in relation to the metastable zone width of about 20% for ice and salt crystallization whereas the refractive index has such an accuracy of 3%.
- Refractive index measurement is potentially a suitable technique for determination of supersaturation in crystallization processes for MgSO<sub>4</sub> system.

#### LIST OF SYMBOLS

T	°C	Measuring temperature
K	mS/cm	Electrical conductivity
C	wt%	Concentration
$C^*$	wt%	Equilibrium concentration at same temperature
$\kappa_{\text{max}}^0$	mS/cm	Maximum conductivity at 0 °C
$\kappa_{max}^{l}$	mS/cm	Maximum conductivity at process temperature
$C_{ m max}^0$	wt%	Maximum concentration at 0 °C
$C_{ m max}^1$	wt%	Maximum concentration at process temperature
$x, x^0$	-	Adjustable parameter with no physical meaning
$x^{I}$	1/T	Adjustable parameter with no physical meaning
$y, y^0$	$1/(\% - w)^2$	Adjustable parameter with no physical meaning
$y^{I}$	$1/(\% - w)^2 T$	Adjustable parameter with no physical meaning
$\sigma_{_{ice}},\sigma_{_{ice}}$	-	Relative supersaturation for ice
A	$RI/(wt\%)^3$	Constant as a function of temperature
В	$RI/(wt\%)^2$	Constant as a function of temperature
D	RI/wt%	Constant as a function of temperature
E	-	Constant as a function of temperature
H	wt%	Concentration measured by conductometer and
		Refractive index method

#### REFERENCES

- Casteel et al. 1972 Casteel, J. F.; Amis, E. S.; Specific conductance of concentrated solutions of magnesium salts in water-ethanol system, *J. Chem. Eng. Data*. 1972, 17, 55.
- De Diego et al. 1997 De Diego, A; Madariaga, J. M.; Chapela, E.; Empirical model of general application to fit (*k*, *c*, *T*) experimental data from concentrated aqueous electrolyte solutions, *Electrochimica Acta*. 1997, 42-9, 1449.
- De Diego et al. 2001 De Diego, A; Usobiaga, A.; Fernández, L. A.; Madariaga, J. M.; Application of the electrical conductivity of concentrated electrolyte solutions to industrial process control and design: from experimental measurement towards prediction through modelling, *Trends in Analytical Chemistry*. 2001, 20-2, 65.
- Fredericks et al. 1994 Fredericks, W.J.; Hammonds, M.C.; Howard, S.B; Rosenberger, F.; Density, thermal expansivity, viscosity and refractive index of lysozyme solutions at crystal growth concentrations, *J. Crystal Growth.* 1994, 141, 183.
- Gmelin 1958 Gmelin; *Gmelins Handbuch der Anorganischen Chemie*. Verlag Chemie, Weinheim, 1958.
- Gores et al. 1980 Gores, H. J.; Barthel, J.; Conductance of salts at moderate and high concentrations in propylene carbonate-dimethoxyethane mixtures at temperatures from -45 °C to 25 °C, *J. Solution Chem.* 1980, 9, 939.
- Hirano et al. 1981 Hirano, E.; Ogawa, T.; Measurements of the concentration gradient around a growing crystal in an aqueous solution by moiré fringes, *J. Crystal. Growth.* 1981, 51, 113.
- Lobo 1989 Lobo, V.M.M.; Handbook of Electrolyte Solutions:

  Literature Data on Thermodynamic and Transport Properties. Elsevier,

  Amsterdam, 1989.
- Rilo et al. 2003 Rilo, E.; Freire, S.; Segade, L.; Cabeza, O.; Franjo, C.; Jimenez, E.; Surface tensions, densities and refractive indexes of mixtures of dibutyl ether and 1-alkanol at *T*=298.15 K, *J. Chem. Thermodynamics*. 2003, 35, 839.

- Russo et al. 1993 Russo, N. A.; Tonso, A. O.; Sicre, E. E.; Liquid refractometry: an approach for a continuous measurement, *Optics & Laser Technology*. 1993, 25-2, 109.
- Takubo et al. 1989 Takubo, H.; Makita, H.; Refractometric studies of NH<sub>4</sub>H<sub>2</sub>PO<sub>4</sub> and KH<sub>2</sub>PO<sub>4</sub> solution growth; experimental setup and refractive index data, *J. Crystal. Growth.* 1989, 94, 469.
- Takubo 1990 Takubo, H; Refractive index as a measure for saturation and supersaturation in crystal growth of water-soluble substances, *J. Crystal Growth*. 1990, 104, 239.
- Valkai et al. 1998 Valkai, S.; Liszi, J.; Szalai, I.; Temperature dependence of the refractive index for three chloromethane liquids at 514.5 nm and 632.8 nm wavelengths, *J. Chem. Thermodynamics*. 1998, 30, 825.
- Werblan et al. 1993 Werblan, L.; Balkowska, A.; Concentrated electrolyte solutions in organic solvents. Their specific conductance and analysis of Casteel—Amis equation, *J. Elecktroanal. Chem.* 1993, 354, 25.
- Widjaja et al. 2002 Widjaja, S.; Himawan, C.; Conductivity Measurements of Magnesium Sulfate Aqueous Solution at High Concentrations and Low Temperatures: Preliminary Study on the Supersaturation Measurements in EFC.

  Lab. for Process Equipment, TUDelft, 2002.
- Yagi et al. 2003 Yagi, T.; Susa, M.; Nagata, K.; Determination of refractive index and electronic polarisability of oxygen for lithium-silicate melts using ellipsometry, *J. Non-Crystallize Solids*. 2003, 315, 54.

## Scaling-up

### Eutectic Freeze Crystallization

3<sup>rd</sup> Generation Cooled Disk Column Crystallizer and A Skid Mounted Unit for Eutectic Freeze Crystallization

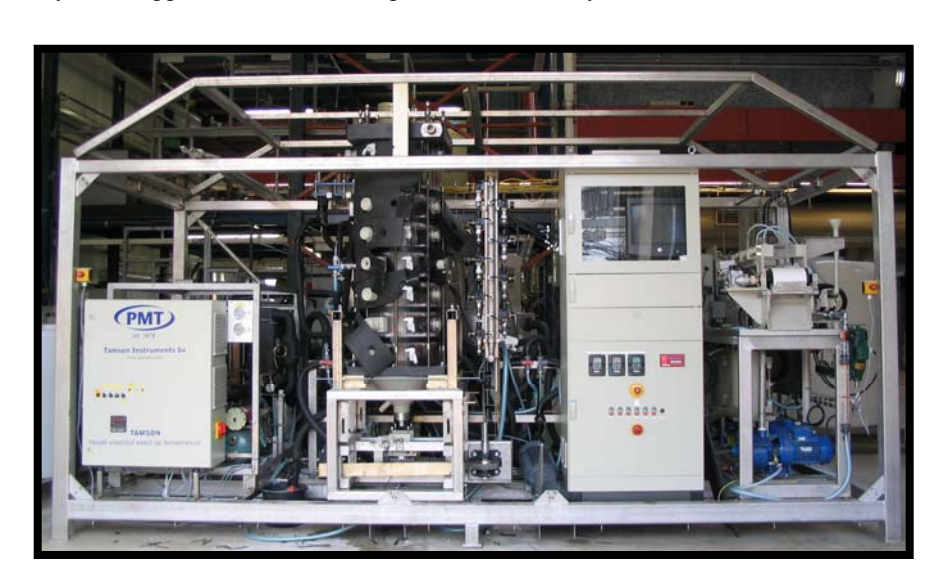
F. Elif Genceli<sup>a</sup>, Daniela Trambitas<sup>a</sup>, Robert Gärtner<sup>a</sup>, Marcos Rodriguez<sup>a</sup>, Geert-Jan Witkamp<sup>a</sup>
<sup>a</sup> Process & Energy Department TUDelft, Deft-The Netherlands

VDI Berichte (1901 II), art. no. D-15, pp. 855-860, 16th International Symposium on Industrial Crystallization, 11-14 Sept 2005, Dresden, Germany.

A sustainable technology: Eutectic freeze crystallization – From batch laboratory to continuous industry applications

**F. Elif Genceli**<sup>a</sup>, **Robert Gärtner**<sup>a</sup>, **Daniela Trambitas**<sup>a</sup>, **Marcos Rodriguez**<sup>a</sup>, **Geert-Jan Witkamp**<sup>a</sup> Process & Energy Department TUDelft, Deft-The Netherlands

Sustainable (Bio)Chemical Process Technology – Incorporating the 6<sup>th</sup> International Conference on Process Intensification, pp. 235-242, 27-29 September 2005, Delft, The Netherlands.



#### **ABSTRACT**

Soluble inorganic salts from industrial processes and aqueous waste streams can be recovered by Eutectic Freeze Crystallization (EFC). Around the eutectic temperature both highly pure salt and ice crystals can be simultaneously recovered as valuable products. Here, the third generation Cooled Disc Column Crystallizer (CDCC-3) and Skid Mounted Unit are presented. CDCC has a capacity of 220-liters, 7 compartments and 7.7 m<sup>2</sup>/m<sup>3</sup> cooling surface area. A complete mobile (skid mounted) pilot unit for industrial applications was designed and constructed, allowing the system to be easily installed and integrated into an industrial plant. The unit consists of the CDCC-3, belt filtration, wash column, separation and storage tanks and special measurement devices (image analysis, data acquisition and a field bus based control system). As a practical application, the skid mounted unit was designed for producing 130 ton/year MgSO<sub>4</sub>·7H<sub>2</sub>O salt. Besides process flow diagrams, the practical performances of the CDCC-3 in terms of heat transfer properties and product quality were investigated. The experimental data were used to estimate the parameters for kinetic relations for nucleation and growth rates for ice and MgSO<sub>4</sub>·11H<sub>2</sub>O salt. For logarithmic mean temperature difference between bulk and coolant temperatures varying between 3.8 and 7.5 K, the heat fluxes were calculated to change from 2.4 to 3.9 kW/m<sup>2</sup> for 30 minutes residence time. Within these operating conditions MgSO<sub>4</sub>·11H<sub>2</sub>O crystals have an average sizes of 90-130 µm and contained less than 0.5 ppm of major impurities. On the other hand, the ice crystals having average sizes between 80-120 µm contained 10 ppm Mg<sup>2+</sup> and SO<sub>4</sub><sup>2-</sup> impurity after four times washing. The growth rates (m.s<sup>-1</sup>) of MgSO<sub>4</sub>·11H<sub>2</sub>O and ice were estimated to be  $G_{salt} = 2 \times 10^{-5} \sigma_{bulk}^2$  and  $G_{ice} = 8 \times 10^{-8} \Delta T_{bulk}$  respectively. The secondary nucleation rates for ice and salt in the bulk were also calculated taking into account the secondary nucleation on the cooled disk walls of the CDCC-3.

#### INTRODUCTION

In industrial processes, such as fertilizer and semiconductor manufacturing, and hydrometallurgy, petrochemical, biochemical processes salt solutions frequently occur as process or wastewater streams. Eutectic Freeze Crystallization (EFC) potentially offers a technically and economically attractive alternative for conventional separation techniques. EFC operates around the eutectic temperature and composition of aqueous solutions, but can treat a wide variety of feed solutions. Both highly pure salt and ice crystals can be simultaneously recovered as valuable products. Theoretically 100% yield and up to 70% energy cost saving (typically 50%) can be achieved compared to triple stage evaporative crystallization. Separation of ice and salt products takes place simultaneously, based on their density difference.

#### **EXPERIMENTAL**

Experimental Set-up: The flow scheme of the process is given in Figure 4.1. The 3<sup>rd</sup> generation Cooled Disk Column Crystallizer (CDCC-3), having 220-liter capacity, contains 7 compartments separated by 6 cooling plates (SS-316 steel). Orifices are built into the outer rims of the disks allowing vertical transport of fluid, ice and salt through the column. The wall is made of transparent PMMA, 6 rotating scrapers made of HMPE on each cooling plate are mounted on a central axis which is connected to a motor with variable speed. In the crystallizer main body, the total cooled surface area per crystallizer volume is 7.7 m<sup>2</sup>/m<sup>3</sup>. Compared to the previous designs [Vaessen 2003, Genceli et al. 2005] the cooled surface area and the volume of the crystallizer are increased. The scrapers are improved for avoiding scaling and all metal parts of the scraper system were isolated. The drive system was changed for a higher motor power. The bottom compartment of the crystallizer was replaced to a conical one and the height of the top compartment was increased for better ice collection. The plate heat exchanger (H-01) supplied from Alfa Laval having 6.6 m<sup>2</sup> surface area is used for the precooling of the feed solution fed to the CDCC-3. The settler (T-02) tank has 120-liters capacity and is made of stainless steel (SS-316). It has a conical bottom for efficient collection of the produced

salt. It is consisting of a cylindrical jacketed vessel on the outer wall, in which cooling liquid passes through. The total cooled surface area per settler tank volume is 7.5 m<sup>2</sup>/m<sup>3</sup>. Spiral-shaped paths inside the jacketed cylinder walls ensure an even distribution of the coolant flow throughout each cylinder. It is stirred with a motor with variable speed. In the hydraulic wash column (WC-01), the produced ice is separated and washed from the impure mother liquor. This is achieved by the formation of a moving ice crystal bed, from which the top part is scraped off and melted. The crystal bed is compressed and transported through the column by the hydraulic force of the mother liquor. Part of the melt, i.e. pure water, is used as a washing liquid and recycled into the crystal bed to wash off the mother liquor. The mother liquor is removed through filtration pipes. The wash column is supplied by TNO and its capacity is 15 kg.h<sup>-1</sup>. The reciprocal tray belt filter (BF-01) is used for the separation of MgSO<sub>4</sub>.11H<sub>2</sub>O salt crystals from mother liquor, and combines counter current washing and drying in a single piece of equipment. BF-01, supplied by Larox-Pannevis, has 0.75 m<sup>2</sup> area, and processes with 1 m<sup>3</sup>/h feed. In the skid, totally 6 membrane pumps are used for the transport of solution and slurry with capacities ranging between 50-2000 l/h. CM-01, supplied by Tamson Instruments B.V., has 10 kW cooling capacity at 0 °C. Freezium<sup>TM</sup> -60 °C solution containing 50 %-w potassium formate was used as coolant. The temperature of the cooling liquid was controlled with an accuracy of ±0.1-0.5 °C. The temperature of the MgSO<sub>4</sub> solution, cooling liquid inlet and outlet temperatures were measured using an ASL F250 precision thermometer connected to PT-100 temperature sensors with an accuracy of ±0.01°C and resolution up to ±0.001 °C. F250 Heraeus Pt-100 Elements (+/- 0.05 °C), a Luci-Cpi Series load cell supplied by Ian Fellows Limited (used as torque meter with an accuracy of ±1 kg), Fisher Rosemount Magnetic Flow Meters (+/- 0.25%) with a Fisher Rosemount Delta-V data acquisition and control system were used.

**Solution:** The used industrial magnesium sulfate solution initially contained 17.4 %-w of MgSO<sub>4</sub> and the following major impurities in (by weight) ppm (mg/kg) level:  $(45\pm10)$  ppm Mn,  $(360\pm60)$  ppm Ca,  $(70\pm10)$  ppm Zn,  $(500\pm100)$  ppm Cl,  $(6\pm4)$  ppm Ni,  $(20\pm5)$  ppm P,  $(370\pm100)$  ppm K,  $(40\pm10)$  ppm Na,  $(20\pm10)$  ppm Mo.

Operating procedure: See Figure 4.1 The CDCC-3 was first filled with MgSO<sub>4</sub> feed solution form the storage tank (T-01) at ambient temperature and (super)cooled in batch mode. The coolant temperature was set in the range between -10 to -14 °C. The initial supercooling, at which seeds of ice and MgSO<sub>4</sub>·11H<sub>2</sub>O salt crystals were introduced, was typically 1.0 °C. These seeds were prepared separately and maintained stable in a cooling chamber. As soon as crystallization of ice and salt occurred, the suspension temperature rose gradually to approach the eutectic temperature and remained stable throughout the experiment. After solids were accumulated, about 0.5-1.0 %-w, which was observed visually, the operation was then switch to continuous mode. The feed liquor was pumped (P-01) from T-01 through a plate heat exchanger (H-01). The scraping rate was a constant 80 rpm which refers to 8 scraper passes per second on any point of the cooling plate. As the result of too good mixing in CDCC-3, at steady state, an intermediate settling tank (T-02) was used for the gravitational separation of ice and salt crystals. From CDCC-3, the top slurry (mainly ice) was withdrawn by overflow and the bottom flow (mainly MgSO<sub>4</sub>·11H<sub>2</sub>O salt) was pumped by a membrane pump (P-02) into T-02. CDCC-3, T-02 and H-01 were cooled down by the connected cooling machine (CM-01). T-02 is mixed by a combined turbine impeller – mixing paddle arrangement to keep the ice crystals as a homogenous, mixed slurry and suspend the salt crystals to prevent blockage in the outlet of the conical bottom. From T-02, the overflow was send to the wash column (WC-01) via P-05 to be separated from the mother liquor. At 0 °C, the mother liquor of eutectic composition was sucked from the ice slurry and discharged back to T-01. MgSO<sub>4</sub>·11H<sub>2</sub>O crystals slurry settled in the T-02 is sent to the belt filter (BF-01) for to be filtered. The mother liquor obtained both from BF-01 and WC-01 were recycled to T-01 via P-04 and P-06 respectively.

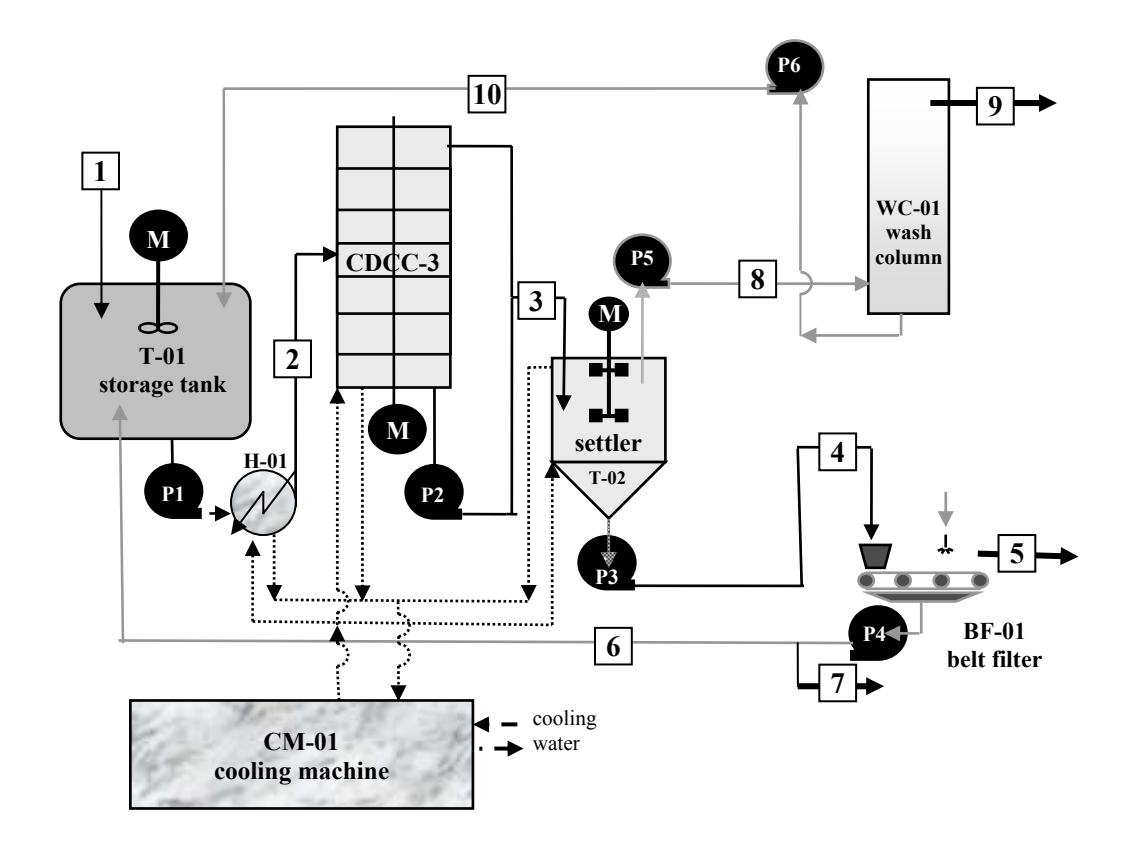


**Figure 4.1**: The flow diagram of MgSO<sub>4</sub>.7H<sub>2</sub>O production with EFC technique (numbers refer to are described in the texts)

Sampling and sample analysis: Slurry samples were taken from the CDCC-3 in batch and continuous mode, the settling tank and the belt filter for defining the production rate, crystal sizes and their quality. The solid was studied by light microscope; photographs were taken of the crystals and the solid content of the slurries determined by filtration (and differential weighing). The control parameter for defining the optimum operation condition was the set temperature of the coolant. The feed flows and thereby the residence time was kept constant at half hour (30 minutes) in all experiments. This value is the lowest residence time due to the restrictions of the pump capacities used in the skid mounted unit. The heat transfer coefficients in the system were determined from measured flows and temperatures and the heat capacities, using the logarithmic temperature difference between coolant and bulk solution as a driving force. The samples of salt crystals were withdrawn every 15 minutes from sampling points of CDCC-3 and

belt filter. The slurry samples were vacuum filtered. On the samples taken from CDCC-3, first gravity separation was applied so ice and salt solid content were measured subsequently and the mother liquor was collected. The cations and anions in the mother liquor and the crystal purity were measured using Inductively Coupled Plasma Atomic Emission Spectrometry (ICP-AES) with an accuracy of ±2.5% and Ion Chromatography with an accuracy of ±3%. Digital photographs of the salt and ice crystals were taken under a Leica WILD M10 stereomicroscope attached with a Nikon Coolpix 4500 camera. The sizes of salt and ice crystals were determined by image analysis. At least 300 crystals were hand counted per one sampling time. The ice and salt impurity contents were measured with Cryo-Laser-Ablation-Induced-Coupled-Plasma-Mass-Spectrograph (cryo-LA-ICP-MS) method. The cryo-LA-ICP-MS consists of the cryo-sample cell, the Bioptic Laser Ablation Unit and the Thermo Finnigan High Resolution ICP-MS. The same sampling procedure was followed as described by Gärtner et al. [Gärtner et al. 2005]. Ice and salt samples were analyzed for Na, K, Mg, Ca, Cr, Mn, Ni, Mo and Cu. The sensitivity of this method for the investigated elements is around 1 ppb or better.

#### RESULTS AND DISCUSSION

As presented in Table 4.1, the temperature of cooling liquid ( $T_{cool}$ ) to CDCC-3 was varied between -10 to -14 °C resulting in heat fluxes from 2.4 to 3.9 W/m<sup>2</sup>. The residence times ( $\tau$ ) for batch were kept constant at 30 minutes after achieving eutectic conditions.

**Table 4.1:** Operating conditions and measurements

Operating	conditions	Heat transfer		Production rate		
T <sub>cool</sub> (°C)	τ (h)	ΔT <sub>log</sub> * (K)	Q <sub>total</sub> (kW)	$\frac{Q_{total}/A_{wall}}{(kW/m^2)}$	x <sub>ice</sub> kg/h	x <sub>salt</sub> kg/h
-10	30	3.8	4.04	2.4	8.3	9.5
-12	30	5.3	5.31	3.2	15.2	16.4
-14	30	7.5	6.48	3.9	17.1	17.4

\* 
$$\Delta T_{log} = (T_{cool,in} - T_{cool,out}) / ln \left( \frac{T_{cool,out} - T_{cryst}}{T_{cool,in} - T_{cryst}} \right)$$

#### Ice and salt crystals

The unwashed ice and MgSO<sub>4</sub>·11H<sub>2</sub>O crystals for after  $5\tau$  residence time are shown in Figure 4.2. Under low heat removal rate with logarithmic temperature difference of 3.8 K, the average crystal sizes of MgSO<sub>4</sub>·11H<sub>2</sub>O and ice were measured to be 130 and 120  $\mu$ m respectively (see Figure 4.2 (a) and (b)). However, under higher heat removal rate with logarithmic temperature difference of 7.5 K, smaller average crystal sizes of 90 and 80  $\mu$ m (for salt and ice respectively) were recorded (see Figure 4.2 (c) and (d)).

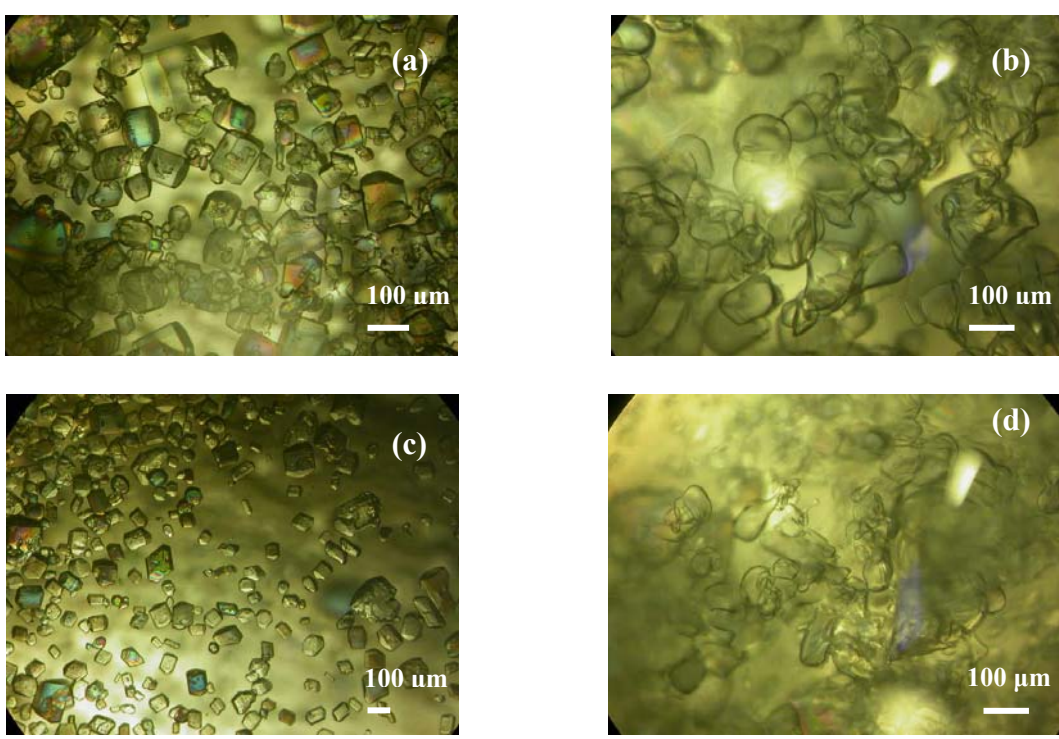


Figure 4.2: Effect of heat removal rate

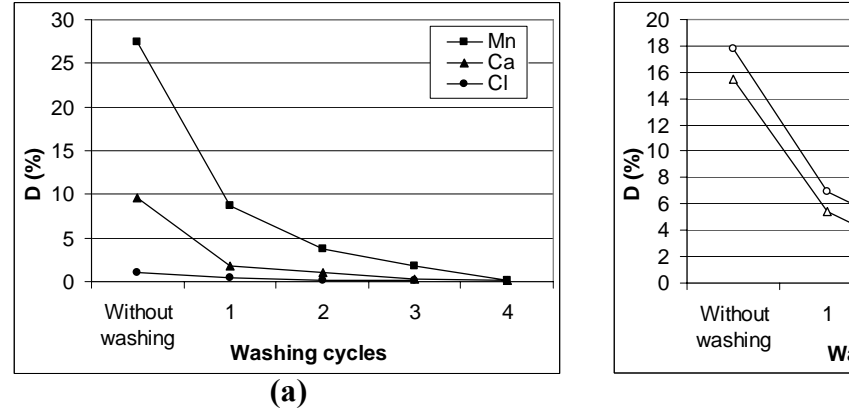
 $MgSO_4\cdot 11H_2O$  crystals under low (a) and high (c) heat removal rates Ice crystals under low (b) and high (d) heat removal rates respectively

The ice crystals are disk shaped with mass based average size between 80 and 120  $\mu$ m. Collecting from the crystallizer, they mainly contain Mg<sup>2+</sup> (3 %-wt) and SO<sub>4</sub><sup>2-</sup> (10-wt%) mother liquor impurity which drops below 50 ppm after washing on the belt filter (filtration of ice on belt filter was also tried) and drops below 10 ppm after four times washing cycle with pure water at 0 °C. The concentration in the ice crystal structure is probably even much lower.

MgSO<sub>4</sub>·11H<sub>2</sub>O crystals are well faceted rectangular shaped with mass based average size between 90 and 130  $\mu$ m. The unwashed salt crystals collected from the crystallizer have as main impurities Ca<sup>2+</sup>, Cl<sup>-</sup> and Mn<sup>2+</sup> ions, in total about 100 ppm, which drops below 10 ppm after the washing step on the belt filter and to below <0.5 ppm after four times washing cycles with pure magnesium sulfate solution prepared at eutectic concentration and precooled to -3 °C.

Solid-solution formation is a frequent occurrence when trying to crystallize apart compounds of similar molecular structure. The closer structurally the wanted and unwanted compounds are, the more likely they are to form a solid-solution. In order to understand solid-solution formation, it is valuable to have a numerical measure of its extent. Molecule 'A' (desired compound) will equilibrate between the crystal phase (C) and the liquor phase (L) according to a partition coefficient, p(A). Likewise molecule 'B' (the impurity) will equilibrate between the crystal and the liquor phase according to another partition coefficient p(B). The ratio of p(A) to p(B) in mole fractions gives a measure of the solid-solution extent 'D' which is short for Distribution [McCauge 2007].





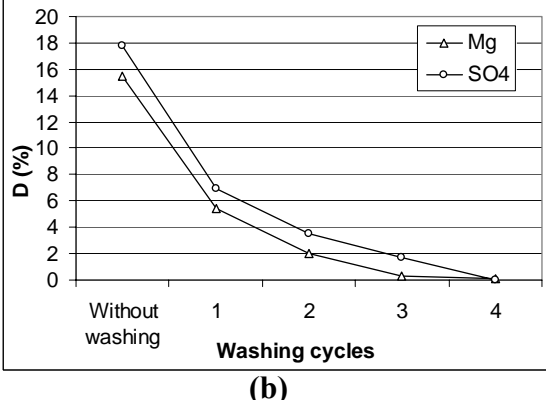


Figure 4.3: Solid-solution extent (D) variation as a function of crystal washing cycles.

(a) MgSO<sub>4</sub>·11H<sub>2</sub>O crystal main impurities: Ca<sup>2+</sup>, Cl<sup>-</sup> and Mn<sup>2+</sup> ions

(b) Ice main impurities: Mg<sup>2+</sup> and SO<sub>4</sub><sup>2-</sup>

Using Equation (4.1), the solid-solution extent of salt and ice crystals are defined as a function of distribution and washing cycles and are presented in Figure 4.3 (a)-(b). The total value of 'D' for MgSO<sub>4</sub>·11H<sub>2</sub>O crystal main impurities (Ca<sup>2+</sup>, Cl<sup>-</sup> and Mn<sup>2+</sup> ions) adds up around 2% (See Figure 4.3a) whereas same value for ice crystal mother liquor impurities of Mg<sup>2+</sup> and SO<sub>4</sub><sup>2-</sup> are around 1% (See Figure 4.3b) after washing the crystals 4 times.

Generally it is desired to have D < 5% for a good resolution and assumed the crystals to have reasonable solid-solution content [McCauge 2007]. The high purities and the great effect of the washing confirm the high selectivity of ice and MgSO<sub>4</sub>·11H<sub>2</sub>O crystals growth under eutectic freeze crystallization.

#### Crystallization Kinetics

Kinetic data (growth and nucleation rates) were estimated with the assumption of an MSMPR (a mixed-suspension, mixed-product removal) crystallizer operated in continuously in steady state [Myerson 2002]. From other research [Himawan 2005] we know that this is not completely true, if only for the influence of the cooled surface on the nucleation of especially ice. This, however, we take into account (see below, step 4).

Moreover, both nucleation in the bulk and near the cooled surface are assumed to be secondary of nature. A visual observation learned that in a clear, undercooled liquid nucleation of ice occurred only when some ice crystals were added, and took place near the scrapers.

We assume that no crystals are present in the feed stream, all crystals are of the same shape, the crystals do not break by attrition and that the crystal growth rate is independent on the crystal size. The relationship between crystal size L, and population density, n (number of crystals per unit size per unit volume of the CDCC) is then directly derived from the population balance shown in Equation 4.2 [Mullin 2001]:

$$n = n_o \exp(-\frac{L}{G\tau}) \tag{4.2}$$

where  $n_o$  (#.m<sup>-4</sup>) is the population density of nuclei (zero-sized crystals) and  $\tau$  is the residence time. A plot of log n versus L gives a straight line of slope  $-(G\tau)^{-1}$  with an intercept at L=0 equal to  $n_o$ . The experimental measurement of crystal size distribution (recorded on a number basis) in the assumed a steady-state MSMPR crystallizer and extrapolation is used to quantify  $n_o$ .

For calculation of growth and nucleation rates briefly the following steps were followed:

- 1. Crystal size distribution (*L*) versus crystal population density in logarithmic scale (*n*) was obtained.
- 2. Slope of the straight line was equal to  $-1/G\tau$  with an intercept at L=0 equal to  $n_o$  (Equation 4.1).
- 3. From the known residence times ( $\tau$ ), the crystal growth rates (G) were calculated.
- 4. Nucleation rate (B) was calculated using growth rate (G) from  $B_{total} = n_o G$ . Nucleation took place both in the bulk and at the walls of the cooling walls. Therefore nucleation rate was defined by using the following equation:  $B_{total} = B_{bulk} + B_{wall}$
- 5. Growth and nucleation rate kinetic parameters were calculated according to the following relations by the following assumptions [Himawan 2005]:
  - a. The growth rates of ice and salt occurred mostly in bulk and modeled with power law kinetics.  $G_{salt}$  was controlled by surface kinetics with spiral growth mechanism, while  $G_{ice}$  was mass transport controlled.
  - b. In the bulk relative supersaturations for salt and ice were defined by  $\sigma_{bulk} = \frac{C_{bulk} C_{eq}}{C_{eq}} \text{ and } \Delta T_{ice} = T_{eq} T_{bulk} \text{ respectively.}$

On the cooling walls the relative supersaturation for salt and ice were defined by

$$\sigma_{wall} = \frac{C_{bulk} - C_{eq,wall}}{C_{eq,wall}} \text{ and } \Delta T_{ice,wall} = T_{eq,wall} - T_{wall} \text{ respectively}.$$

- $C_{eq}$  and  $C_{eq,wall}$  were the equilibrium concentration of MgSO<sub>4</sub>.11H<sub>2</sub>O at  $T_{bulk}$  and  $T_{bulk,wall}$  respectively; whereas  $T_{eq}$  and  $T_{eq,wall}$  were the temperature (freeze depression point of ice) at  $C_{bulk}$  and  $C_{bulk,wall}$  respectively.
- c. From freeze concentration literature, secondary ice nucleation was chosen which was proportional to total crystal surface area  $m_{2,ice}$  and second order of supercooling  $\Delta T_{ice}$  [Evans et al. 1974, Kane et al. 1975, Shirai et al. 1990, Louhi 1996].
- d. The expression for MgSO<sub>4</sub>.11H<sub>2</sub>O secondary nucleation was chosen to the form reported for MgSO<sub>4</sub>.7H<sub>2</sub>O [Bauer et al. 1974, Tai et al. 1975].
- e. The wall nucleation rates were taken to be proportional to the available total cooling surface area per crystallizer volume  $(A_{wall}/V_{cryst})$  and to the salt solid content  $M_{T,salt}$  or ice crystals area  $m_{2,ice}$ , implying the importance of crystals-crystals and crystals-wall collisions in these zones.

In Table 4.2 the kinetic expressions introduced in the model are presented.

**Table 4.2:** Kinetic expressions applied in eutectic freeze crystallization for CDCC-3

Kinetics	Salt	Ice	
Growth rate	$G_{salt} = k_{g,salt} \sigma_{bulk}^2$	$G_{ice} = k_{g,ice} \Delta T_{bulk}$	ms <sup>-1</sup>
Secondary nucleation -bulk-	$B_{salt} = k_{b,salt} M_{T,salt} \sigma_{bulk}^2$	$B_{ice} = k_{b,ice} m_{2,ice} \Delta T_{ice}^2$	#m <sup>-3</sup> s <sup>-1</sup>
Secondary nucleation -wall-	$B_{salt,wall} = k_{b,salt,wall} \left( \frac{A_{wall}}{V_{cryst}} \right) M_{T,salt} \sigma_{wall}^{2}$	$B_{ice,wall} = k_{b,ice,wall} \left( \frac{A_{wall}}{V_{cryst}} \right) m_{2,ice} \Delta T_{wall}^{2}$	#m <sup>-3</sup> s <sup>-1</sup>

The growth rate kinetic parameters  $(k_g)$  for salt and ice crystals were estimated from the Equations given in Table 4.2 and Figure 4.4. It can be seen that the error can be quite high.

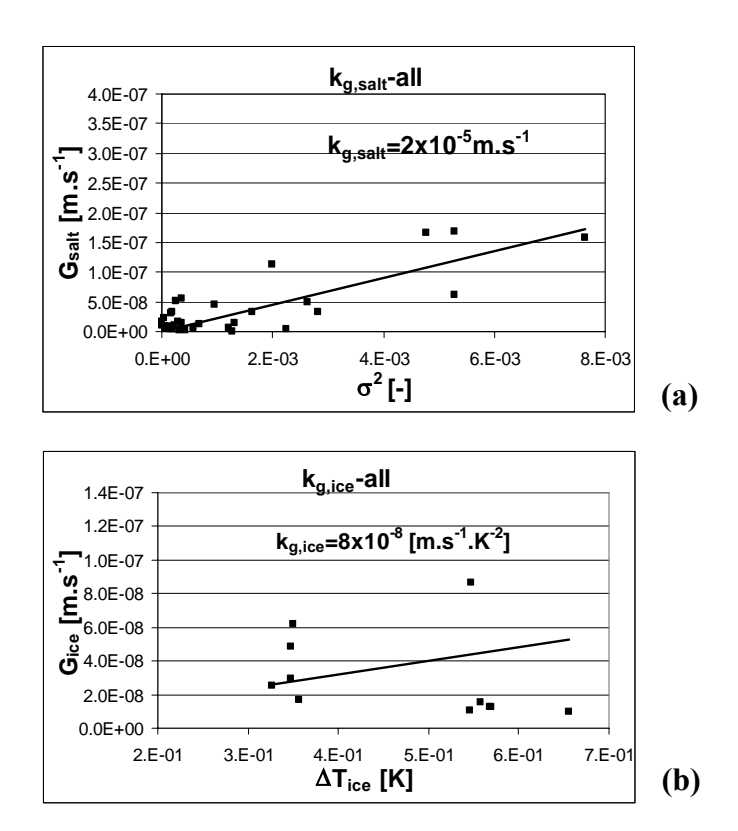


**Figure 4.4:** (a) MgSO<sub>4</sub>·11H<sub>2</sub>O crystals growth rate kinetic parameters (b) Ice growth rate kinetic parameters

The nucleation rate kinetic parameters ( $k_{b,salt-bulk}$ ,  $k_{b,salt-wall}$ ,  $k_{b,ice-bulk}$ ,  $k_{b,ice-wall}$ ) for salt and ice crystals were estimated form the Equations given in Table 4.2 and Figure 4.5.

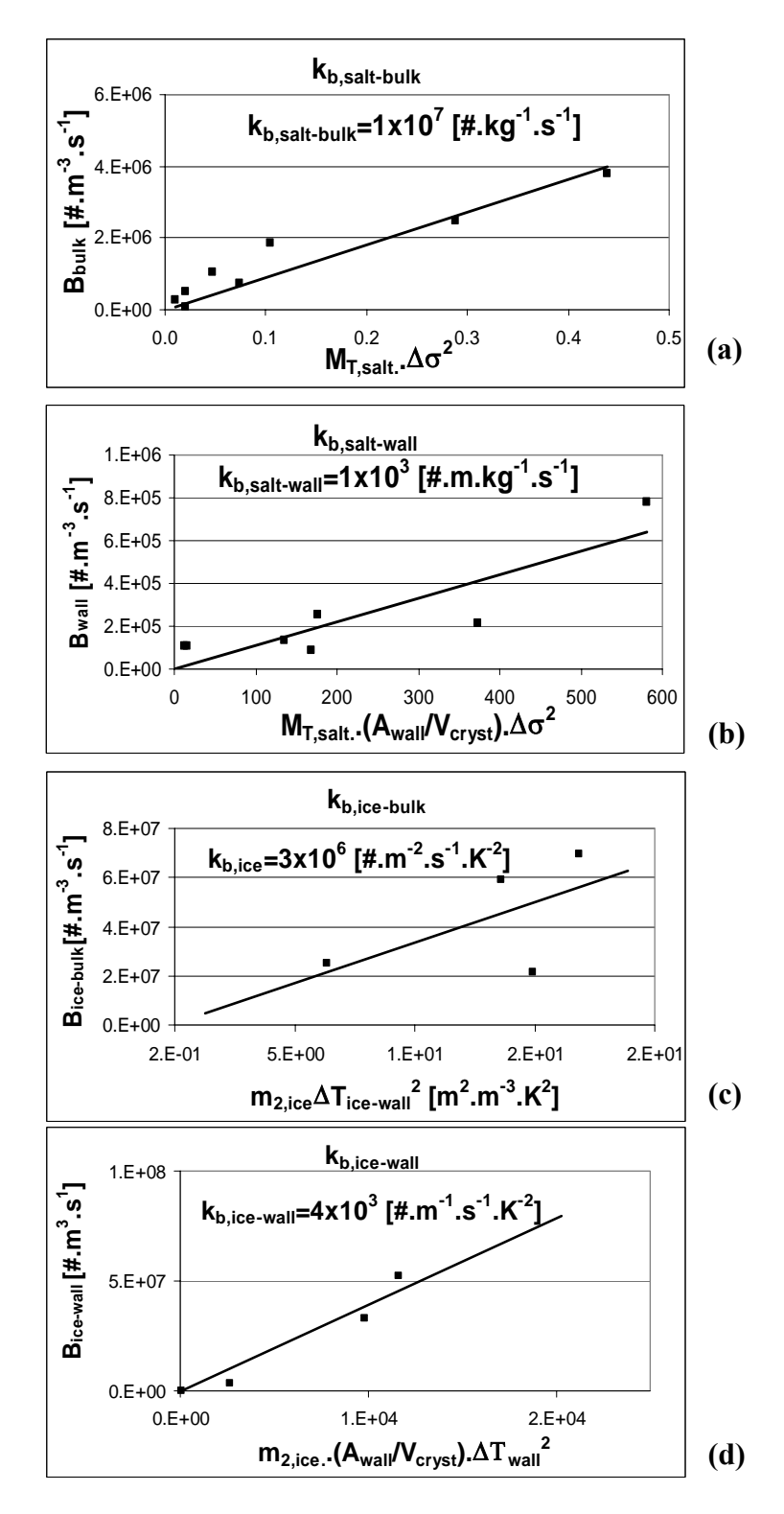


**Figure 4.5:** (a) MgSO<sub>4</sub>·11H<sub>2</sub>O crystals bulk nucleation rate kinetic parameters (b) MgSO<sub>4</sub>·11H<sub>2</sub>O crystals wall nucleation rate kinetic parameters

- (c) Ice crystals bulk nucleation rate kinetic parameters
- (d) Ice crystals wall nucleation rate kinetic parameters

From Figures 4.4 and 4.5 the estimated growth and nucleation kinetic parameters for ice and salt crystals are summarized in Table 4.3. These parameters could be used for simulation studies.

<b>Table 4.3:</b>	Estimated	kinetic	parameters	for	CDCC
-------------------	-----------	---------	------------	-----	------

Parameters	Salt		Ice	
$k_g$	$2 \times 10^{-5}$	[m.s <sup>-1</sup> ]	$8 \times 10^{-8}$	[m.s <sup>-1</sup> .K <sup>-1</sup> ]
$k_b$	1×10 <sup>7</sup>	[#.kg <sup>-1</sup> .s <sup>-1</sup> ]	3×10 <sup>6</sup>	[#.m <sup>-2</sup> .s <sup>-1</sup> .K <sup>-2</sup> ]
$k_{b,wall}$	$1\times10^3$	[#.m.kg <sup>-1</sup> .s <sup>-1</sup> ]	$4\times10^3$	[#.m <sup>-1</sup> .s <sup>-1</sup> .K <sup>-2</sup> ]

Trends of salt and ice *nucleation rates* and *supersaturations* versus *run time* for ice and salt crystallization are given in Figure 4.6. The nucleation rate for salt is dominated by that in the bulk whereas nucleation of ice takes place more at at the wall.

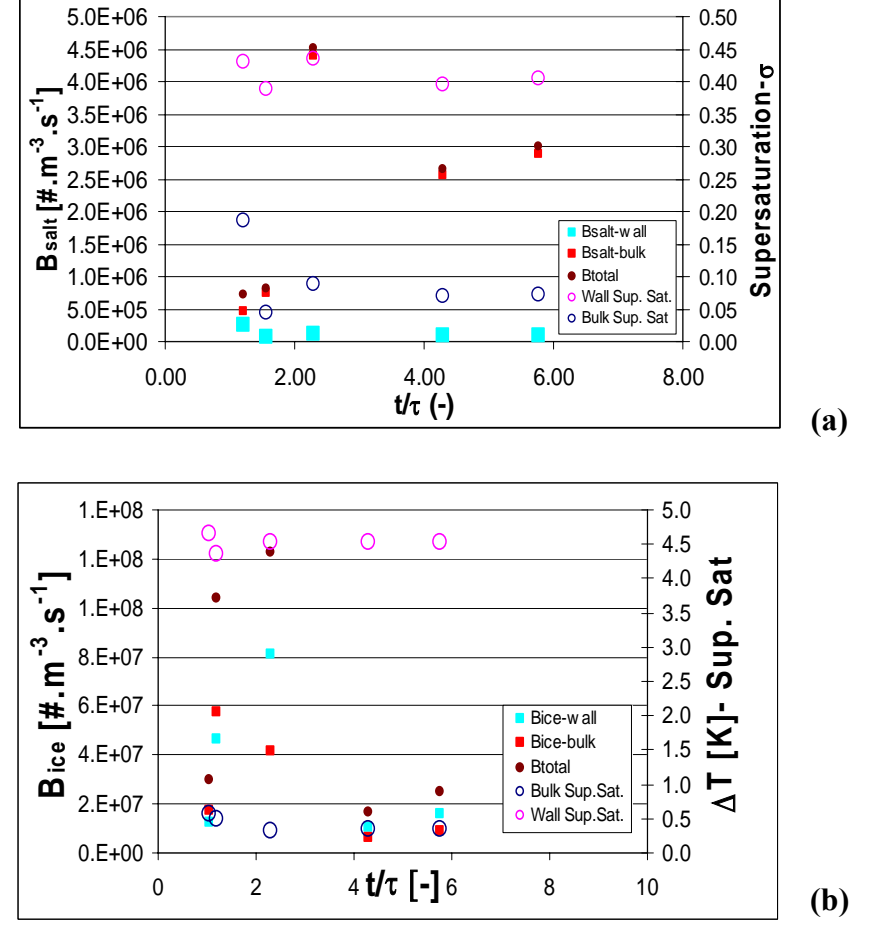


**Figure 4.6:** Trends of ice and salt nucleation rates versus runtime  $(A_{wall}/V_{cryst}=7.7 \text{ m}^2\text{m}^{-3})$ 

Kinetic parameters of ice and MgSO<sub>4</sub>·11H<sub>2</sub>O salt crystallization under Eutectic Freeze Crystallization in CDCC are derived from the data collected under steady state operation conditions at different set temperatures (heat fluxes) and for 30 minutes residence time. The growth rate for ice varied between  $G_{ice}$   $5\times10^{-9}-7\times10^{-8}\,\text{m.s}^{-1}$  within the supersaturation of  $\Delta T_{ice}$  0.05-0.66 °C and salt  $G_{salt}$   $1.3\times10^{-9}-1.3\times10^{-7}\,\text{m.s}^{-1}$  within the supersaturation range of  $\sigma_{bulk}$  0.008-0.08.

The growth rate of ice is lower than in previous studies [Shirai et al. 1990, Louhi-Kultanen 1996] but comparable with that in a SCWC [Himawan 2004]. This might be due to the ice crystals captured inside the compartments around the axis. Similar to Himawan's work,  $G_{salt}$  is of the same magnitude as that in literature [Mershmann 1995] only with a slight lower value due to EFC low operating temperature.

The supersaturations for ice and salt near the wall are much higher than in bulk as shown in Figure 4.6. According to Figure 4.6 (a), the salt effective nucleation rates (i.e. wall plus bulk nucleation rates) are dominated by nucleation in the bulk. On the other hand, the ice effective nucleation rates are dominated by nucleation at the wall (see Figure 4.6 (b)).

The effective nucleation rates vary for  $B_{ice}$  and for  $B_{salt}$  as follows (according to experimental data for different supersaturations):  $3 \cdot 10^7 - 1 \cdot 10^8 \text{ \#.m}^{-3}.\text{s}^{-1}$  and  $8 \cdot 10^5 - 4.5 \cdot 10^6 \text{\#.m}^{-3}.\text{s}^{-1}$  respectively.

#### CONCLUSIONS

The third generation crystallizer for EFC applications (CDCC-3) and the design of the complete mobile skid mounted unit are presented. The practical performance of the CDCC-3 was investigated in terms of heat transfer properties and product quality for MgSO<sub>4</sub> solution. For logarithmic mean temperature difference between bulk and coolant temperatures varying between 3.8 to 7.5 K, the heat fluxes were calculated to change from 2.4 to 3.9 kW/m<sup>2</sup> for 30 minutes residence time. Within these operating conditions, well faceted MgSO<sub>4</sub>·11H<sub>2</sub>O crystals had a mean size of 90-130  $\mu$ m. They contained less than 0.5 ppm of major impurities. The disk-shaped ice crystals having mean sizes of 80-120  $\mu$ m contained 10 ppm Mg<sup>2+</sup> and SO<sub>4</sub><sup>2-</sup> impurity after four times washing. The growth rates (m.s<sup>-1</sup>) of MgSO<sub>4</sub>·11H<sub>2</sub>O and ice were estimated to be  $G_{salt} = 2 \times 10^{-5} \sigma_{bulk}^2$  and  $G_{lce} = 8 \times 10^{-8} \Delta T_{bulk}$  respectively. Both the secondary nucleation rates for ice and salt in the bulk as well as near the cooled surface of the CDCC-3 were calculated form the experimental data. The supersaturations for ice and salt at the wall are much higher than in bulk. The salt nucleation rates were calculated to be dominated by nucleation in the bulk while for the ice the nucleation was dominated by nucleation at the wall.

### REFERENCES

- Bauer et al. 1974 Bauer, L. G.; Larson, M. A.; Dallons, V. J.; Contact Nucleation of MgSO<sub>4</sub>·7H<sub>2</sub>O in a Continuous MSMPR Crystallizer, *Chem. Eng. Sci.* 1974, 29, 1253.
- Evans et al. 1974 Evans, T. W.; Sarofim, A. F.; Margolis, G.; Models of secondary nucleation Attributable to Crystal-Crystallizer and Crystal-Crystal Collisions, A*IChe J.* 1974, 20(5), 959-966.
- Gärtner et al. 2005 Gärtner, R.S.; Genceli, F.E.; Trambitas, D.O.; Witkamp G.J.; Impurity gradients in solution-grown ice and MgSO<sub>4</sub>·12H<sub>2</sub>O crystals measured by cryo-laser ablation and high-resolution-induced-coupled plasma mass spectrograph, *Journal of Crystal Growth*. 2005, 275(1-2), e1773-1778.
- Genceli et al. 2005a Genceli, F. E.; Gärtner, R.; Witkamp, G. J.; Eutectic Freeze Crystallization in a 2<sup>nd</sup> Generation Cooled Disk Column Crystallizer for MgSO<sub>4</sub>-H<sub>2</sub>O System, *Journal of Crystal Growth.* 2005, 275(1-2), e1369-e1372.
- Himawan 2005 Himawan, C.; Characterization and Population Balance Modelling of Eutectic Freeze Crystallization. PhD dissertation, Delft, 2005.
- Kane et al. 1975 Kane, S. G.; Evans, T. W.; Brian, P. L. T.; Sarofim, A. F.; The kinetics of the secondary nucleation of ice: Implications to the operation of continuous crystallizers, *Desalination*. 1975, 17, 3-16.
- Louhi-Kultanen 1996 Louhi-Kultanen, M.; Concentration and purification by crystallization, *Acta Polytechnica Scandinavica, Chemical Technology Series*. 1996, no. 241.
- McCague 2007 McCague, R,; A measure of the solid-solution extent useful for crystallization resolution studies, *Tetrahedron Letters*. 2007, 48, 869-872.
- Mersmann 1995 Mersmann, A.; General prediction of statistically mean growth rates of a crystal collective, *J. Crystal Growth.* 1995, 147, 181.
- Mullin 2001 Mullin, J. W. Crystallization. 4<sup>th</sup> ed., Butterworth-Heinemann, Boston, 2001.
- Myerson 2002 Myerson, A. S.; *Handbook of Industrial Crystallization*. 2<sup>nd</sup> ed., Butterworth-Heinemann, 2002.

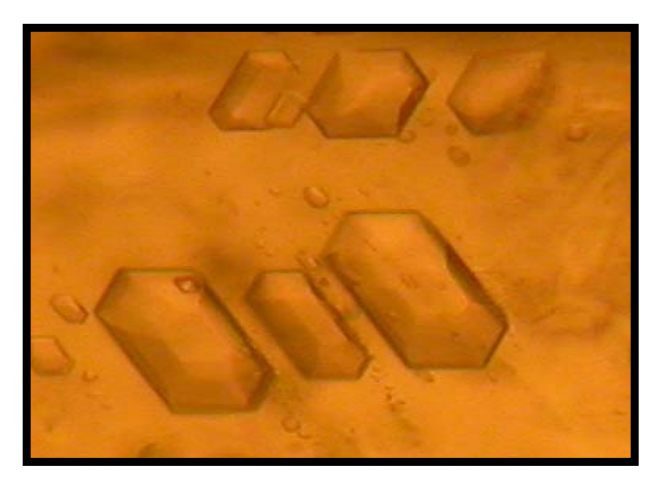
- Shirai et al. 1990 Shirai, Y.; Louhi-Kultanen, M.; Palosaari, S.; Nakanishi, K.; Matsuno, R.; Comments on the prediction of ice crystal size distribution in a continuous crystallizer, *Chem. Eng. Sci.* 1990, 45, 4, 1147.
- Tai et al. 1975 Tai, C. Y.; McCbe, W. L.; Rousseau, R. W.; Contact nucleation of various crystal types, *AIChe J.* 1975, 2(5), 375.
- Vaessen et al. 2002 Vaessen, R. J. C.; Himawan, C.; Witkamp, G. J.; Scale formation of ice from electrolyte solutions on a scraped surface heat exchanger plate, *Journal of Crystal Growth*. 2002, 237-239.
- Vaessen 2003 Vaessen, R. J. C.; *Development of Scraped Eutectic Freeze Crystallizers*. PhD dissertation, Delft, 2003.
- Van der Ham et al. 1999 Van der Ham, F.; Witkamp, G. J.; De Graauw, J.; Rosmalen,
  G. M.; Eutectic Freeze Crystallization Simultaneous Formation and Separation of
  Two Solid Phases, *Journal of Crystal Growth*. 1999, 198/199, 744-748.
- Van der Ham et al. 2003 Van der Ham, F.; Seckler, M. M.; Witkamp, G. J.; Eutectic Freeze Crystallization in a New Apparatus: The Cooled Disk Column Crystallizer, *Chemical Engineering and Processing*. 2003, 43(2), 161-167.

# Chapter 5

# Crystallization and characterization of a new Magnesium Sulfate Hydrate -MgSO<sub>4</sub>·11H<sub>2</sub>O-

## F. Elif Genceli<sup>a</sup>, Martin Lutz<sup>b</sup>, Anthony L. Spek <sup>b</sup>, Geert-Jan Witkamp<sup>a</sup>

Crystal Growth & Design, 2007, 7(12), pp. 2460-2466



<sup>&</sup>lt;sup>a</sup> Process & Energy Department TUDelft, Deft-The Netherlands

<sup>&</sup>lt;sup>b</sup> Crystal and Structural Chemistry, Bijvoet Center for Biomolecular Research, Utrecht- The Netherlands

### **ABSTRACT**

The MgSO<sub>4</sub> crystal hydrate formed below approx. 0 °C was proven to be the undecahydrate, MgSO<sub>4</sub>·11H<sub>2</sub>O -Meridianiite- instead of the reported dodecahydrate MgSO<sub>4</sub>·12H<sub>2</sub>O. The crystals were grown from solution by eutectic freeze and by cooling crystallization. The crystal structure analysis and the molecular arrangement of these crystals were determined using single crystal X-ray diffraction (XRD). Reflections were measured at a temperature of 110(2) K. The structure is triclinic with space group  $P\overline{\ 1}$ (no. 2). The crystal is a colorless block with the following parameters F.W. = 318.55,  $0.54 \times 0.24 \times 0.18 \text{ mm}^3$ , a = 6.72548(7), b = 6.77937(14), c = 17.2898(5) Å,  $\alpha =$ 88.255(1),  $\beta = 89.478(2)$ ,  $\gamma = 62.598(1)^{\circ}$ , V = 699.54(3) Å<sup>3</sup>, Z = 2,  $D_{calc} = 1.512$  g/cm<sup>3</sup>,  $\mu$ = 0.343 mm<sup>-1</sup>. Raman spectroscopy was used for characterizing MgSO<sub>4</sub>·11H<sub>2</sub>O and for comparing the vibrational spectra with MgSO<sub>4</sub>·7H<sub>2</sub>O salt. Between the two salts there are significant differences mainly in the type of interactions of water with sulfate groups in the lattice, in view of the different O-H stretching vibrations, as well as sulfate, O-H...O (sulfate) and O-Mg-O bands vibrational modes. Thermo gravimetric analysis confirmed the stochiometry of the MgSO<sub>4</sub>·11H<sub>2</sub>O salt. Additionally the Miller indices of the major faces of MgSO<sub>4</sub>·11H<sub>2</sub>O crystals were defined.

### **INTRODUCTION**

The MgSO<sub>4</sub>-H<sub>2</sub>O system is not only of industrial interest, but is also a commonly used model system for crystallization investigations. MgSO<sub>4</sub> crystallizes in a large number of different hydrated forms at different working concentrations and temperatures [Gmelin 1958, Baur 1964, Ramalingom et al. 2001, Zalki et al. 1964, Aleksovska et al. 1998]. In this chapter we prove that the magnesium sulfate salt formed at low temperatures is described by the formula MgSO<sub>4</sub>·11H<sub>2</sub>O, the commonly reported MgSO<sub>4</sub>·12H<sub>2</sub>O being incorrect. We also present the synthesis and structure of MgSO<sub>4</sub>·11H<sub>2</sub>O crystals. We have developed the Eutectic Freeze Crystallization (EFC) technique as production method for various salts, including magnesium sulphate from industrial solutions [Himawan et al. 2006, Genceli et al. 2005a]. EFC is a promising technique for processing waste and process streams of mixed aqueous electrolyte/organic solutions, yielding highly pure water and salt. Single crystals synthesized by EFC and cooling crystallization methods were characterized using single crystal X-ray diffraction (XRD).

According to the phase diagram of MgSO<sub>4</sub>-H<sub>2</sub>O system, MgSO<sub>4</sub>·12H<sub>2</sub>O (magnesium sulphate dodecahydrate) is the stable form around the eutectic point (concentration 17.3-21.4 %-w MgSO<sub>4</sub> and temperature between -3.9 to 1.8 °C) [Gmelin 1958, Marion et al. 1999, Pillay et al. 2005, Smith et al. 1928, Meyer et al. 1928, Hogenboom et al. 1995, Chernogorenko 1956].

The low temperature MgSO<sub>4</sub> hydrate crystal form (which we now know to have been MgSO<sub>4</sub>·11H<sub>2</sub>O, the undecahydrate) was discovered by Carl Julius Fritzsche in 1837 [Fritzche 1837]. Observing the crystallization behavior of a magnesium solution left outside in winter, he realized that at temperatures lower than 0 °C, small-whitish-agglomerated or large-transparent crystals occur, which are different from epsomite (MgSO<sub>4</sub>·7H<sub>2</sub>O) crystals. Fritzsche mentioned that those crystals transform into MgSO<sub>4</sub>·7H<sub>2</sub>O at temperatures above 0 °C. For defining the water content of the new magnesium sulphate salt, he dried a single salt first with a blotting paper and then either with flame or air drying in cold weather. From the mass balance he proposed the crystal

has either 12 or 11 water molecules and by repeating the experiments he concluded (erroneously) that the crystals are in the form of MgSO<sub>4</sub>·12H<sub>2</sub>O.

Frederick Cottrell, whose work had been published by Van't Hoff et. al. in 1901, established the eutectic point ice-undecahydrate at -3.9 °C and peritectic undecahydrate-heptahydrate at +1.8 °C [Van't Hoff et al. 1901], reported as data for the dodecahydrate.

Marion et al. estimated the parameters of the Pitzer model and activity data for dodecahydrate using solubility data [Marion et al. 1999]. Pillay et al. improved Marion's model to fit more accurately their recent solubility data of MgSO<sub>4</sub>·12H<sub>2</sub>O [Pillay et al. 2005]. These data need to be recalculated given the new knowledge that it was the undecahydrate. Density and viscosity properties of MgSO<sub>4</sub>·11H<sub>2</sub>O have also been studied [Kargel 1991, Kajiwara et al. 2003].

We used MgSO<sub>4</sub> as a model solution while developing Eutectic Freeze Crystallization technology and initially accepted that the salt produced at eutectic point was MgSO<sub>4</sub>·12H<sub>2</sub>O crystals [Himawan et al. 2005-2006, Genceli et al. 2005a-2005b-2005c]. The effects of the eutectic crystallizer design and the operation conditions on the salt quality considering kinetic relations for the population balance, impurity content, nucleation and growth rates were investigated before [Genceli et al. 2005a, Himawan et al. 2005, Gaertner et al. 2005]. Using eutectic freeze crystallization, combining data of many experiments from industrial waste MgSO<sub>4</sub> solution in continuous scraped cooled wall crystallizers and scraped cooled disk column crystallizer, the nucleation and crystal growth rates of MgSO<sub>4</sub>·11H<sub>2</sub>O salt were found to be  $B = 1 \times 10^7 M_T \sigma^2$  (#m<sup>-3</sup>s<sup>-1</sup>) and  $G = 2.10^{-5} \sigma^2$  (ms<sup>-1</sup>) as a function of supersaturation ( $\sigma$ ) and solid concentration (M<sub>T</sub>) [Genceli et al. 2005a, Himawan et al. 2005]. Similarly in batch scraped crystallizers, the nucleation and crystal growth rates of MgSO<sub>4</sub>·11H<sub>2</sub>O salt were found to be best described as [ Himawan et al. 2005]:

Nucleation rate: 
$$B = (6.5 \pm 5.0).10^7 M_T^{(0.20 \pm 0.06)} \sigma^{(1.7 \pm 0.1)} \quad (\# \text{m}^{-3} \text{s}^{-1})$$
 (5.1)

Growth rate : 
$$G_{salt} = (3.9 \pm 1.7).10^{-6} \sigma^{(1.8 \pm 0.2)}$$
 (ms<sup>-1</sup>)

The second order of the growth rate of Equation 5.2 in supersaturation suggests a spiral growth mechanism.

Considering the lack of MgSO<sub>4</sub>·12H<sub>2</sub>O crystal structure data, we analyzed the salt crystals produced at eutectic freeze or cooling crystallization around the eutectic point by single-crystal XRD. Surprisingly instead of the expected MgSO<sub>4</sub>·12H<sub>2</sub>O a MgSO<sub>4</sub>·11H<sub>2</sub>O crystal structure was found. This discovery implies that MgSO<sub>4</sub>·11H<sub>2</sub>O has mistakenly been denoted as MgSO<sub>4</sub>·12H<sub>2</sub>O, and since 1837, it has been named incorrectly. The purpose of this work was to correct this misconception and investigate properties of MgSO<sub>4</sub>·11H<sub>2</sub>O salt such as crystallization morphology and habit, crystal structure and Raman spectra.

### **EXPERIMENTAL SECTIONS**

### Experimental Setups

Experiments were performed in three different set-ups.

The first setup was a 15 liter, batch type, Scraped Cooled Wall Crystallizer (SCWC) designed for EFC processes. Cooling was achieved by circulating Kryo-85 cooling liquid through a thermostatic unit, Lauda RUK 90 SW. In so doing, the temperature of the cooling liquid was controlled with an accuracy of  $\pm 0.1$ -0.5 °C. The temperature of the MgSO<sub>4</sub> solution was measured using an ASL F250 precision thermometer connected to a PT-100 temperature sensor with an accuracy of  $\pm 0.01$  °C and a resolution of 0.001 °C. More detailed description of the set-up is given elsewhere [Genceli et al. 2005b].

The second setup was 220 liters, continuous type, Cooled Disk Column Crystallizer (CDCC) built in a skid mounted unit designed for EFC applications. Freezium<sup>TM</sup>-60 °C was used as secondary cooling medium in the cooling machine, in the cooling disks, and

in the plate heat exchanger pre-cooler. During continuous EFC operation, salt and ice were sent together with the mother liquid form the CDCC to the settler in which the gravitational separation of ice and salt occurs because of their density differences. From the settler, salt was sent to a Larox-Pannevis reciprocal tray belt filter (0.2 m<sup>2</sup> filtration area) for the separation of crystals from mother liquor. The temperature of the cooling machine was controlled with an accuracy of  $\pm 0.1$ -0.5 °C whereas the temperatures of the MgSO<sub>4</sub> solution, cooling liquid inlets and outlets were measured with PT-100 temperature sensors with an accuracy of  $\pm 0.01$  °C and a resolution of 0.001 °C. The CDCC, cooling machine, settler, plate heat exchanger, belt filter, measuring devices (temperature sensors, flow meters, torque meter), data acquisition and control system are described in more detail elsewhere [Genceli et al. 2005c].

The third setup was 2 liter, batch type, cylindrical jacketed glass vessel located in a climate room. The vessel was equipped with a three-leg scraper to prevent ice and scaling at the wall as to provide mixing. Cooling was achieved by circulating Kryo-51 coolant from a Lauda RK 8 KP bath through the cylinder jacket, with similar accuracies as for the setup described first above. The temperature of the climate room was regulated simultaneously with the crystallizer set temperature.

### **Preparation of Solutions**

18-20 %-w MgSO<sub>4</sub> solutions, prepared with 99.99 %-w MgSO<sub>4</sub>·7H<sub>2</sub>O (J.T. Baker) and ultra pure water of 18.2 m $\Omega$  were used in the first and third experimental setups.

In the second experimental setup, industrial magnesium sulfate solution from ex-flue gas desulphurization was used. It initially contained 17-19 %-w MgSO<sub>4</sub> with the following major impurities in ppm (mg/kg) level: 300±60 ppm Ca, 550±100 ppm K, 70±5 ppm In, 60±10 ppm Na, 60±8 ppm Zn, 50±10 Co, 30±10 ppm Mn, 20±10 ppm Mo, 9±2 ppm B, 4±2 ppm Ni, 25±10 ppm P, 10±5 ppm Pb.

The magnesium sulfate concentrations of the solutions were measured offline using picnometer density measurements with an error of  $\pm 0.15$  %-w. Inductively Coupled

Plasma Atomic Emission Spectrometry (ICP-AES) and Ion Chromatograph were used to measure the cations and anions concentrations in the mother liquor and in the crystals with an error of  $\pm 2.5\%$ .

### Experimental Procedure

Experimental Setups: Unseeded batch crystallization experiments in first and third setups were started stabilizing the solution at 10 °C for two hours. The mixing rate was 80 rpm. A cooling rate of 4 °C/hour was applied until a temperature jump due to exothermic formation of the salt crystals was detected. When crystallization occurred, the coolant temperature was kept constant. After 10-15 minutes, a natural cooling profile was started. Natural cooling profiles were achieved by immediately cooling down the coolant medium to a certain constant temperature and let the crystallizer respond. Every 30 minutes salt samples were collected with a pre-cooled syringe form the bottom outlets of the crystallizer. All salt samples were directly vacuum filtered using a jacket-cooled filter. The data from the temperature sensors were collected every 20 seconds and were recorded with Lab View.

In the second setup, similar to the previous ones, first nucleation was allowed to occur in batch mode by super cooling without seeding. Reaching eutectic conditions, two products -ice and salt crystals- were formed inside the crystallizer. When ice and salt crystals reached to  $\approx 200$  and 250  $\mu m$  mean diameter size, the crystallizer was switched to continuous operation. MgSO4 feed solution was passed through the pre-cooler and fed to the crystallizer. Inside the crystallizer the residence time was varied between 15 minutes to 1 hour, with the coolant set temperature set between -10 to -14 °C. The slurries (ice, salt, and solution at eutectic composition and temperature) leaving the crystallizer were fed to the settler for gravitational separation. From the settler, the bottom flow (salt and solution) was pumped to the belt filter for filtering off the mother liquor. Salt samples from the crystallizer and settling tank were taken into a pre-cooled beaker and immediately vacuum filtered using a jacket-cooled filter. Salt samples from the belt filter were also collected after filtration.

**Picturing and Salt Preserving:** Salt samples from each setup were observed under a Leica WILD M10 stereomicroscope equipped with a Nikon Coolpix 4500 camera.

The salt crystals collected from three different setups were preserved well isolated at -20 °C for the structure determination. As they dissolve above 1.8 °C and recrystallize in to MgSO<sub>4</sub>·7H<sub>2</sub>O (epsomite) form.

*XRD Measurement:* 40989 Reflections were measured at a temperature of 110(2) K up to a resolution of (sin  $\theta/\lambda$ )<sub>max</sub> = 0.90 Å<sup>-1</sup> on a Nonius KappaCCD diffractometer with rotating anode and graphite monochromator ( $\lambda$  = 0.71073 Å). The intensities were obtained with Eval14 [Sheldrick et al. 1997a] using an accurate description of the crystal form and the diffraction geometry. An absorption correction based on multiple measured reflections was applied [Sheldrick et al. 1997b] (0.83-0.94 correction range). 8564 reflections were unique (R<sub>int</sub> = 0.019). The structure was solved with Direct Methods [Duisenberg et al. 2003] and refined with SHELXL-97 [Sheldrick et al. 1999] on F<sup>2</sup> of all reflections. Non-hydrogen atoms were refined freely with anisotropic displacement parameters. All hydrogen atoms were located in the difference Fourier map and refined freely with isotropic displacement parameters. 245 parameters were refined with no restraints. R1/wR2 [I > 2σ(I)]: 0.0222/0.0545. R1/wR2 [all reflections]: 0.0313/0.0577. S = 1.084. The residual electron density is between -0.43 and 0.40 e/Å<sup>3</sup>. Geometry calculations, drawings and checking for higher symmetry were performed with the PLATON package [Spek 2003].

Thermogravimetric Analysis: The Thermogravimetric analysis (TGA) of the crystal was done with a SDT 2960 (TA Instruments) with a temperature accuracy and precision of  $\pm 1$  °C and  $\pm 0.5$  °C respectively and a weight sensitivity of 0.1 µg and weight accuracy of  $\pm 1$  %. TGA was carried out in helium atmosphere (with a purge rate of 100 ml/min) at a heating rate of 5 °C/min. from 27 °C to 300 °C.

Micro Raman Spectroscopy: Raman spectroscopy was applied for characterization of the MgSO<sub>4</sub>·11H<sub>2</sub>O crystals. A Renishaw Ramanscope System 2000, equipped with a 20 mW Ar<sup>+</sup> laser (λ=514 nm) was used to record Raman spectra. A Leica DMLM PL Fluotar L50x/0.55 microscope was used to determine the analyzed surface of the sample. The spectral resolution was ~1 cm<sup>-1</sup> within the range of 100-4000 cm<sup>-1</sup>. To investigate the sample at low temperature preventing recrystallization into MgSO<sub>4</sub>·7H<sub>2</sub>O, MgSO<sub>4</sub>·11H<sub>2</sub>O crystals were kept inside an insulating vessel filled with frozen carbon dioxide prior to the measurements. A Linkam THM600 flow cell was used for the measurement below the freezing point. The cell was precooled by circulating ethylene glycol, which was set at -10 °C and by placing frozen carbon dioxide (dry ice) inside the cell. After substantial pre-cooling of the cell, the sample was placed inside and the spectra were recorded. At ambient temperature, i.e. 20 °C, the spectra of MgSO<sub>4</sub>·7H<sub>2</sub>O crystals were also measured for comparison. Crystals in the range of 100-4000 cm<sup>-1</sup> were analyzed by continuous extended scanning, with a detection time of 100 s.

### **RESULTS AND DISCUSSION**

### The crystals

Salt samples, crystallized using pure and industrial magnesium sulfate solutions, were collected from three different crystallizer setups (running either batch or continuous mode) and from the belt filter. The samples were produced using eutectic freeze or cooling crystallization working near the equilibrium line between E and P as shown in Figure 5.1.

From the photo in Figure 5.2 it can be seen that the crystals are well faceted, which matches with the earlier suggested spiral crystal growth based on Equation 5.2.

All the salt samples either directly filtered from the crystallizer or taken from the belt filter were found to be MgSO<sub>4</sub>·11H<sub>2</sub>O crystals.

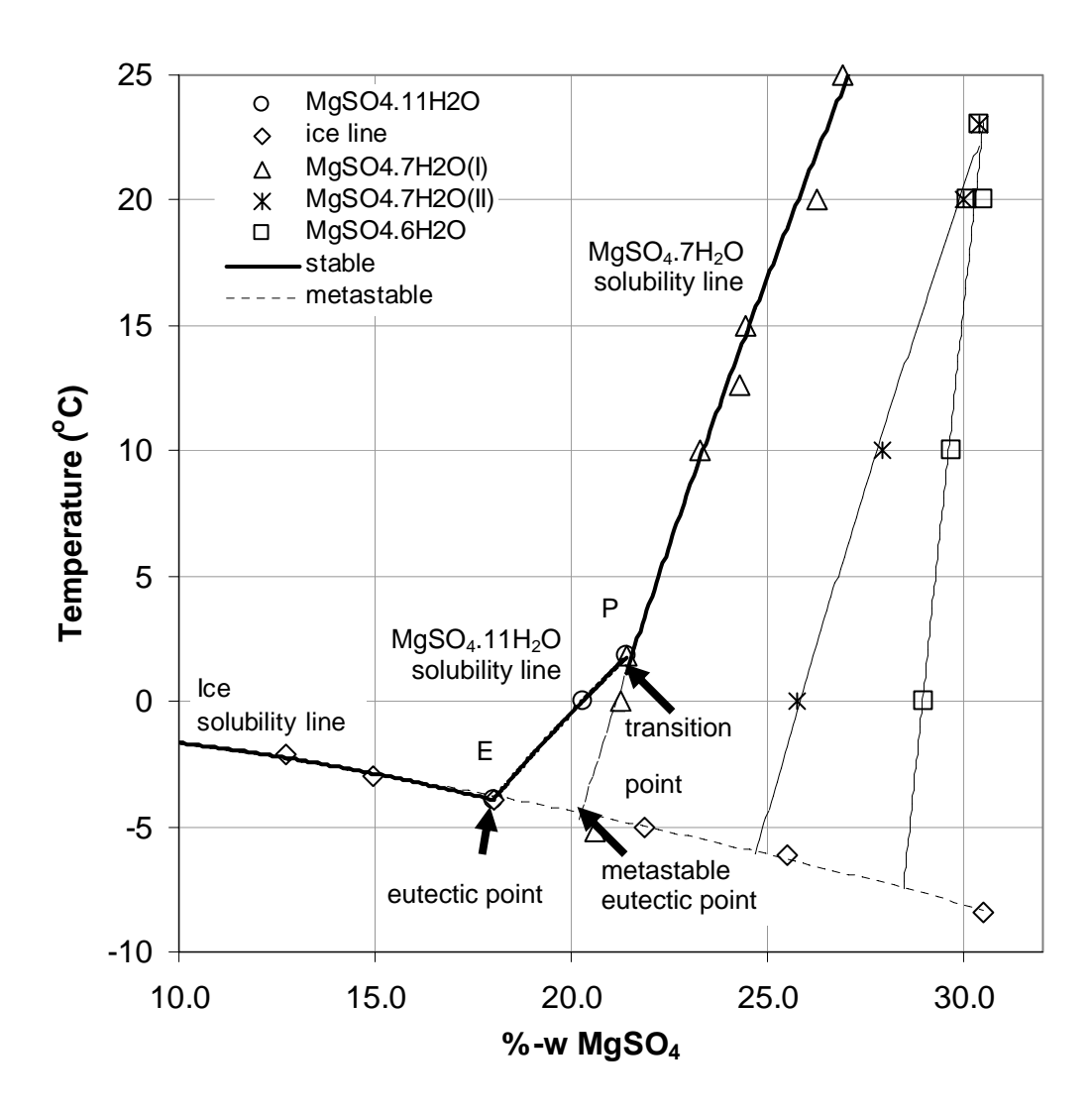


**Figure 5.1:** Phase diagram of the MgSO<sub>4</sub>-H<sub>2</sub>O system. E is the eutectic point and P is the peritectic.

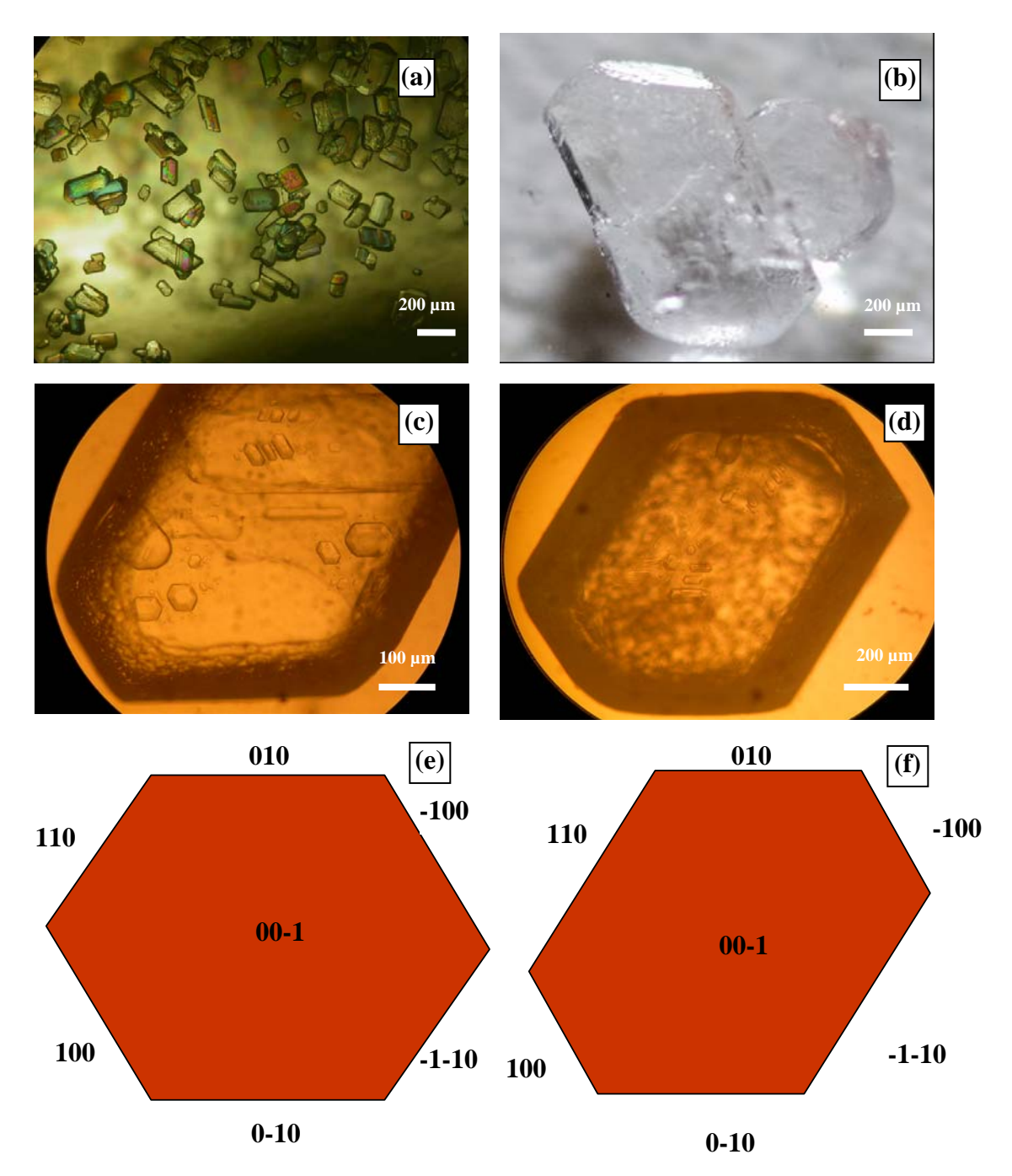


**Figure 5.2:** (a)-(b)-(d) Optical images of MgSO<sub>4</sub>·11H<sub>2</sub>O

- (c) Mother liquor inclusions (negative crystals) in a MgSO<sub>4</sub>·11H<sub>2</sub>O crystal
- (e) The predicted BFDH morphology of MgSO<sub>4</sub>·11H<sub>2</sub>O
- (f) The suggested face indexing of crystal 2d

### XRD Measurements: Crystal Structure Determination

[Mg(H<sub>2</sub>O)<sub>6</sub>](SO<sub>4</sub>)·5H<sub>2</sub>O (MgSO<sub>4</sub>·11H<sub>2</sub>O), Fw = 318.55, colorless block, 0.54 x 0.24 x 0.18 mm<sup>3</sup>, triclinic, P  $\overline{1}$  (no. 2), a = 6.72548(7), b = 6.77937(14), c = 17.2898(5) Å,  $\alpha$  = 88.255(1),  $\beta$  = 89.478(2),  $\gamma$  = 62.598(1)°, V = 699.54(3) Å<sup>3</sup>, Z = 2, D<sub>calc</sub> = 1.512 g/cm<sup>3</sup>,  $\mu$  = 0.343 mm<sup>-1</sup>.

Compound  $[Mg(H_2O)_6](SO_4)\cdot 5H_2O$  crystallizes in the centrosymmetric triclinic space group  $P\overline{1}$ . Two magnesium atoms occupy two independent inversion centres of this space group (Wyckoff positions e and h). Both magnesium atoms are octahedrally surrounded by six coordinated water molecules. Thus the asymmetric unit of the crystal structure contains two half molecules of  $Mg(H_2O)_6$ . Further there are one sulphate molecule and five uncoordinated water molecules in the asymmetric unit. The Mg-O distances are in the range of 2.0383(4) - 2.0701(4) Å, which is in the expected range for hexahydrated magnesium [Bock et al. 1994]. The *cis* angles range from 87.603(17)-92.397(17) °, while all *trans* angles are 180° by inversion symmetry. Consequently the distortions of the two independent octahedrons are very small with RMS-deviations [Pilati et al. 1998] from perfect  $O_b$  symmetry of only 0.0219 and 0.0364, respectively.

The coordinated water molecules differ in their geometries. The angles between the least-squares plane of the water molecules O5, O8, O9, and O10 and the corresponding Mg-O vectors are 6.3, 16.6, 7.0, and 5.7°, respectively, indicating an essentially trigonal coordination mode [McIntyre et al. 1990]. At O6 and O7 these angles are larger with 33.5 and 23.2°, respectively, and the water molecules are thus bent. The reason for this is the intermolecular hydrogen bonding: O6 and O7 are the only coordinated water molecules which are acceptors of hydrogen bonds. The angles between the Mg-O bond and the hydrogen bonded O...H direction are 84.6(3) and 94.2(4) °, respectively.

At the measurement temperature of 110 K the two  $Mg(H_2O)_6$  octahedra differ significantly in their thermal motion. While the octahedron at Mg1 has an R-value of 0.080 [Schomaker et al. 1986] and can be described as a rigid body, the R-value at Mg2 is

0.184 and has thus much more internal freedom. We assume that this is a consequence of the different hydrogen bond pattern of the two octahedra (*vide supra*).

All water molecules act as hydrogen bond donors. Hydrogen bond acceptors are all sulphate oxygens, all uncoordinated water oxygens and the coordinated water oxygens O6 and O7 (*vide supra*). Overall this leads to an infinite, three-dimensional hydrogen bonded network. Sulfate oxygen O1 accepts two hydrogen bonds and has a significantly shorter S-O distance than O2, O3, and O4, which accept three hydrogen bonds, respectively. Each of the uncoordinated water oxygen atoms accept two hydrogen bonds and have thus an essentially tetrahedral environment.

Hydrogen bonding interactions, and selected bond lengths [Å] and bond angles [°] in  $[Mg(H_2O)_6](SO_4)\cdot 5H_2O$  are given in Tables 5.1 and 5.2 respectively. In Figure 5.3, bifurcated hydrogen bond at hydrogen atom H15 is shown. The angle sum at H15 is 357.0(18) ° and the symmetry operation viii is 1-x, 2-y, 1-z. Displacement ellipsoid plot of  $[Mg(H_2O)_6](SO_4)\cdot 5H_2O$ , drawn at the 50% probability level is shown in Figure 5.4. Packing of  $[Mg(H_2O)_6](SO_4)\cdot 5H_2O$  in the crystal is shown in Figure 5.5.

A comparison of the current 11-aqua MgSO<sub>4</sub> crystal structure with the 7-aqua structure (MgSO<sub>4</sub>·7H<sub>2</sub>O, Epsomite) [Calleri et al. 1984, Lutz et al. 2005] shows that they both contain Mg(H<sub>2</sub>O)<sub>6</sub> cations and SO<sub>4</sub> anions. The difference is the number of 5 and 1 non-coordinating H<sub>2</sub>O molecules respectively. This leads to completely different observed hydrogen bonding systems. Nine out of the twelve hydrogen atoms of the 6 molecules that coordinate around Mg are hydrogen bonded to SO<sub>4</sub> for the 7aq structure where this number is only three out of twelve for the 11aq structure. This analysis can be completed with a comparison with the crystal structure of MgSO<sub>4</sub>·6H<sub>2</sub>O [Batsanov 2000] that contains only Mg(H<sub>2</sub>O)<sub>6</sub> cations and SO<sub>4</sub> anions. In this structure 11 out of 12 of the hydrogen bonds are to SO<sub>4</sub>.

**Table 5.1:** Hydrogen bonding interactions in [Mg(H<sub>2</sub>O)<sub>6</sub>](SO<sub>4</sub>)·5H<sub>2</sub>O

D-HA	D-H [Å]	HA [Å]	DA [Å]	D-HA [°]
O5-H1O12	0.815(12)	1.932(12)	2.7416(6)	172.5(12)
O5-H2O13	0.797(13)	1.926(13)	2.7197(6)	174.1(13)
O6-H3O12 <sup>iii</sup>	0.831(12)	1.957(12)	2.7813(6)	171.2(12)
O6-H4O15	0.819(12)	1.904(12)	2.7192(6)	173.3(11)
О7-Н5О14	0.819(12)	1.945(12)	2.7534(6)	169.2(11)
O7-H6O13 <sup>iii</sup>	0.858(13)	1.854(13)	2.7111(6)	178.0(13)
O8-H7O4	0.769(12)	2.082(12)	2.8472(6)	172.9(12)
O8-H8O14 <sup>i</sup>	0.807(12)	2.053(12)	2.8524(6)	170.6(11)
O9-H9O11 <sup>iv</sup>	0.849(12)	1.892(12)	2.7337(6)	170.9(11)
O9-H10O4 <sup>v</sup>	0.823(12)	2.039(12)	2.8469(6)	166.8(11)
O10-H11O11 <sup>ii</sup>	0.869(12)	1.886(12)	2.7520(6)	174.4(11)
O10-H12O4 <sup>vi</sup>	0.785(12)	2.044(12)	2.8139(6)	166.5(11)
O11-H13O2 <sup>iii</sup>	0.865(13)	1.969(13)	2.8188(6)	167.1(12)
O11-H14O1 <sup>vii</sup>	0.856(13)	1.896(13)	2.7502(6)	176.0(12)
O12-H15O6 <sup>viii</sup>	0.803(14)	2.591(14)	3.1748(6)	130.8(12)
O12-H15O7 <sup>viii</sup>	0.803(14)	2.236(14)	2.9692(6)	151.9(13)
O12-H16O3	0.837(12)	1.949(12)	2.7847(6)	175.6(11)
O13-H17O15 <sup>viii</sup>	0.842(13)	1.886(13)	2.7274(6)	178.9(12)
O13-H18O2 <sup>ix</sup>	0.829(13)	1.891(13)	2.7023(5)	165.9(12)
O14-H19O2 <sup>ix</sup>	0.829(13)	1.984(13)	2.8119(6)	176.6(12)
O14-H20O3 <sup>viii</sup>	0.799(12)	2.063(12)	2.8391(6)	163.9(11)
O15-H21O3	0.826(11)	1.941(11)	2.7464(6)	164.6(11)
O15-H22O1 <sup>iii</sup>	0.800(13)	1.891(13)	2.6775(6)	167.2(12)

Symmetry operations: *i*: 1-x, 1-y, 1-z; *ii*: 1-x, 1-y, -z; *iii*: x-1, y, z; *iv*: x+1, y, z; *v*: 2-x, 1-y, -z; *vi*: 1-x, 2-y, -z, *vii*: x-1, y-1, z; *viii*: 1-x, 2-y, 1-z; *ix*: 2-x, 1-y, 1-z.

**Table 5.2:** Selected bond lengths [Å] and bond angles [°] in [Mg(H<sub>2</sub>O)<sub>6</sub>](SO<sub>4</sub>)·5H<sub>2</sub>O

Mg1-O5	2.0383(4)	Mg1-O6	2.0625(4)
Mg1-O7	2.0700(4)	Mg2-O8	2.0701(4)
Mg2-O9	2.0510(4)	Mg2-O10	2.0545(4)
S1-O1	1.4648(4)	S1-O2	1.4827(4)
S1-O3	1.4816(4)	S1-O4	1.4737(4)
O5-Mg1-O6	89.989(18)	O5-Mg1-O7	90.791(18)
O6-Mg1-O7	89.827(17)	O8-Mg2-O9	87.603(17)
O8-Mg2-O10	89.945(18)	O9-Mg2-O10	89.346(17)

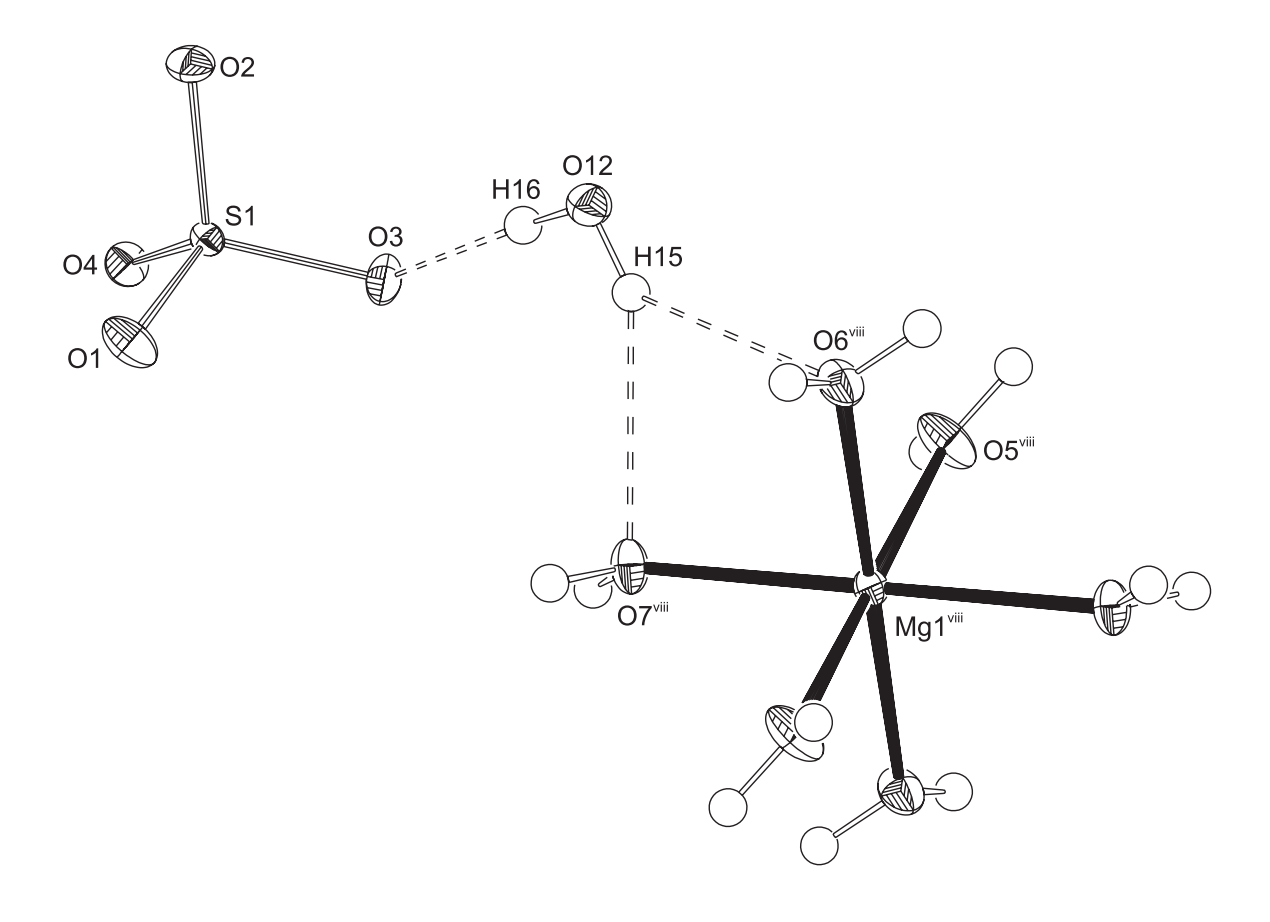


**Figure 5.3:** Bifurcated hydrogen bond at hydrogen atom H15. The angle sum at H15 is 357.0(18) °. Symmetry operation viii: 1-x, 2-y, 1-z.

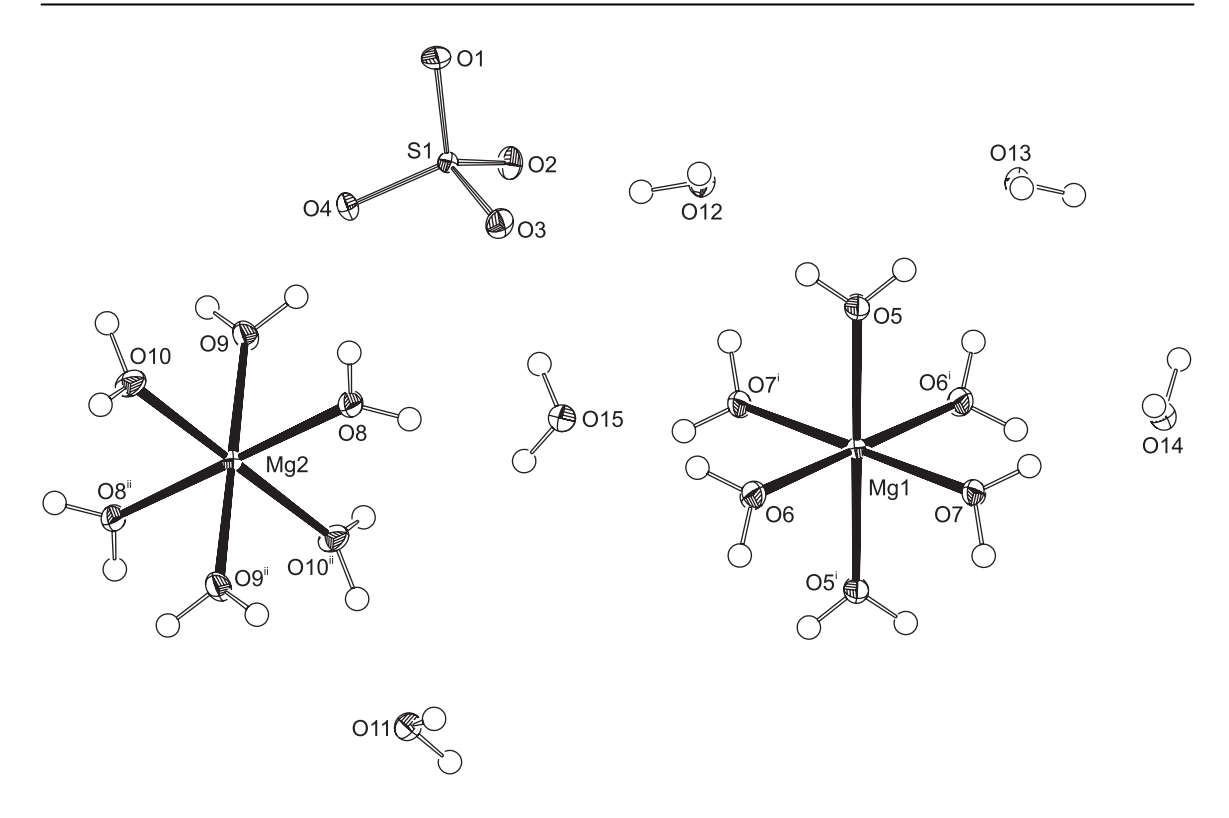


**Figure 5.4:** Displacement ellipsoid plot of  $[Mg(H_2O)_6](SO_4)\cdot 5H_2O$ , drawn at the 50% probability level. Symmetry operations *i*: 1-x, 1-y, 1-z; *ii*: 1-x, 1-y, -z.

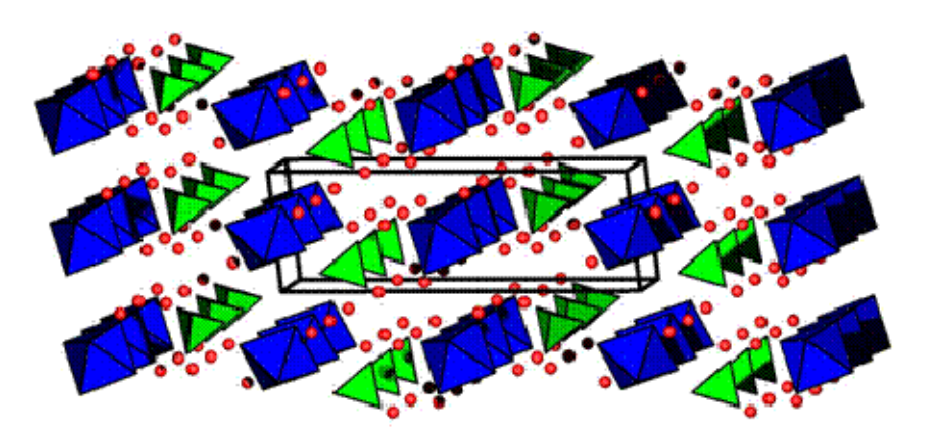


**Figure 5.5:** Packing of [Mg(H<sub>2</sub>O)<sub>6</sub>](SO<sub>4</sub>)·5H<sub>2</sub>O in the crystal. Hydrogen atoms are omitted for clarity. The Mg(H<sub>2</sub>O)<sub>6</sub> octahedra are drawn in blue, the sulfate tetrahedra in green and the uncoordinated water oxygen atoms as red spheres of arbitrary radii.

### Thermal Analysis

The thermogram of MgSO<sub>4</sub>·11H<sub>2</sub>O is illustrated in Figure 4.6. In the TGA trace, there is a broad continuous weight loss till 225  $^{\circ}$ C which belongs to the dehydration step by the elimination of eleven water molecules.

The average relative weight loss of eight samples (typically 25 mg) was  $62.33\% \pm 0.38\%$  which corresponded to the theoretical value of 62.21% within the error limit.

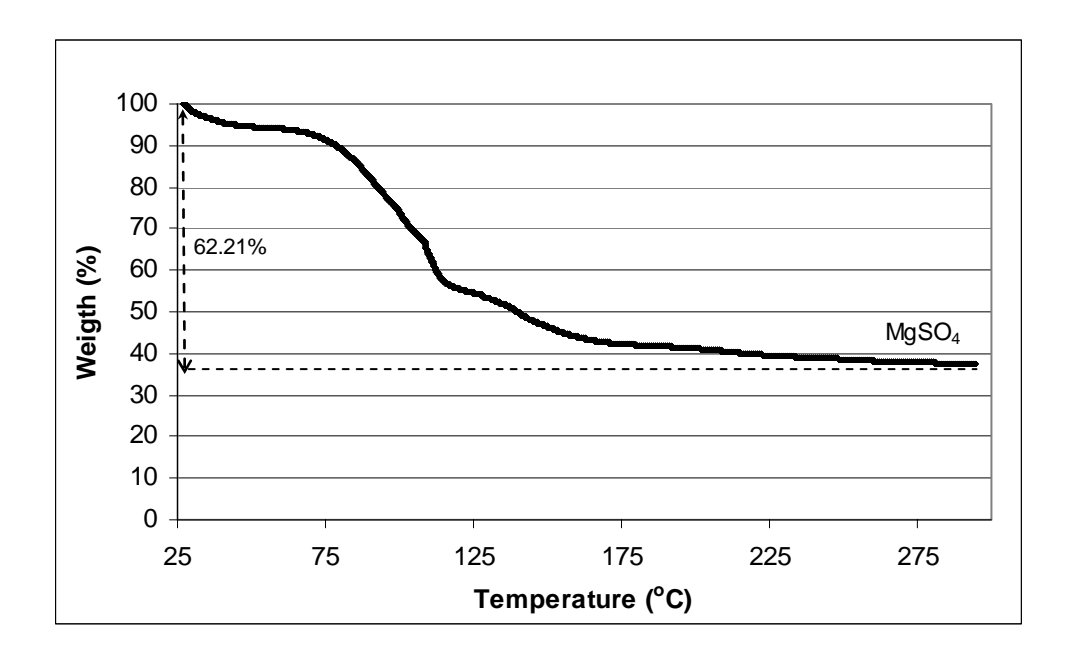


**Figure 5.6:** TGA Curve of MgSO<sub>4</sub>·11H<sub>2</sub>O

### Micro Raman Spectroscopy

The spectra of MgSO<sub>4</sub>·11H<sub>2</sub>O and MgSO<sub>4</sub>·7H<sub>2</sub>O are presented in Figure 5.7. The most significant peak is the SO<sub>4</sub><sup>2-</sup> associated symmetric stretching band at 986 cm<sup>-1</sup> for MgSO<sub>4</sub>·7H<sub>2</sub>O, which is shifted slightly to 990 cm<sup>-1</sup> for MgSO<sub>4</sub>·11H<sub>2</sub>O. MgSO<sub>4</sub>·11H<sub>2</sub>O has additional sulfate modes at 1116 cm<sup>-1</sup> and 1071 cm<sup>-1</sup> [Makreski et al. 2005]. Sulfate related Raman bands for MgSO<sub>4</sub>·7H<sub>2</sub>O has a different Raman pattern with maxima at 1139 cm<sup>-1</sup>, 1101 cm<sup>-1</sup> and 1067 cm<sup>-1</sup>.

For MgSO<sub>4</sub>·11H<sub>2</sub>O, a water bending mode [Makreski et al. 2005] is observed between 409-490 cm<sup>-1</sup> having a maximum at 444 cm<sup>-1</sup> and a sulfate mode between 585-680 cm<sup>-1</sup> with a maximum at 620 cm<sup>-1</sup>. For MgSO<sub>4</sub>·7H<sub>2</sub>O the same bands for water and sulfate can be observed and are located between 418-496 cm<sup>-1</sup> having a maximum at 455 cm<sup>-1</sup> and in the range of 566-668 cm<sup>-1</sup>, having a maximum at 618 cm<sup>-1</sup>, respectively.

Raman bands reported at 379 cm<sup>-1</sup> for Mg-O [Makreski et al. 2005] vibrations of MgSO<sub>4</sub>·7H<sub>2</sub>O are not present in the spectrum of MgSO<sub>4</sub>·11H<sub>2</sub>O in Figure 4.7.

The bands at 255 and 177 cm<sup>-1</sup> for MgSO<sub>4</sub>·7H<sub>2</sub>O are close to the frequency values observed in the literature [Parsk et al. 1966], and have been assigned to O-H...O (sulfate) entities in the crystal structure (255 cm<sup>-1</sup>), and to O-Mg-O deformations, respectively. For MgSO<sub>4</sub>·11H<sub>2</sub>O, the O-H...O (sulfate) vibration is located at lower energies (233 cm<sup>-1</sup>) than given in the literature for MgSO<sub>4</sub>·7H<sub>2</sub>O (255 cm<sup>-1</sup>), most likely due to the presence of additional lattice water. On the contrary, the corresponding O-Mg-O band for MgSO<sub>4</sub>·11H<sub>2</sub>O seems to be shifted to a higher wave number, i.e. 190 cm<sup>-1</sup>.

The stretching modes of water incorporated in the lattice are located in the 2900-3700 cm<sup>-1</sup> region. For MgSO<sub>4</sub>·11H<sub>2</sub>O, there seems to be one dominant band having a maximum at 3395 cm<sup>-1</sup>, with potential shoulders at 3520, 3300 and 3150 cm<sup>-1</sup>. For MgSO<sub>4</sub>·7H<sub>2</sub>O, two bands are resolved at 3427 cm<sup>-1</sup> and 3325 cm<sup>-1</sup>, including a shoulder at 3212 cm<sup>-1</sup>. The bands located at 1669 cm<sup>-1</sup> for MgSO<sub>4</sub>·11H<sub>2</sub>O and at 1678 cm<sup>-1</sup> for MgSO<sub>4</sub>·7H<sub>2</sub>O, respectively, can be assigned to bending modes of intracrystalline water [Socrates et al. 2001].

Summarizing, by comparing the vibrational spectra of the MgSO<sub>4</sub>·11H<sub>2</sub>O and MgSO<sub>4</sub>·7H<sub>2</sub>O salts, it can be concluded that significant differences exist in the type of interactions of water with sulfate groups in the lattice, in view of the different O-H stretching vibrations, as well as sulfate, O-H...O (sulfate) and O-Mg-O bands vibrational modes.

It should be noted that the Raman spectrum of MgSO<sub>4</sub>·11H<sub>2</sub>O is very similar to the spectra of a salt found as inclusions denoted as MgSO<sub>4</sub>·12H<sub>2</sub>O but presumably the undecahydrate form in Holocene ice cores from Dome Fuji-East Antarctica [Ohno et al. 2005]. The strongest SO<sub>4</sub><sup>2-</sup> band is in both cases located at 989 cm<sup>-1</sup> (symmetrical stretching mode), including the weaker modes maximizing at 1117 cm<sup>-1</sup> and 1071 cm<sup>-1</sup>. This suggests that micro inclusions of MgSO<sub>4</sub> salt preserved inside ice core at low temperature to some extent contain MgSO<sub>4</sub>·11H<sub>2</sub>O salt.

Natural occurrence of MgSO<sub>4</sub>·11H<sub>2</sub>O crystals has been found in sea ice inclusions from Saroma Lake-Japan, recognized as a valid mineral by International Mineralogical Association (IMA) Commission and named "Meridianiite". The existence of Meridianiite mineral in sea ice has been proven by showing the excellent Micro Raman Spectra vibrational harmony between the synthetic MgSO<sub>4</sub>·11H<sub>2</sub>O and the inclusions in the sea ice sample [Genceli et al. 2008].

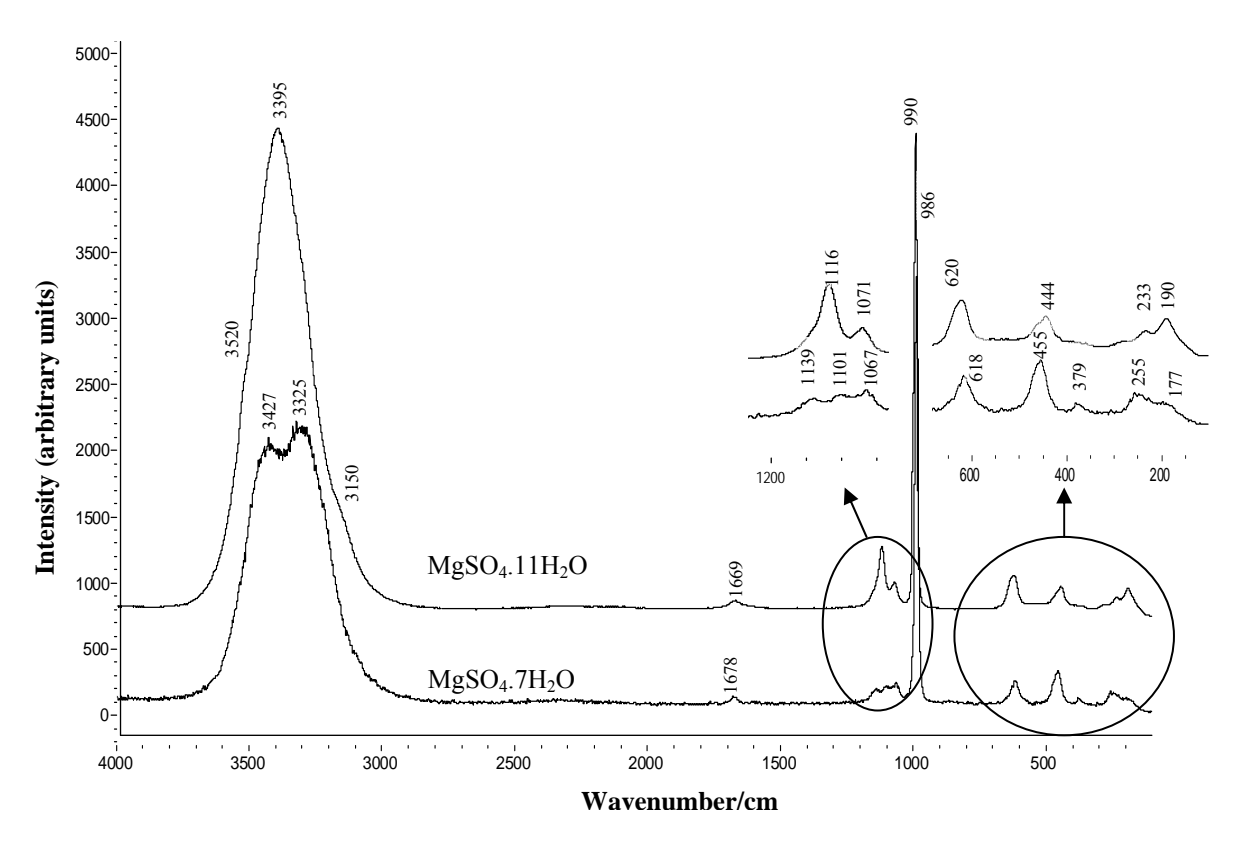


**Figure 5.7:** Raman Spectra of MgSO<sub>4</sub>·11H<sub>2</sub>O and MgSO<sub>4</sub>·7H<sub>2</sub>O Crystals

### Molecular Modelling

On the basis of XRD data, single crystal structure and cell parameters were determined. The morphology module of Cerius<sup>2</sup> v.3.9 (Accelys) was used to determine the BFDH morphology [Eerden et al. 1995] (in vacuum) shown in Figure 5.2e. Measuring the angles between the faces in the crystals, a suggestion for face indexing of the experimental morphology in Figure 5.2d is given in Figure 5.2f. The experimental (5.2d, 5.2f) 110 and 110 faces grow slightly slower than 010 and 010, probably due to solvent effects. The 001 face is dominant both in the BFDH and experimental morphology.

### **Inclusions**

Small pockets of mother liquor (inclusions) are visible in the interior of the crystal in Figure 5.1c. Inclusions develop during the course of crystal growth [Mullin 2001]. These inclusions show as negative crystals (mother liquor inclusions bounded by the crystal faces of that crystal) which have a similar morphology as the MgSO<sub>4</sub>·11H<sub>2</sub>O crystal. Under isothermal conditions inclusion may change shape or unite as the internal system adjusts itself towards the condition of minimum surface energy [Denbig et al. 1966]. It is proposed that the large inclusions (negative crystals) result from the formation of liquid parent inclusions and the subsequent inward growth and coalescence during long storage of the crystals [Hu et al. 1996]. The inclusions vary in size from 50-200 μm.

### **CONCLUSION**

This chapter corrects the misconception in literature for MgSO<sub>4</sub>·11H<sub>2</sub>O crystals mistakenly labeled MgSO<sub>4</sub>·12H<sub>2</sub>O by Fritzsche in 1837. [Mg(H<sub>2</sub>O)<sub>6</sub>](SO<sub>4</sub>)·5H<sub>2</sub>O (MgSO<sub>4</sub>·11H<sub>2</sub>O), was grown from magnesium sulfate solution by eutectic freezing and by cooling crystallization around eutectic conditions. Single crystal XRD studies were carried out at a temperature of 110(2) K and crystal structure *-triclinic with space group*  $P\overline{I}$  (no. 2)- and cell parameters -a = 6.72548(7), b = 6.77937(14), c = 17.2898(5) Å,  $\alpha = 88.255(1)$ ,  $\beta = 89.478(2)$ ,  $\gamma = 62.598(1)$ °, V = 699.54(3) Å<sup>3</sup>, Z = 2- were calculated. Thermo gravimetric analysis, proved the stochiometry of the MgSO<sub>4</sub>·11H<sub>2</sub>O salt. The

corrected phase diagram of MgSO<sub>4</sub> for the range 17.3-21.4 %-w MgSO<sub>4</sub> and temperature -3.9-+1.8 °C is given. The Raman spectrum of MgSO<sub>4</sub>·11H<sub>2</sub>O showed significant differences with that of MgSO<sub>4</sub>·7H<sub>2</sub>O. The natural occurrence of MgSO<sub>4</sub>·11H<sub>2</sub>O in sea ice inclusions from Saroma Lake-Japan, its recognition by IMA as a mineral and its name -Meridianiite- has been announced. The Miller indices of MgSO<sub>4</sub>·11H<sub>2</sub>O crystals are also presented. Negative crystals, formed in inclusions, exhibited the same morphology.

### **ACKNOWLEDGMENT**

This work was supported by the EET (Energy, Ecology and Technology) program of the Ministries of Economic Affairs, VROM, O&W and Kemira, Nedmag, Larox-Pannevis, TNO, DSM and was also supported (M.L., A.L.S.) by the Council for Chemical Sciences of the Netherlands Organization for Scientific Research (CW-NWO). We would also like to thank Dr. Joop Ter Horst for morphology prediction, Hirokazu Shibata and Dr. Guido Mul for Raman Spectroscopy and Duco Bosma for TGA measurements.

### SUPPORTING INFORMATION AVAILABLE

Crystallographic files in CIF format is available free of charge via the Internet at http://pubs.acs.org.

### REFERENCES

- Aleksovska et al. 1998 Aleksovska, S.; Petrusevski, V. M.; Soptrajanov, B.; *Acta Cryst.* 1998, B54, 564-567.
- Batsanov 2000 Batsanov, A. S.; *Acta Cryst.* 2000, C56, e230-e231.
- Baur, W. H.; Acta Cryst. 1964, 17, 1361-1369.
- Bock et al.1994 Bock, C.W.; Kaufman, A.; Glusker, J.P.; *Inorg. Chem.* 1994, 33, 419-427.
- Calleri et al. 1984 Calleri, M.; Gavetti, G.; Ivaldi, G.; Rubbo. M; *Acta Cryst*. 1984, B40, 218-222.
- Chernogorenko 1956 Chernogorenko, V. B.; *Zhurnal Neorganicheskoi Khimii.* 1956, Vol. I, No.2, 317-322.
- Denbigh et al. 1966 Denbigh, K. G.; White, E. T.; *Chemical Engineering Science*. 1966, 21, 739-754.
- Duisenberg et al. 2003 Duisenberg, A. J. M.; Kroon-Batenburg, L. M. J.; Schreurs, A. M. M.; *J. Appl. Cryst.* 2003, 36, 220–229.
- Eerden et al. 1995 Van der Eerden, J.P.; Bruinsma O. S. L.; Science and Technology of Crystal Growth. Kluwer Academic Publishers, 1995.
- Fritzche 1837 Fritzche, C. J.; Ueber eine neue Verbindung der schwefelsauren Talkerde mit wasser. Annalen der Physik und Chemie. *Poggendorff's Annalen*. 1837, 42, 577-580.
- Genceli et al. 2005a Genceli, F. E.; Gaertner, R. S.; Witkamp, G. J.; *J. Crystal Growth.* 2005, 275(1-2), e1369-e1372.
- Genceli et al. 2005b Genceli, F. E.; Himawan, C.; Witkamp, G. J.; *J. Crystal Growth.* 2005, 275(1-2), e1757-e1762.
- Genceli et al. 2005c Genceli, F.E.; Trambitas, D.O.; Gärtner, R.S.; Rodriguez, M.; Witkamp, G.J.; VDI Berichte (1901 II). 2005, 855-860.
- Genceli et al. 2008 Genceli, F. E.; Horikawa, S.; Iizuka, Y.; Sakurai, T.; Hondoh, T.; Kawamura, T.; Witkamp, G. J.; *Journal of Glaciology* (submitted).
- Gmelin 1958 Gmelin; *Gmelins Handbuch der Anorganischen Chemie*. Verlag Chemie, Weinheim, 1958.

- Himawan et al. 2005 Himawan, C.; *Characterization and Population Balance Modelling of Eutectic Freeze Crystallization*. PhD Dissertation, Delft University of Technology, The Netherlands, 2005.
- Himawan et al. 2006 Himawan, C.; Kramer, H. J. M.; Witkamp, G. J.; *Sep. Pur. Tech.* 2006, 50, 240-248.
- Hogenboom et al. 1995 Hogenboom, D. L.; Kargel, J. S.; Ganasan, J. P.; Lee, L.; *Icarus*. 1995, 115, 258-277.
- Hu et al. 1996 Hu, X. B.; Jiang, S. S.; Huang, X. R.; Zeng, W.; Lui, W. J.; Chen, C. T.; Zhoa, Q. L.; Jiang, J. H.; Wang, Y. L.; Tian, Y. L.; Han, Y. J.; *Crystal Growth.* 1996, 163, 266-271.
- Kajiwara et al. 2003 Kajiwara, K.; Yabe, K.; Hashitani, T.; *CryoLetters*. 2003, 24, 143-148.
- Kargel 1991 Kargel, J. S.; *Icarus*. 1991, 94, 368-390.
- Lutz et al. 2005 Lutz, M.; Spek, A. L.; *Private Communication*. 2005.
- Makreski et al. 2005 Makreski, P.; Jovanovski, G.; Dimitrovska, S.; *Vibrational Spectroscopy*. 2005, 39, 229-239.
- Marion et al. 1999 Marion, G. M.; Farren, R. E.; *Geochim. Cosmochim. Acta.* 1999, 63(9), 1305-1318.
- McIntyre et al. 1990 McIntyre, G. J.; Ptasiewicz-Bak, H.; Olovsson, I.; *Acta Cryst*. 1990, B46, 27-39.
- Meyer et al. 1928 Meyer, J.; Aulich, W.; *Zeitschrift für Anorganische Chemie*. 1928, 127, 329.
- Mullin 2001 Mullin J. W.; Crystallization- 4<sup>th</sup> Ed. Elsevier, 2001.
- Ohno et al. 2005 Ohno, H.; Igarashi, M.; Hondoh, T.; *Earth and Planetary Science Letters*. 2005, 232, 171-178.
- Parsk et al. 1966 Parsk, H. J.; Boutin, H.; *Journal of Chemical Physics*. 1966, 45, 3284.
- Pilati et al. 1998 Pilati, T.; Forni, A.; *J. Appl. Cryst.* 1998, 31, 503-504.
- Pillay et al. 2005 Pillay, V.; Gaertner, R. S.; Himawan, C.; Seckler, M. M.; Lewis, A. E.; Witkamp, G. J.; *J. Chem. Eng. Data.* 2005, 50(2), 551-555.

- Ramalingom et al. 2001 Ramalingom, S.; Podder, J.; Narayana Kalkura, S.; *Cryst. Res. Technol.* 2001, 36(12), 1357-1364.
- Schomaker et al. 1986 Schomaker, V.; Trueblood, K. N.; *Acta Cryst.* 1986, B24, 63-76.
- Sheldrick et al. 1997a Sheldrick, G.; M. SHELXS-97: Program for Crystal Structure Solution. Universität Göttingen, Germany, 1997.
- Sheldrick et al. 1997b Sheldrick, G. M.; *SHELXL-97: Program for Crystal Structure Refinement*. Universität Göttingen, Germany, 1997.
- Sheldrick et al.1999 Sheldrick, G.; M. SADABS: Area-Detector Absorption Correction, v2. 10. Universität Göttingen, Germany, 1999.
- Smith et al. 1928 Smits, A.; Rinse, J.; Koymans, L. H.; Zeitschrift für Physikalische Chemie. Abt. A. Chem. 1928, 135, 78-84.
- Socrates et al. 2001 Socrates, G.; *Infrared and Raman Characteristic Group Frequencies-Tables and Charts*. John Wiley & Sons, 3<sup>rd</sup> edition, 2001.
- Spek 2003 Spek, A. L.; J. Appl. Cryst. 2003, 36, 7-13.
- Van't Hoff et al. 1901 Van't Hoff, J. H.; Meyerhoffer, W.; Smith, N. Sitzungsberichte der Königlich Preussischen Akadem. 1901, 1034-1044.
- Zalki et al. 1964 Zalkin, A.; Ruben, H.; Templeton, D. H.; *Acta Cryst.* 1964, 17, 235-240.

# Meridianiite: Detected In Ice

F. Elif Genceli<sup>a</sup> , Shinichirou Horikawa<sup>b</sup> , Yoshinori Iizuka<sup>b</sup> , Toshimitsu Sakurai<sup>b</sup> , Takeo Hondoh<sup>b</sup> , Toshiyuki Kawamura<sup>b</sup> , Geert-Jan Witkamp<sup>a</sup>

Submitted for publication to Journal of Glaciology



<sup>&</sup>lt;sup>a</sup> Process & Energy Department TUDelft, Deft-The Netherlands

<sup>&</sup>lt;sup>b</sup> Institute of Low Temperature Science, Hokkaido University, Sapporo-Japan Crystal Growth & Design

### **ABSTRACT**

Inclusions affect the behaviour of ice, and their characterization helps to understand the formation history of the ice. Recently the low temperature magnesium sulfate salt was found to have the formula MgSO<sub>4</sub>·11H<sub>2</sub>O [Genceli et al. 2007, Peterson et al. 2006]. This paper describes the discovery of the natural occurrence of the MgSO<sub>4</sub>·11H<sub>2</sub>O new mineral -Meridianiite- as salt inclusions in sea ice from Saroma Lake-Japan and in Antarctic ice. Existence of meridianiite was confirmed using Micro Raman spectroscopy technique by comparing and presenting the excellent harmony between the Raman spectra of synthetic MgSO<sub>4</sub>·11H<sub>2</sub>O and the inclusions. Epsomite and mirabilite Raman Spectra are also presented to be compared with the one of meridianiite. Both sea ice and Antarctic ice meridianiite inclusions have similar morphology with the synthetic MgSO<sub>4</sub>·11H<sub>2</sub>O crystals. Meridianiite stability strongly depends on temperature, atmospheric conditions and is sensitive to the relative humidity of the environment. Dehydration to lower hydration levels occurs in the presence of non-ideal cases for meridianiite.

### INTRODUCTION

Seasonal sea ice strongly modulates global climate and ecology through its insulating and sea composition regulation effect. Small changes in atmosphere/ocean/ice composition ratio may lead to significant changes in the nature of the sea ice cover and the ecological life. Minerals detected in sea ice as inclusions would introduce one more parameter to understand the ecological and global climatic balance.

On the other hand the presence of minerals in Antarctic ice would provide significant information on the past atmospheric composition. The snowfall composition buried over time contains the records of the history in ice which could successfully be used in climate and environmental studies [Kotlyakov et al. 2004, Kekonen et al. 2005].

This work demonstrates the occurrence of inclusions of the recently discovered mineral – Meridianiite- in sea ice and Antarctic ice.

The MgSO<sub>4</sub>·11H<sub>2</sub>O crystal structure was recently solved as triclinic with space group  $P \ \overline{1}$  (no. 2). MgSO<sub>4</sub>·11H<sub>2</sub>O was previously described as MgSO<sub>4</sub>·12H<sub>2</sub>O by Fritzsche in 1837 (Fritzsche, 1837). Via dehydration by weight loss, Fritzsche tried to estimate the water content of the salt, which led to an error by one water molecule. MgSO<sub>4</sub>·11H<sub>2</sub>O crystal is a colorless needle with the following parameters F.W.=318.55, 0.54×0.24×0.18 mm<sup>3</sup>, a = 6.72548(7), b = 6.77937(14), c = 17.2898(5) Å,  $\alpha$  = 88.255(1),  $\beta$  = 89.478(2),  $\gamma$  = 62.598(1)°, V=699.54(3) Å<sup>3</sup>, Z = 2,  $D_{calc}$  = 1.512 g/cm<sup>3</sup>,  $\mu$  = 0.343 mm<sup>-1</sup> [Genceli et al. 2007].

On Earth, Epsomite (MgSO<sub>4</sub>·7H<sub>2</sub>O) is present in many places like crusts and efflorescences in coal or metal mines, limestone caves, in the oxidized zones of sulfide ore deposits and in salt lakes and playas. According to the phase diagram of the MgSO<sub>4</sub>·H<sub>2</sub>O aqueous system under atmospheric pressure presented in Figure 6.1, MgSO<sub>4</sub>·11H<sub>2</sub>O is stable around its eutectic point: concentration between 17.3-21.4 wt% MgSO<sub>4</sub> and temperature between -3.9 to 1.8 °C. In nature MgSO<sub>4</sub>·11H<sub>2</sub>O formation likely occurs

around eutectic conditions where supersaturation with respect to temperature and concentration is achieved. If the temperature of the epsomite reservoir goes below 1.8 °C, meridianiite formation occurs instead of epsomite.

Previously Antarctic ice impurities were checked using SEM/EDS method [Baker et al. 2003, Barnes et al. 2004]. Later Ohno et. al. used Micro Raman Spectroscopy to examine micro-inclusions in polar ice form Dome Fuji to determine the salt composition. It was found that the inclusions were mainly sulfate salts with small amount of other soluble salts and insoluble dust [Ohno et al. 2005, Ohno et al. 2006].

To identify the chemical composition in sea ice and Antarctic ice inclusions, SEM/EDS method and Micro Raman spectroscopy were used.

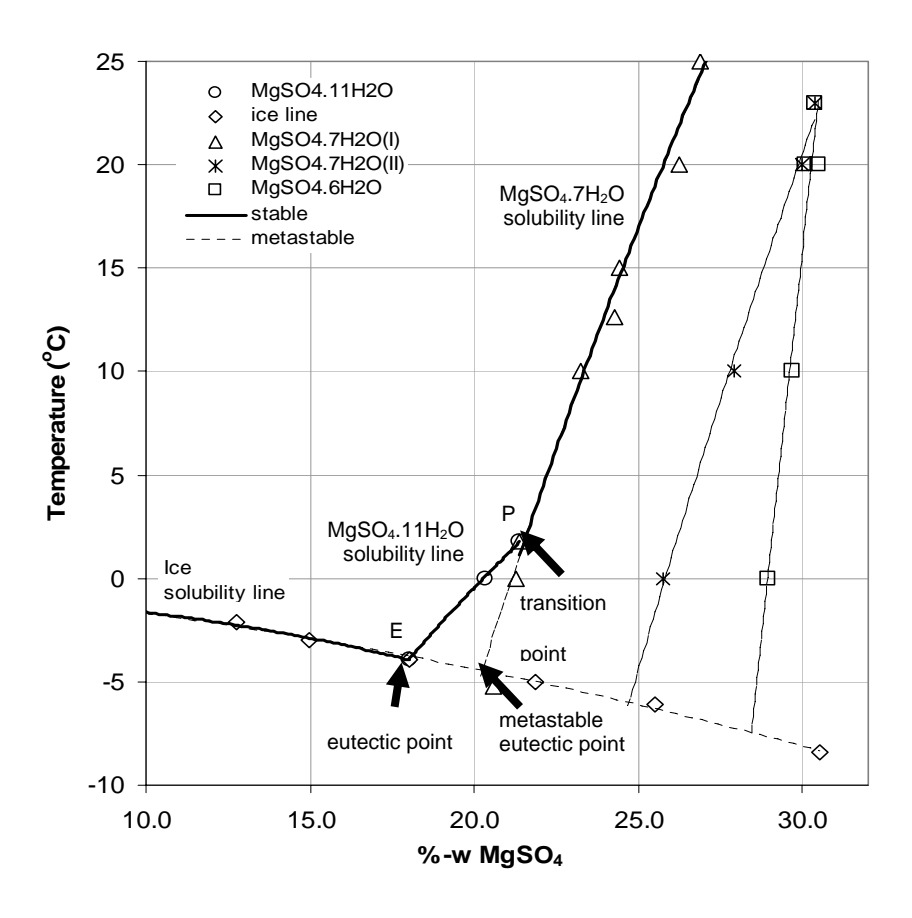


**Figure 6.1:** Phase diagram of the MgSO<sub>4</sub>-H<sub>2</sub>O system [Genceli et al. 2007] E is the eutectic point and P is the peritectic

### SAMPLING METHODS

For Sea Ice: The sea ice samples were collected from Lake Saroma (Saroma-Ko), the third largest lake of Japan located on the north-eastern shore of Hokkaido Island about 30 km away from Abashiri City. Saroma Lake is a semi-enclosed embayment connected with two openings to the Sea of Okhotsk. Most of the lake surface is covered with sea-ice during winter [Kawamura et al. 2004]. The map of Hokkaido Island, the location of Saroma Lake and sampling stations are shown in Figure 6.2.

The sea ice samples were picked from the core sampled at Station # 4 (44°07'N, 143°57'E) on March, 2006 with Core Number of 06.03.07-St.4. The sections of the sea ice core samples are shown in Figure 6.3. The sampling temperatures at 5, 10, 15, 25, 30, 35 and 40 cm below the sea level were +0.08, -0.30, -0.13, -0.28, -0.12, -0.32 and -0.29 °C respectively. However, in this work the (colder) top sections (surface) of the ice core which are in direct contact with air were analyzed. The lowest air and ice surface temperatures during March 2006 were -16.4 °C and -20.6 °C respectively and the average day temperature recorded by Kawamura et al. for air was -3.9 °C and ice surface was -2.8 °C [Kawamura, T., private communication 2007].

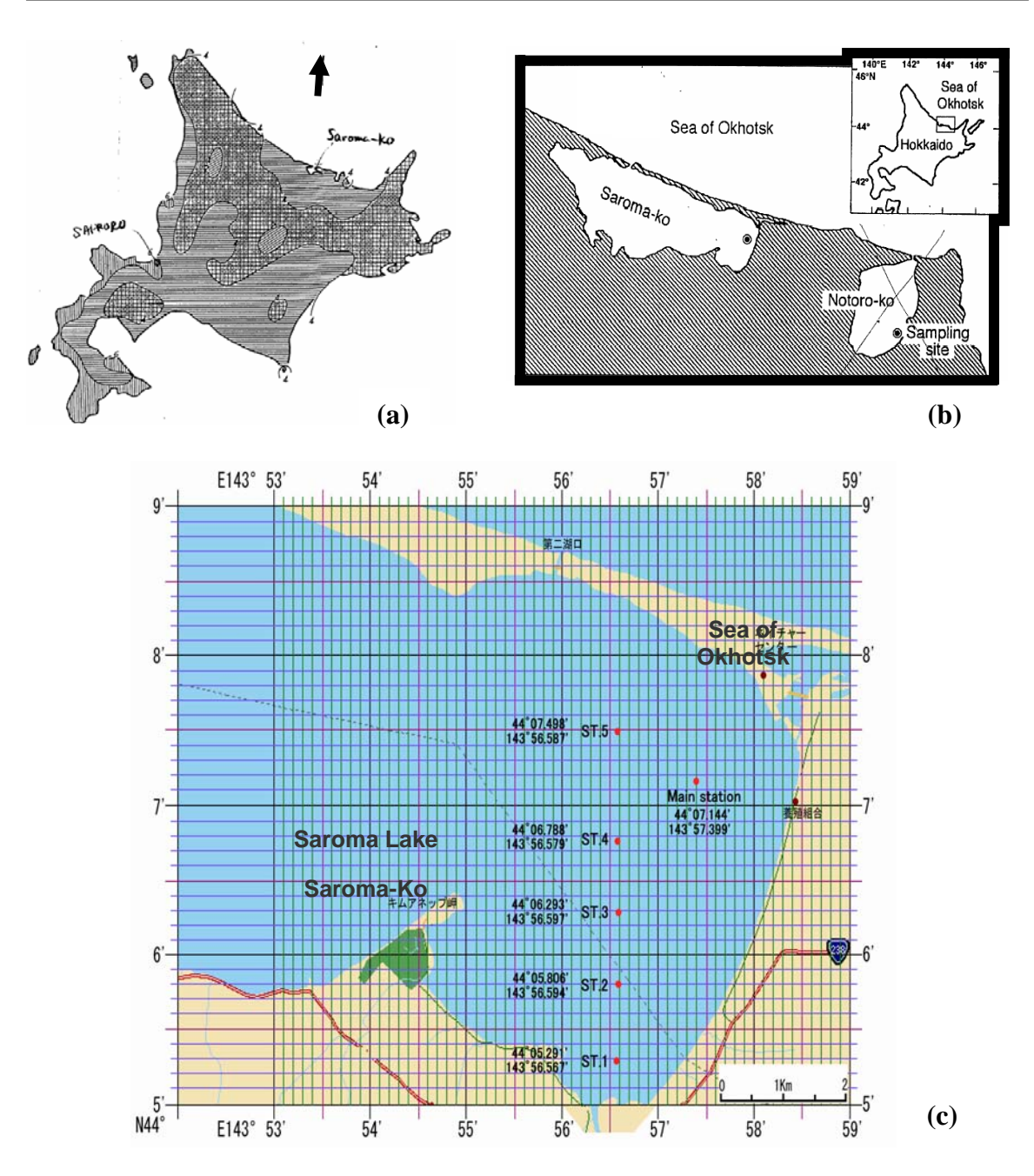


Figure 6.2: (a) The map of Hokkaido Island

- (b) Map of Saroma Lake
- (c) Location of sampling stations

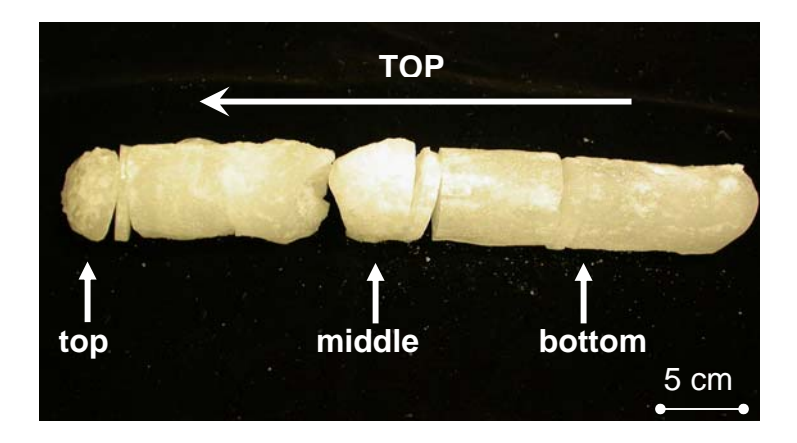


Figure 6.3: Picture of Sea Ice Core

The analyzed samples were taken from the sea ice surface (Section H1). Ice temperature was measured in-situ immediately after extraction of the cores, using calibrated thermistor probes (TECHNOL SEVEN, D617) inserted in drilled small holes at the exact diameter of the probe. Precision of the measurement was  $\pm 0.1$ °C.

After collecting, the samples were stored in the cold room of the Low Temperature Institute of Hokkaido University at -15 °C almost at the lowest exposed air temperature (-16.4 °C) and a little bit higher than the lowest measured surface ice temperature in the lake (-20.6 °C).

Ice forms by the gradual decrease of the sea water temperature where the remaining brine becomes increasingly saline. Since ice can generally contain no salt in the ice body, the brine is rejected into the underlying sea water. However, a portion of brine can become mechanically trapped in the ice matrix [Wakatsuchi et al. 1987]. As cooling continues, different solid salts also crystallize from the brine. However, they crystallize over a temperature range as opposed to a fixed eutectic temperature [Weeks et al. 1982]. According to phase relations of sea water, crystallization of salts depends upon the temperature of the ice [Assur 1958]. Precipitation of the salts from sea ice brine at various temperatures was deduced from changes in brine composition and stability ranges of individual salts in the corresponding pure salt water systems [Sinha 1977]. The solubility of one salt affects the solubility of the other due to their shifting pseudo

eutectic. Therefore different salts in sea ice crystallize at their shifting, pseudo eutectic temperatures.

As mentioned earlier, the pure MgSO<sub>4</sub>-H<sub>2</sub>O aqueous system crystallizes in MgSO<sub>4</sub>·11H<sub>2</sub>O form below +1.8 °C and has a eutectic point at -3.9 °C and 17.3 wt% MgSO<sub>4</sub> concentration [Genceli et al. 2007]. Presence of impurities (composition of the brine), and their quality and quantities shift the eutectic point to lower temperatures for the related salt. Therefore the formation of MgSO<sub>4</sub>·11H<sub>2</sub>O from sea brine composition is not known accurately. However, salt inclusions were detected in the samples which were stored and measured at -15 °C. Knowing the lowest ice exposure air temperature during March 2006 was -16.4 °C, it is reasonable to assume that the samples from the surface sea ice were kept intact during sampling and analysis.

For Antarctic Ice: The ice core used in this study was collected from Dome Fuji Station in East Antarctica at the 3810 m asl summit of the East Dronning Maud Land Plateau from location 77°19'S, 39°42'E. Map of Dome Fuji Station in East Antarctica is presented in Figure 4. The average snow temperature at 10 meters depth was measured - 58 °C. Further information about the sampling station geographical settings could be found in elsewhere [Dome-F Deep Coring Group 1998].

After collecting, the samples were stored in the cold room of the Low Temperature Institute of Hokkaido University at -50 °C. Samples from 362 and 576 meter depths having core numbers 03-124 and 05-156 respectively were analyzed in this work.

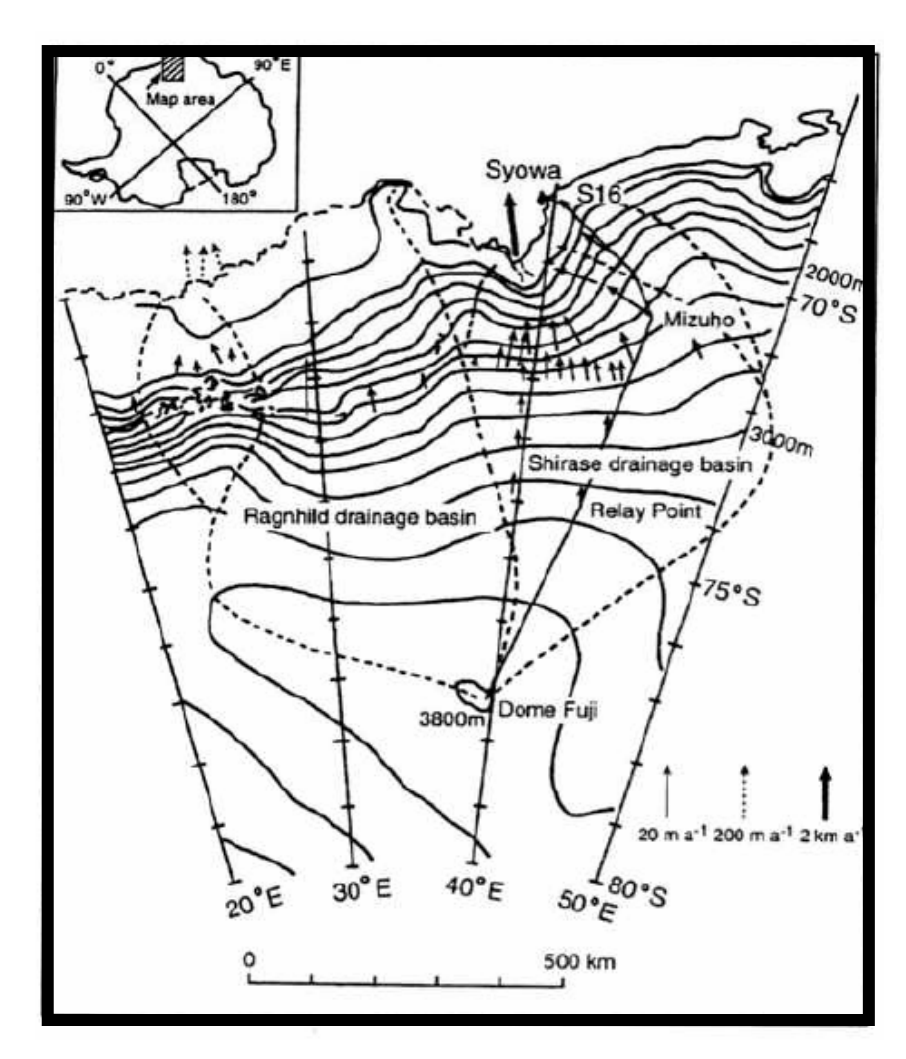


**Figure 6.4:** Map of Dome Fuji Station in East Antarctica [Dome-F Deep Coring Group 1998]

## **EXPERIMENTAL**

Synthetic MgSO<sub>4</sub>·11H<sub>2</sub>O Preparation: 20 wt% MgSO<sub>4</sub> solution, prepared form 99 wt% MgSO<sub>4</sub>·7H<sub>2</sub>O (J.T. Baker) and ultra pure water of 18.2 mΩ, was used for synthesizing MgSO<sub>4</sub>·11H<sub>2</sub>O crystals. Before starting crystallization, the solution was mixed inside a jacketed-crystallizer around 25 °C for a minimum of  $\pm 1$  hour to create a homogeneous solution. The cooling liquid -controlled by the cooling machine- was circulated through the jacketed crystallizer. A cooling rate of 4 °C/hour was applied until the nucleation of MgSO<sub>4</sub>·11H<sub>2</sub>O salt occurred. Afterwards the coolant temperature was set to -3 °C, until

the system reached equilibrium. Analyzes of synthetic MgSO<sub>4</sub>·11H<sub>2</sub>O crystal was used to compare with the analysis of ice inclusions.

For proving the natural existence of MgSO<sub>4</sub>·11H<sub>2</sub>O in nature, ice inclusion analysis were compared to synthetic MgSO<sub>4</sub>·11H<sub>2</sub>O crystal analysis. By this way their similarity is shown.

**Preparation of the Ice Samples:** Surface of top section of the sea ice samples and samples form 362 and 576 meter depth of Antarctic ice were prepared by cutting with a band saw into  $10 \times 10 \times 3$  mm<sup>3</sup> pieces. The upper and lower sides of the samples were then flattened (polished) with a microtome in clean-cold chamber at -15 °C.

Analysis Techniques: Determination of chemical compositions of the inclusions in both ice samples was not possible by direct methods due to extremely small sizes (few µm), their low crystal (compound) content and high solubility in water. As the inclusions were captured in ice, the measurements had to be done at low temperature, below 0 °C.

Micro-Raman Spectroscopy was used for inclusion observations and composition identification of the brine pockets of sea ice at low temperature. Raman Spectra of synthetic MgSO<sub>4</sub>·11H<sub>2</sub>O crystals measured under similar conditions were compared with the observed spectra of the inclusions. Jobin-Yvon T64000 triple monochromator equipped with a CCD detector was used for obtaining back-scattered Micro-Raman Spectra. The ice samples were placed into a cold chamber on an x-y translation stage of a microscope. Sample was kept in atmospheric conditions and cooling was achieved indirectly by N<sub>2</sub> gas circulation through the chamber keeping the sample temperature at -15±0.5 °C. Laser light of wavelength 514.5 nm and power 100 mW was focused to a diameter of about 1  $\mu$ m on the specimen using a long-working-distance objective lens with a 6 mm focal length (Mitutoyo, M Plan Apo 100×). The absolute frequency of the monochromator was calibrated with neon emission lines. The spectral resolution was ~1 cm<sup>-1</sup> within the range of 100-4000 cm<sup>-1</sup> with a detection time of 60 s.

Inductively Coupled Plasma Atomic Emission Spectrometry (ICP-AES) and Ion Chromatography were used to measure the cations and anions sea ice sample identifications with an error of  $\pm 2.5\%$ .

JEOL 6340LV Scanning Electron Microscope (SEM) equipped with Energy-Dispersive X-ray Spectrometer (EDS) was also tried for ice inclusions' composition determination at low temperature. Samples for SEM were fixed to stainless holder having a window for transparent microscope observation. The specimen was dropped into Liquid Nitrogen and vacuumed at that temperature, and transferred into SEM with a vacuumed pod using Alto-2100 (Oxford Instruments). After defining the position of targeted sample, SEM-EDS was used at -160 °C and under vacuum for their chemical characterization.

## **RESULTS**

It was found that the sea ice inclusions were typically 5-20 micrometer in diameter as shown in Figure 6.5 (a)-(b). Most of them were within the ice grains. The chemical composition of the sea ice samples measured by ICP-AES is presented in Table 6.1.

**Table 6.1:** Overall chemical composition of the sea ice samples

Constituent	Amount	Value
Co	7	[ppb]
Cu	8	[ppb]
Ni	10	[ppb]
Cr	11	[ppb]
V	11	[ppb]
Mn	12	[ppb]
Ga	65	[ppb]
Fe	125	[ppb]
Sr	130	[ppb]
Zn	150	[ppb]
Ba	820	[ppb]
K	7	[ppm]
Ca	9	[ppm]
Mg	14	[ppm]
$SO_4$	47	[ppm]
Na	115	[ppm]
Cl	300	[ppm]

Antarctic ice inclusions were typically 1-5 micrometer in diameter as presented in Figure 6.5 (c). Similar to sea ice inclusions they are mostly within the ice grains. The average concentrations of ion species ( $\mu$ molL<sup>-1</sup>) from 362 and 576 meter depths were measured using ion chromatography (Dionex 500) with an error better than  $\pm 0.01$   $\mu$ molL<sup>-1</sup> and are presented in Table 6.2 [Ohno et al. 2005].

**Table 6.2:** Chemical composition of Antarctic Ice from 362 and 576 meter depths [Ohno et al. 2005]

Constituent	Depth		Value
	362	576	meter
MSA	0.15	0.19	μmolL <sup>-1</sup>
Cl	2.48	5.36	μmolL <sup>-1</sup>
NO <sub>3</sub>	0.20	1.62	μmolL <sup>-1</sup>
$SO_4$	0.96	2.48	μmolL <sup>-1</sup>
Na	2.15	5.29	μmolL <sup>-1</sup>
Mg	0.20	0.89	μmolL <sup>-1</sup>
Ca	0.26	1.55	μmolL <sup>-1</sup>

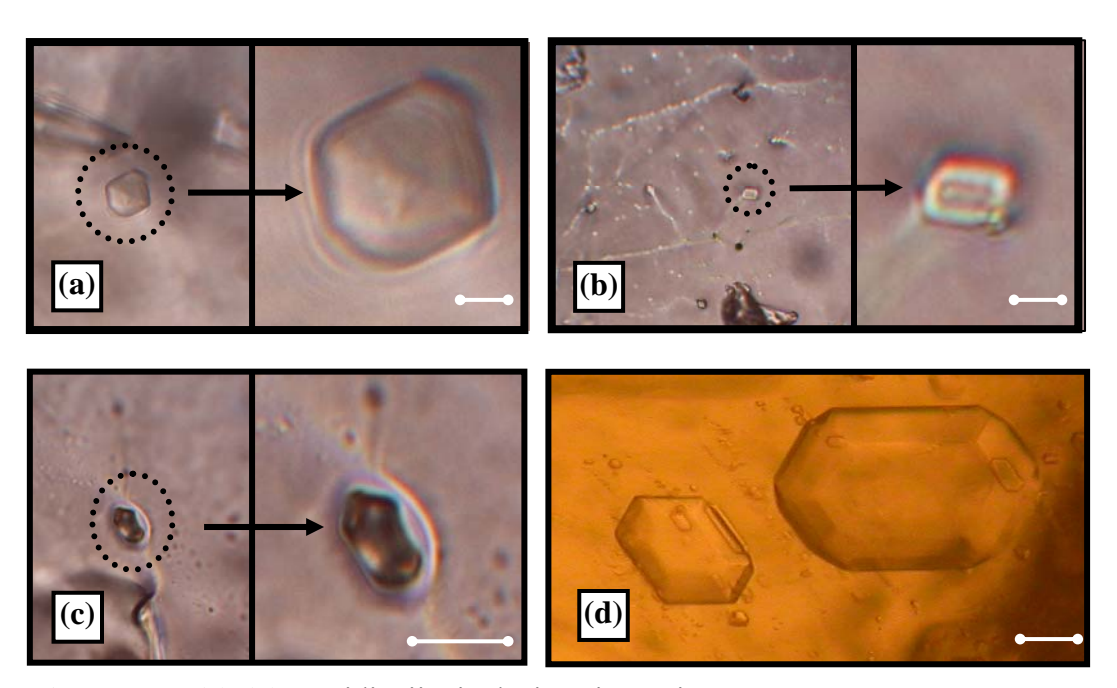


Figure 6.5: (a)-(b) Meridianiite inclusions in sea ice

- (c) Antarctic ice inclusions
- (d) Optical images of synthetic MgSO<sub>4</sub>·11H<sub>2</sub>O and negative crystals

<sup>\*</sup> The scale bar in each image is 5  $\mu m$ 

In Figure 6.5 (d) the morphology of synthetic  $MgSO_4\cdot 11H_2O$  crystals are presented with the picture of negative crystals. The morphological similarity with the synthetic crystals to meridianiite inclusions of sea ice -Figure 6.5 (a) and (b)- and Antarctic ice -Figure 6.5 (c)- could be observed.

## **SEM-EDS Results**

Checking the synthetic MgSO<sub>4</sub>·11H<sub>2</sub>O under SEM-EDS showed that the crystals deformed even at -160 °C when vacuum was applied. In Figure 6.6 (a) the original crystal image, whereas in Figure 6.6 (b) and (c) the deformed amorphous meridianiite images after 15 minutes and 1 hour are presented respectively. Due to vacuum, the crystal was dehydrated which could also be followed by Mg/O ratio increase in time and ended up as a porous structure of kieserite (MgSO<sub>4</sub>·H<sub>2</sub>O). Beside temperature restrictions, meridianiite stability depends also on relative humidity and atmospheric conditions.

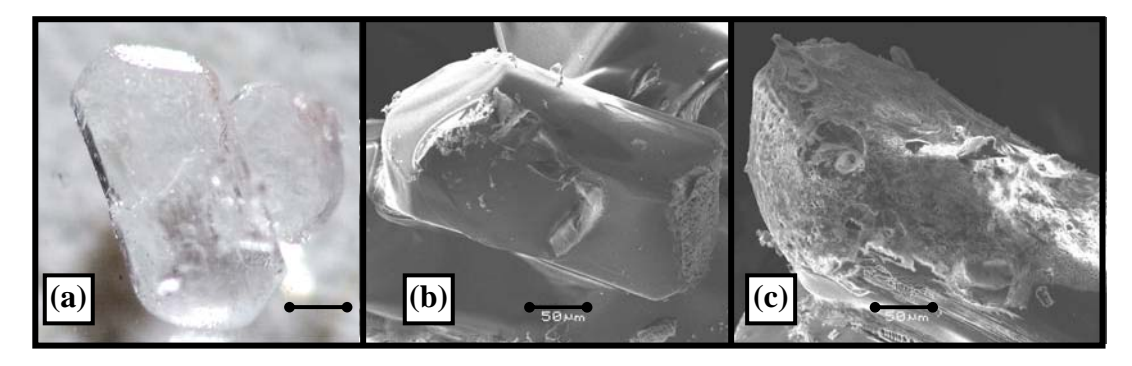


**Figure 6.6:** (a)-(b)-(c) Synthetic MgSO<sub>4</sub>·11H<sub>2</sub>O crystal deformation under vacuum \* The scale bar in each image is 50 μm.

In general, dehydration is a common behavior of hydrated sulfate salts and soluble salts. The phase transition reaction can be a highly dynamic process strongly influenced by variation of temperature and relative humidity in the surrounding environment [Cardell et al. 2007].

Therefore using SEM-EDS technique was not a suitable method for characterizing meridianiite both in synthetic  $MgSO_4\cdot11H_2O$  and in daughter minerals in ice inclusions.

For direct analysis, the salt inclusions were tried to be extracted from ice location by ice sublimation under atmospheric conditions in cold room at -15°C with 11 % relative humidity. Although it was possible to sublimate ice, similar to SEM-EDS applications dehydration of inclusions was inevitable.

## Micro Raman Spectroscopy

Since extracting the inclusions and analyzing those using direct methods was not possible, Micro Raman Spectroscopy was the only and the most powerful technique to identify the inclusions inside the ice samples. Inclusions were analyzed by Micro Raman Spectroscopy under atmospheric pressure by indirect cooling in a chamber kept at -15 °C at 5% relative humidity for sea ice whereas at -50 °C at < 5% relative humidity for Antarctic ice samples. Synthetic MgSO<sub>4</sub>·11H<sub>2</sub>O and inclusions detected in the sea and Antarctic ice were compared via Micro Raman spectra to demonstrate the identity between them.

*Micro Raman Spectroscopy of Sea Ice Inclusion:* Micro Raman Spectra of sea ice inclusions and synthetic MgSO<sub>4</sub>·11H<sub>2</sub>O salt for low-frequency ranges (0-2000 cm<sup>-1</sup>) and for high-frequency ranges (2000-4000 cm<sup>-1</sup>) are presented in Figures 6.7-6.10. As the aforesaid inclusions were located in the sea ice crystals, it was not possible to remove the dominant ice bands from their spectra. Therefore sea ice Raman Spectra are also presented for comparison in Figures 6.11-6.12. In the Figures bands belong to ice are presented with a black highlight.

The most significant peak is the  $SO_4^{2-}$  associated symmetric stretching band [Genceli et. al. 2007] at 989.85 cm<sup>-1</sup> for synthetic MgSO<sub>4</sub>·11H<sub>2</sub>O and at 989.77 cm<sup>-1</sup> for the sea ice inclusion.

Synthetic MgSO<sub>4</sub>·11H<sub>2</sub>O have sulfate modes [Makreski et al. 2005, Genceli et al. 2007] at 1116.37 cm<sup>-1</sup>, 1069.54 cm<sup>-1</sup> and 619.18 cm<sup>-1</sup>. Similarly in the sea ice inclusions these modes are located at 1116.69 cm<sup>-1</sup>, 1071.07 cm<sup>-1</sup> and 620.61 cm<sup>-1</sup>.

For synthetic MgSO<sub>4</sub>·11H<sub>2</sub>O, a water bending mode [Makreski et al. 2005, Genceli et al. 2007] is observed to have a maximum at 443.64 cm<sup>-1</sup> connected with a small peak at 457.22 cm<sup>-1</sup>. In sea ice inclusions, the same mode is also detected at 444.68 cm<sup>-1</sup> with a shoulder at 457.60 cm<sup>-1</sup>.

The effect of O-H...O (sulfate) [Parsk et al. 1966, Genceli et al. 2007] vibration located at 232.42 cm<sup>-1</sup> for synthetic MgSO<sub>4</sub>·11H<sub>2</sub>O is not detectable in sea ice inclusions as the presence of a strong ice stretching band at 214.86 cm<sup>-1</sup> with a resolved mode at 293.62 cm<sup>-1</sup> hides this band. In sea ice, similar bands are detected at 215.15 cm<sup>-1</sup> and 292.06 cm<sup>-1</sup>.

The O-Mg-O band [Parsk et al. 1966, Genceli et al. 2007] for synthetic MgSO<sub>4</sub>·11H<sub>2</sub>O seems to be located at 188.23 cm<sup>-1</sup> whereas in sea ice inclusions at 188.41 cm<sup>-1</sup>.

The stretching modes of crystal water in the lattice are located in the 2900-3700 cm<sup>-1</sup> region [Genceli et al. 2007]. For synthetic MgSO<sub>4</sub>·11H<sub>2</sub>O, there is one dominant band having a maximum at 3392.71 cm<sup>-1</sup>, with potential shoulders at 3520.67, 3469.99, 3304.05 and 3150.80 cm<sup>-1</sup>. Similarly, sea ice inclusion has that dominant band at 3400.48 cm<sup>-1</sup> and shoulders located at 3544.89, 3472.93 and 3302.58 cm<sup>-1</sup>.

In sea ice inclusion Raman Spectra, extra water bands due to presence of ice surrounding the inclusions are detected at 3264.62, 3141.43 and 2188.37 cm<sup>-1</sup>. Pure sea ice has the same equivalence bands at 3265.52, 3141.13 and 2186.97 cm<sup>-1</sup>.

The bands located at 1672.67 cm<sup>-1</sup> for synthetic MgSO<sub>4</sub>:11H<sub>2</sub>O and at 1672.97 cm<sup>-1</sup> for sea ice inclusion are interpreted as the bending mode of intracrystalline water [Socrates 2001, Genceli et al. 2007].

Summarizing all, by showing the excellent Micro Raman Spectra vibrational harmony between the synthetic MgSO<sub>4</sub>·11H<sub>2</sub>O and the inclusions of sea ice sample, the natural occurrence of "Meridianiite" as a mineral in sea ice is proven. The daughter minerals in

inclusions of sea ice may have been formed through freezing of sea ice followed by concentration of the sea brine captured in the ice and the meridianiite crystallization out of this brine.

Natural occurrence of meridianiite, on the surface of a frozen pond in central British Columbia Canada in a tree trunk was also presented in the work of Peterson et. all. The powder diffraction, refractive indices, infrared transmission spectra and reflectance infrared spectrum measurements of meridianiite were presented [Peterson et al. 2007].

Meridianiite has been submitted and recognized as a valid mineral species by the International Mineralogical Association Commission. The full submission to the IMA commission including powder diffraction data, physical properties has been deposited. The crystal structure data of meridianiite was presented in [Genceli et al. 2007, Peterson et al. 2006, Peterson et al. 2007].

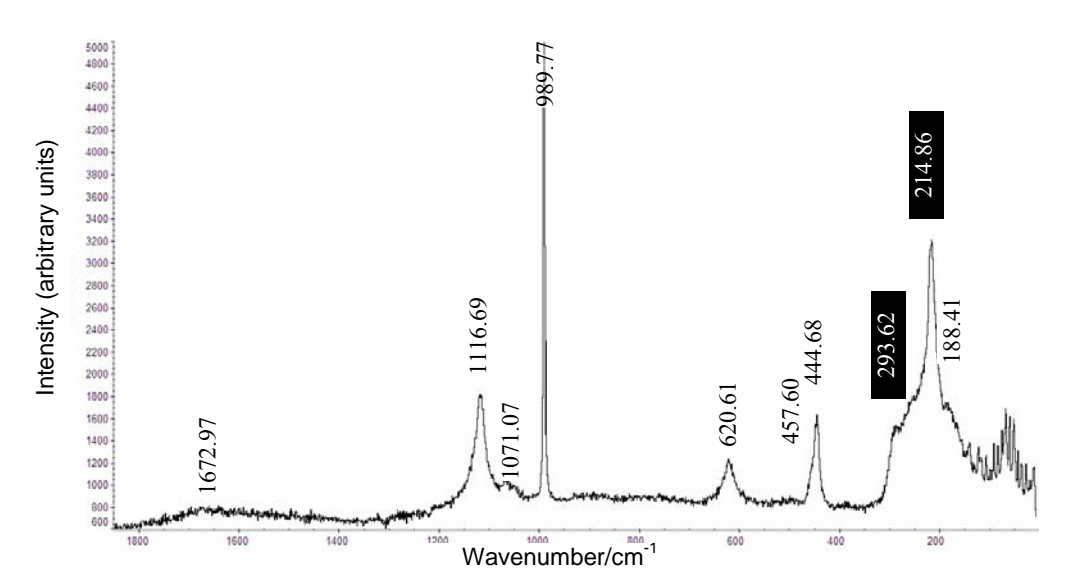


Figure 6.7: Low-frequency range of meridianiite inclusion

Note: Ice bands are highlighted with black

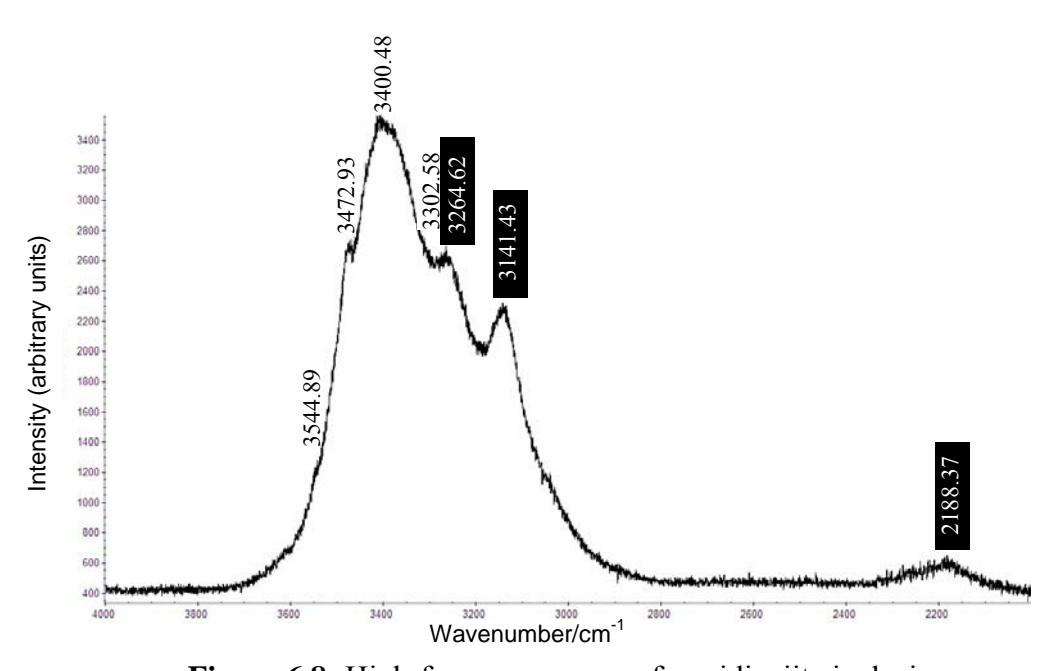
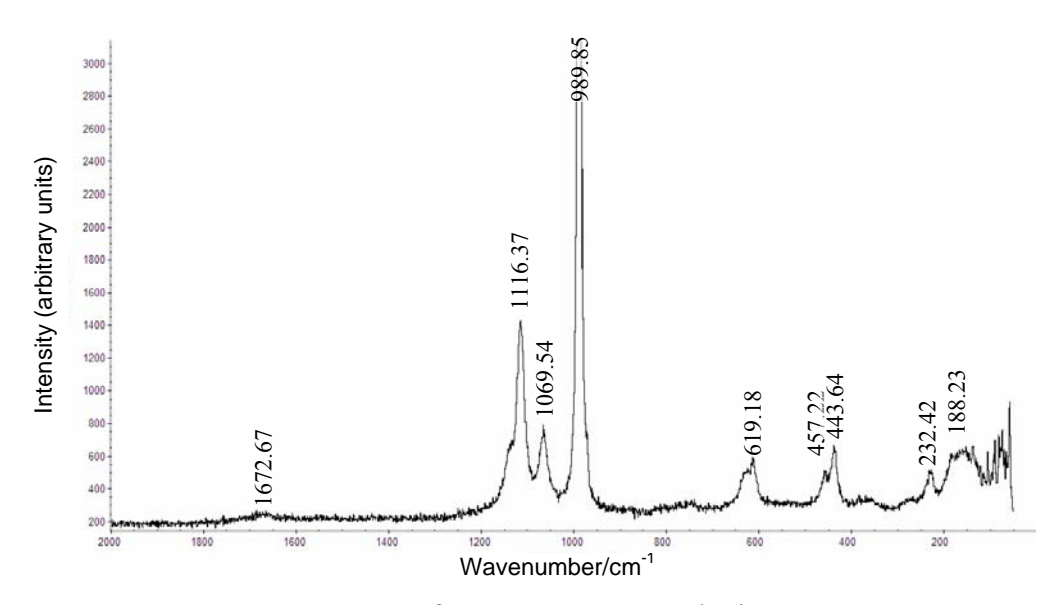
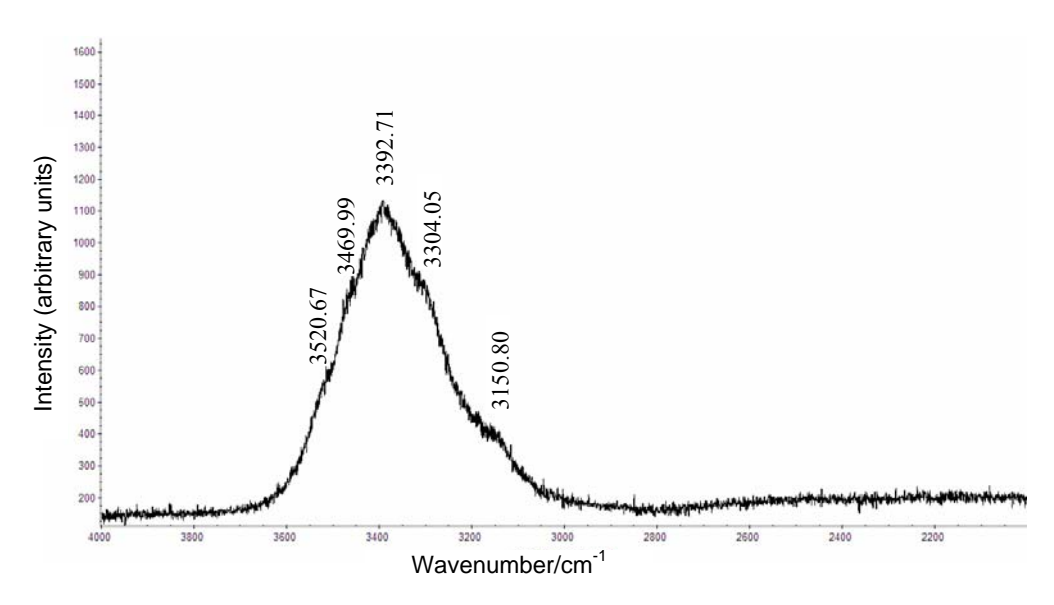


Figure 6.8: High-frequency range of meridianiite inclusion

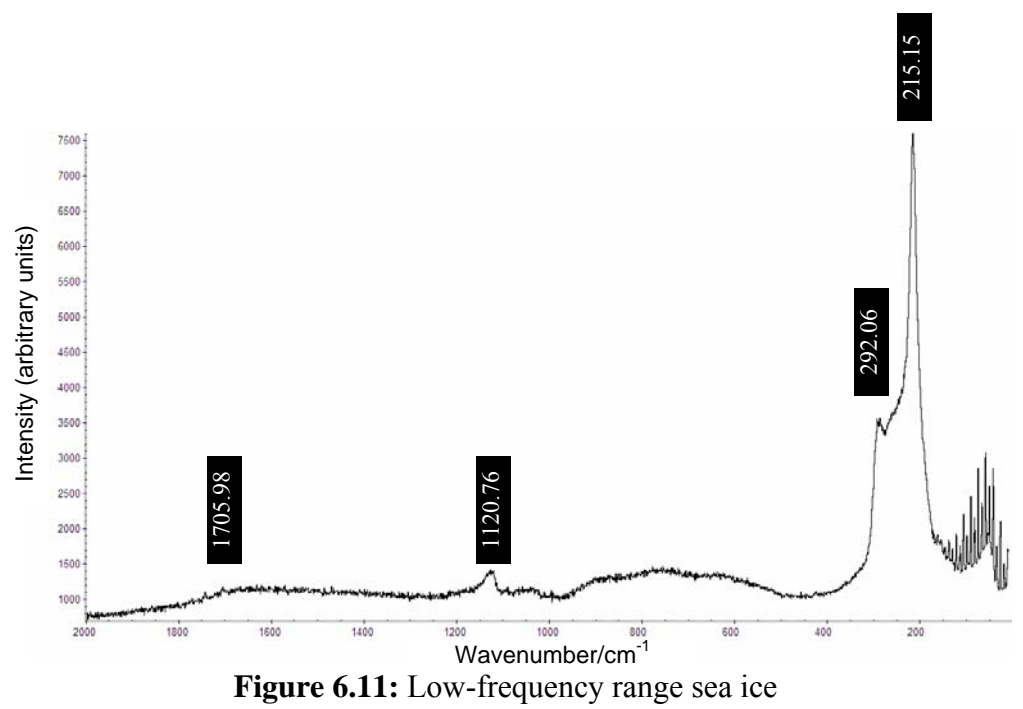
Note: Ice bands are highlighted with black



**Figure 6.9:** Low-frequency range synthetic MgSO<sub>4</sub>·11H<sub>2</sub>O



**Figure 6.10:** High-frequency range synthetic MgSO<sub>4</sub>·11H<sub>2</sub>O



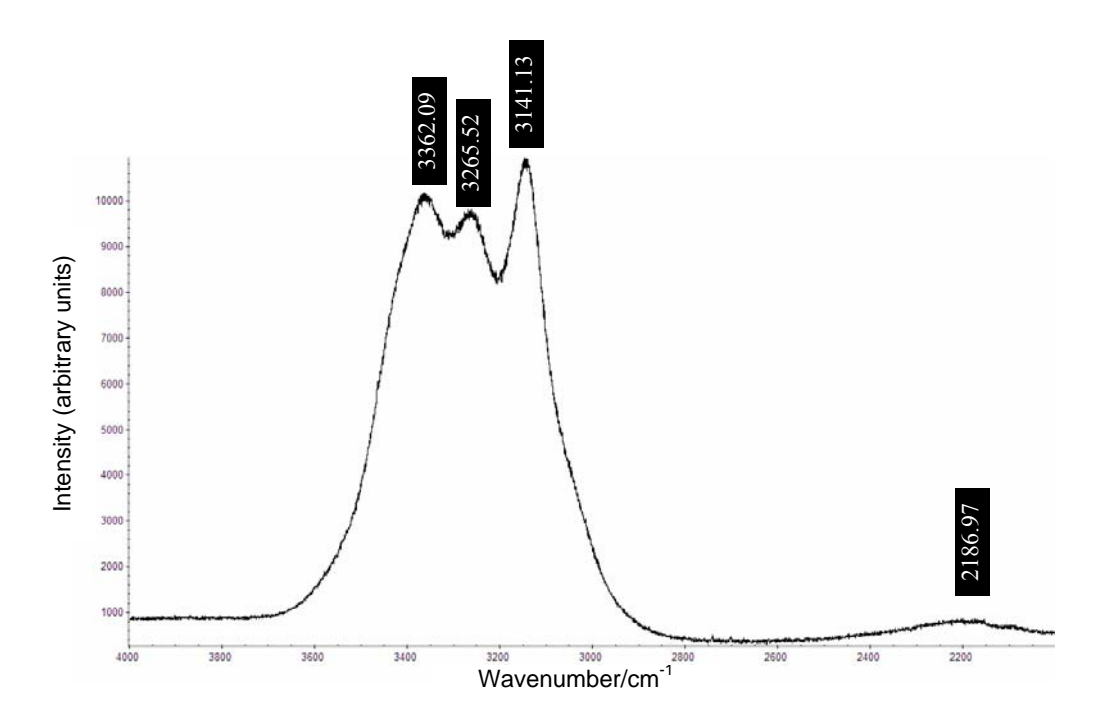
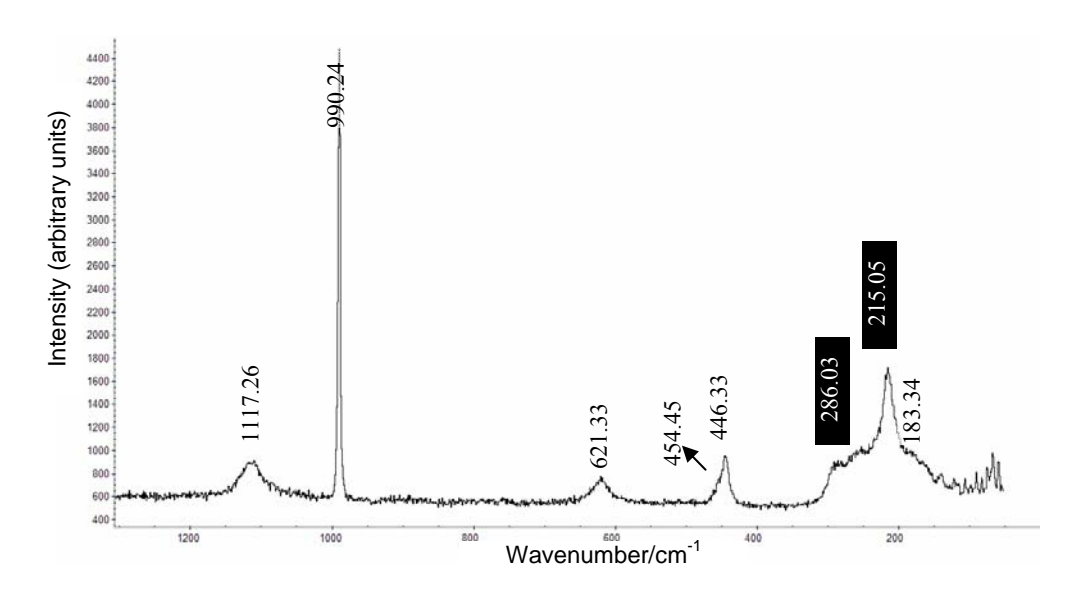


Figure 6.12: High-frequency range sea ice

*Micro Raman Spectroscopy of Antarctic Ice Inclusion:* Meridianiite likely occurs also in inclusions found in Holocene ice cores from Dome Fuji-East Antarctica [Ohno et al. 2005]. The aforesaid Antarctic ice samples were simultaneously analyzed during this work using Micro Raman spectroscopy. Due to the small sizes of the inclusions ranging between 1-5 μm, it was not possible to measure the whole spectrum from a single inclusion. In Figure 6.13, Micro Raman Spectra of an Antarctic ice sample inclusion for low-frequency range (0-1300 cm<sup>-1</sup>) is presented. The higher frequency ranges (1300-4000 cm<sup>-1</sup>) of the same inclusion for incorporated water in the lattice and for intracrystalline water bands could not be collected.

In the spectra presented in Figure 6.13 for Antarctic ice inclusion, the most significant peak is the SO<sub>4</sub><sup>2-</sup> associated symmetric stretching band at 990.24 cm<sup>-1</sup> and the sulfate modes at 1117.26 cm<sup>-1</sup> and 621.33 cm<sup>-1</sup>. The sulfate mode around 1069.54 cm<sup>-1</sup> for the synthetic MgSO<sub>4</sub>·11H<sub>2</sub>O is not very clear in Antarctic ice inclusion. The water bending mode is observed to have a maximum at 446.33 cm<sup>-1</sup> connected with a shoulder at 454.45 cm<sup>-1</sup>. Similar to sea ice inclusions, the strong ice stretching band at 215.05 cm<sup>-1</sup> with a resolved mode at 286.03 cm<sup>-1</sup> hide the band of O-H...O (sulfate) vibration located at 232.42 cm<sup>-1</sup>. The O-Mg-O band is located at 183.24 cm<sup>-1</sup>.

The Micro Raman Spectra for low vibrations of Antarctic ice inclusion match well with the one from synthetic MgSO<sub>4</sub>·11H<sub>2</sub>O. This suggests that micro inclusions of MgSO<sub>4</sub> salt preserved inside Antarctic ice core very likely contain meridianiite mineral. Meridianiite possibly formed as inclusions in Antarctic ice during different glacial periods by the reaction of acid-gas particles (H<sub>2</sub>SO<sub>4</sub> and HNO<sub>3</sub>) with sea-salt aerosols or terrestrial dusts during their transport through the atmosphere and while they were in snow pack [Röthlisberger et al. 2000, Ohno et al. 2006].



**Figure 6.13:** Low-frequency range of meridianiite inclusion in Antarctic Note: Ice bands are highlighted with black

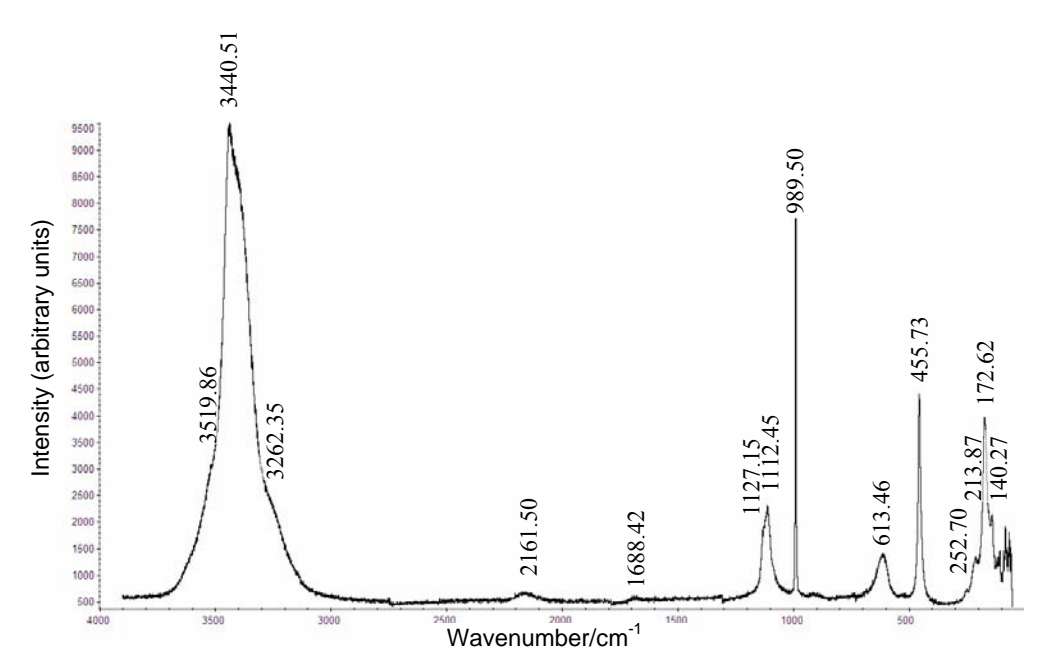


Figure 6.14: Micro Raman Spectra of synthetic mirabilite

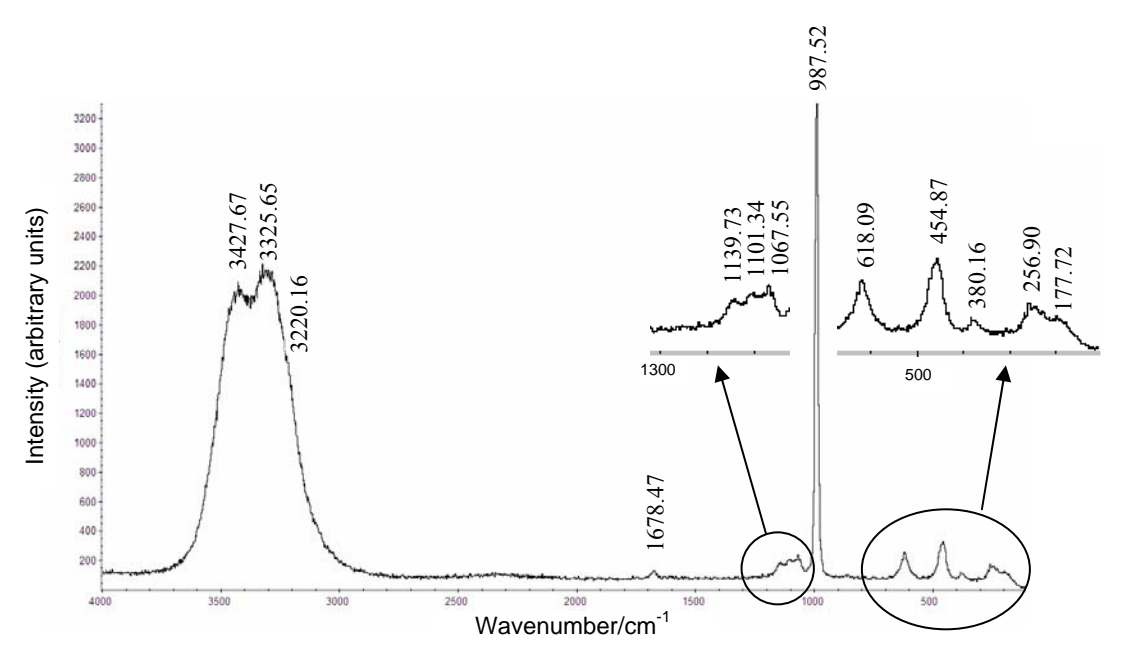


Figure 6.15: Micro Raman Spectra of synthetic epsomite [Genceli et al. 2007]

Micro Raman Spectroscopy of Mirabilite: Raman Spectra of the associated mineral of mirabilite (Na<sub>2</sub>SO<sub>4</sub>·10H<sub>2</sub>O) was also determined in sea ice and Antarctic ice as inclusions. In Figure 6.14, the Raman Spectra of synthetic mirabilite is presented to solve the ambiguity that was faced in the work of Ohno et al. in detecting the difference between the inclusions MgSO<sub>4</sub>·11H<sub>2</sub>O (defined as MgSO<sub>4</sub>·12H<sub>2</sub>O) and Na<sub>2</sub>SO<sub>4</sub>·10H<sub>2</sub>O in Holocene ice cores from Dome Fuji-East Antarctica [Ohno et al. 2005]. Synthetic mirabilite Raman Spectra were collected under atmospheric pressure in a cooling chamber at -15 °C with the same operational conditions applied for meridianiite. Comparing spectra given in Figures 6.9-6.10 of meridianiite, to Figure 6.14 of mirabilite only harmonizes at  $SO_4^{2-}$  symmetric stretching band at 989.50 cm<sup>-1</sup>. The rest of the spectrum differs from that of mirabilite such as with the presence of  $v_2$  mode at 455.73,  $v_3$  mode at 1112.45 and 1127.45 cm<sup>-1</sup> and  $v_4$  mode at 613.46 cm<sup>-1</sup> [Murugan et al. 2000]. Mirabilite has an OH-band located at wavenumber ranged from 3100 to 3700 cm<sup>-1</sup> [Xu et al. 1999]. The stretching water mode incorporated in the lattice has a maximum band at 3440.51 cm<sup>-1</sup> and potential shoulders at 3519.86 and 3262.35 cm<sup>-1</sup>. Detailed mirabilite Raman Spectra indexing is not available in literature. Therefore the assignment of Raman

Spectra picks was not done in this work very elaborate. On the other hand presenting the different spectra for meridianiite and mirabilite supports the reliability of our technique and eradicates the doubts that the reader may have for distinguishing the difference between meridianiite and mirabilite inclusions.

*Micro Raman Spectroscopy of Epsomite:* For comparing the Micro Raman Spectrum of synthetic epsomite (MgSO<sub>4</sub>·7H<sub>2</sub>O) salt measured at -10 °C is also shown in Figure 6.15 [Genceli et al. 2007]. For MgSO<sub>4</sub>·7H<sub>2</sub>O most significant peak of SO<sub>4</sub><sup>2-</sup> associated symmetric stretching band at 987.52 cm<sup>-1</sup> and more sulfate related Raman bands with maxima at 1139.73 cm<sup>-1</sup>, 1101.34 cm<sup>-1</sup> and 1067.55 cm<sup>-1</sup>. A water bending mode is located between 418-496 cm<sup>-1</sup> having a maximum at 454.87 cm<sup>-1</sup> and a sulfate mode in the range of 566-668 cm<sup>-1</sup>, having a maximum at 618.09 cm<sup>-1</sup>. Mg-O vibration band located at 380.16 cm<sup>-1</sup> for MgSO<sub>4</sub>·7H<sub>2</sub>O is not present for meridianiite. The bands at 256.90 and 177.72 cm<sup>-1</sup> are assigned to O-H...O (sulfate) entities in the crystal structure and to O-Mg-O deformations, respectively. The stretching modes of water are two bands resolved at 3427.67 cm<sup>-1</sup> and 3325.65 cm<sup>-1</sup>, including a shoulder at 3220.16 cm<sup>-1</sup>. Intracrystalline water assignment is located at 1678.47 cm<sup>-1</sup>.

Comparing the vibrational spectra of the epsomite and meridianiite salts, it is very obvious to detect the existence of significant differences due to presence of different structural bonding of the two salts.

#### **CONCLUSION**

Meridianiite, deposited and recognized as a valid mineral by International Mineralogical Association Commission, was found in sea ice inclusions from Saroma Lake-Japan. The excellent Micro Raman Spectra match of the Japanese sea ice daughter crystals to synthetic MgSO<sub>4</sub>·11H<sub>2</sub>O crystals is presented as the evidence of this existence.

Antarctic ice core inclusions from Dome Fuji perfectly match with the Micro Raman Spectra for low vibrations of synthetic MgSO<sub>4</sub>·11H<sub>2</sub>O. This evidence indicates the

possible existence of meridianiite in Antarctic ice. The extremely small size of the inclusions (ranging between 1-5  $\mu$ m) was the greatest obstacle for not measuring the whole Micro Raman spectrum from a single inclusion.

The Raman spectrum of MgSO<sub>4</sub>·11H<sub>2</sub>O (meridianiite) showed significant differences with that of MgSO<sub>4</sub>·7H<sub>2</sub>O (epsomite) and Na<sub>2</sub>SO<sub>4</sub>·10H<sub>2</sub>O (mirabilite).

Beside temperature restrictions of keeping MgSO<sub>4</sub>·11H<sub>2</sub>O below +1.8 °C (at atmospheric pressure) for preventing recrystallization into epsomite, meridianiite stability depends on relative humidity and atmospheric conditions. Meridianiite deforms and dehydrates very easily into lower hydrated-MgSO<sub>4</sub> crystal structures even at -160 °C when vacuum is applied or relative humidity is low. Therefore SEM-EDS technique was not suitable for our research to detect meridianiite inclusions in sea and Antarctic ice samples.

#### ACKNOWLEDGMENT

We would like to thank to Dr. Ernst Burke -Chairman of IMA Commission on New Minerals- for all his support and help during this work.

## REFERENCES

- Assur 1958 Assur, A.; Composition of sea ice and its tensile strength, U.S. Natl. Acad. Sci. NRC Pub. 1958, 598, 106-138.
- Baker et al. 2003 Baker, L.; Cullen, D.; SEM/EDS observations of impurities in polar ice: artefacts or not?, *Journal of Glaciology*. 2003, 49(165), 184-190.
- Barnes et al. 2004 Barnes, P. R. F.; Wolff. E. W.; Distribution of soluble impurities in cold glacial ice, *Journal of Glaciology*. 2004, 50(170), 311-324.
- Cardell et al. 2007 Cardell, C.; Sánchez-Navas, A.; Olmo-Reyes, F. J.; Martin-Ramos, J. D.; Power X-Ray Thermodiffraction Study of Mirabilite and Epsomite Dehydration Effects of Direct IR-Irradiation on Samples, *Analytical Chemistry*. 2007, 79, 4455-4462.
- Dome-F Deep Coring Group 1998 Dome-F Deep Coring Group; Deep ice-core drilling at Dome Fuji and glaciological studies in east Dronning Maud Land, Antarctica, *Annals of Glaciology*. 1998, 27, 333-337.
- Fritzche 1837 Fritzche, C. J.; Ueber eine neue Verbindung der schwefelsauren Talkerde mit wasser. Annalen der Physik und Chemie. *Poggendorff's Annale.*, 1837, 42, 577-580.
- Genceli et al. 2007 Genceli, F. E.; Lutz, M.; Spek, A. L.; Witkamp G. J.; Crystallization and Characterization of a New Magnesium Sulfate Hydrate MgSO<sub>4</sub>·11H<sub>2</sub>O-, *Crystal Growth & Design.* 2007, 7(12), 2460-2466.
- Kawamura et al. 2004 Kawamura, T.; Shirasawa, K.; Ishikawa, M.; Takatsuka, T.; Daibou T.; Leppäranta, M.; On The Annual Variation of Characteristics of Snow and Ice in Lake Saroma, 17<sup>th</sup> International Symposium on Ice, Saint Petersburg, Russia, International Association of Hydraulic Engineering and Research. 2004, 212-220.
- Makreski et al. 2005 Makreski, P.; Jovanovski G.; Dimitrovska, S.; *Vibrational Spectroscopy*. 2005, 39, 229-239.
- Murugan et al. 2000 Murugan, R.; Ghule, A.; Chang, H.; Thermo-Raman spectroscopic studies on polymorphism in Na<sub>2</sub>SO<sub>4</sub>, *Journal of Physics: Condensed Matter*. 2000, 12, 677-700.

- Ohno et al. 2005 Ohno, H.; Igarashi M.; Hondoh, T.; Salt inclusions in polar ice core: Location and chemical form of water-soluble impurities, *Earth and Planetary Science Letters*. 2005, 232, 171-178.
- Ohno et al. 2006 Ohno, H.; Igarashi M.; Hondoh, T.; Characteristics of salt inclusions in polar ice from Dome Fuji, East Antarctica, *Geophysical Research Letters*. 2006, 33(8), L08501.
- Parsk et al. 1966 Parsk, H. J.; Boutin, H.; Low-Frequency Motions of H<sub>2</sub>O Molecules in Crystals III, *Journal of Chemical Physics*. 1966, 45, 3284.
- Peterson et al. 2006 Peterson, R.C.; Wang. R.; Crystal Molds on Mars: Melting of a possible new mineral species to create Martian chaotic terrain, *Geology*. 2006, 34, 957-960.
- Peterson et al. 2007 Peterson, R.C.; Nelson, W.; Madu B.; Shurvell, H. F.; Meridianiite: a new mineral species observed on Earth and predicted to exist on Mars, *American Mineralogist*. 2007, 92, 1756-1759.
- Röthlisberger et al. 2000 Röthlisberger, R.; Hutterli, M.A.; Sommer, S.; Wolff E.W.; Mulvaney R.; Factors Controlling Nitrate in Ice Cores: Evidence from the Dome C Deep Ice Core, *Journal of Geophysical Research*. 2000, 105(D16), 20565-20572.
- Sinha 1977 Sinha, N.K.; Instruments and Methods Technique for Studying Structure of Sea Ice, *Journal of Glaciology*. 1977, 18(79), 315-323.
- Socrates et al. 2001 Socrates, G.; *Infrared and Raman Characteristic Group Frequencies-Tables and Charts*. John Wiley & Sons, 3<sup>rd</sup> edition, 2001.
- Wakatsuchi et al. 1987 Wakatsuchi, M.; Kawamura, T.; Formation processes of brine drainage channels in sea ice, *Journal of Geophysical Research*. 1987, 92(C7), 7195-7197.
- Weeks et al. 1982 Weeks, W. F.; Ackley, S. F.; The growth, structure, and properties of sea ice, *CRREL Monograph*. 1982, 82(1), 4.
- Xu et al. 1999 Xu, B.; Schweiger, G.; In-situ Raman Observation of phase transformation of Na<sub>2</sub>SO<sub>4</sub> during the hydration/dehydration cycles on single levitated microparticle, *Journal of Aerosol Science*. 1999, 30, S379-S380.

# Coupled heat and mass transfer during crystallization of $MgSO_4\cdot 7H_2O$ on a cooled surface

F. Elif Genceli<sup>a</sup>, Marcos Rodriguez<sup>a</sup>, Signe Kjelstrup <sup>a, b</sup>, Geert-Jan Witkamp<sup>a</sup>

<sup>&</sup>lt;sup>a</sup> Process & Energy Department TUDelft, Deft-The Netherlands

<sup>&</sup>lt;sup>b</sup> Department of Chemistry, Faculty of Natural Science and Technology, Norwegian University of Science and Technology, Trondheim- Norway

## **ABSTRACT**

Crystal growth of MgSO<sub>4</sub> aqueous solution on a cooled surface has been studied theoretically and experimentally. The excess entropy production rate for heat and mass transport into, out of and across the interface was used to define the fluxes and forces of the system. The method describes the interface as a separate (two-dimensional) phase in local equilibrium. Coupled heat and mass flux equations from non-equilibrium thermodynamics were defined for crystal growth and the temperature jump at the interface of the growing crystal. All interface transfer resistivities were determined using MgSO<sub>4</sub>·7H<sub>2</sub>O crystallization on a cooled surface as an example case. The coupling coefficient showed that between 20 and 30% of the enthalpy of crystallization is returned to the liquid side during crystal growth. The coupling of heat and mass transport equations at liquid-solid interface has not been described before.

#### INTRODUCTION

Assume a crystal growing on a cooled solid surface from an aqueous solution. Furthermore, we consider only the flat parts of the growth layers on the crystal surface, e.g. we disregard steps and kinks, and surface integration phenomena, for a moment. Then it can be expected that coupled heat and mass transfer effects, when calculated with the Onsager equations, will in principle be noticeable and will lead to a temperature jump at the interface [Kjelstrup et al. 2008], apart from the regular thermal and concentration diffusion boundary layers. Using crystallization of MgSO<sub>4</sub>·7H<sub>2</sub>O on a cooled metal surface covered with TLC (Thermochromatic Liquid Crystal) sheet as an example case, we distinguish between the following thermodynamic phases; the homogeneous solution phase, crystal phase, TLC covered metal phase, and the (described as two-dimensional) interfaces between the homogeneous phases: which are the solid-solid interface between the crystal and TLC covered metal, and the liquid-solid interface between the liquid and crystal. In this work we neglect the contribution solid-solid interface between crystal and TLC covered metal.

First, the equations of transport of heat and mass through this series of layers, and their application and predictions, are set up. All transport equations are in principle governed by the second law of thermodynamics. The theory of non-equilibrium thermodynamics can be used to derive these rate equations, including those which apply to the interface, in a systematic manner, assuming that the second law remains valid locally. We shall document here a temperature jump at the crystal interface during crystallization of MgSO<sub>4</sub>·7H<sub>2</sub>O. The jump is predicted by irreversible thermodynamics. We can thus interpret the measured temperature jump and give the surface transfer resistivities.

General expressions for the excess entropy production rate of an interface were already derived a long time ago [Bedeaux et al. 1976, Bedeaux 1986, Albano et al. 1987] for curved interfaces that were allowed to move in space and change their curvature. Such an analysis is rather complicated, and simplifications are required. A first attempt to use non-equilibrium thermodynamics in the description of crystallization was made by Ratkje

and Flesland [Ratkje et al. 1995] in their studies of freeze concentration of ice from an aqueous solution. That study did not take into account the heterogeneous nature of the problem, however, which is essential [Chen et al. 1997]. Badam et al. recent measured the temperature jump in the liquid vapour interface and show the importance of coupling coefficient [Badam et al. 2007].

We are now able to take advantage of the results of Kjelstrup and Bedeaux 1996, in their development of coupled transport equations for a planar liquid-vapor interface, and include the heterogeneous nature of the system [Kjelstrup et al. 1996]. An interface does not exist without its bounding phases, and the transport processes in question therefore address a heterogeneous system: the system made up by two homogeneous phases and the interface between these. One may still question the need to invoke this level of detail in the description, but we shall see, this is the only way to describe properly the simultaneous transport of heat and mass, in a way that is consistent with the second law of thermodynamics.

The aim of this work is to estimate the magnitude of the temperature jump and to quantify the effect of the coupling of heat and mass transport.

The chapter is organized as follows. After a description of the coupled transport of heat and mass in terms of non-equilibrium thermodynamics across some heterogeneous layers in theory section, we describe an experimental system and experiments to test the theory in experimental section. The data analysis methodology is described in data analysis section. Results from measurements of temperature differences across the layers, a discussion and a comparison with other theoretical methods of data reduction are done in results and discussion part. We conclude on the general perspectives on the method.

## **THEORY**

## The System

A schematic drawing of the crystallization system just on the cooled surface is shown in Figure 7.1. The homogeneous liquid phase is indicated by  $(\ell)$ , the crystal phase by (s). The area between the solution and the crystal layers is called interface (i), having a thickness of  $\delta^i$  though it is considered thermodynamically as a two dimensional phase. In Figure 7.1, the variation of the MgSO<sub>4</sub> concentration is shown from liquid to solid phase. The x-axis of Figure 7.1 has coordinates for concentration in kmol.m<sup>-3</sup> whereas y-axis has coordinates in variable  $\mu$ m.

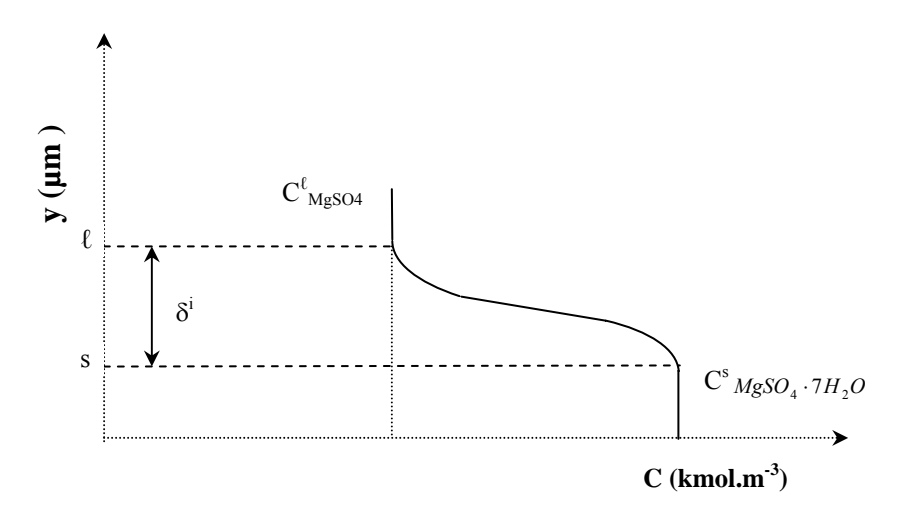
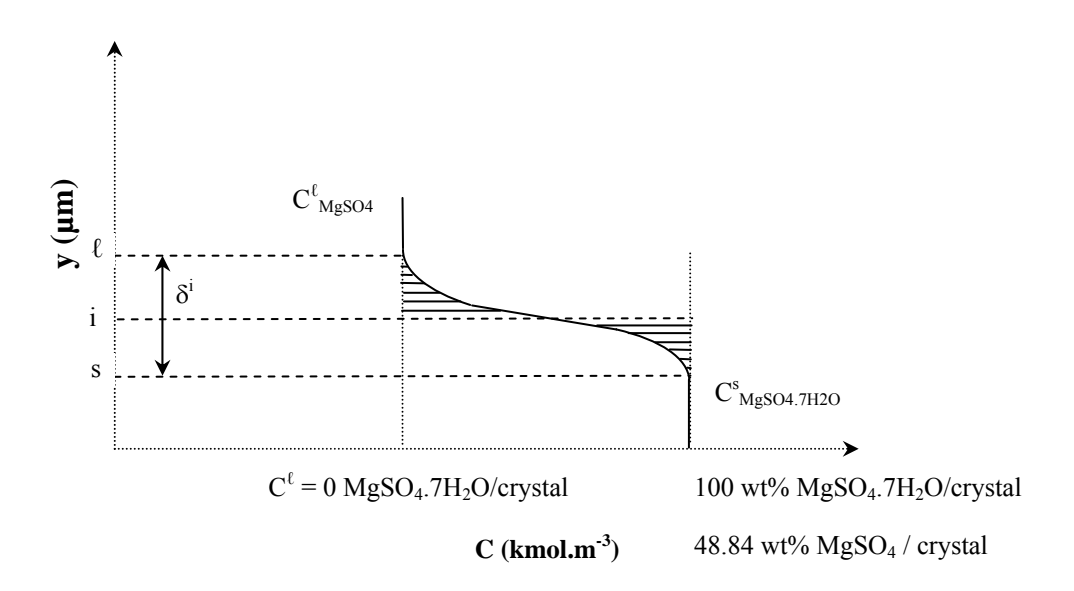


Figure 7.1: Variation in the molar density of the crystal % MgSO<sub>4</sub>·7H<sub>2</sub>O

The three homogeneous phases; the TLC covered metal phase, the crystal phase and the solution have all a thickness of the order of millimetre. The interface between the crystal and the TLC covered metal does not involve any mass flux, and the contact resistance to heat transport through this layer will be neglected.

# Excess Densities for the Surface

In a macroscopic description, not only the homogenous phases, but also the interface (between solution and the crystal) is a separate thermodynamic phase system. The thermodynamic properties of the interface are given by the values of the excess densities as defined by Gibbs [1961]. Excess concentration means the integral of the concentration above (or below) the values of the nearby phases. The location of the *equimolar* interface is such that the surplus of moles of the component on one side of the interface is equal to the deficiency of moles of the component on the other side of the interface. The value of these densities and the location of the interface will be defined through the example of a liquid-solid interface in crystallization system. Figure 7.2 shows the equimolar surface of MgSO<sub>4</sub>·7H<sub>2</sub>O by the horizontal line at i.



**Figure 7.2:** Determination of position of the equimolar surface of MgSO<sub>4</sub> crystallization The areas between the curve and the bulk densities on both sides of the lines are the same

Calculation and determination of the location of this plane (for excess surface concentration, excess density, excess internal energy, excess enthalpy, the surface tension and the excess entropy) is explained in detail else where [Bedeaux et al. 2005].

# Heat and Mass Transport, and the Entropy Production Equations for Crystallization

For analyzing crystallization of the MgSO<sub>4</sub>·7H<sub>2</sub>O salt on the heat exchanger surface, the heat and mass transfer equations must be defined from the entropy production for three different regions, i.e. at points "s", " $\ell$ " and "i" to obtain the temperature, concentration and heat and mass flux profiles.

## 1. Salt Layer "s":

The frame of reference for the transports of heat and mass is the interface of the salt crystals growing at the wall into the solution so the observer is moving with the interface. Transport (through the interface) from the solution into the cold wall is chosen to be the positive direction of transport.

Mass transport for "s": The mass flux into the interface is an aqueous solution and out is salt crystals. At this stage mass conservation is valid, giving:

$$J^{\ell} = J^{s} \tag{7.1}$$

The mass flux is calculated by the measured crystal growth rate ( $v^{salt}$ ) using,

$$J^{s} = \rho_{salt} v^{salt} \tag{7.2}$$

Heat transport in "s": The heat flux into the salt can be determined on the coolant side when the salt is growing on the wall. From the energy balance of the coolant, we define the total heat going though the wall  $(J'_a)$  is equal to the heat flux through the salt  $(J'_a)$ .

$$J'_{q} = J'^{s}_{q} \tag{7.3}$$

Entropy production for "s": The entropy production of the salt is,

$$\sigma^{s} = J_{q}^{'s} \frac{d}{dx} \left( \frac{1}{T} \right) \tag{7.4}$$

The pure salt has only transport of heat. We use Fourier's law as the linear law for heat transport giving,

$$J_q^{'s} = -\lambda^{salt} \frac{dT}{dx} \tag{7.5}$$

Having constant heat flux and thermal conductivity, the temperature profile of the salt on the TLC surface would be,

$$T^{s} - T^{TLC} = \frac{\delta^{salt}}{\lambda^{salt}} J_{q}^{'s} \tag{7.6}$$

If we include the heat exchanger metal wall and the thermo liquid crystal (TLC) coating layer as well,

$$T^{s} - T^{c} = \left(\frac{\delta^{salt}}{\lambda^{salt}} + \frac{\delta^{TLC}}{\lambda^{TLC}} + \frac{\delta^{wall}}{\lambda^{wall}}\right) J_{q}^{s}$$
(7.7)

# 2. Liquid Layer "\ell":

Entropy production for " $\ell$ ": In the liquid side of the interface the entropy production has two terms namely heat flux and mass flow rate.

$$\sigma^{\ell} = J_q^{\ell} \frac{d}{dx} \left(\frac{1}{T}\right) - J^{\ell} \frac{1}{T} \frac{d\mu_{T,salt-aq}}{dx}$$

$$\tag{7.8}$$

The heat and mass transport and the entropy production equations for the liquid layer in frond of the interface are defined with the following equations:

Mass transport for " $\ell$ ": Mass flux on the salt side calculated via Equation (7.2) and due to mass conservation assumption given in Equation (7.1), mass flux on the liquid side ( $J^{\ell}$ ) is found.

Heat transport for " $\ell$ ": The heat flux for the related layer is defined in similar form to the salt layer given in Equation 7.5:

$$J_q^{'\ell} = -\lambda^{salt-aq} \frac{dT}{dx} \tag{7.9}$$

Equation 7.9 gives a continuous profile away from the surface. We have then neglected the coupling of heat and mass in the solution. The Soret coefficient in liquids is small in many cases.

## 3. At the Interface "i":

In the crystallization system, the interface is the most interesting layer compared to the others as all the reaction takes place over the interface. The layer is defined as a two-dimensional thermodynamic system by excess densities explained under Theory- *The System*.

Extrapolating the measured temperature profiles both from the solid side and from the liquid side up to their contact point (the interface) shows the temperature discontinuity across the solid-liquid interface. We chose interface at the equimolar surface of the salt.

Heat and mass transport for "i": At the interface, the energy conservation for onedimensional transport gives,

$$J_{q}^{is} + J \cdot H_{cryst.}^{s} = J_{q}^{i\ell} + J \cdot H_{cryst.}^{\ell}$$

$$J_{q}^{is} = J_{q}^{i\ell} + \Delta H_{cryst.} J$$

$$J \cdot (H_{cryst.}^{s} - H_{cryst.}^{\ell}) = J_{q}^{i\ell} - J_{q}^{is} < 0$$

$$(7.10)$$

In equation (7.10), it is seen that, the enthalpy of crystallization can partly be transported into the salt  $J_q^{is} > 0$  and partly be going back into the mother liquid  $J_q^{i\ell} < 0$ . The relative fraction of the enthalpy of crystallization carried by the fluxes at uniform temperature is given by the resistance to heat transfer and the so-called heats of transfer, see definitions below.

Entropy production for "i": The entropy production for the interface has three terms at the steady state. Two of them are from the heat conduction in and out of the interface and

one from mass transport across it [Kjelstrup et al. 2008]. The entropy production for the salt in the interface could be defined as follows,

$$\sigma^{i} = J_{q}^{is} \Delta_{i,s} \left(\frac{1}{T}\right) + J_{q}^{i\ell} \Delta_{\ell,i} \left(\frac{1}{T}\right) - J \frac{1}{T^{i}} \Delta_{\ell,s} \mu_{T}(T^{i})$$

$$(7.11)$$

The expression for the entropy production given in Equation 7.11 is valid for crystal growth. Subscript i,s means that the difference is taken between the salt and the surface, the subscript  $\ell,i$  means a difference between the surface and the solution; while  $\ell,s$  means across the surface (i.e. between salt and the solution). As the mass flux of the salt into and out of the surface is constant, the chemical driving force into and out of the surface were combined. Due to the fact of inequality of  $J_q^{is} \neq J_q^{i\ell}$ , the other terms in Equation 7.11 can not be combined in the similar way. The expression describes all energy lost as heat at the interface.

It is not convenient to have a driving force depending on the temperature of the surface. By introducing the energy balance into the entropy production and by using the identity given in Equation 7.12, both the surface temperature and one of the heat fluxes could be eliminated from Equation 7.11.

$$\frac{1}{T^{i}} \Delta_{\ell,s} \mu_{T}(T^{i}) = \frac{1}{T^{i}} \left( \mu^{s}(T^{i}) - \mu^{\ell}(T^{i}) \right) = \frac{1}{T^{\ell}} \left( \mu^{s}(T^{\ell}) - \mu^{\ell}(T^{\ell}) + (H^{s} - H^{\ell})(\frac{1}{T^{i}} - \frac{1}{T^{s}}) \right)$$
(7.12)

The entropy production for the interface could be rewritten in the following form

$$\sigma^{i} = J_{q}^{is} \Delta_{\ell,s} \left(\frac{1}{T}\right) + J\left(-\frac{1}{T^{\ell}} \Delta_{\ell,s} \mu_{T}(T^{\ell})\right) \tag{7.13}$$

The thermodynamic driving forces for transport of heat and mass from the entropy production are as follows:

$$\Delta_{\ell,s}\left(\frac{I}{T}\right) = \frac{I}{T^s} - \frac{I}{T^\ell} = \frac{\Delta_{s,\ell}T}{T^\ell T^s} \approx \frac{\Delta_{s,\ell}T}{(T^\ell)^2} = -\frac{\Delta_{\ell,s}T}{(T^\ell)^2}$$

$$-\frac{1}{T^{\ell}} \Delta_{\ell,s} \mu_T(T^{\ell}) = -\frac{RT^{\ell}}{T^{\ell}} ln \frac{a^s(T^{\ell})}{a^{\ell}(T^{\ell})} = -R ln \frac{a^s(T^{\ell})}{a^{\ell}(T^{\ell})}$$

$$(7.14)$$

The activity of the salt in the liquid is given at the liquid temperature near the surface, at  $T^{\ell}$ . Since the activity of the salt is more difficult to obtain, the activity of the liquid that would have been in equilibrium with the salt at the temperature  $T^{\ell}$  is taken in Equation 7.14. The activity is calculated from the saturation curve using Pitzer Model.

## Equations of Transport for Crystal Growth

For the surface there is a linear relation between the thermodynamic forces and the conjugate fluxes. In steady state, force-flux relations between the interface (i) and the salt side (s) in terms of resistivities can be written for constant mass flux and almost constant heat flux as follows:

$$-\frac{\Delta_{\ell,s}(T)}{(T^{\ell})^{2}} = R_{qq}^{i,s} J_{q}^{'s} + R_{q\mu}^{i,s} J$$

$$-\frac{1}{T^{\ell}} \Delta_{\ell,s} \mu_{T}(T^{\ell}) = R_{\mu q}^{i,s} J_{q}^{'s} + R_{\mu \mu}^{i,s} J$$
(7.15)

These equations express that there are jumps in the intensive variables like the temperature and the chemical potential at the surface and that  $T^i \neq T^s$ ,  $T^\ell$  as seen in Figure 7.2. This fact is normally not taken into account in the description of phase transitions [Pronk 2006, Mersmann 2001]. In Equation 7.15,  $R^{i,s}_{qq}$  and  $R^{i,s}_{\mu\mu}$  are the two main interface resistivities to heat and mass transfer respectively; and  $R^{i,s}_{q\mu}$  and  $R^{i,s}_{\mu q}$  are the coupling film resistivities for the interface. According to Onsager relations  $R^{i,s}_{q\mu} = R^{i,s}_{\mu q}$  are equal. The "heat of transfer"  $q^{*i,s}$  for the salt side of the surface is defined by the coefficient ratio.

$$q^{*i,s} \equiv \left(\frac{J_q^{is}}{J}\right)_{T^s = T^\ell} = -\frac{R_{q\mu}^{i,s}}{R_{qq}^{i,s}} \tag{7.16}$$

By Equation 7.16, the stationary state heat flux equation is defined as follows:

$$J_{q}^{\prime s} = -\frac{1}{R_{qq}^{i,s}} \frac{\Delta_{\ell,s}(T)}{(T^{\ell})^{2}} + q^{*i,s} J$$
(7.17)

Substituting Equation 7.10 into Equation 7.15, using Equation 7.12 we obtain the following relations between the resistivities for the salt side and the liquid side heat flux [Xu et al. 2006, Kjelstrup et al. 2008]:

$$\begin{split} R_{qq}^{i,s} &= R_{qq}^{i,\ell} \\ R_{q\mu}^{i,s} &= R_{\mu q}^{i,\ell} - \Delta H_{cryst.} R_{qq}^{i,\ell} \\ R_{\mu\mu}^{i,s} &= R_{\mu\mu}^{i,\ell} - 2\Delta H_{cryst.} R_{\mu q}^{i,\ell} + (\Delta H_{cryst.})^2 R_{qq}^{i,\ell} \end{split} \tag{7.18}$$

The heat transfer coefficient ratio  $q^{*i,s}$  for the liquid side of the surface is defined by,

$$q^{*i,\ell} \equiv \left(\frac{J'^{\ell}_{q}}{J}\right)_{T^{s}=T^{\ell}} = -\frac{R^{i,\ell}_{q\mu}}{R^{i,\ell}_{qq}}$$
(7.19)

Equation 7.20 is derived from Equations 7.16 and 7.19 which shows that the assumption of zero cross coefficients violates thermodynamic laws [Kjelstrup et al. 2008].

$$q^{*i,s} - q^{*i,\ell} = \Delta H_{cryst.} \tag{7.20}$$

The fraction of enthalpy carried out via the cooled surface into the salt is defined with the parameter k,

$$k = \frac{q^{*i,s}}{\Delta H_{crvst.}} \tag{7.21}$$

## **EXPERIMENTAL**

## Experimental Setup and Sampling

The schematic drawing of the 10 liter crystallizer and the experimental setup used in this study is shown in Figure 7.3. The top and the vertical sides of the crystallizer are

transparent. The bottom surface of the crystallizer consisted of a vertical metal wall used as heat exchanger to regulate the bulk temperature. The crystallizer was indirectly cooled via circulating ethylene glycol from the Lauda RK 8 KP cooling machine through the heat exchanger. The temperature of the cooling machine was controlled with an accuracy of  $\pm 0.1$ -0.5 °C.

Temperature of inlet ( $T^c_{in}$ ) and outlet ( $T^c_{out}$ ) of the coolant to crystallizer and bulk solution temperatures at four locations in the crystallizer (1.7 mm  $T^1$ , 6.7 mm  $T^2$ , 11.7 mm  $T^3$  and 25 cm  $T^4$  away from the bottom surface) were measured with ASL F250 precision thermometer connected to PT-100 temperature sensors with an accuracy of  $\pm 0.01$  °C and resolution up to  $\pm 0.001$  °C in every 2 seconds. The temperature and coolant flow rate data were collected in a computer using Lab-View data acquisition program. The experimental system was thermal insulated wherever appropriate besides the top part.

The temperature at the bottom surface wall (T<sup>w</sup>) was screened by a thermochromatic liquid crystal (TLC, Hallcrest R33C1W) sheet layer placed over it. TLC, changes its colour with temperature, with a working range between 33- 34 °C. The TLC-sheet is illuminated using a slide projector with a halogen lamp (colour temperature 3400 °K, 320 W). Its light is passed through a linear polarising filter, and then projected via a mirror onto the bottom of the tank under an angle of incidence of 75°. The tank bottom was observed from above through a second polarizer using a Cannon Powershot S2 IS digital photo camera. The two polarizers suppress unwanted reflections on the water surface and small scratches in the TLC-sheet, resulting in more saturated TLC-reflected colours. Inline color screening of TLC surface photographic image series (jpeg-compressed, 2592\*1944 px) were recorded and transferred to a PC every 2 seconds, on which further image processing was done using MatLab, v. 6.0 [Delfos et al. 2002].

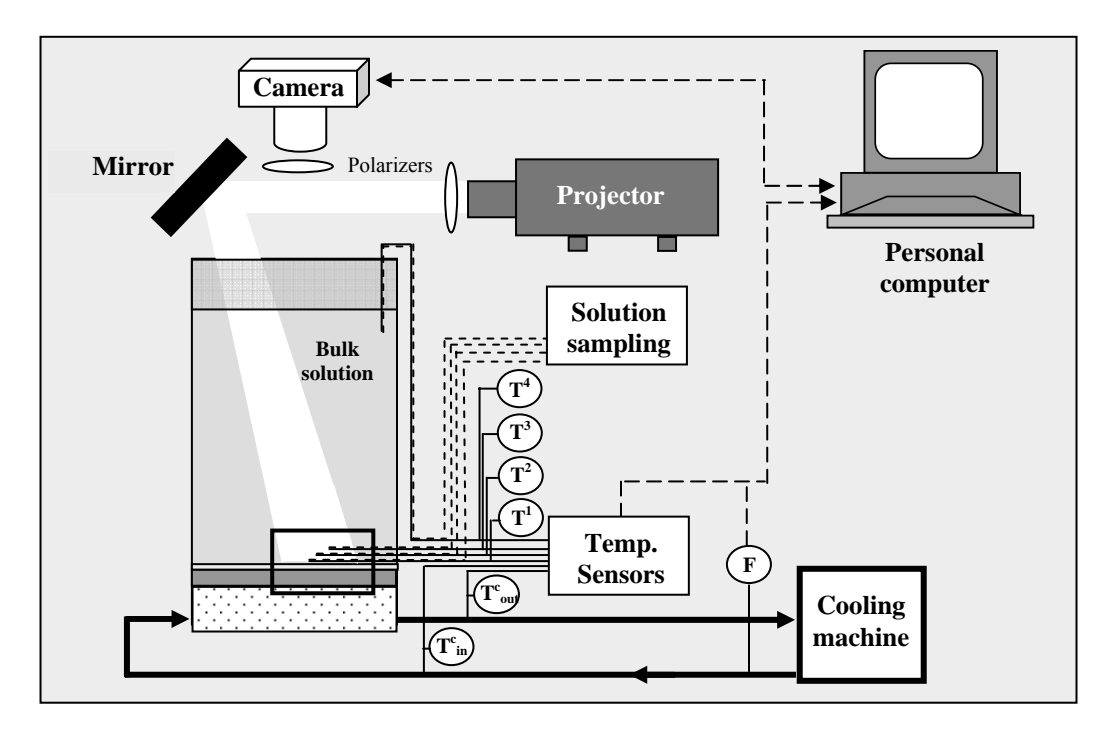


**Figure 7.3:** The schematic view of the experimental setup

Concentration profile within the crystallizer was defined through the solution samples collected from the syringes connected to the wires attached next to the 4 temperature sensors located at 1.7 mm, 6.7 mm, 11.7 mm and 25 cm away from the bottom surface. Collected sample concentrations were determined offline using Inductive Coupled Plasma Atomic Emission Spectrometry (ICP-AES) and Ion Chromatograph with an error of  $\pm 2.5$  %, and picnometer density measurement with an error of  $\pm 0.15$  wt%.

The surface of the crystallizer shown in Figure 7.3 is magnified in Figure 7.4. The temperatures at the cooled surface, metal wall, TLC surface and on salt surface layers are labelled as  $T^c$ ,  $T^w$ ,  $T^{TLC}$  and  $T^s$  correspondingly. The thickness of the stainless steel 316 metal wall and TLC are 1 mm and 0.13 mm respectively. The interface thickness ( $\delta^i$ ) is not known. The interface temperature on the liquid side ( $T^\ell$ ) is determined by linear extrapolation of the liquid temperature to the salt interface.

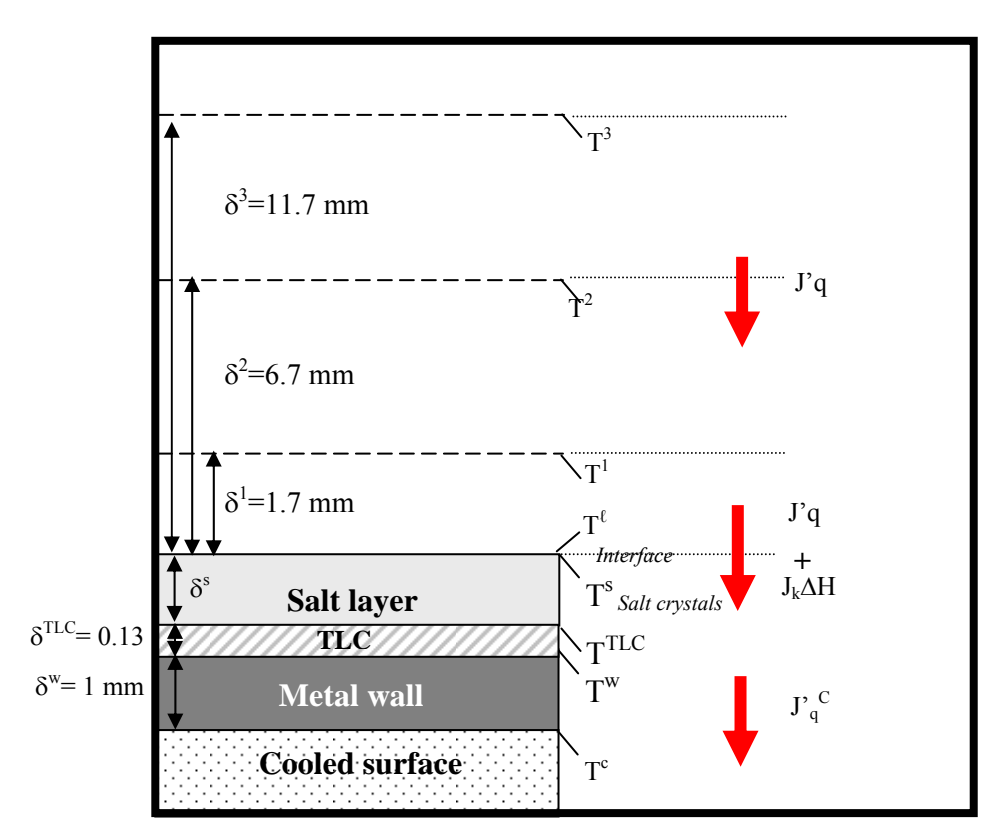


**Figure 7.4:** The magnified view\* of the surface of Figure 7.3.

\*Figure is not drawn proportional to its origin.

k: fraction of the enthalpy of crystallization carried out via the cooled surface, see Equation 7.21

#### **Chemicals**

29.72 wt% MgSO<sub>4</sub> solution, prepared with 99.99 wt% MgSO<sub>4</sub>·7H<sub>2</sub>O (J.T. Baker) and ultra pure water of  $18.2 \text{ m}\Omega$  were used in the experimental setups.

## Experimental Procedure

Calibration: Calibration of the TLC-colours was done in situ during a gradual cool-down and heat-up procedure. Pre-heated MgSO<sub>4</sub> solution was fed into the crystallizer. When  $T^1$  -the first temperature sensor in the bulk- and  $T^w$  -the metal stainless steel metal plate temperature- readings were stabilized at the same value, the picture of the TLC surface was taken. The Red-Green-Blue (RGB) image files were mapped to Hue-Saturation-Intensity (HSI) files using MatLab's rgb2hsv procedure. Based on the Hue values H, we

obtained a one-to-one relationship ('calibration curve') for T vs. H (provided 32.5 °C < T < 36 °C), which was shown to depend hardly on illumination intensity and with an accuracy of  $\pm 0.03$  °C [Delfos et al.2002]. This procedure was repeated many times for absolute TLC color temperature assignment.

Experiment: The pre-heated MgSO<sub>4</sub> solution was fed into the crystallizer and stabilized at 37 °C for 10 minutes. When a homogenous temperature profile was achieved, the solution was cooled down indirectly through the crystallizer's bottom wall as heat flows from the solution to the coolant. Under steady-state conditions and in the presence of any crystals, the temperature profile and the heat flux from the solution into the coolant were continuous. The saturation temperature of the solution for the related MgSO<sub>4</sub> concentration was calculated to be 35.7 °C [Pronk 2006]. When the solution was cooled below its saturation temperature, MgSO<sub>4</sub>·7H<sub>2</sub>O crystallization nucleation on the cold surface was initiated via seeding at time zero. As the epsomite crystallization process is exothermic and generated heat into the system, the temperature profile and heat flux were not continuous anymore. A temperature jump was seen at the locations where crystals nucleate and grow. The crystallization on the cooled surface is visualized by naked eye and by digital pictures. The temperature jump in the interface due to nucleation and growth of MgSO<sub>4</sub>·7H<sub>2</sub>O crystals were confirmed by the calculations using the values of TLC and temperature sensor measurements.

### **DATA ANALYSIS**

The salt surface temperature ( $T^s$ ) was derived from the coolant heat flux given in Equation 7.6, whereas the liquid side temperature ( $T^{\ell}$ ) was calculated via linear extrapolation from the temperature sensor readings located in the bulk ( $T^1$ ,  $T^2$ ,  $T^3$ ) to the interface thickness.

TLC temperature values for crystal growing areas and crystals-free areas were extracted from the pictures.

The thickness of the salt ( $\delta^s$ ) growing into the liquid direction and the mass flux (J) of the crystals were estimated using four different approaches all of which overlap perfectly well with each other. These approaches were using the Image J program for measuring the crystal size changes in time, weighing the crystal amount at the end of the experiment and also doing concentration measurement in the beginning and at the end of the experiment and extracting the mass flux value form Equation 7.10.

The chemical potential difference in Equation 7.15 was calculated using Pitzer model. The program presented by [Pillay et al. 2005] was modified for higher temperature calculations for MgSO<sub>4</sub>·7H<sub>2</sub>O salt application.

The various equations and the constants needed in the calculations are presented in Appendix I.

#### RESULTS AND DISCUSSION

In Figure 7.5, single (a-c)  $MgSO_4 \cdot 7H_2O$  crystal photos on the TLC surface are presented. The transparency property of  $MgSO_4 \cdot 7H_2O$  crystals allows us to follow the temperature profiles of the TLC surface both on crystal-free and for the crystal covered areas. Undistinguished crystal borders on the post-processing temperature images (b)-(d) are supporting this fact. The part of heat (due to heat of crystallization) evolved in the crystal side is transferred both under and near the borders of the crystal on the TLC.

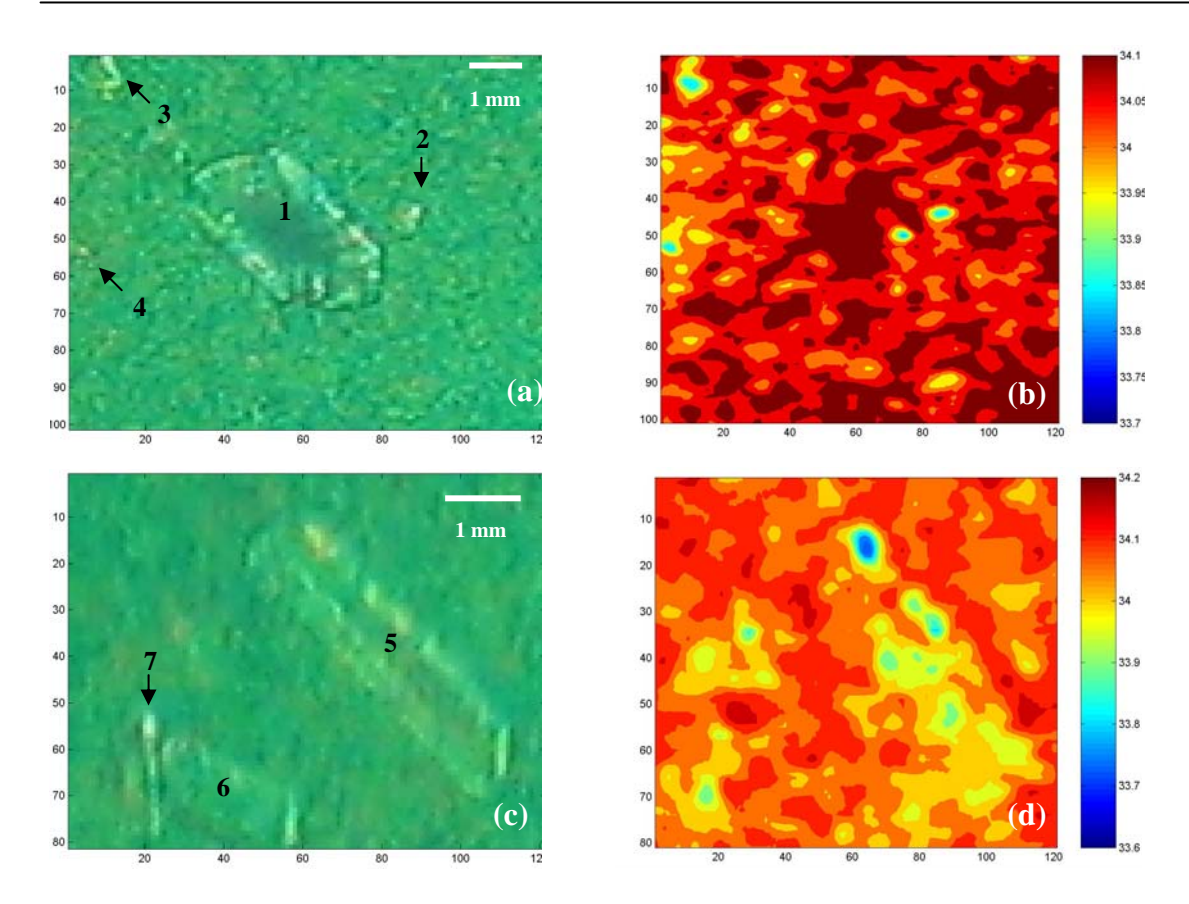
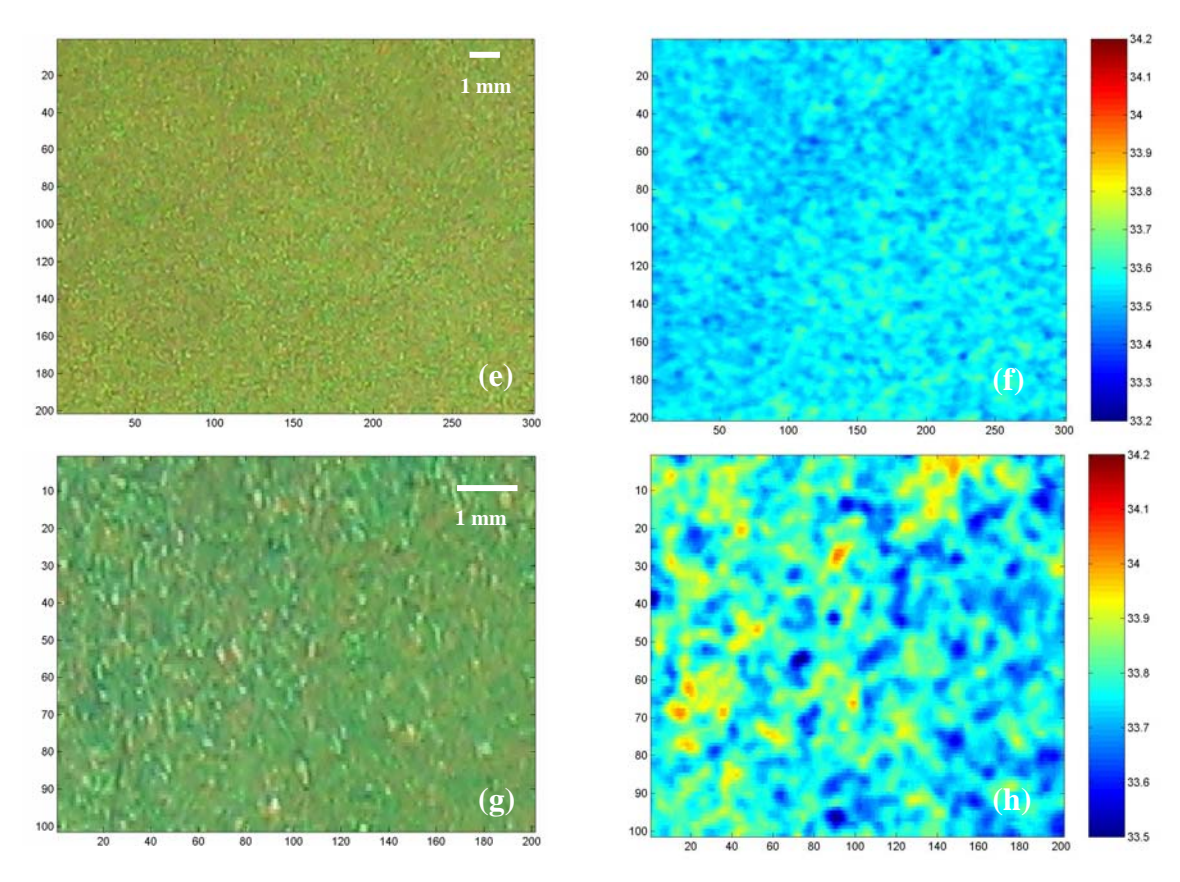


Figure 7.5: (a)-(c) Picture of single crystals (labelled 1 to 7) on the TLC surface
(b)-(d) Crystals post-processing temperature images on the TLC surface
\* 1 pixel is 65μm

Crystallization is a dynamic process in which molecules or ions dissolve and absorb on the crystal surface simultaneously during growth. Therefore warmer or colder temperature readings under the crystals compared to the surrounding is possible before stationary state conditions are established and can be detected in the post-processing temperature images. Figure 7.5(a)-(d) is an example of presenting the single crystal temperature reading on the TLC. It is seen in the photos (a) and (c) under the crystals numbered 1 and 6, the temperature readings are warmer than the surroundings crystal free area. However, for the crystals numbered 2-5 and 7 the under crystal temperature readings are colder than their surroundings. Additionally the different optical properties such as the refractive index and the morphology of the crystal may affect the subjected crystal temperature readings.

The effect of heat generated from heat of crystallization and transported through the crystal is not only conducted under the crystal but also evolved in the horizontal direction of the TLC. Therefore the TLC temperature reading collected near the crystals does not represent the TLC temperature reading for crystal free area.



**Figure 7.6:** Picture of crystal free (e) and crystal covered (g) areas on the TLC surface and their post-processing temperature images (f), (h)

\* 1 pixel is 65µm

Taking into account of all those facts, the temperature data collection from TLC readings using single crystal values was avoided. Instead, the representative temperature readings were collected for the same moment from two different areas covered with and without crystals. By using *crystal group average temperature values*, these little variations due to the optical properties and heat distribution in the horizontal direction of the TLC are minimized and included in the accuracy of  $\pm 0.03$  °C. In Figure 7.6(e) a photo for the crystal-free area and in (f) its post-processing temperature images are presented. The

averaged TLC temperature reading for crystal free areas for this moment is determined as 33.6 °C. For the same moment, an area covered with crystals and its post-processing temperature image is also presented in Figures 7.6(g) and (h) respectively with an average temperature reading value of 33.75 °C.

The interface, salt layer,  $T^1$  and  $T^2$  locations versus time are shown in Figure 7.7. The time zero refers to the seeding moment.

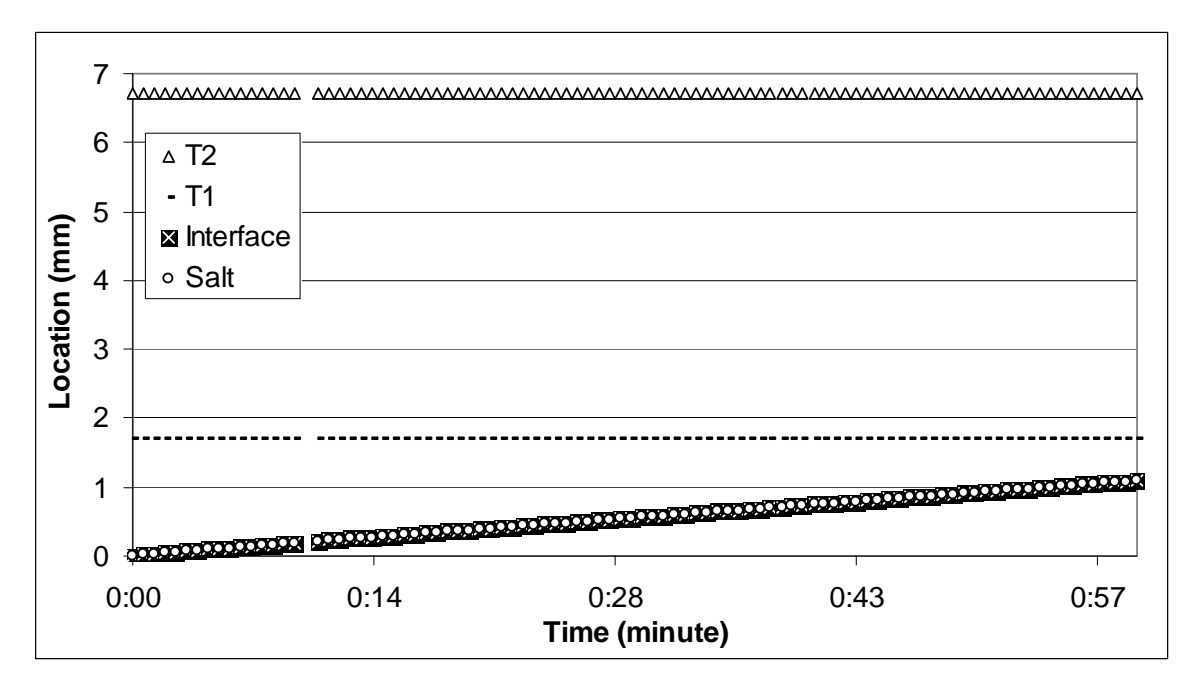


**Figure 7.7:** Location of  $T^1$ ,  $T^2$  temperature sensor and  $T^s$ ,  $T^{\ell}$  temperature locations versus time.

The temperature readings and the results obtained following the procedure described in Data Analysis section are presented in Figure 7.8. Temperature jumps across the interface  $T^{\ell}$ - $T^{s}$  are calculated 0.2 °C.

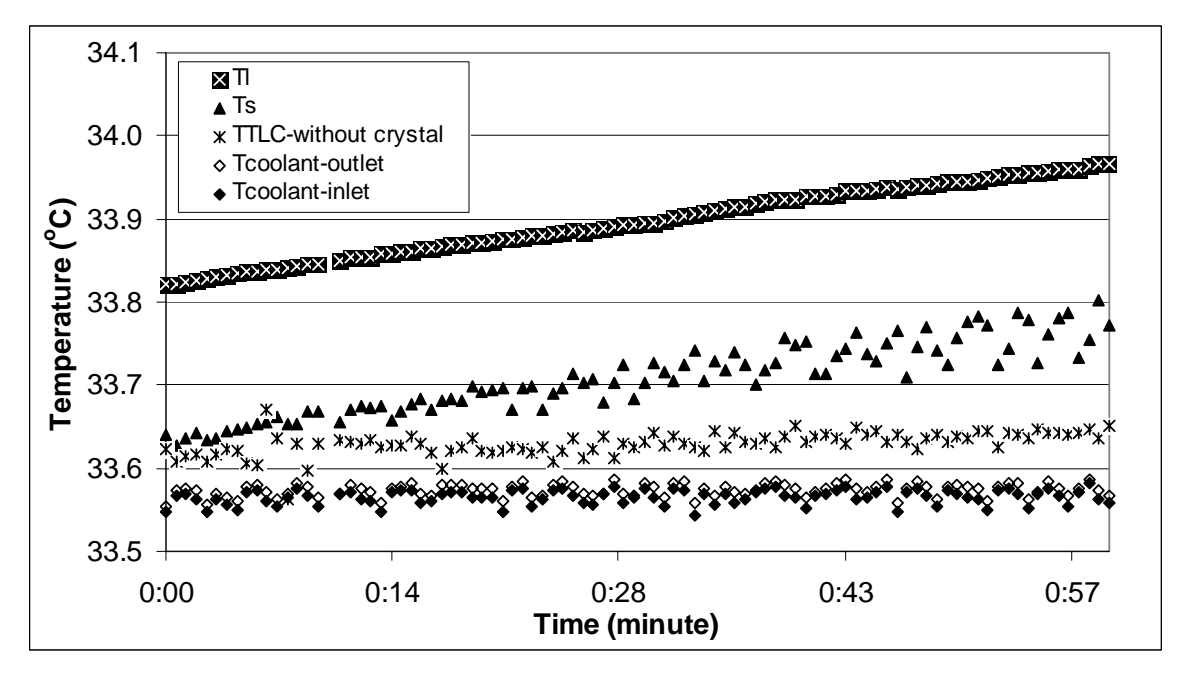


**Figure 7.8:** Coolant ( $T_{inlet}$ ,  $T_{outlet}$ ),  $T^{TLC}$ -without crystal,  $T^s$  and  $T^\ell$  temperatures versus time.

The indications of consistency of our measurement are listed below.

- The coolant inlet temperature has lower values than the coolant outlet temperature,
- The measured wall and calculated wall temperatures were always equal to each other,
- The T<sup>TLC</sup>-<sub>without crystal</sub> (crystal free area on TLC) temperature measurements were constant during the entire experiment.
- As discussed before, the crystals shapes can not be detected in the TLC post-processing temperature images (see Figures 7.5(a)-(d)). This is due to the transparency property of MgSO<sub>4</sub>·7H<sub>2</sub>O crystals. This property allows us to use temperature readings under the crystals.

The heat of transfer for the salt side divided by the enthalpy of crystallization, the ratio k, was presented in Figure 7.9. The ratio is calculated using the coupling coefficient ratio over the resistivity to heat transfer at zero salt growth formulated in Equation 7.16.

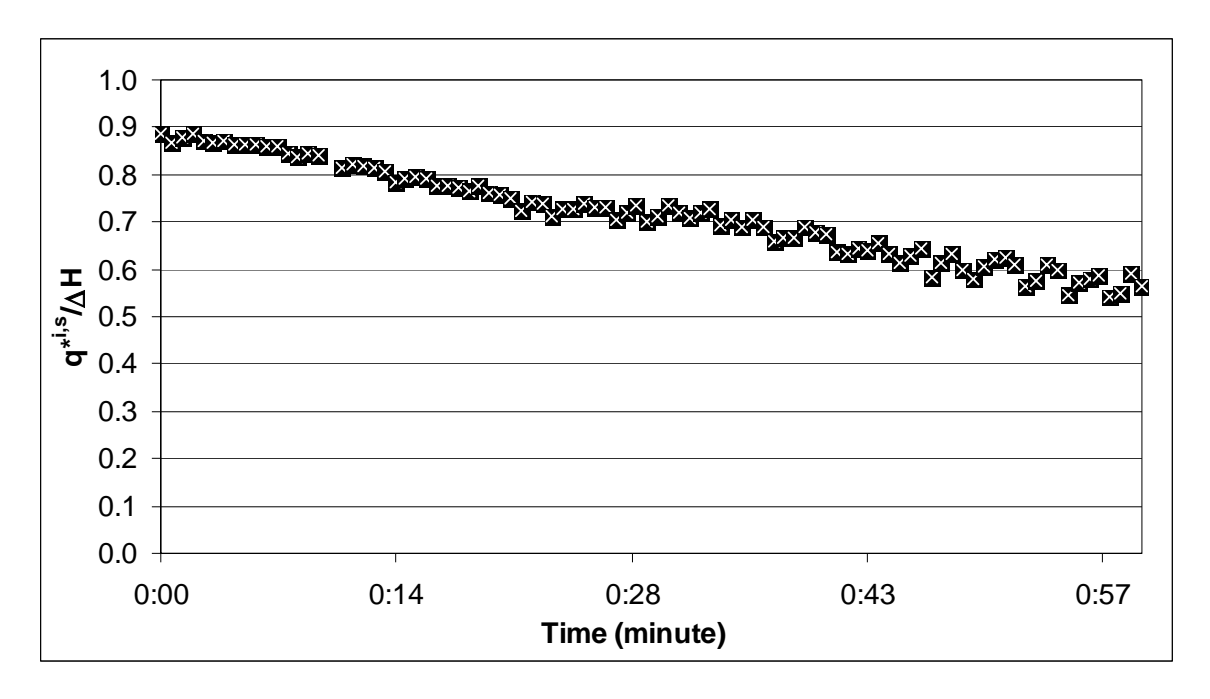


Figure 7.9: The fraction of the enthalpy of crystallization that returns to the solid side

In crystallization calculations [Pronk 2006, Mersmann 2001] it is frequently assumed that all of the heat of crystallization is transferred into the cold side (i.e. to the salt side). In Figure 7.9, the calculated heat of transfer divided by the enthalpy of crystallization  $q^{*i.s}/\Delta H$  is presented to show the error one can do using this assumption. It is clear that typically 70-80% of this heat is transferred into the solid side whereas 20-30% of this latent heat is released is transferred back into the liquid side during MgSO<sub>4</sub>·7H<sub>2</sub>O crystallization. The assumption of sending all the heat of phase transition to the cold side may be quantified by this method of description. While the error may not seem very big in this case, it is case dependent, and might well be larger in other systems.

The description allows also for calculation of  $R_{\mu\mu}$ , the interface mass resistivity, using equation 7.15 and the coupling coefficients  $R_{q\mu} = R_{\mu q}$ . By taking advantage of the Onsager set of equations, we have a new alternative to overcome (resolve) the difficulty of finding the temperature jump in the absence of a heat flux.

In the Appendix 7.1, the input values are shown. In Table 7.1, calculated driving forces and the coefficients for one time period during the experiment is presented. The interface resistivity coefficients for heat transfer ( $R_{qq}$ ) and mass transfer ( $R_{\mu\mu}$ ) are calculated as  $2.1 \times 10^{-7}$  m<sup>2</sup>.K<sup>-1</sup>.W<sup>-1</sup> and  $1.26 \times 10^3$  J. m<sup>2</sup>.s.K<sup>-1</sup>.mol<sup>-2</sup> respectively. The coupling film resistivity coefficients ( $R_{q\mu} = R_{\mu q}$ ) are calculated -3.88×10<sup>-3</sup> m<sup>2</sup>.s.K<sup>-1</sup>mol<sup>-1</sup>.

It is now possible to calculate the minimum chemical driving force, or degree of supersaturation at the temperature near the phase boundary that is needed to overcome the temperature jump before crystallization can take place. We obtain from Equation 7.15 for J=0 the criteria to have MgSO<sub>4</sub>·7H<sub>2</sub>O crystallization:

$$\frac{\Delta_{s,\ell}(T)}{T^{\ell}} \le 0.5 \times 10^{-4} \Delta \mu_T(T^{\ell}) \tag{7.22}$$

This inequality explains that crystallization may be hindered, not only by activation energy, but also by thermal force acting in an unfavourable way. Such a relation may help us to explain scaling formation on cold surfaces.

From Equation 7.15 a relation between the coolant side heat flux and mass flux can be derived.

$$J = -\frac{1}{T^{\ell}} \Delta \mu_T(T^{\ell}) \frac{1}{R_{\mu\mu}^{i,s}} - \frac{R_{\mu q}^{i,s}}{R_{\mu\mu}^{i,s}} J_q^{'s}$$
(7.23)

Equation 7.23 presents that a bigger the heat flux on the salt side promotes crystallization. In other words when the cooling rate is larger, the growth rate of the crystals increases. Mass transfer on to the crystal surface becomes more difficult if  $\Delta_{s,\ell}(T)$  becomes too large and  $J_q^{-1s}$  is reduced on the cost of  $J_q^{-1\ell}$ .

An analogy between conductive heat transfer coefficient ( $\lambda$ ) and heat resistivity ( $R_{qq}$ ) can be derived. The general heat transfer flux (q'') relation according to Fourier's law is

proportional to the temperature  $(\frac{\Delta T}{\Delta z})$  gradient in the direction of the heat transfer and the thermal conductivity coefficient ( $\lambda$ ) [Incropera et al.1990].

$$q'' = -\lambda \frac{\Delta_{\ell,s}(T)}{\Delta z} \tag{7.24}$$

The force-flux relation in case of no mass transport can be simplified from Equation (7.15) and heat flux  $(J_q^{'s})$  can be defined as a function of heat resistivity  $(R_{qq}^{i,s})$  and temperature difference.

$$J_{q}^{'s} = -\frac{1}{R_{qq}^{i,s}} \cdot \frac{\Delta_{\ell,s}(T)}{(T^{\ell})^{2}}$$
(7.25)

Equalling Equations (7.24) and (7.25) knowing that  $q'' = J_q^{'s}$ , the conduction heat transfer coefficient can be written in terms of heat resistivity as shown in Equation (7.26).

$$\lambda = \frac{\Delta z}{R_{qq}^{i,s} (T^{\ell})^2} \tag{7.26}$$

 $\Delta z$  is assumed 0.3 µm as the interface thickness ( $\delta^{1}$ ) value. Using bulk side interface temperature and heat resistivity, the thermal conductivity coefficient ( $\lambda$ ) calculated as  $1.5 \times 10^{-5} \text{ W.m}^{-1}.\text{K}^{-1}$  which is lower than bulk thermal conductivity value calculated for water-MgSO<sub>4</sub> system relation deduced from Melinder having value of 0.6 W.m<sup>-1</sup>.K<sup>-1</sup> [Melinder 1997, Pronk 2006]. By replacing the bulk thermal conductivity value in Equation 7.26 the interface thickness is calculated 12 mm.

Similar analogy can be derived between convective mass transfer coefficient  $(D_{AB})$  and mass resistivity  $(R_{\mu\mu})$ . The general molar mass transfer flux  $(N_A')$  relation according to Fick's law presented in Equation (7.27) is proportional to the molar concentration gradient  $(\frac{\Delta C_A}{\Delta z})$  and the convection mass transfer coefficient  $(D_{AB})$  [Incropera et al. 1990].

$$N_A' = -D_{AB} \frac{\Delta C_A}{\Delta z} \tag{7.27}$$

The force-flux relation in case of no heat transport can also be simplified from Equation (7.15) and mass flux (J) can be defined as a function of heat resistivity ( $R_{\mu\mu}^{i,s}$ ) and chemical potential or in other worlds concentration differences.

$$J = -\frac{1}{R_{\mu\mu}^{i,s} T^{\ell}} \Delta_{\ell,s} \mu_{T}(T^{\ell}) = -\frac{1}{R_{\mu\mu}^{i,s} T^{\ell}} R T^{\ell} \frac{\Delta_{\ell,s}(C)}{C^{\ell}}$$
(7.28)

Equalling Equations (7.27) and (7.28) knowing that  $N_A' = J$ , the convection mass transfer coefficient can be written in terms of mass resistivity as shown in Equation (7.29).

$$D_{AB} = \frac{\Delta z R}{R_{\mu\mu}^{i,s} C^{\ell}} \tag{7.29}$$

Choosing the  $\Delta z$  value as assuming the interface thickness 0.3  $\mu$ m ( $\delta^i$ ), and using the C<sup> $\ell$ </sup> concentration 2.33 mol/m<sup> $\delta$ </sup>, the  $D_{AB}$  is calculated as  $8.5 \times 10^{-10}$  m<sup> $\delta$ </sup>/s. This value is comparable to diffusion coefficient of water-MgSO<sub> $\delta$ </sub> system relation deduced from Gmelin and Lobo for same concentration and temperature by having the value of  $8.8 \times 10^{-10}$  m<sup> $\delta$ </sup>.s<sup>-1</sup> [Gmelin 1952, Lobo 1989, Pronk 2006].

**Table 7.1:** Summary of the crystallization experiments

<b>Driving forces</b>		Unit
$n rac{a^s(T^\ell)}{a^\ell(T^\ell)}$		
$ma^{\ell}(T^{\ell})$	-0.30	-
$\Delta_{\ell,s}\mu_{T}(T^{\ell}) = RT^{\ell} \ln \frac{a^{s}(T^{\ell})}{a^{\ell}(T^{\ell})}$	-768.58	J.mol <sup>-1</sup>
$-\frac{\varDelta_{\ell,s}T}{(T^{\ell})^2}$		
$(T^{\ell})^2$	$2.02 \times 10^{-6}$	K <sup>-1</sup>
Coefficients		Unit
$ig  R_{qq}^{i,s}$	2.10×10 <sup>-7</sup>	$m^2.K^{-1}W^{-1}$
$R_{q\mu}^{i,s}=R_{q\mu}^{i,s}$	$-3.88 \times 10^{-3}$	m <sup>2</sup> .s.K <sup>-1</sup> mol <sup>-1</sup>
$R^{i,s}_{\mu\mu}$	$1.26 \times 10^{3}$	J.m <sup>2</sup> .s.K <sup>-1</sup> mol <sup>-2</sup>
h	$1.5 \times 10^{-5}$	W. m <sup>-2</sup> .K <sup>-1</sup>
$D_{AB}$	$8.5 \times 10^{-10}$	$\mathrm{m}^2.\mathrm{s}^{-1}$
Calculated values		Unit
	$1.84 \times 10^4$	J.mol <sup>-1</sup>
$q^{*,s}/\Delta H$	0.77	
1 9	$-5.57 \times 10^3$	J.mol <sup>-1</sup>
$q^{*,\ell}/\Delta H$	-0.23	

## **CONCLUSION**

Crystallization is mostly an exothermic process. According to irreversible thermodynamics, the heat released during crystallization at the interface is distributed to both the liquid and solid phases which are in contact with the interface also for isothermal conditions. We present the temperature jump between the solid and the liquid side of the interface and the heat of transfer for both sides of the surface, using For MgSO<sub>4</sub>·7H<sub>2</sub>O crystal growth on a cold surface as example. For epsomite crystal growth rate of  $2.33 \times 10^{-3}$  mol.m<sup>-2</sup>.s<sup>-1</sup>, around 20-30% of the heat of crystallization is calculated to be transferred back into the liquid side. The interface resistivity to mass transfer ( $R_{qq}^{i,s}$ ) is  $1.26 \times 10^3$  J.m<sup>2</sup>.s.K<sup>-1</sup>.mol<sup>-2</sup>, while the interface resistivity to heat transfer ( $R_{qq}^{i,s}$ ) is  $2.1 \times 10^{-7}$  m<sup>2</sup>.K<sup>-1</sup>.W<sup>-1</sup>. This is the first time of coupling heat and mass transfer equation at liquid-solid interface description and heat of distribution calculation during crystallization is documented.

**Appendix 7.1:** Equations and constants

Constants		Unit
Cp <sup>freezium</sup>	$= 0.00274T(^{\circ}C) + 2.818$	kJ.kg <sup>-1</sup> .K <sup>-1</sup>
$\rho^{\text{freezium}}$	$=-0.4T(^{\circ}C)+1289$	kg.m <sup>-3</sup>
<sup>*</sup>	$= 5.6 \times 10^{-1} + 2 \times 10^{-3} (T) - 6.9 \times 10^{-6} (T)^{2}$	kg.iii
$\lambda_{aq}^{MgSO_4}$ [T (°C), C= wt%]		1 1
	$-6.4 \times 10^{-4} (C) - 2.3 \times 10^{6} (C)(T) + 7.8 \times 10^{-9} (C)(T)^{2}$	W.m <sup>-1</sup> .K <sup>-1</sup>
$\lambda_{salt}^{MgSO_4}$ [Thermtest 2007]	2.427	$W.m^{-1}.K^{-1}$
netal=wall		
$\lambda_{solid}^{metal=wall}$	5	$W.m^{-1}.K^{-1}$
$\lambda_{solid}^{TLC}$	0.16	$W.m^{-1}.K^{-1}$
A TT MgSO.	0.10	W.III .K
$\Delta H_{cryst.}^{MgSO_4}$	395	J.kmol <sup>-1</sup>
$C_{eq}^{MgSO_4}$	$= 21.3 + 0.206 \times T(^{\circ}C) + 0.000833 \times T^{2}(^{\circ}C)$	wt%
A <sup>cold surface</sup>	0.031	$m^2$
$\delta^w$	5	mm
$\delta^{TLC}$	0.13	mm
$A_{cooled}$	0.0314	$m^2$
$\rho_{salt}$	1680	kg.m <sup>-3</sup> (for MgSO <sub>4</sub> ·7H <sub>2</sub> O)
Measured data		Unit & Source
T <sup>c</sup> <sub>in</sub>	33.572	°C (PT100)
$T_{\text{out}}^{\text{c}}$ $T^{TLC}$	33.579	°C (PT100)
$T^1$	33.666	°C (photos-without crystal) °C (PT100)
$\begin{array}{ c c c c c c c c c c c c c c c c c c c$	33.933	,
$\begin{array}{c} 1 \\ T^3 \end{array}$	34.274 34.805	°C (PT100) °C (PT100)
F <sup>coolant</sup>	374.60	l.h <sup>-1</sup>
$\delta^{s}$	0.35	mm
	0.55	
Calculated values		Unit
T <sup>c</sup> log	33.575	°C
Cnfraggium	3.659	kJ.kg <sup>-1</sup> .K <sup>-1</sup>
T <sup>TLC</sup> without crystal	33.625	°C
1	33.681	°C
$T^\ell$	33.869	°C
J	2.33×10 <sup>-3</sup>	mol.m <sup>-2</sup> .s <sup>-1</sup>
J'cq	108.20	W.m <sup>-2</sup>
J' <sub>q</sub>	52.37	W.m <sup>-2</sup>
$J\Delta H_{cryst.}$	55.83	$W.m^{-2}$ $W.m^{-2}$
$J_q^{'\ell}$	31.02 0.937	W.m <sup>-2</sup> (for no mass flux)
$a_{w-\ell}$	0.937	
$egin{aligned} a_{Mg-\ell} \ a_{SO4-\ell} \end{aligned}$	0.093	
$a_{\text{W-S}}$	0.945	
$a_{\text{W-S}}$ $a_{\text{Mg-S}}$	0.085	
$a_{SO4-s}$	0.085	
**3U4-8		

## **List of Captions**

List of Symb	ols			
а	activity	-		
C	concentration	mol.m <sup>-3</sup>		
Ср	specific heat	kJ.kg <sup>-1</sup> .K <sup>-1</sup>		
$D_{AB}$	convection mass transfer coefficient	$m^2.s^{-1}$		
$\Delta H_{cryst.}$	Heat of crystallization	J.mol <sup>-1</sup>		
h cryst.	convection heat transfer coefficient	$W.m^{-2}.K^{-1}$		
J	mass flux	$mol.m^{-2}.s^{-1}$		
$J'_q$	heat flux	J.m <sup>-2</sup> .s <sup>-1</sup>		
k	enthalpy fraction transferred to the coolant side	-		
N <sub>A</sub> '	convective mass flux	$mol.s^{-1}.m^{-2}$		
R	ideal gas constant	J.K <sup>-1</sup> . mol <sup>-1</sup>		
$R_{qq}^{i,s}$	heat transfer resistivity of the surface to the salt side	$m^2.s^1.J^{-1}.K^{-1}$		
$R^{i,s}_{\mu\mu}$	mass transfer resistivity of the surface to the salt side	J.K <sup>-1</sup> . mol <sup>-2</sup> . m <sup>-2</sup> .s <sup>-1</sup>		
$R_{q\mu}^{i,s}=R_{q\mu}^{i,s}$	coupling film resistivities of the surface to the salt side	$m^2.s^1.mol^{-1}.K^{-1}$		
$R_{qq}^{i,s}$	heat transfer resistivity of the surface to the liquid side	$m^2.s^1.J^{-1}.K^{-1}$		
$R^{i,s}_{\mu\mu}$	mass transfer resistivity of the surface to the liquid side	J.K <sup>-1</sup> . mol <sup>-2</sup> . m <sup>-2</sup> .s <sup>-1</sup>		
$R_{q\mu}^{i,s}=R_{q\mu}^{i,s}$	coupling film resistivities of the surface to the liquid side	$m^2.s^1.mol^{-1}.K^{-1}$		
q"	convective heat flux	W.m <sup>-2</sup>		
q* <sup>i,s</sup>	heat of transfer coefficient ratio to the salt side of the surface	J.mol <sup>-1</sup>		
$q^{*i,\ell}$	heat of transfer coefficient ratio to the liquid side of the surface	J.mol <sup>-1</sup>		
T	temperature	°C		
Z	distance from the salt surface	m		
Greek symbo	Greek symbols			
δ	thickness	μm, mm		
λ	thermal conductivity	$W.m^{-1}.K^{-1}$		
$\mu$	chemical potential	J. K <sup>-1</sup>		
v	measured velocity, salt growth rate	$\mathrm{m.s}^{-1}$		
$\rho$	density at the given condition	kmol.m <sup>-3</sup>		
σ	entropy production	$W.m^{-2}.K^{-1}$		
Sub-Superscripts				
c	coolant			
i	interface			
$\ell$	liquid			
S	salt			
TLC	thermo liquid crystal			

#### REFERENCES

- Albanoet al. 1987 Albano, A. M.; Bedeaux, D.; Non-equilibrium eletrothermodynamics and polarizable multicomponent fluid with an interface, *Physica A.* 1987, 147:407-435.
- Badam et al. 2007 Badam, V. K.; Kumar, V.; Durst, F.; Danov, K.; Experimental and theoretical investigations on interfacial temperature jumps during evaporation, *Experimental Thermal and Fluid Sciences*. In press, 2007.
- Bedeaux et al. 1976 Bedeaux, D.; Albano, A. M.; Mazur, P.; Boundary conditions and nonequilibrium thermodynamics, *Pyhsica A.* 1976, 82: 438-462.
- Bedeaux 1986 Bedeaux, D.; Non-equilibrium thermodynamics and statistical physics of surface, *Adv. Chem. Phys.* 1986, 64:47-109.
- Bedeaux et al. 1999 Bedeaux, D.; Kjelstrup, S.; Transfer coefficients for evaporation, *Physica A*. 1999, 270, 413-426.
- Bedeaux et al. 2005 Bedeaux, D.; Kjelstrup, S.; Heat, Mass and Charge Transport, and Chemical Reactiona at Surfaces, *Int. J. of Thermodynamics*. 2005, Vol. 8, (No. 1), pp. 25-41.
- Chandler 1964 Chandler, J. L.; Effect of supersaturation and flow conditions on the initiation of scale formation, *Transaction of the Institution of Chemical Engineers*, 1964, 42, 24-34.
- Chen et al. 1997 Chen, X. C.; Chen, P.; Free, K. W.; A note on the two models of ice growth velocity in aqueous solutions derived from an irreversible thermodynamics analysis and the conventional heat and mass transfer theory, *Journal of Food Engineering*. 1997, 31, 395-402.
- Delfos et al. 2002 Delfos, R.; Lagerwaard, R.; Roos, M.; Bottom temperature structure in low-conductivity Rayleigh-Benard convection, *EUROTHERM-71 Visualization, Imaging and Data Analysis in Convective Heat and Mass Transfer*—October 28-30 2002, Reims- France.
- Flesland 1995 Fleslands, O.; Freeze concentration by layer crystallization, *Drying Technology.* 1995, 13 (8&9), 1713-1739.

- Genceli et al. 2007 Genceli, F. E.; Lutz, M.; Spek, A. L.; Witkamp G. J.; Crystallization and Characterization of a New Magnesium Sulfate Hydrate MgSO<sub>4</sub>·11H<sub>2</sub>O-, *Crystal Growth & Design*. 2007, 7(12), 2460-2466.
- Gibbs 1961 Gibbs, J. W.; *The Scientific Papers of J.W. Gibbs.* Dover, New York, 1961.
- Gmelin 1952 *Gmelins Handbuch der Anorganschen Chemie.* 8<sup>th</sup> ed., Deutsche Chemische Gesellschaft, Weinheim: Verlag Chemie.
- Goldman et al. 1981 Goldman, G.; Spott, G.; Krustenbildung in kristallisationsangen: eine neue praxisnahe Meßmethode, *Chemie Ingenieur Technik*, 1981, 53, 713-716.
- Ham et al. 2004 Van der Ham, F.; Seckler, M. M.; Witkamp, G. J.; Eutectic Crystallization in a Newly Design Crystallizer: The Cooled Disk Column Crystallizer, *Chem. Eng. Process.* 2004, 43(2), 161.
- Hodgman 1972 Hodgman, C. D.; *Handbook of Chemistry and Physics*. 64<sup>th</sup> ed., 1972.
- Incropera et al. 1990 Incropera, F. P.; De Witt, D. P.; *Fundamentals of Heat and Mass Transfer*. John Wiley & Sons, 3<sup>rd</sup> ed., 1990.
- Kjelstrup et al. 1996 Kjelstrup Ratkje, S.; Bedeaux, D.; The overpotential as a surface singularity described by nonequilibrium thermodynamics, *Journal of the Electrochemical Society*. 1996, 143(3), 779-89.
- Kjelstrup et al. 2008 Kjelstrup, S.; Bedeaux, D.; *Non-equilibrium thermodynamic of heterogeneous systems*. Series on Advances in Statistical Mechanics, Vol. 16, World Scientific, Singapore, 2008.
- Lobo 1989 Lobo, V. M. M.; *Handbook of Electrolyte Solutions*. Amsterdam: Elsevier, 1989.
- Lunardini 1991 Lunardini, V. J.; *Heat Transfer with Freezing and Thawing*. Elsevier Science Publication Co., Amsterdam, 1991.
- Mark et al. 1981 Mark, H. F., et al.; *Kirk-Othmer Enyclopedia of chemical technology.*, 3<sup>rd</sup> ed., Vol. 14, 1981.

- Melinder 1997 Melinder, Å; *Thermophysical Properties of Liquid Secondary Refrigerants. Charts and Tables.* Paris: International Institute of Refrigeration, 1997.
- Mersmann 2001 Mersmann, A.; *Crystallization Technology Handbook*, Second edition. New York: Marcel Dekker Inc., 2001.
- Pillay et al. 2005 Pillay, V.; Gaertner, R. S.; Himawan, C.; Seckler, M. M.; Lewis, A. E.; Witkamp, G. J.; MgSO<sub>4</sub>+H<sub>2</sub>O System at Eutectic Conditions and Thermodynamic Solubility Products of MgSO<sub>4</sub>.12H<sub>2</sub>O(s) and MgSO<sub>4</sub>.7H<sub>2</sub>O(s), *J. Chem. Eng. Data.* 2005, 50(2), 551-555.
- Pronk 2006 Pronk, P.; Fluidized bed heat exchangers to prevent fouling in ice slurry systems and industrial crystallizers. PhD Dissertation, Delft University of Technology: The Netherlands, 2006.
- Qin, F. G. F.; Chen, X. D.; Russel, A. B.; Heat transfer at the Subcooled-Scraped Surface with/without Phase Change, *AIChE Journal*. 2003, Vol. 49, No.8, 1947-1955.
- Qin et al. 2004 Qin, F. G. F.; Chen, X. D.; Farid, M. M.; Growth kinetics of ice films spreading on a subcooled solid surface, *Separation and Purification Technology*. 2004, Vol 39, 109-121.
- Ratkje et al. 1995 Ratje, S. K.; Flesland, O.; Modelling the freeze concentration process by irreversible thermodynamics, *J. Food Eng.* 1995, 25, 553-567.
- Thermtest 2007 Thermal conductivity database of materials http://www.thermtest.com
- Toussaint et al. 1974 Toussaint, A. G.; Donders, A. J. M.; The mixing criterion in crystallization by cooling, *Chemical Engineering Science*, 1974, 29, 237-245.
- Vaessen et al. 2003 Vaessen, R. J. C.; Janse; B. H. J.; Seckler, M. M.; Witkamp, G. J.; Evaluation of the Performance of a newly developed eutectic freeze crystallizer: Scraped Cooled Wall Crystallizer, *Trans. IChemE.* 2003, 81(A), 1363.
- Veverka et al. 1979 Veverka, F., Nyvlt, J.; Growth of scale on a cooling surface during the stirring of a crystal suspension, *Chemiky Prumysl*, 1979, 29, 123-127, 580-582, 623-626.

- Wedekind 2006 Wedekind, J.; *Nano-Droplets at birth Computer Experiments on Gas Phase Nucleation*. PhD Dissertation, University of Koln: Germany, ISBN 10: 3-86727-084-4, ISBN 13: 978-3-86727-084-7, 2006.
- Xu et al. 2006 Xu, J.; Kjelstrup, S.; Bedeaux, D.; Røsjorde, A.; Rekvig, L.; Verification of Onsager's reciprocal relations for evaporation and condensation using non-equilibrium molecular dynamics, *Journal of Colloid and Interface Science*. 2006, 299, 455-463.

# Chapter 8

# Cyclic Innovation Model Application:

## Eutectic Freeze Crystallization

## Cyclic Innovation Model Application: Eutectic Freeze Crystallization

## F. Elif Genceli<sup>a</sup>, Dap Hartmann<sup>b</sup>, Geert-Jan Witkamp<sup>a</sup>, Guus Berkhout<sup>b</sup>

Part 2 within a series *Innovating the Innovation* by Berkhout, Hartmann et al.

Prepared for publication in Separation and Purification Technology

<sup>&</sup>lt;sup>a</sup> Process Equipment. 3ME, Delft University of Technology, Delft-The Netherlands

<sup>&</sup>lt;sup>b</sup> Management & Governance Department, Delft University of Technology, Delft-The Netherlands

## **ABSTRACT**

Separation technology is a key enabler in medical, mining, food, paper, chemical, pharmaceutical and biotechnological processes. With a perfect separation, no waste is generated while the best quality product is produced. Separations, however, are costly in terms of equipment and power consumption. In the process industry more than half of the overall costs are due to separations. In virtually all cases, the actual power consumption far exceeds the exergy amount. It is estimated that yearly almost 10<sup>20</sup> J could be saved by more efficient separations of salts or acids from aqueous systems alone. Moreover, huge amounts of valuable industrial aqueous streams that are currently too energy intensive to be treated and are disposed of, could be decomposed into valuable materials instead, if only the separation technology to do so were available.

For the industrial or waste streams containing moderate to higher salt or acid concentrations, Eutectic Freeze Crystallization (EFC) is a very promising technology for perfect separation. EFC turns a solution into pure ice and pure salts and/or acids, at 100% efficiency (apart from a bleed stream) and saves up to 90% (typically 50%) of the energy costs compared to evaporative crystallization. In addition, the low operating temperature allows for cheap construction steel to be used, avoids decomposition of organics, is sanitary favourable and is very safe for process operators. EFC not only can replace existing technologies, but is also enables completely new processes to be designed, as it constitutes a new unit operation.

A consortium including scientists, users and an equipment manufacturer has recently developed an efficient EFC technology to a pilot plant scale. Now it is time to accelerate the transition of this science-based technological knowledge into a green business. A very helpful methodology to do that is described by the Cyclic Innovation Model (CIM), which was developed from real-life experience [Berkhout 2006]. CIM describes a process of *multi-value innovation* by coupled cycles of change, connecting science and business in a symbiotic manner. This chapter describes how such an acceleration of turning technology into business can be achieved. We will illustrate this with three concrete examples.

## INTRODUCTION

Many regular industrial process or waste streams -for example from the chemical process industry, (hydro-)metallurgy, electronics industry, biological industry, food industry, agricultural industrial- contain high concentrations of dissolved salts and/or acids (throughout the text for "salts" also "acids" can be read). Recovery of these salts is important for economic and environmental reasons. Separation processes are essential for almost every industrial process, either for the recovery of the salts in the production step or for the reduction of waste streams in the purification step.

High energy consumption is the major drawback for most of the current separation technologies. In addition, current separation technologies are rarely 100% selective. In the process industry more than half of the costs both for equipment and for energy are spent on separations. In most cases, the energy consumption far exceeds the theoretically required amount, where a factor of hundred is no exception. Development and implementation of more efficient technologies is necessary to save roughly  $10^{20}$  J/y (almost  $10^{10}$  barrels of oil equivalent, or about  $10^{13}$  kg CO<sub>2</sub> emission), currently consumed for separations of salts or acids from aqueous systems [Energy 2004], and for environmental reasons. Moreover, huge amounts of valuable industrial aqueous streams that are currently too energy intensive to be treated (and are therefore disposed of) can be considered as raw materials when the right separation technology becomes available. New aqueous separation technologies also will allow completely new, more efficient process flow diagrams to be designed.

Economically attractive, energy- and environmentally-friendly processes are necessary to ensure the sustainability of our society. This multi-value role of innovation has great significance in the light of the annual increase in energy consumption, world population, and municipal and industrial water consumption/withdrawal generation. These worrying figures and their predicted future values are presented in the Figures 8.1-8.4 and show a strong increase over time. Without stricter precautions and the use of innovative technologies, the rise will be even steeper due to the multiplication by the increasing

world population. Therefore, future innovation should aim at sustainable business. We call that multi-value innovation.

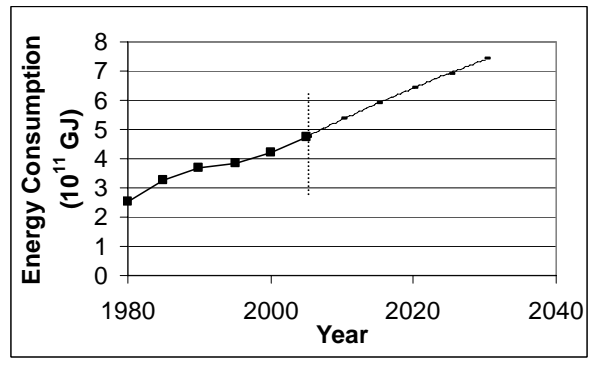


**Figure 8.1:** World energy consumption 1980-2030 [Energy 2004]

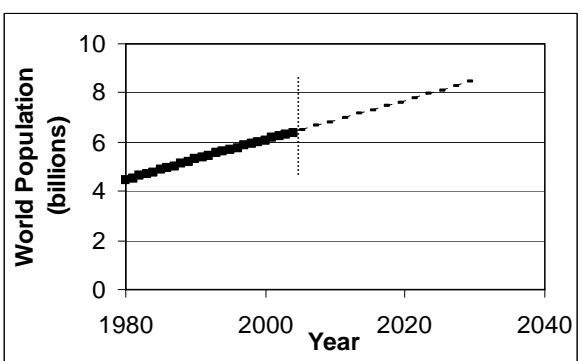


**Figure 8.2:** World population 1980-2030 [Energy 2004]

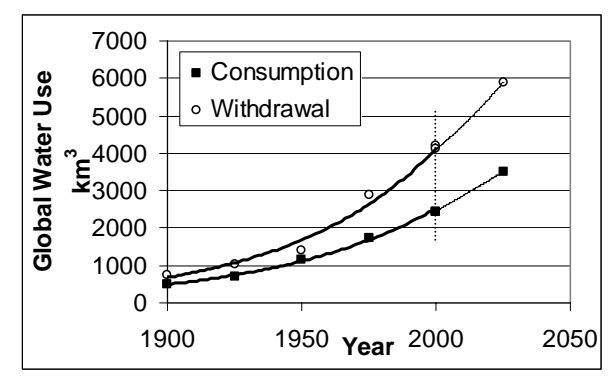


**Figure 8.3:** Global fresh water use: Withdrawal and consumption [United Nations 2007]

**Withdrawal** is the removal of freshwater from water resources or reservoirs for use in agriculture, industry or domestic purpose.

**Consumption** is the use of water by humans from natural water resources or reservoirs for agriculture, industry or domestic purpose.

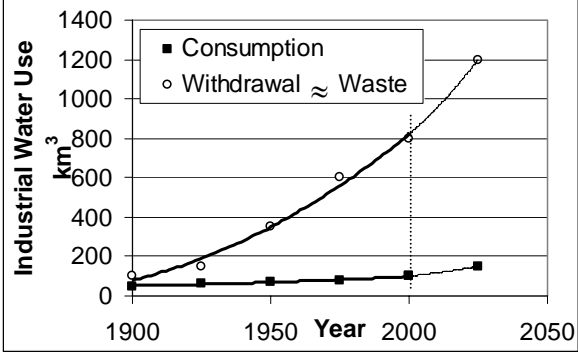


**Figure 8.4:** Global industrial water use: Withdrawal and consumption by industry [United Nations 2007]

**Withdrawal** is the removal of freshwater from water resources or reservoirs for use in industry. **Consumption** is the use of water by humans from natural water resources or reservoirs for industry purposes.

Currently, huge amounts of valuable industrial aqueous streams cause pollution and damage ecological systems. It has been suggested that water pollution is the leading worldwide cause of death and disease [Pink 2006, West 2006], and that it accounts for the death of more than 14,000 people daily [West 2006]. An estimated 15-20% of worldwide water use is industrial (Figure 8.3-8.4) [United Nations 2007, Wikipedia 2007]. Metallurgy, chemical, food-beverages, and the wood-paper industries are the most waste-

producing sectors. Industrial waste volumes reach close to 2000 kg/capita/year in South Korea and drop to less than 20 kg/capita/year in Brazil. Between these two extremes, average volumes range between 400 and 700 kg/capita/year in OECD countries [Veolia 2007]. Generally, waste holders do not want to go on public record; instead they prefer to hide their problems. Diluting these streams, to governmentally accepted concentration levels, is the cheapest solution. However, this 'solution' discharges the same amount of waste to the environment and contaminates even more clean water by the dilution process. Due to the difficulty of estimating waste stream volumes, it is very hard to estimate the value of the world industrial waste market. The value of the non-hazardous industrial waste market is estimated at \$147 billion for Japan, Europe (EU15, Norway and Switzerland), the United States, South Korea, Australia and Mexico. The market is largest in Japan, at an estimated \$67 billion. [Veolia 2007]. Hazardous waste is even more difficult to estimate. For the EU, US, Canada, Japan, South Korea, Thailand, China, Mexico, India and South Africa the amount of hazardous waste is estimated at approximately 150 million metric tons [Veolia 2007]. These huge amounts of (valuable) industrial aqueous streams are disposed of because existing treatment methods consume too much energy or cannot handle the solutions. These streams could easily be turned into valuable products once an affordable treatment technology is available. The new wasteto-products paradigm which treats waste streams as raw materials is environmentally crucial for recycling and protecting the world's natural resources, and also economically favourable by decreasing the production cost.

Recently, the separation of valuable non-ferro metals (copper, aluminum, nickel, zinc and silver) and clean building materials from bottom ashes of incinerated domestic waste was achieved by using a newly developed 'wet eddy separator' technology patented by the TU Delft and the Amsterdam Afval Energie Bedrijf (AEB) [Rem et al. 2004, Hartmann 2006]. In Europe, 220 million tons of domestic waste is generated annually. When incinerated, these bottom ashes which used to be a problem causing waste can be regarded as a precious raw material containing 500 kton of copper and 500 kton of aluminum (annually), with a total value of 2 billion Euros [Hartmann 2006].

Similar to the domestic waste separation case, for aqueous process and waste streams, new technologies are being developed to recover valuable salts in an energetically favorable way. For certain types of aqueous streams, new technologies such as reverse osmosis, multiple stage evaporation with mechanical vapour recompression, and combined heat-power generation have come a long way to enhance the efficiency. However, for systems containing higher salt (or acid) concentrations, there is no efficient technology available yet.

At this point Eutectic Freeze Crystallization (EFC) [Van der Ham 1999, Vaessen 2003, Himawan 2005, Genceli 2005a-c] is a strong future technology candidate for separation of the dissolved salts and process water from industrial or waste streams. EFC, described in more detail further below, offers a technologically and economically attractive alternative to conventional separation techniques by recovering pure salt and water product from process or waste streams, thus saving energy or turning waste into raw materials in an energetically favourable way (more close to the theoretically required amount). Besides, EFC is an entirely new type of unit operation which allows completely new, more efficient flowsheets to be designed. EFC operates around the eutectic temperature of aqueous solutions and can treat a wide variety of feed solutions without adding any further solvents or chemicals. EFC is complementary to reverse osmosis for concentrated streams and dissolved inorganic and organic mixtures. With a theoretical yield of 100% and an energy cost saving of up to 90% compared to evaporative crystallization, EFC delivers two products simultaneously: pure salt and pure ice crystals. Separating those products is easily accomplished on account of their density differences. In the past, a combination of lacking equipment and prejudices ('cooling is too expensive', 'the crystals will never be pure') has hampered the development and implementation of EFC.

From an economic and environmental point of view fast industrial implementation of the EFC technology is desirable which will realize a major breakthrough due to lower power consumption, less waste generation and a higher product yield of high purity. Two pilot

demonstrations at industrial sites have been successfully performed, and the next issue for commercialization is an industrial production unit design and construction.

EFC is an example of a potential so called multi-value innovation. Such an innovation creates economic, ecologic and social added-value and integrates these three dimensions of societal change as illustrated in Figure 8.5. A vision of the future (providing the goals), a transition path (showing the strategy) and a process model (for execution) are the three interconnected parts of the multi-innovation concept [Berkhout et al. 2006]. Starting from the current situation to achieve the vision of the future, a transition path has to be followed. Berkhout describes the transition path as an expedition: the goals are clear but the road to success is unknown.

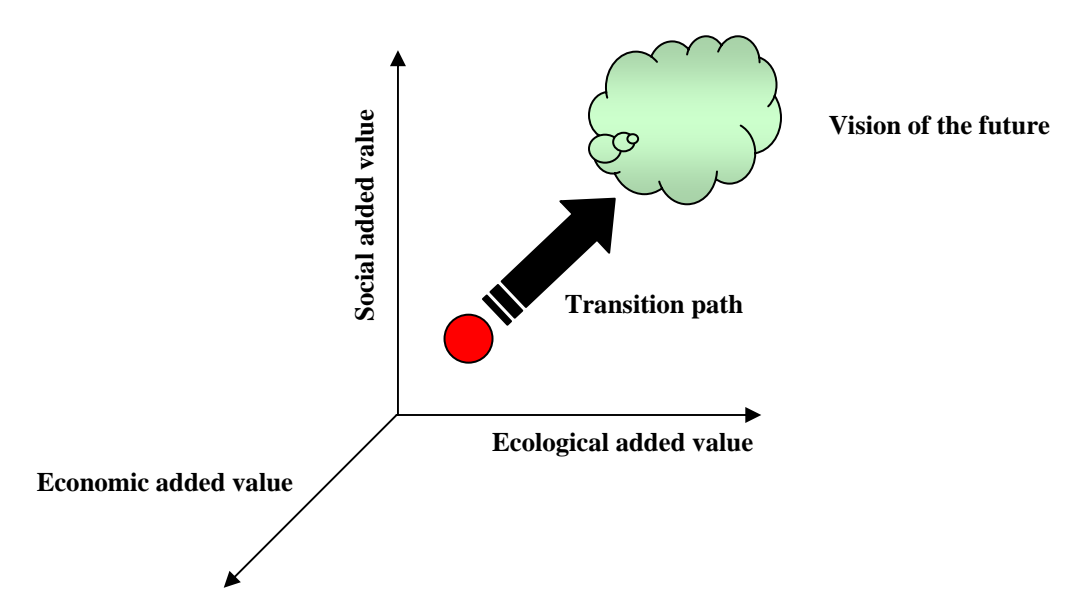


**Figure 8.5:** Multi-value innovation aims at the creation of economic, ecologic and social added value by growing from the present situation to the vision of the future [Berkhout et al. 2007].

Current situation

Traditionally, innovations are considered as linear chains of sequential actions, where each stage requires a certain amount of time, in effect holding up the next stage. This is one important reason for the traditional time and cost intensive implementation trajectory. The time between invention and successful implementation can be reduced by

simultaneous actions using the Cyclic Innovation Model (CIM) which considers the innovation process as symbiotic 'cycles of change', where developments take place in all cycles simultaneously. In CIM, the innovation activities connect science with business as well as technology with markets in a cyclic manner [Berkhout 2000, Berkhout et al. 2006, 2007].

The aim of the work described in this chapter is to develop the application of the Cyclic Innovation Model, for the case of commercial application of the innovative Eutectic Freeze Crystallization Technology. CIM is used as the process model for traversing this transition path.

#### VISION OF THE FUTURE

Innovation is the process of *successfully* introducing a new solution in terms of new products, processes and services or any combination thereof into the market. Innovation is a matter of bringing together what is *technically possible* and what is *socially desirable* [Berkhout et al. 2007]. It is a crucial strategy to stay in business, especially for high-technology companies that want to be leaders rather than followers ('the winner takes all').

Innovation starts by having an ambitious vision of the future (see Figure 8.5). Such a vision is essential to focus the attention of the actors (organizations) involved and persuade them to replace their existing (conventional) technologies by new technologies that can accomplish the goals in the vision. Success can only be achieved when this vision of the future is shared by all actors.

In our vision of the future is to split aqueous solutions, containing dissolved salts, acids and organic compounds into pure water, pure salts, pure acids and pure organic materials, using not more than the energy which is theoretically required, i.e. what natures asks us. The necessary equipment will be very affordable so that the product yield will more than cover the total processing costs.

The required theoretical energy can be calculated from thermodynamics and is independent of the process since it is a physical entity. It is mostly very low. For instance to crystallize NaCl from its saturated solution (26 wt.%) theoretically costs 111 kJ/kg produced NaCl, while for a single stage evaporation roughly 5 MJ of thermal energy are needed and highly optimised multiple stage evaporative processes still use about 2 MJ in the form of steam.

Having such an ideal process implies there will be no more waste from aqueous process streams, raw materials can be used completely and transformed into ultra pure products. In other words, the waste to products concept could be implemented to completeness. This not only counts for simple salts, acids, water and organic materials, but also for more complex and/or high added value products.

If the ideal process would be available, we could for instance win the uranium (3 microgram/kg) from sea water and make available 360 times as much U as we can access now [Hermann, 2005]. Similarly new process routes for metals, petrochemical, food processing involving large amounts of water would become feasible, revolutionizing our way of designing processes. Therefore, not only existing aqueous process streams could be treated feasibly, but also many other types of material flow. It would certainly be a base for powerful innovations.

EFC brings us a step closer to this ideal process. In the transition to the ideal process we consider eutectic freezing as an intermediate goal. It saves up to 90% compared to evaporative crystallization. Even then, however, the amount of exergy required to perform the separation is still tens of times the theoretical amount.

## TRANSITION PATH

In realising the vision of the future for low energy consumption, less waste generation and higher raw materials recovery from waste streams, a transition path has to be followed starting from the current situation of energy intensive, more waste-generating and little waste recycling. The transition path visualizes the envisaged road -from the present to the future- by showing the anticipated innovations ('the big steps') for the short, medium and long-term. For a fast implementation of the new technology, generally the following obstacles have to be overcome [Berkhout et. al. 2007]:

- Successful life cycle management of current production plants
- A risk-averse culture in the majority of the chemical industry
- Linear innovation paths causing long times to market

Investment requirements are considered to be an important obstacle in the adoption of the new separation process. In the current economic structure of the chemical industry, the lifetime of production plants are large and returns on investment are relatively low. Therefore, new technologies requiring large capital expenditure are unlikely to be adopted from an economic point of view. This hurdle has seriously limited a more widespread use of promising technologies in the past [Kroon 2006].

A second obstacle along the transition path is considered to be uncertainty. A new way of processing always involves risks, because the concept has not yet been proven on a large scale. Therefore, as long as the current production method is making an acceptable profit, industry will be risk averse and stick with optimizing current production concepts ('life cycle management'). Radical change must primarily come from environmental and social forces, rather than economical incentives [Kroon 2006].

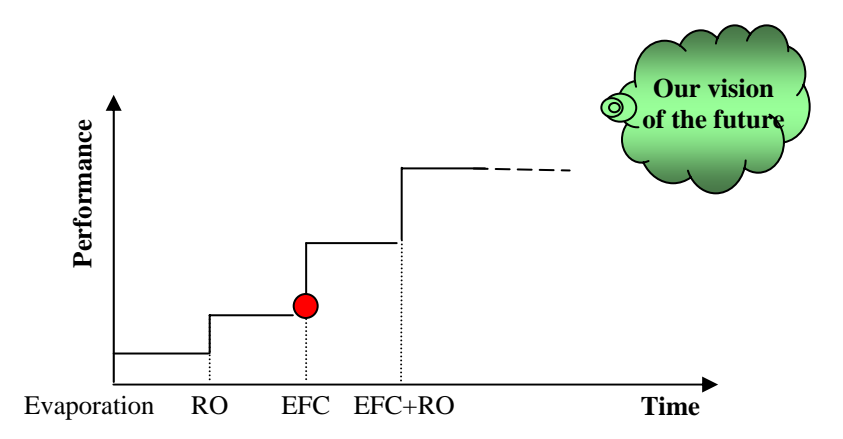


**Figure 8.6:** Intermediate innovations along the transition path, leading to our vision of the Future Current situation

Figure 8.6 shows the radical change along the transition path. Realization of the goal set in our vision will take place step by step. The development and application of reverse osmosis (RO) for clean, dilute salt solutions can be seen as the most recent big step. EFC technology (mainly for more concentrated solutions) for commercialization is in progress. EFC presently covers 10% of the way towards reaching its targeted future vision. Commercialisation EFC by starting up of a company for exploiting the technology is seen as the next big step. It is expected that the third big step following that is created by combining RO and EFC technologies.

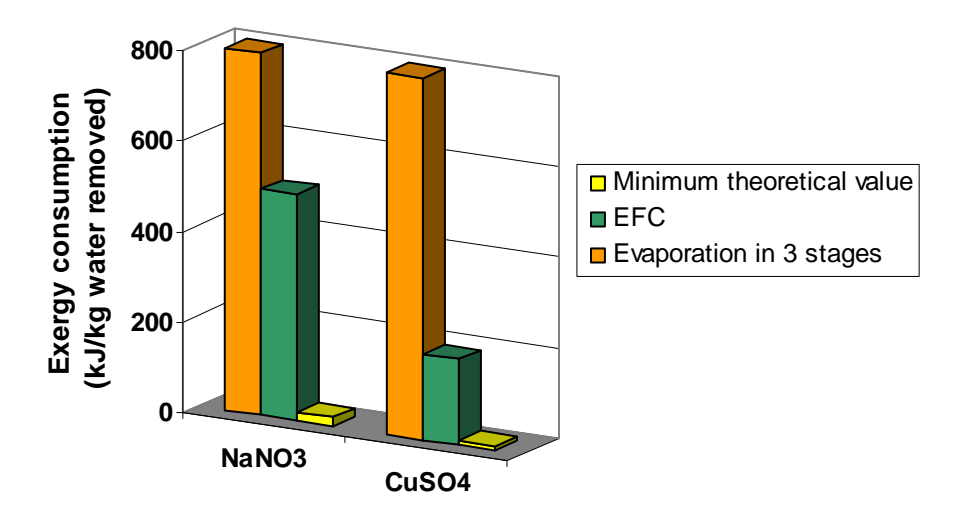


Figure 8.7: EFC brings us closer to our ideal (theoretical) process [Van der Ham 1999]

There is no doubt that on our path towards full realization of our vision new, yet unknown technologies are necessary. EFC brings us more close to the theoretical energy as can be seen in the Figure 8.7, but is still away from it. Therefore, new steps need to be taken. Consider now the transition where full scale EFC is implemented where possible.

Drivers for introducing EFC are: a high and increasing energy price, the higher economic value of products when they are pure, its safe operation and the pressure of society to contribute to the problem of climate change. Also at small scale all the advantages can be achieved. EFC is attractive to further treat the concentrated streams delivered by reverse osmosis (RO), which is the most efficient existing process for producing pure water from clean dilute salt streams. Therefore, RO and EFC mutually enhance there attractiveness. This implies that present applications of RO form part of the market for EFC.

Factors hampering the transition to a situation where EFC is applied wherever attractive are a risk averse industries which prefer proven technologies such as evaporation. Current evaporative crystallization plants will not easily be replaced by EFC. Especially for certain highly optimised large scale multiple stage evaporative plants (e.g. for NaCl) using the waste heat from powerplants EFC will not be in view.

We think that early EFC applications are in the high added value products field, such as for recovery of valuable materials e.g. from the semiconductor industry, cheese brines, Mo winning from blow down streams of SMPO plants.

Equipment manufacturers form roughly two groups: the true innovators and those who wait for specified orders from process industry and produce at low cost and margins (jobbers). EFC equipment might be produced by either of the two, but clearly at least one of the first category is needed. In the transition not only innovative user, but also an innovative producer will be needed.

For new applications, now untreated process streams which now become profitable to treat, we do not have to overcome the difficulty of replacing a successful life cycle management of an existing production plant. Establishing a successful demonstration and proving its sustainability to uses of the conventional separation technology will broaden the market for EFC. Probably first some higher added value products will be made with EFC.

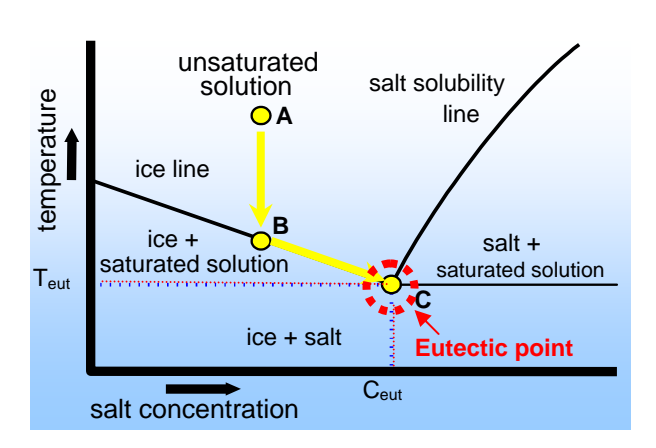
EFC, has already overcome most of the uncertainties on the transition path, as the concept was proven on a large scale with two successfully demonstrations (Appendix I) at site. Many unknowns for the long-term process aspects such as continuous stable operation, equipment robustness, costs and its impacts on the environment were answered as a result of the successful cooperation between the companies, research institutes and universities [Genceli et al. 2005a, 2005b, 2005c].

## **EUTECTIC FREEZE CRYSTALLIZATION, the process**

It is possible to apply EFC technology for the recovery of dissolved salts from industrial process streams, waste streams or underground water of the mining industry [Van der Ham 1999, Vaessen 2003, Himawan 2005]. EFC has an inherent stability by operating around the eutectic point (eutectic temperature and concentration) of the aqueous solutions. The principle of EFC can be described using a phase diagram of a binary saltwater mixture, shown in Figure 8.8. If a solution in the unsaturated regime with a concentration lower than eutectic composition (**A**) is cooled down below its freezing point, ice crystals start to form (**B**). Further cooling decreases the temperature, and increases the concentration through the formation of ice crystals along the ice line **B** to **C**. At point **C** (the eutectic point: the intersection of the ice and salt solubility lines), the liquid concentration reaches saturation and further cooling will result in the formation of ice and salt crystals simultaneously. Similarly, starting with a solution at higher concentration than eutectic composition will first result in the formation of salt and reach the eutectic point by following the salt solubility line. The two solid products (ice and salt) are separated gravitationally during the production inside the crystallizer due to their

density difference. Salt crystals sink to the bottom of the solution while the ice crystals rise to the surface, as shown in Figure 8.9.

Stepakoff [Stepakoff et al. 1974], Barduhn [Barduhn et al. 1979], and Swenne and Thoenes [Swenne 1983, Swenne et al. 1985] made the first studies of a eutectic freeze crystallization process for brine disposal and concentration of industrial wastewater, of natural waters and of sodium chloride production from solution mining. In the late 1990's, Van der Ham and Witkamp developed a eutectic freeze crystallization process using indirect cooling.



ice

**Figure 8.8:** Eutectic phase diagram of an aqueous solution

**Figure 8.9:** Gravitational separation of ice and salt crystals formed by EFC

He proved the feasibility of EFC technology for the waste water treatment of aqueous systems like NaNO<sub>3</sub>, CuSO<sub>4</sub>, NH<sub>4</sub>H<sub>2</sub>PO<sub>4</sub> and an industrial case for a KNO<sub>3</sub>–HNO<sub>3</sub>-H<sub>2</sub>O process stream [Van de Ham 1999, Van de Ham et al. 1999-2003]. Following the work of Van der Ham, in 1998 Vaessen designed and constructed two types of 100-liter eutectic freeze crystallizers: The cooled disc column crystallizer (CDCC) and the scraped cooled wall crystallizer (SCWC). He evaluated their technical performance based on the treatment of ternary aqueous KNO<sub>3</sub>–HNO<sub>3</sub> solutions [Vaessen 2003, Vaessen et al. 2003a-2003b]. Besides indirect cooling, Vaessen also studied direct cooling with the help of CO<sub>2</sub> clathrates by changing the eutectic temperature by crystallizing CO<sub>2</sub> clathrates instead of normal ice [Vaessen et al. 1999]. In 2002, Himawan applied EFC technology to recover magnesium sulphate and ice from an industrial magnesium sulphate stream

from ex-flue gas desulphurization, and developed a general model for continuous eutectic freeze crystallization in a scraped surface crystallizer based on population balances [Himawan 2005, Himawan et al. 2002-2006]. Following Himawan's work, Genceli further studied using MgSO<sub>4</sub> aqueous streams under EFC with the second generation (150-liter capacity and 5.6 m<sup>2</sup>m<sup>-3</sup> cooling area) cooled disc column crystallizer (CDCC-2) [Genceli et al. 2005a]. A heat flux of 1.1 to 3.9 kWm<sup>-2</sup> was achieved at a temperature difference between coolant and crystallizer bulk solution of 3 to 6.4 K and a residence time of 1-3 h. Genceli reported that CDCC-2 had a good crystallization performance and reduced scaling compared to previous designs, allowing a much higher (up to 2x) heat transfer rate and thus production rate (in kgs<sup>-1</sup>m<sup>-3</sup> of the main crystallizer body) of 0.024 kgs<sup>-1</sup>m<sup>-3</sup> for ice and 0.017 kgs<sup>-1</sup>m<sup>-3</sup> for MgSO<sub>4</sub>·11H<sub>2</sub>O salt [Genceli et al. 2005b]. Based on the previous studies, EFC technology was scaled up and a complete mobile skid mounted unit for EFC applications was designed and constructed for 130 ton/year MgSO<sub>4</sub>·7H<sub>2</sub>O and water production. This project was carried out together with industrial partners, allowing the system to be easily installed and connected to an industrial plant [Genceli et al. 2005c].

Two successful demonstrations served as important milestones of the project. The first one was at Nedmag-Veendam in May 2005, treating a waste magnesium sulphate stream from ex-flue gas desulphurization with continuous 20 kg/h epsomite and 20 kg/h ice production rates. The second demonstration took place at AVR-Rotterdam in April 2007, treating an industrial sodium (bi-)carbonate stream with continuous 30 kg/h ice and 1 kg/h Na<sub>2</sub>CO<sub>3</sub>·10H<sub>2</sub>O production rates.

The key properties of being less susceptible to corrosion, preventing poisonous fume discharges and avoiding the undesirable side effects of adding extra chemicals for waste water treatment, make EFC technology environmentally friendly. The low operating temperature allows for cheap construction steel to be used as corrosion is rarely an issue, avoids decomposition of organics (dangerous when nitrates are present), is sanitary favourable and is safe for process operators. Furthermore, no poisonous fumes are

generated at these low temperatures. The cold operation also has advantages when temperature sensitive compounds are treated (e.g. in the food industry) or when bacterial growth has to be kept under control.

EFC consumes less power (less than 50% of the power required by triple-stage evaporative crystallization), and has (theoretically) a 100% yield (contrary to membrane technologies). The yield is only limited by the desired bleed stream of non-crystallizable compounds (e.g. organics) [Ham 1999]. These advantages make EFC economically attractive as well as ecologically sustainable. Economically and technically EFC is complementary to reverse osmosis, which is very effective in clean systems up to a few % salts but can not crystallize salts from their saturated solutions. Another favourable characteristic of EFC is its wide inorganic and organic solution applicability range. In addition to separating organic and inorganic salts from their binary solutions, EFC is capable of separating highly purified salts from mixtures of inorganic and organic streams. EFC allows the separation of each salt due to its fixed eutectic point without contamination from other dissolved salts or impurities. Because cooling crystallization is a very selective process, the chance of impurities in the product is very low. Hence, using EFC technology significantly increases the product quality.

Depending on the composition of the feed stream and the requirements of the client, the EFC operational frame can be adjusted. It is also possible to operate EFC with tailor-made operational parameters according to the priority of the product (process water or salt recovery). EFC systems can be economically designed for small as well as large systems and can serve a wide variety of industrial sectors which are in need of process water, waste water treatment, organic or inorganic salt recovery, or a temperature sensitive operation to preserve product quality.

EFC not only can replace existing technologies but enables completely new processes to be designed, as it constitutes a new unit operation. For instance, a process where reverse osmosis does the first concentration step up to 5 wt% salt and EFC produces crystalline product and more clean water, combines the two processes at their greatest strengths.

## Eutectic Freeze Crystallization Application Cases

KNO<sub>3</sub> treatment: During the production of starch from potatoes, a KNO<sub>3</sub> stream containing 16 wt% KNO<sub>3</sub>, 1.1 wt% HNO<sub>3</sub> and 3345 ppm organic material is generated. Recovery of valuable the KNO<sub>3</sub> salt and pure water from this aqueous waste stream is desirable to reduce the amount of generated waste and to conserve chemicals. Below, EFC separation technology is compared to conventional evaporative crystallization [Van der Ham 1999, Vaessen 2003].

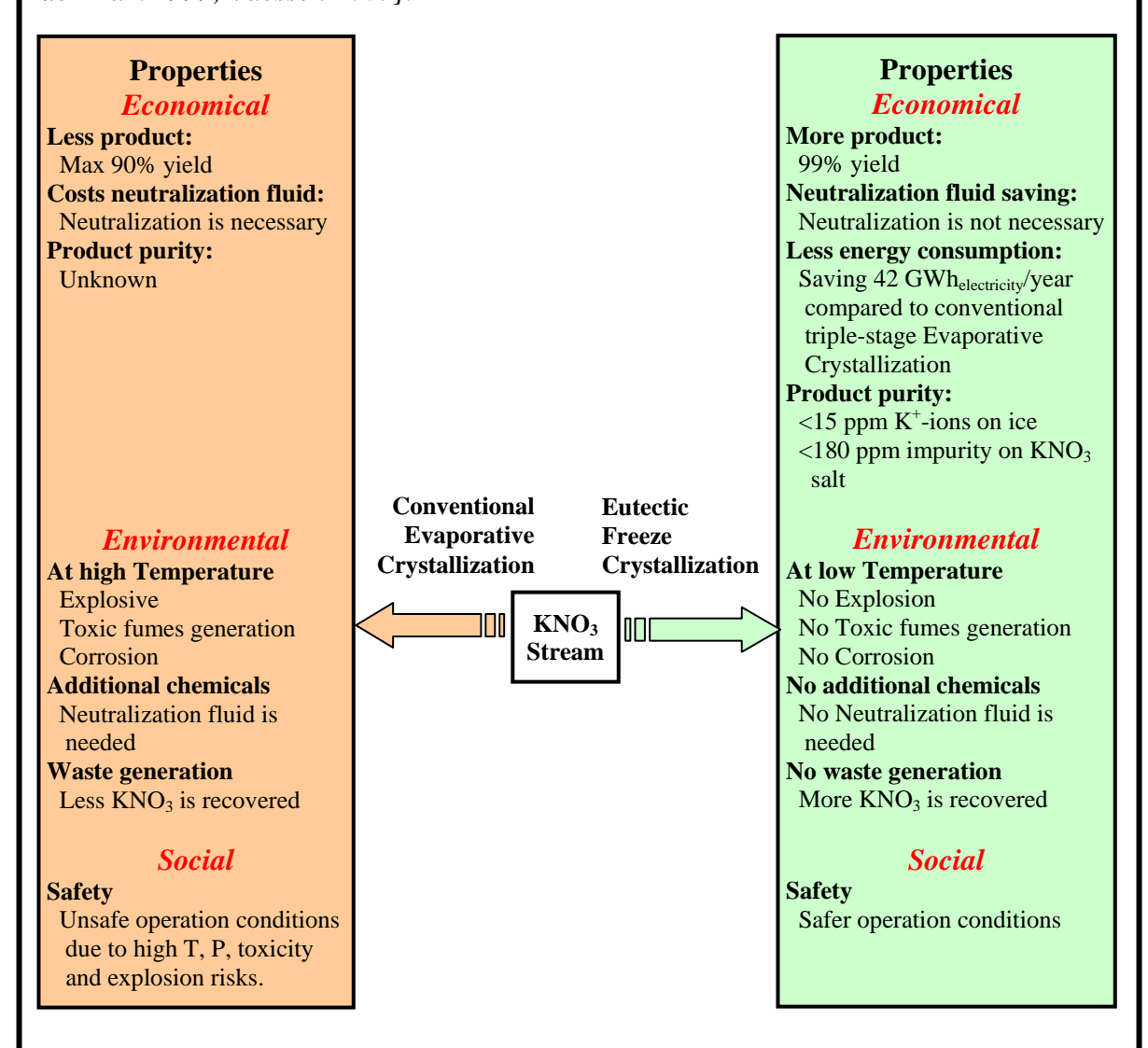


Figure 8.10: KNO<sub>3</sub> stream treatment

**Sodium** (bi-)carbonate treatment: Water-soluble sodium bicarbonate (NaHCO<sub>3</sub>) and sodium carbonate (Na<sub>2</sub>CO<sub>3</sub>) have many industrial uses. At AVR-Europoort about 300.000 tons of alkaline industrial waste water is incinerated every year, yielding a sodium (bi-)carbonate solution (about 5 wt%) with about 1 g/L Molybdenum, the so-called blow-down solution [Envirochemie 2007].

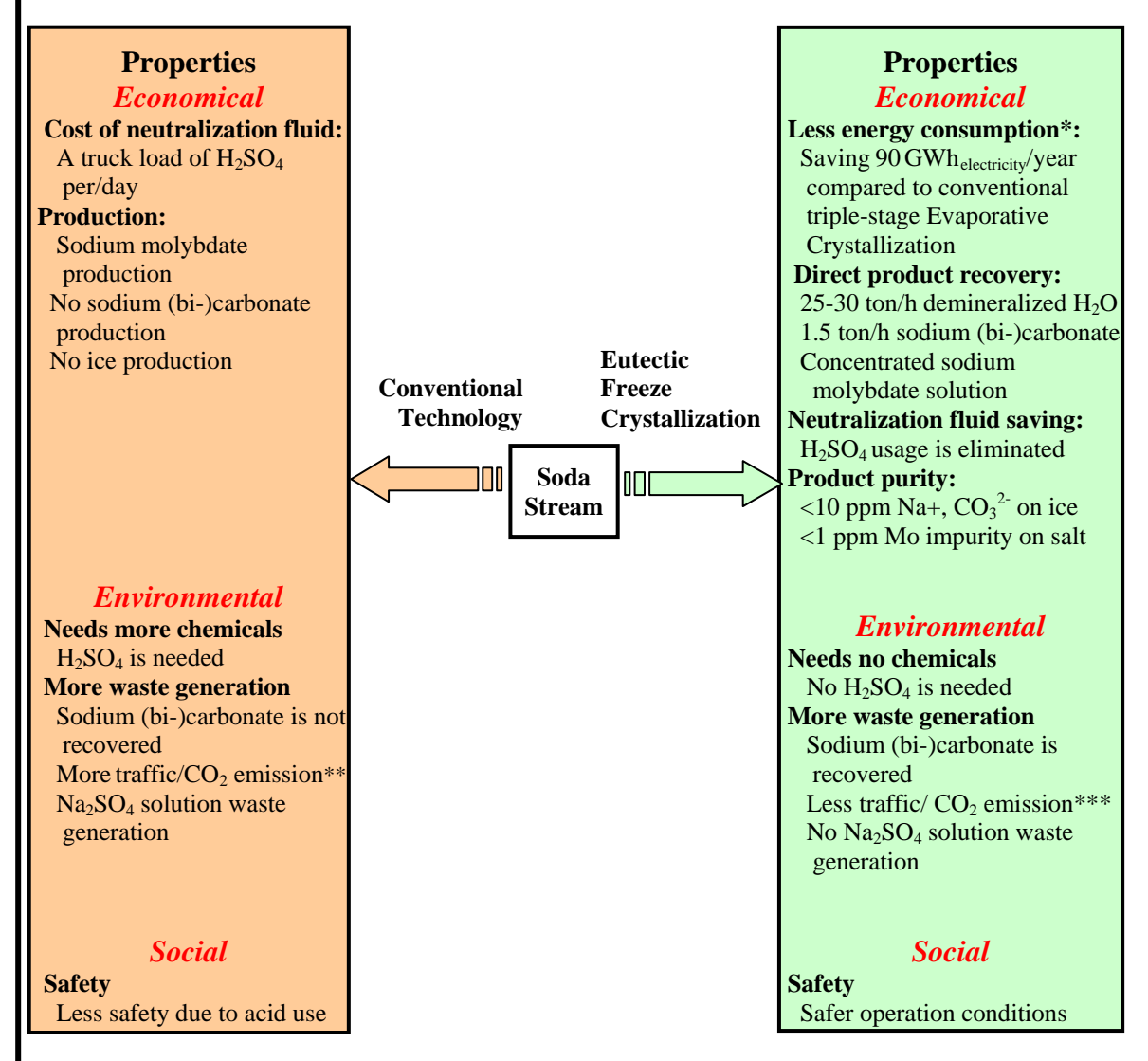
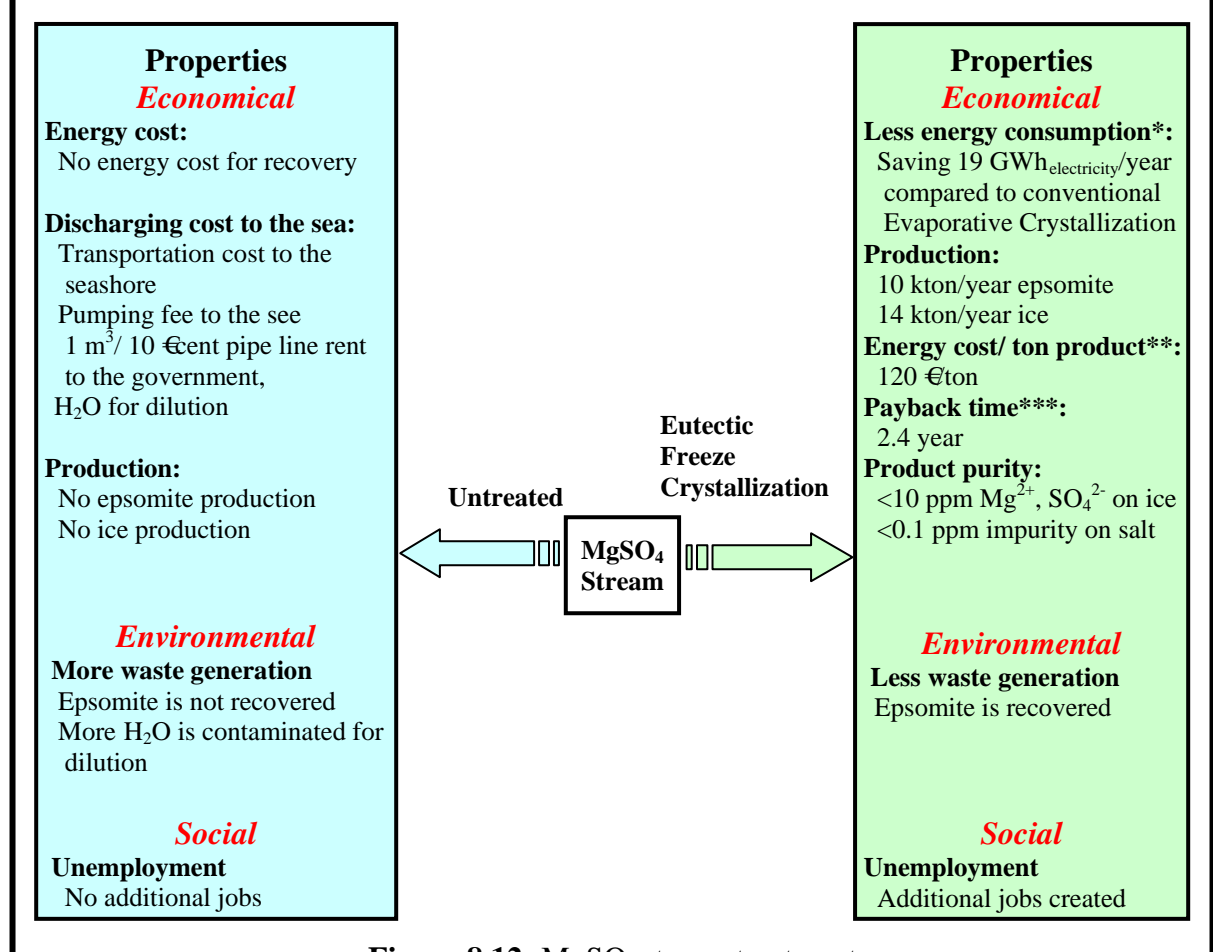


Figure 8.11: Soda stream treatment

- \* Due to the fact that Sodium (bi-)carbonate is not currently produced using Conventional Technology, the energy price for the production of Sodium (bi-)carbonate using EFC technology is compared to triple-stage Evaporative Crystallization technology.
- \*\* One extra truck on the road which burns fossil fuel, produces CO<sub>2</sub> and adds to traffic congestion.
- \*\*\* One less truck on the road. No fossil fuel consumption, no CO<sub>2</sub> emission, and adds to traffic congestion.

MgSO<sub>4</sub> treatment: Combustion of fossil fuels may cause severe air contamination due to the emission of (among others) sulphur dioxide. To prevent such pollution, a flue gas desulphurization process is commonly installed. The SO<sub>2</sub> in the flue gas is absorbed in an aqueous solution of magnesium hydroxide, yielding a solution containing MgSO<sub>4</sub>. An MgSO<sub>4</sub> stream is harmless for the environment when dumped into the sea in low concentration. MgSO<sub>4</sub> can be recovered and utilized further, e.g. as a fertilizer. It has been shown recently that EFC is a promising technology for this purpose. Below, 10 kton/year MgSO<sub>4</sub>·7H<sub>2</sub>O (epsomite) recovery using EFC technology is compared to an untreated solution discharge alternative [Himawan 2005, Genceli et al. 2005a-b].



**Figure 8.12:** MgSO<sub>4</sub> stream treatment

- \* Due to the fact that Epsomite is not currently produced, the energy price for the production of Epsomite using EFC technology is compared to Evaporative Crystallization technology.
- \*\* Assuming Utility costs of steam price is 25 €ton, natural gas 0.5 €Nm³. electricity 0.1 €kWh.
- \*\*\* Pay back time: Ratio between the total investments to cash flow.

The advantages of EFC technology are best explained using three example application cases from industry: KNO<sub>3</sub>, sodium (bi-)carbonate and MgSO<sub>4</sub> containing industrial streams of various origin as presented in Figures 8.10, 8.11 and 8.12 respectively.

Recovering KNO<sub>3</sub> by EFC technology is economically, socially, environmentally, energetically and qualitatively superior to conventional triple-stage Evaporative Crystallization technology with respect to higher yield (99%), less energy consumption (saves 42 GWh<sub>electricity</sub>/year energy), high purity ice and salt production and higher safety operating conditions (See Figure 8.10).

The EFC application to sodium (bi-)carbonate stream is the second example case. In current treatment technology as the first step, sulphuric acid is used to neutralize the soda stream. Afterwards, sodium molybdate from this neutralized stream is recovered by ion exchanger and the remaining sodium sulphate solution is disposed into the environment. The current technology does not allow sodium (bi-)carbonate recovery. However, using EFC technology, sodium (bi-)carbonate crystals, ice and concentrated sodium molybdate solution recovery is possible. Therefore, EFC energy consumption for the related products is compared to conventional triple-stage evaporative crystallization and presented to save yearly 90 GWh<sub>electricity</sub> energy. Triple-stage evaporation of the blowdown stream would yield sodium carbonate mono-hydrate crystals contaminated with sodium molybdate whereas the product purity (sodium carbonate deca-hydrate salt and ice) using EFC technology would be very high. The environmental and social superiority of EFC technology is also presented in Figure 8.11.

Different from the previous 2 cases in the third application example, the treatment of a MgSO<sub>4</sub> stream with EFC is compared with the untreated situation instead of with a conventional technology. The stream can be dumped into the sea in low concentrations without causing any environmental pollution. Figure 8.12 presents the consequences of this comparison. Treating the stream has the advantages of recovering the epsomite mineral and ice crystals, lowering the waste generation and having social and

environmental benefits. The ice and salt products are highly pure. Having a payback time of 2.4 years makes EFC an attractive investment. These benefits will eventually outweigh the advantage of energy savings in the untreated case.

The exergy saving of EFC compared to the conventional 3-Step Evaporation Crystallization technology for several salt streams are presented in Figure 8.13 [Van der Ham, 1999]. It is seen that EFC typically saves 50% exergy. When compared to single stage evaporation the exergy saving is up to 90%.

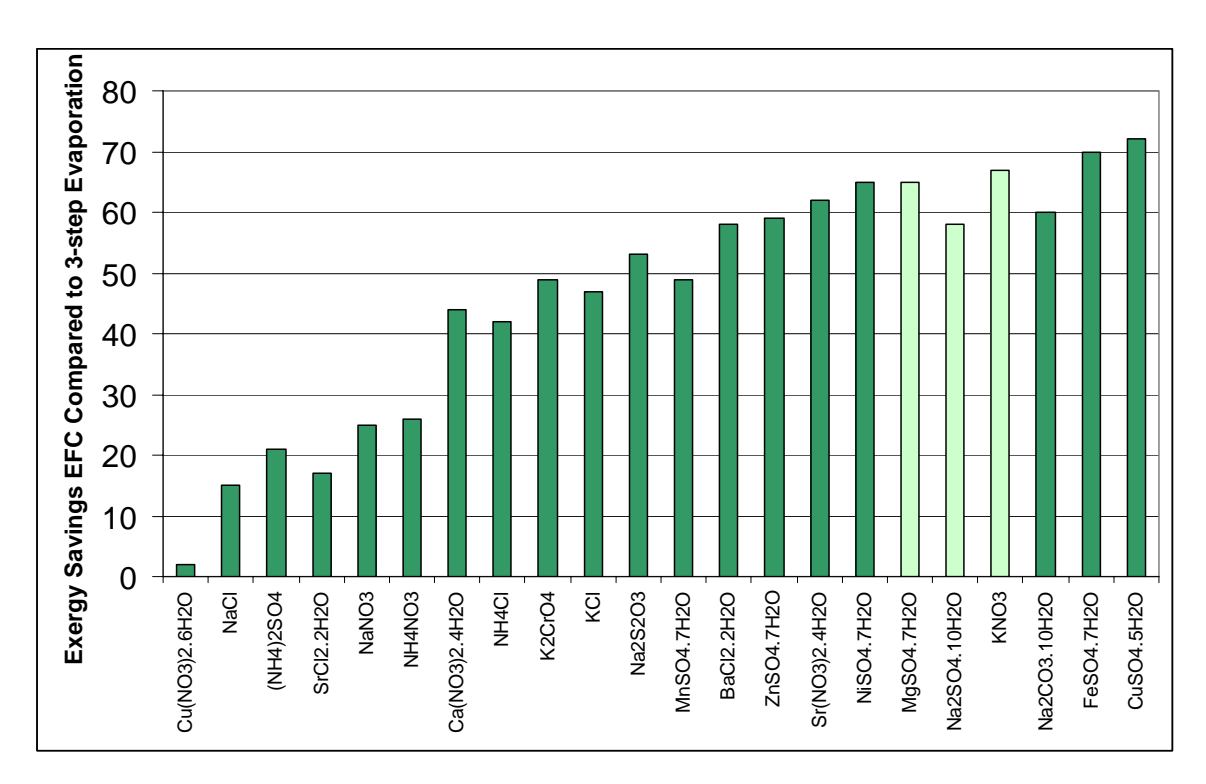


**Figure 8.13:** Exergy savings diagram [Van der Ham, 1999]

#### CYCLIC INNOVATION MODEL

## **Process Model**

Traditional innovation models describe the processes along the transition path as a pipeline: governmental investments in scientific research must lead to application-oriented development routes which subsequently – with the aid of risk capital – ought to

result in successful market introductions. If we invest enough in science and technology then the rest will work out all right, that is the reasoning.<sup>1</sup> Such a linear science-push approach in innovation policies is still taking place on a large scale, with the result that the innovation system cannot flourish [Berkhout et al. 2007].

Chesbrough shows that the in-house, stage-gate model —a pipeline where promising ideas are developed toward successful products and services- can be extended to a more open version, that allows external interactions from outside the pipeline [Chesbrough 2003]. This pipeline was extended by Robert Kirschbaum by introducing the possibility of spinin and spin-out [Kirschbaum 2005].

Successful innovation processes are not a matter of one-way pipelines, but rather of interlocking cycles with feedforward and feedback connections: from linear to nonlinear thinking. In that way, a symbiotic environment is created in which the soft sciences are linked to engineering, and where the hard sciences connect with valorization goals. The links, which go forwards and backwards (cyclic processes), are an essential feature of dynamic systems [Forrester 1961, Senge 1994]. To improve the scientific insight into innovation processes, we should make feedback more explicit in our models [Berkhout et al. 2007].

## The Principle of Cyclical Interaction

With the explicit addition of feedback paths, process models along transition paths are represented by two-way interactions, leading to cyclic processes.<sup>2</sup> With the presence of feedback, organizations are continuously exposed to reactions of their environment, providing them with an important source of information and inspiration. In addition –thanks to feedback— organizations are constantly confronted with the consequences of their actions, preferably through built-in 'early signals'. In that way quick adjustments can be made in the event of unexpected occurrences. And, last but not least, the cyclical architecture also ensures that mistakes can be learned from, a very important property for innovation.

In summary, the combination of feedforward and feedback –cyclic interaction– is a fundamental property of dynamic systems. It also provides the basic elements to model the dynamic culture in innovative organizations: start quickly, adjust quickly and learn quickly.<sup>3</sup> [Berkhout et al. 2007]

### Elementary Building Block

Figure 8.14 illustrates the basic principle. **A** represents an entity that maintains a cyclical interaction with entity **X**. Examples are interactions between governments and their citizens, commercial organizations and their customers, hospitals and their patients, etc. A particularly interesting example is the innovation strategy of large companies with respect to spinning-out (**A**-to-**X**) and spinning-in (**X**-to-**A**) start-ups. New in-house ideas are developed outside the original business unit and, after successful prototyping, reintroduced in the organization where it all started. It is interesting to note that by including the time axis Figure 8.13 transforms into a helix [Berkhout et al. 2007].

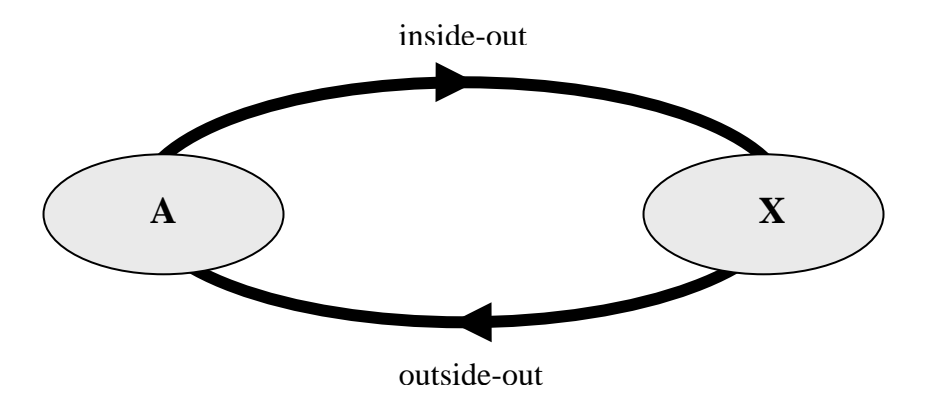


**Figure 8.14:** Cyclical Interaction is the Basis for Open Innovation and a Precondition for Operational Flexibility. *Note:* It is also a necessary condition for sustainability. Here, A and X represent two interacting entities [Berkhout et al. 2007].

### **Dynamics around Technological Research**

Figure 8.15 shows two linked basic units – the double loop – in which technological research plays a central role. The cyclical interaction processes for the development of new technology take place in the so-called technical oriented sciences cycle (the left-hand

side of Figure 8.15) with the help of a wide range of disciplines from the hard sciences.<sup>4</sup> Technological research in this cycle is a multi-disciplinary activity: a team of scientists from different disciplines of the hard sciences is needed to develop a new technology (many-to-one relationship).

Similarly, the cyclical interaction processes for the development of new products take place in the integrated engineering cycle (the right-hand side of Figure 8.15). Modern product development is a multi-technology activity: a package of different –often patented– technologies is needed to design and prototype a new product (many-to-one relationship). Like multi-disciplinary science, here too we see that many different specialists are needed to succeed. In most industrial sectors the creativity, knowledge and skills of specialized suppliers play an important role in making the engineering process successful. This is consistent with the open innovation concept [Berkhout et al. 2007].

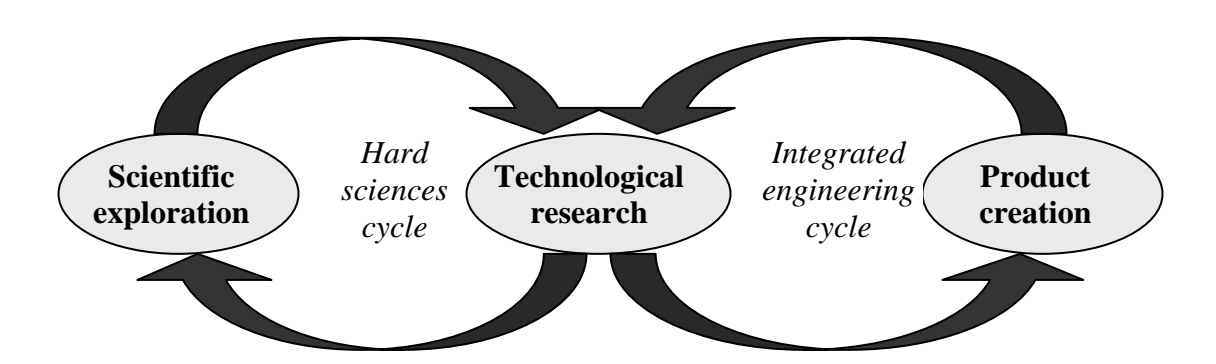


**Figure 8.15:** The Dynamic Surrounding Technological Research Are Driven by the Cyclical Interaction between New Scientific Insights into Technical-Oriented Processes (Left-Hand Side) and New Functional Requirements for Process-Product Combinations (Right-Hand Side) [Berkhout et al. 2007].

## **Dynamics around Market Transitions**

Figure 8.16 also shows two linked cycles, but in this case it is the world of social change rather than the world of technical change that plays the central role. The cyclical interaction processes for the development of new insights into changes in demand—causing emerging and receding markets—take place in the social-oriented sciences cycle (left-hand side of Figure 8.16) with the help of a wide range of different disciplines from

the soft sciences.<sup>5</sup> With these insights, new socio-technical solutions can be developed faster and with less economic risk. Anticipating changes in demand is very much a multi-disciplinary activity: a team of disciplinary experts from the soft sciences is needed to explain and extrapolate shifts in societal needs and concerns as well as shifts in trade conditions (many-to-one relationship) [Berkhout et al. 2007].

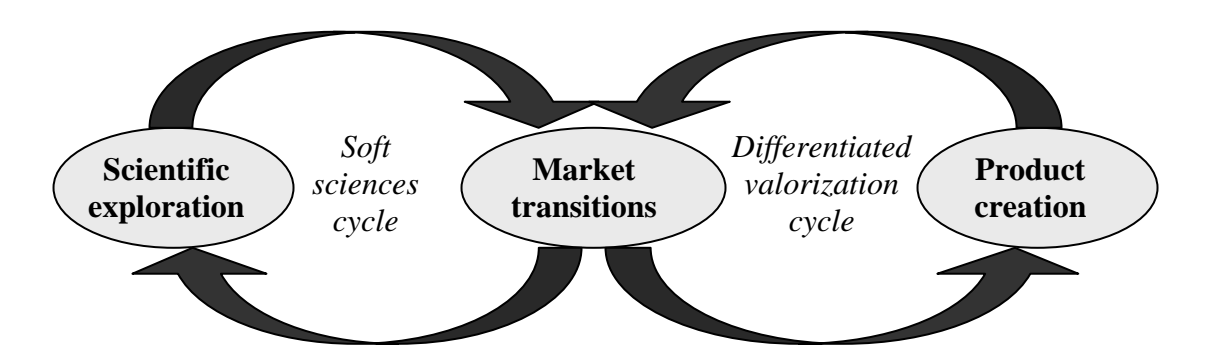


**Figure 8.16:** The Dynamic around Market Transitions are Driven by the Cyclical Interaction between New Scientific Insights into Changing Socio-Economic Behavior (Left-Hand Side) and Industrial Investments in New Product-Service Combinations (Right-Hand Side) [Berkhout et al. 2007].

### The Cyclic Process Model

If we compare Figures 8.15 and 8.16, the dual nature of scientific exploration and product creation becomes clear: science has both hard and soft aspects and product creation has both technical and social aspects. Figure 8.17 combines Figures 8.15 and 8.16. The result is the Cyclic Innovation Model (CIM), a systems view of change processes —and their interactions— as they take place in an open innovation arena: hard and soft sciences as well as engineering and valorization are brought together in a coherent system of processes. The combination of the involved changes leads to a wealth of opportunities. Here, entrepreneurship plays a central role: making use of those opportunities. Without the drive of entrepreneurs there is no innovation, and without innovation there is not new business [Berkhout et al. 2007].

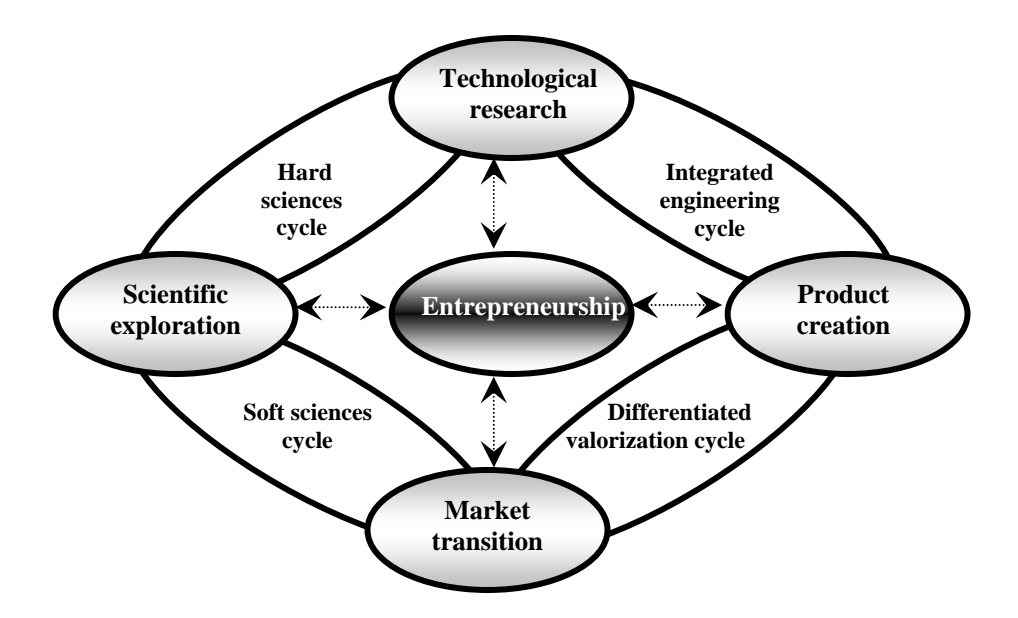


**Figure 8.17:** Cyclic Innovation Model (CIM), Presenting the Processes in Innovation by a Circle of Change. *Note:* In the model, changes in science (left) and industry (right) and changes in technology (top) and markets (bottom) are cyclically interconnected. It requires an open society to realize a rapid circulation along the circle, clockwise and anti-clockwise. The combination of all these changes creates an abundance of opportunities and it requires entrepreneurship to transform those opportunities into value for society (valorization) [Berkhout et al. 2007].

The first striking feature of Figure 8.17 is that the architecture is not a chain but a *circle*: Innovations build on innovations.<sup>6</sup> Ideas create new developments, successes create new challenges and failures create new insights. The creation of value is constantly accumulating<sup>7</sup>.

New instruments will be needed to preserve the strength of the dynamics in the circle. Large-scale failures like the dotcom debacle in 2000 undermine the confidence in the innovation economy and cause investment capital to become scarce. In terms of the cyclic process model: the processes of change are decoupled. The economy enters a phase of stagnation in which companies focus on existing business at lower cost (life-cycle management), until institutional adaptations are made and investment capital becomes available again to spur innovation. The dynamics in the circle then accelerate again. Carlota Perez calls this phase the turning point in a technological revolution [Perez 2002, Berkhout et al. 2007].

Figure 8.17 also shows that the proposed model portrays a system of dynamic processes –circle of change– with four 'nodes of change': scientific exploration, technological research, product creation and market transitions. But more importantly, between these nodes there are 'cycles of change' by which the dynamic processes in the nodes influence each other. In other words, they inspire, correct and supplement each other (first-order dependency).

This produces a system of linked cycles, which in turn also influence each other (higher-order dependencies). The result is a more or less synchronized regime of interconnected dynamic processes that spark a creative interaction between changes in science (left-hand side) and industry (right-hand side), and between changes in technology (top) and market (bottom). The combination of change and entrepreneurship is at the basis of innovation.

Autonomous social transitions manifest themselves in markets as changes in the need for products and services (the demand). Think of the huge influence of education and emancipation on a society. On the other hand, autonomous technological developments generate new products and services (the supply). Think of the huge influence of internet and mobile communication technology on a society. It is the cyclic interaction of both autonomous innovation drivers, social and technical, that will create new business with a maximum value for society.

Several variations exist in the proposed cyclic process model, depending on which goals we would like to achieve. For instance, if we would like to emphasize changes in society at large –combining economic and social values– then 'market transitions' should be replaced by 'societal transitions' in Figure 8.17. Similarly, if we would like to emphasize changes in today's energy system –aiming at renewable source– then 'market transitions' should be replaced by 'energy transitions'.

For the coming decades, environmental values will become one of the biggest drivers in innovation worldwide. This means that the transition node in the cyclic process model should be focused on changes in the global ecological system: 'ecological transitions' [Berkhout et al. 2007].

The details of CIM will be discussed in the following lines using EFC application example case.

## Innovation recovery of valuable salts with EFC

The innovations in which all four nodes contribute are called class 4. EFC application in separation industry is a class 4 innovation. CIM is performed with actors who are responsible for committing their challenges. The challenges, actors and responsibilities for accelerating the implementation of EFC science and technology are indicated in Figure 8.18.

Challenges in the demand: The chemical industry is growing day by day with the increasing population and chemical product consumption. For the same reason, clean and process water consumption of the population and the industries are increasing fast, at increasing rates as depicted in Figures 8.3 and 8.4. The salt (and acids) production involve mining industries or raw materials processing and separation of aqueous process and waste streams. Conventional salt recovery or waste stream treatment processes in several cases consume too much power and generate too much chemical waste. The environmental awareness of the governments and society pushes the technology developers and the users for more sustainable technologies with reduced waste generation and energy consumption.

EFC fulfils a societal demand for reducing energy, raw materials use, and pollution. Proper governmental regulations should, however, also be directed at fulfilling the same goals, otherwise the innovation is hampered. For instance, partly due to untimely and too locally imposed regulations the cleanest wet phosphoric acid plants in the world in the Rotterdam area, could not compete well anymore with those abroad (where no regulations were imposed) and had to close down as a result of which the heavy metal import in the Netherlands via phosphate fertiliser even increased, and the yearly

production of two million tons of high quality gypsum (already approved by the ministry for construction purposes) could not take place.

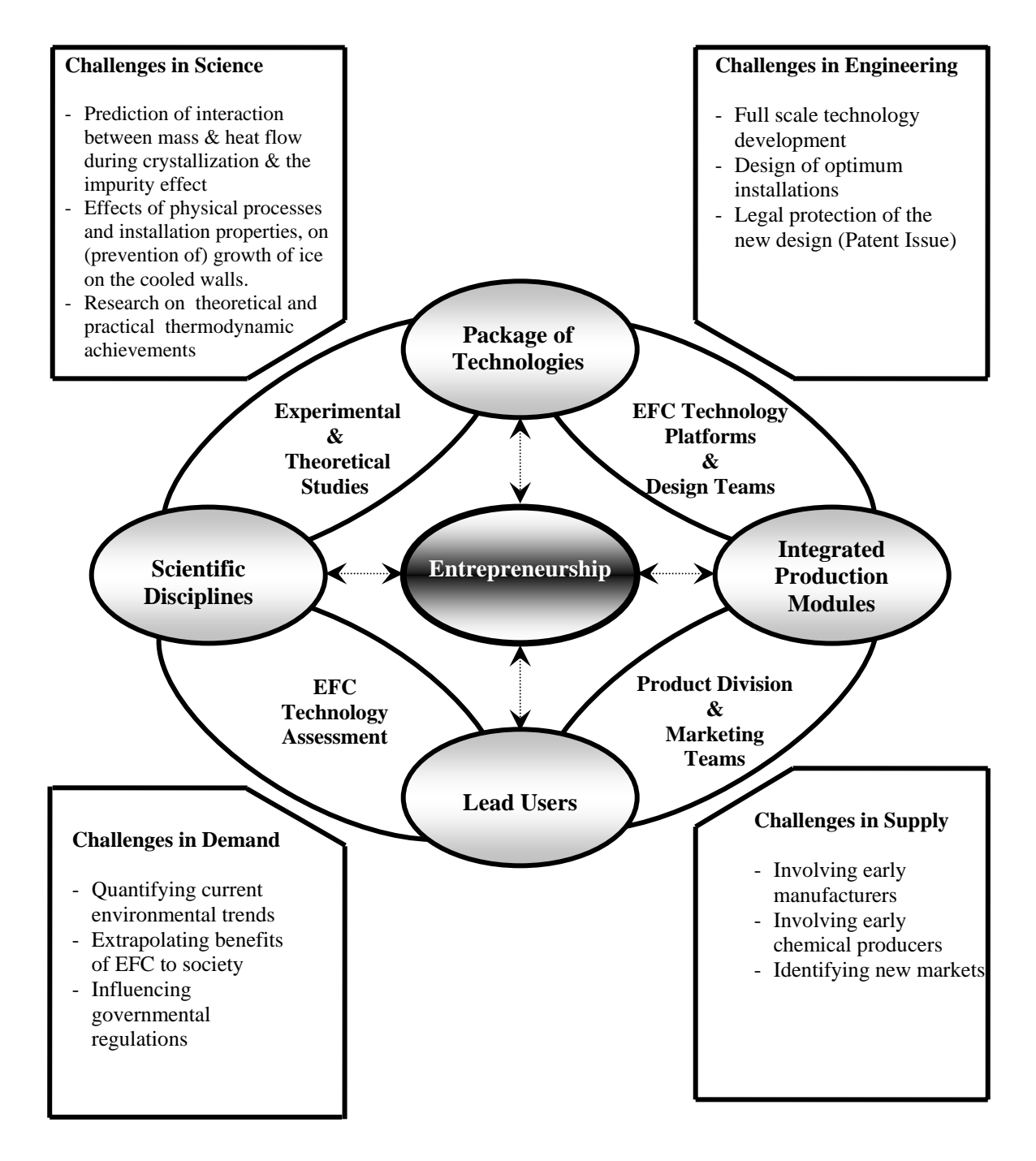


Figure 8.18: The Cyclic Innovation Model for accelerating commercial use of EFC Technology

- Challenges in supply: Product quality and specifications have to be developed in cooperation with early equipment manufacturers and early chemicals producers, as robust production and profitability are the first requirements from the business holders. New product-market combinations have to be identified.
- Challenges in engineering: Engineers from industry and applied researchers from hard sciences have to cooperate in the engineering cycle for development of full scale installations. During the EFC research and technology period for over 10 years, the industrial engineering and hard sciences always have worked side by side to develop robust EFC equipment and production technology for those. Two types of crystallizers (three generations of Cooled Disc Column Crystallizer and two generations of Scraped Cooled Wall Crystallizer) were designed, constructed and developed by the university and the industrial partners based on the experimental results and performance reports of applied researchers (university). Based on knowledge about the process and the equipment a complete mobile (skid mounted) pilot unit for industrial applications was designed and constructed. The work culminated in two successful demonstrations at actual production plant locations for two different EFC applications. The next challenges in engineering are developments of the full scale from current optimum installations and legal protection of the new design.
- Challenges in science: Thermodynamic analyses of practical and theoretical separations serve to define theoretical limits of EFC. The interactions between the physical processes and the installation properties have to be investigated, in particular in view of the scale formation (growth of ice or salt onto the cooling surfaces) and its prevention on the cooled surfaces. Higher heat transfer efficiencies increase the salt production rate and bring down salt production costs. Currently it is not possible to predict the maximum allowable (before encrustation occurs) temperature difference between cooled wall and the crystalliser fluid as a function of surface material type and its roughness, scraper material and construction, and all types of process conditions. Models to predict crystallization related phenomena such as coupled mass and heat flows during crystallization and the growth retarding effects of impurities have to be developed.

For each aqueous stream, EFC has its own specific implementation parameters. Eutectic points, kinetic parameters (nucleation and growth rates as a function of supersaturation and solution composition) for the salts or acids, impurity effects, and process parameters for each system have to be determined.

- Class 4 innovation: EFC is an example for a class 4 innovation as it is based on innovation contributions in all four nodes.

#### CONCLUSIONS

Eutectic Freeze Crystallization offers an economically, environmentally and socially attractive alternative for conventional separation techniques. A wide variety of process or waste streams can be treated with EFC, recovering both pure salt and ice crystals simultaneously from the feed stream using less energy and generating less waste. Moreover, huge amounts of valuable industrial aqueous streams that are currently too much energy intensive to be treated, could be commercially decompose into valuable materials when using EFC technology. The separation burden will be changed into a blessing by producing raw materials from waste streams by spending less energy. This inline with the green concept: 'from cradle to cradle' [McDonough et al. 2002].

To accelerate industrial implementation of EFC technology, the innovation concept represented by the Cyclic Innovation Model (CIM) is proposed. CIM presents innovation by symbiotic networks that connect science, technology, business and market in a cyclic manner.

## **NOTES** [Berkhout et al. 2007]

- 1. The innovation policy in the European Union aims at R&D budgets of the member states that amount to at least 3 % of their GNP.
- 2. A cycle consists of processes occurring repeatedly, each time with new starting conditions and a changing context. The dynamics in a cycle are determined by the cycle time and the amount of change per cycle.
- 3. It is appropriate to quote Charles Darwin here: 'the ones that survive are those that adapt'.
- 4. Disciplines from the hard sciences include specialist knowledge in the natural and life sciences.
- 5. Disciplines in the soft sciences include specialist knowledge in behavioral and social sciences.
- 6. Innovation guru Tom Peters (1997) also makes use of the circular architecture, displaying 15 ideas around a 'circle of innovation'.
- 7. The accumulation of innovations is visualized by the transition path.

#### REFERENCES

- Barduhn et al. 1979 Barduhn, A. J.; Manudhane, A.; Temperatures Required for Eutectic Freezing of Natural Waters, *Desalination*. 1979, 28, 233-241.
- Berkhout 2000 Berkhout, A. J.; The Dynamic Role of Knowledge in Innovation. An Integrated Framework of Cyclic Networks for the Assessment of Technological Change and Sustainable Growth. Delft University Press, Delft, 2000.
- Berkhout et al. 2006 Berkhout, A. J.; Hartmann, D.; Duin, P. van der; Ortt, R.; Innovating the Innovation Process, *Int. J. Technol. Management*. 2006, 34, Nos. 3/4, 390-404.
- Berkhout et al. 2007 Berkhout, A. J.; Van der Duin, P.; Hartmann, D.; Ortt, R.; Advances in the Study of Entrepreneurship, Innovation and Economic Growth Volume 17- The Cyclic Nature of Innovation: Connection Hard Sciences with Soft Values. Elsevier, 2007.
- Chesbrough 2003 Chesbrough, H.; Open innovation: The new imperative for creating and profiting from technology. 2003, Boston: Harvard Business School Press.
- Energy 2004 Energy Information Administration, International Energy Annual 2004, http://www.eia.doe.gov
- Envirochemie 2007 Envirochemie Technology for Water, 2007 http://www.envirochemie.nl/Materiaalterugwinning-AVR.76.0.html
- Forrester 1961 Forrester, J.; *Industrial dynamics*. 1961, Cambridge: Productivity Press.
- Genceli et al. 2005a Genceli, F. E.; Gärtner, R.; Witkamp, G. J.; Eutectic Freeze Crystallization in a 2<sup>nd</sup> Generation Cooled Disk Column Crystallizer for MgSO<sub>4</sub>.H<sub>2</sub>O System, *Journal of Crystal Growth*. 2005, 275(1-2), e1369-e1372.
- Genceli et al. 2005b Genceli, F.E.; Trambitas, D.O.; Gärtner, R.S.; Rodriguez, M.; Witkamp, G.J.; *VDI Berichte* (1901 II). 2005, 855-860.

- Genceli et al. 2005c Genceli F.E.; Gärtner R.S.; Trambitas D.; Rodriguez M.; Witkamp G.J.; A sustainable technology: Eutectic freeze crystallization-From batch laboratory to continuous industry applications, *Sustainable (Bio)Chemical Process Technology Incorporating the 6th International Conference on Process Intensification*. 2005, pp. 235-242, Delft, The Netherlands.
- Gleick 2007 Gleick, P.; *The World's Water 2006-2007: The Biennial Report on Freshwater Resources.* Island Press, Washington DC, 2007.
- Hartmann 2006 Hartmann, D.; Gold from garbage: Delft technology reclaims valuable metals from incinerated domestic waste in an Amsterdam test factory, *Delft Outlook*. 2006.
- Hermann 2005 Hermann W. A.; Quantifying global exergy resources, *Energy*. 2006, 31, 1685-1702.
- Himawan et al. 2002 Himawan, C.; Vaessen, R. J. C.; Seckler, M. M.; Witkamp,
   G. J.; Recovery of Magnesium Sulfate and Ice from Magnesium Sulfate Industrial
   Solution by Eutectic Freezing, *Proceeding of the 15<sup>th</sup> International Symposium on Industrial Crystallization*. 2002, Sorrento-Italy, 951-955.
- Himawan 2005 Himawan, C.; Characterization and Population Balance Modelling of Eutectic Freeze Crystallization. PhD dissertation, Delft, 2005.
- Himawan et al. 2006 Himawan, C.; Kramer, H. J. M.; Witkamp, G. J.; *Sep. Pur. Tech.* 2006, 50, 240-248.
- Kirschbaum 2005 Kirschbaum, R.; Open innovation in practice, *Research-Technology Management*, (July-August) 2005, 24-28.
- Kroon 2006 Kroon, M. C.; *Combined Reactions and Separations Using Ionic Liquids and Carbon Dioxide*. PhD dissertation. Delft, 2006.
- McDonough et al. 2002 McDonough, W.; Braungart, M.; Cradle to Cradle/ Remaking the Way We Make Things. 2002, North Point Press, New York.
- Perez 2002 Perez, C.; *Technical Revolutions and Financial Capital, the Dynamics of Bubbles and Golden Ages.* 2002, Edward Elgar Publishing Limited, UK.
- Pink 2006 Pink, D. H.; Investing in Tomorrow's Liquid Gold, *Yahoo*. April 19, 2006.

- Rem 2004 Rem, P. C.; De Vries, C.; Van Kooy, L. A.; Bevilacqua, P.; Reuter, M. A.; The Amsterdam pilot on bottom ash, *Minerals Engineering*. 2004, 17, 363-365.
- Senge 1994 Senge. P. M.; The Fifth Discipline, the Art and Practice of the Learning Organization. 1994, NY: Doubleday.
- Stepakoff et al. 1974 Stepakoff G. L.; Siegelman, D.; Johnson, R.; Gibson, W.; Development of a Eutectic Freezing Process for Brine Disposal, *Desalination*. 1974, 15, 25-38.
- Swenne 1983 Swenne, D. A.; *The Eutectic Crystallization of NaCl.2H*<sub>2</sub>*O and Ice*. PhD dissertation, Eindhoven, 1983.
- Swenne et al. 1985 Swenne D. A.; Thoenes, D.; The eutectic crystallization of sodium chloride dihydrate and ice, *Journal of Separation Process Technology*. 1985, 6, 17-25.
- United Nations 2007 United Nations Environment Programme/Grid-Arendal.

  Maps and Graphics, http://maps.grida.no
- Vaessen et al. 1999 Vaessen, R. J. C.; Van der Ham, F.; Witkamp, G. J.; Shifting Eutectic Conditions by Use of CO<sub>2</sub> Clathrates in Eutectic Freeze Crystallization, *Ann. N. Y. Acad. Sci.* 1999, 912, 483-495.
- Vaessen 2003 Vaessen, R. J. C.; *Development of Scraped Eutectic Freeze Crystallizers*. PhD dissertation, Delft, 2003.
- Vaessen et al. 2003a Vaessen, R. J. C.; Seckler, M. M.; Witkamp, G. J.; Eutectic Freeze Crystallization with an Aqueous KNO<sub>3</sub>-HNO<sub>3</sub> Solution in a 100-liter Cooled Disc Column Crystallizer, *Industrial Engineering and Chemistry Research*. 2003a, 42(20), 4874-4880.
- Vaessen et al. 2003b
   Vaessen, R. J. C.; Janse, B. J. H.; Seckler, M. M.; Witkamp,
   G. J.; Evaluation of the Performance of a Newly Developed Eutectic Freeze
   Crystallizer Scraped Cooled Wall Crystallizer, *Chemical Engineering Research* and Design. 2003b, 81(A10), 1363-1372.
- Van der Ham 1999 Van der Ham, F.; *Eutectic Freeze Crystallization*. PhD dissertation, Delft, 1999.

- Van der Ham 1998 Van der Ham, F.; Witkamp, G.J.; de Graauw, J.; G.M. van Rosmalen; Eutectic Freeze Crystallization: Application to Process Streams and Waste Water Purification, *Chem. Eng. Proc.* 1998, *37*(2), 207.
- Van der Ham et al.1999 Van der Ham, F.; Witkamp, G. J.; De Graauw, J.; Rosmalen,
  G. M.; Eutectic Freeze Crystallization Simultaneous Formation and Separation of
  Two Solid Phases, *Journal of Crystal Growth*. 1999, 198/199, 744-748.
- Van der Ham et al. 2003 Van der Ham, F.; Seckler, M. M.; Witkamp, G. J.; Eutectic Freeze Crystallization in a New Apparatus: The Cooled Disk Column Crystallizer, *Chemical Engineering and Processing*. 2003, 43(2), 161-167.
- Veolia 2007 Cyclope and Veolia Environmental Services; *Waste to resource abstract:* An abstract of "2006 World Waste Survey" by. 2007, http://www.veoliaenvironmentalservices.com
- West 2006 West, L; World Water Day: A Billion People Worldwide Lack Safe Drinking Water, *About*. March 26, 2006.
- Wikipedia 2007 Wikipedia-The Free Encyclopedia: Water resources, 2007, http://en.wikipedia.org/wiki/Water\_resources

## **APPENDIX**

Status of Eutectic Freeze Crystallization

English summary

Nederlandse samenvatting

Özet (Turkish summary)

Acknowledgments

Curriculum vitae

List of publications

# Status of Eutectic Freeze Crystallization

In 1996 Umicore courageously granted a Delft proposal to investigate the possibilities of applying freezing of water as a means to effectuate the crystallization of sodium nitrate to win this salt back from a process stream, despite opinions stating that processes based on cooling are always too expensive and that EFC would never yield a pure product. Based on the results, Kemira Ventures Rozenburg and Novem decided to sponsor a follow up, focusing on K (as nitrate) from potatoes (with Avebe) and culminating in the promotion work of Frank van der Ham (1999). By this time Shell sponsored TUD to investigate EFC on potassium phosphate from polyol mixtures and SMPO plant waste streams. Realization came that EFC could become very attractive provided that the scientific and technological levels were raised in a multidisciplinary program.

The first phase of the EFC project 'proof of principle' between 1997-2000 was followed by the second phase of the project 'development till pilot plant'. The second phase was achieved with the project partners TUD, TNO, DSM, Kemira, Nedmag and Larox-Pannevis between 2001-2007. The major challenge of EFC technology was the development of a suitable crystallizer -the Cooled Disk Column Crystallizer (CDCC)- for the simultaneous, continuous production and separation of both ice and salt; and demonstrating the industrial partners the successful continuous operation of the system. A complete mobile skid mounted unit for Eutectic Freeze Crystallization applications was designed and constructed together with industrial partners, allowing the system to be easily installed and connected to an industrial plant. As the first practical application, a demonstration at the site of Nedmag in Veendam was performed in April 2005 for the recovery of magnesium sulphate as hydrates from washing liquid from ex-flue gas desulphurization (see Figure A1). One week of successful demonstration proved the potential of EFC technology to the industrial partners and to potential end users. The pilot plant was operated in continuous production mode 12 hours per day for a week and produced up to 25 kg/hour of each ice and salt with a mean production rate of 12 kg/hour. Both products (i.e. ice and salt) were well filterable and of technical purity. The results of the first, industrial test run even exceeded the expectations for process stability and production capacity.

In March 2007 the skid mounted crystallizer with auxiliary equipment was moved to AVR in the Rotterdam port area. At AVR Europoort yearly about 300.000 tons of alkaline industrial waste water are incinerated, yielding a sodium (bi-)carbonate solution (about 5wt%) with about 1 g/L Mo, the so-called blow down solution. Currently at the expense of one tank truck of H<sub>2</sub>SO<sub>4</sub> per day this stream is neutralized to allow for Mo winning, and disposed. Using EFC, valuable pure crystalline sodium(bi-) carbonate can be obtained directly (1.5 ton/hr calculated as water-free salt), 25 to 30 tons of dematerialized water/h), the H<sub>2</sub>SO<sub>4</sub> use is eliminated and a concentrated sodium molybdate solution can be produces. Apart from these environmental benefits, also about 90 GWh electricity per year are calculated to be saved. During two weeks of demonstration (see Figure A2), using (part of) the actual blow down stream from the industrial waste water treatment plant of AVR, pure soda en pure ice were produced, with amounts of sodium bicarbonate as well. At the low operating temperature of about -4 C the decahydrate sodium carbonate salt was formed. The uptake of Mo in the soda crystals lies below 1 mg/kg. The purity is limited by the efficiency with which the mother liquor is washed from the crystals.

Over the last ten years many potential applications were discovered, many of them unexpected, and investigated. EFC can be applied to most combinations of acids and salts, with (in-)organic impurities allowed. About 20 systems were investigated experimentally as well. With the basic design of an EFC plant at AVR by KH-Engineering (Schiedam) under way, the "death valley" between research and proven technology is currently being crossed. This is an important step towards wider scale implementation of EFC. Next to this design, extending practical and theoretical EFC knowledge has a high priority now.











Figure A1: Demonstration of EFC Skid at Nedmag Industries, Veendam-Netherlands, April 2005











Figure A2: Demonstration of EFC Skid at AVR Industries, Rozenburg-Netherlands, March 2007

## **English summary**

## Scaling-up Eutectic Freeze Crystallization

Economical issues, global competition and changing stricter environmental regulations force (bio-)chemical plant owners and therefore the technology developers to pursue cleaner and more energy friendly yet cheaper processing equipment. Knowing that in the process industry more than half of the equipment and energy costs are due to separations, while the theoretical separation energy is 10-100 times lower than what actually is used, roughly  $10^{20}$  J energy could be saved yearly by establishing more efficient separation systems. Moreover, currently huge amounts of valuable industrial aqueous streams are disposed of as existing treatment methods consume too much energy or cannot handle the solutions. However, they could easily be turned into valuable raw materials once an affordable treatment technology is available.

Such a novel crystallization technology, Eutectic Freeze Crystallization (EFC) has been investigated and further developed in this thesis work. EFC operates around the eutectic temperature and composition of aqueous solutions and can be used for recovery of (valuable) dissolved salts (and/or or acids) and water from a wide variety of aqueous process streams. 100 % theoretical yield and up to 90% energy cost saving compared to evaporative crystallization make EFC technology very attractive. Using EFC, processes producing large quantities of saline solutions could be carried out in an ecologically and economically attractive way. It offers extremely high levels of purity of the end products and avoids undesirable side effects related to working at elevated temperatures (e.g. poisonous fumes when working with nitric acid) or avoids having to add extra chemicals for water treatment. It can also be applied in the food or pharmaceutical industry where high temperature operating conditions have to be avoided to preserve product quality. If the feed stream is clean and dilute enough to allow pre-concentration with reverse osmosis, EFC would form an elegant combination with reverse osmosis.

EFC is not only a new unit operation for processing, but it also changes the focus from cost to value by introducing a new separation process which can convert waste into raw materials.

An introduction and a brief summary of earlier work are given in *Chapter 1*.

## Objectives of this thesis work are:

- to develop eutectic freeze crystallization equipment and the technology for industrial scale.
- to understand eutectic freeze crystallization physical phenomena on the basis of experimental analysis and optimization of the hybrid eutectic type of crystallizer.
- to investigate some unexplored fundamental aspects about the MgSO<sub>4</sub> model solution.
- to understand nucleation and growth from a MgSO<sub>4</sub> aqueous solution on cooled surfaces theoretically and experimentally also in relation to scale formation prevention.
- to connect science and business and suggest a model for fast implementation of eutectic freeze crystallization technology in the industry.

The experimental study on pilot scale Cooled Disc Column Crystallizer (CDCC-2) designed for continuous EFC operation is presented in *Chapter 2*. The crystallizer having 150-liter capacity and 5.6 m<sup>2</sup>/m<sup>3</sup> cooling area was tested for an industrial MgSO<sub>4</sub> stream. Compared to the previous EFC crystallizer designs, CDCC-2 performance was evaluated in terms of heat transfer; ice and salt sizes, production and growth rates.

Inline solution concentration and supersaturation determinations have key importance on crystallization evaluation experiments and process control of eutectic freeze crystallization due to its simultaneous ice and salt production feature. For that reason application of conductivity and refractive index measurement techniques for inline concentration and supersaturation measurements of MgSO<sub>4</sub> solution was studied in *Chapter 3*. An industrial MgSO<sub>4</sub> solution having concentration range between 16 to 22 wt% and temperature range between 10 to -5 °C was investigated. Conductivity

measurements were correlated to concentrations and temperature with the empirical Casteel-Amis equation whereas refractivity index measurements were correlated to concentrations and temperature with a developed empirical model. The metastable lines for ice and salt of MgSO<sub>4</sub> system were drawn based on the measurements at the onset of crystallization upon cooling of several solution concentrations. In the working range of EFC, the relative supersaturations were calculated to be  $\sigma_{icemax}$ =0.2 and  $\sigma_{saltmax}$ =0.23. The error in conductivity in relation to the metastable zone width was roughly 20% and in refractive index measurements 3%.

Chapter 4 presents the third generation Cooled Disc Column Crystallizer (CDCC-3) and Skid Mounted Unit, designed and constructed for 130 ton/year MgSO<sub>4</sub>·7H<sub>2</sub>O and water production capacities. The completely mobile skid mounted unit consists of the CDCC-3, a belt filter, a wash column, storage tanks and special measurement devices namely image analysis, data acquisition and a field bus based control system. Practical performance of CDCC-3, having 220-liters capacity, 7 compartments and 7.7 m<sup>2</sup>/m<sup>3</sup> cooling surface area, was evaluated in terms of heat transfer properties and product qualities. For 30 minutes of residence time and varying logarithmic mean temperature differences between bulk and coolant temperatures for CDCC-3, the heat fluxes were calculated and average crystal sizes and impurity contents for MgSO<sub>4</sub> aqueous system were measured. The experimental data were used to estimate the parameters for kinetic relations for nucleation and growth rates for ice and MgSO<sub>4</sub>·11H<sub>2</sub>O salt.

As previously mentioned few times, in this thesis work a MgSO<sub>4</sub> aqueous solution was used as model system for understanding EFC physical phenomena and for developing the technology. For a more elaborate research, MgSO<sub>4</sub> salt crystal structure at eutectic conditions was studied and reported in *Chapter 5*. The MgSO<sub>4</sub> crystal hydrate formed below approximately 0 °C was proven to be MgSO<sub>4</sub>·11H<sub>2</sub>O (undecahydrate) instead of the common reported MgSO<sub>4</sub>·12H<sub>2</sub>O (dodecahydrate). The crystals were grown from solution by eutectic freeze and by cooling crystallization. The crystal structure analysis and the molecular arrangement of these crystals were determined using single crystal

X-ray diffraction. Raman spectroscopy was used for characterizing MgSO<sub>4</sub>·11H<sub>2</sub>O and for comparing the vibrational spectra with MgSO<sub>4</sub>·7H<sub>2</sub>O salt. Between the two salts there are significant differences mainly in the type of interactions of water with sulfate groups in the lattice, in view of the different O-H stretching vibrations, as well as sulfate, O-H...O (sulfate) and O-Mg-O bands vibrational modes. Thermo gravimetric analysis confirmed the stochiometry of the MgSO<sub>4</sub>·11H<sub>2</sub>O salt. Additionally the Miller indices of the major faces of MgSO<sub>4</sub>·11H<sub>2</sub>O crystals were defined.

Resolving the formula of MgSO<sub>4</sub>·11H<sub>2</sub>O brought up the idea of finding the related molecule in nature and depositing as a new mineral species. *Chapter 6* covers the discovery of the natural occurrence of the MgSO<sub>4</sub>·11H<sub>2</sub>O new mineral -Meridianiite- as salt inclusions in sea ice from Saroma Lake-Japan and in Antarctic ice. Existence of meridianiite was confirmed using Micro Raman spectroscopy technique by comparing and presenting the excellent harmony between the Raman spectra of synthetic MgSO<sub>4</sub>·11H<sub>2</sub>O and the inclusions. Epsomite and mirabilite Raman Spectra are also presented to be compared with the one of meridianiite. Both sea ice and Antarctic ice meridianiite inclusions have similar morphology with the synthetic MgSO<sub>4</sub>·11H<sub>2</sub>O crystals.

In *Chapter 7* nucleation and crystal growth of MgSO<sub>4</sub> aqueous solution on a cooled surface were studied theoretically and experimentally. Better understanding of these phenomena is extremely important for scale prevention on cooled surfaces in order to lower the operational costs in industrial crystallizers. The excess entropy production rate for heat and mass transport into, out of and across the interface was used to define the fluxes and forces of the system. The method describes the interface as a separate (two-dimensional) phase in local equilibrium. Coupled heat and mass flux equations from non-equilibrium thermodynamics (Onsager theory with reciprocal relations) were defined for crystal growth and the temperature jump at the interface of the growing crystal. All interface transfer resistivities were determined using MgSO<sub>4</sub>·7H<sub>2</sub>O crystallization on a cooled surface as an example case. The coupling coefficient showed the distribution ratio of heat of crystallization between the salt and liquid phases.

From an economical and an environmental point of view, fast implementation of eutectic freeze crystallization is desired. During the last ten years the successful cooperation between the knowledge institutes, an equipment manufacturer and the users (process industries) developed EFC up to the pilot scale state. Suggestions for the fastest implementation of EFC technology to the market were made based on the Cyclic Innovation Model (CIM) which considers the innovation process as coupled 'cycles of change', where developments take place in all cycles simultaneously and are driven by an entrepreneur. Traditionally, innovations are considered as linear chains of independent actions, where each stage requires a considerable amount of time, holding up the next stage. This is one important reason for the traditional long implementation trajectory. CIM overcomes the obstacles that linear chain innovation faces by triggering developments in all cycles and collaborating all involved actors in coupled networks. *Chapter 8* aims to describe the cyclic innovation model and to set a path for commercialization of the eutectic freeze crystallization technology.

## **Nederlandse samenvatting**

# Eutectische Vrieskristallisatie Opschalen

Economische kwesties, globale competitie en veranderende striktere milieuwetgeving dwingen (bio-)chemische fabriekseigenaren en daarom de technologieontwikkelaars tot het nastreven van schonere, energievriendelijker en toch goedkopere procesapparatuur. Wetende dat in de procesindustrie meer dan de helft van de kosten voor apparatuur en energie gerelateerd zijn aan scheidingen, terwijl de theoretische scheidingsenergie 10-100 maal lager is dan wat feitelijk gebruikt wordt, zou jaarlijks ongeveer 10<sup>20</sup> J aan energie bespaard kunnen worden door efficiëntere scheidingssystemen in te voeren. Bovendien worden vandaag de dag grote hoeveelheden waardevolle industriële waterige stromen gedumpt doordat bestaande behandelingsmethoden te veel energie gebruiken of niet in staat zijn de oplossingen te behandelen. Ze zouden echter eenvoudig in waardevolle grondstoffen kunnen worden omgezet zodra een betaalbare verwerkingstechnologie beschikbaar is.

Een dergelijke nieuwe kristallisatietechnologie, Eutectic Freeze Crystallization (EFC), is onderzocht en verder ontwikkeld in dit promotiewerk. EFC opereert rondom de eutectische temperatuur en samenstelling van waterige oplossingen en kan gebruikt worden voor de winning van (waardevolle) opgeloste zouten (en/of zuren) en water vanuit een breed spectrum aan industriële waterige processtromen. 100% theoretische tot 90% opbrengst en oplopende energiebesparing vergeleken verdampingskristallisatie maken EFC technologie zeer aantrekkelijk. Gebruikmakend van EFC kunnen processen die grote hoeveelheden zouthoudende oplossingen produceren op een ecologisch en economisch aantrekkelijke manier uitgevoerd worden. Het biedt extreem zuiverheid van de eindproducten en voorkomt nevenverschijnselen gerelateerd aan het werken bij verhoogde temperatuur (bijvoorbeeld giftige dampen bij het werken met salpeterzuur) of voorkomt de noodzaak om extra chemicaliën toe te voegen voor waterzuivering. Het kan ook worden toegepast in de voedingsmiddelenindustrie en farmaceutische industrie waar condities met hoge temperaturen vermeden moeten worden om de productkwaliteit te waarborgen. Als de voedingsstroom schoon en verdund genoeg is om vooraf te concentreren met omgekeerde osmose, zou EFC een elegante combinatie met omgekeerde osmose kunnen vormen.

EFC is niet alleen een nieuwe processtap, maar het weerlegt ook de werkzaamheden van kosten naar waarde door de introductie van een nieuw scheidingsproces dat afval kan omzetten in grondstoffen.

Een introductie en korte samenvatting van eerder werk zijn gegeven in *Hoofdstuk 1*.

## Doelstellingen van dit promotiewerk zijn:

- Het ontwikkelen van apparatuur en technologie voor eutectische vrieskristallisatie op industriële schaal.
- Het begrijpen van de fysische fenomenen van eutectische vrieskristallisatie op basis van experimentele analyse en optimalisatie van de hybride type eutectische kristallisator.
- Het onderzoeken van enkele nog niet verkende fundamentele aspecten van de MgSO<sub>4</sub> modeloplossing.
- Het begrijpen van nucleatie en groei vanuit een waterige MgSO<sub>4</sub> oplossing op gekoelde oppervlakken, theoretisch en experimenteel ook in relatie tot het voorkomen van aankorsting.
- Het verbinden van wetenschap en bedrijfsleven en het voorstellen van een model voor de snelle implementatie van eutectische vrieskristallisatie in de industrie.

De experimentele studie op proeffabriekschaal met de Cooled Disc Column Crystallizer (CDCC-2) ontworpen voor continue EFC operatie wordt gepresenteerd in *Hoofdstuk 2*. De kristallisator met een capaciteit van 150 liter en 5,6 m<sup>2</sup>/m<sup>3</sup> koeloppervlak is getest voor een industriële MgSO<sub>4</sub> stroom. In vergelijking met voorgaande ontwerpen van EFC kristallisatoren zijn de CDCC-2 prestaties geëvalueerd in termen van warmteoverdracht, ijs- en zoutgrootte, productie en groeisnelheden.

In-line bepaling van concentratie en oververzadiging zijn van groot belang voor evaluatie van kristallisatie-experimenten en de procesbesturing van eutectische vrieskristallisatie vanwege de simultane ijs- en zoutproductie. Om deze reden is de toepassing van meettechnieken voor geleidbaarheid en brekingsindex voor in-line metingen van concentratie en oververzadiging van een MgSO<sub>4</sub> oplossing bestudeerd in *Hoofdstuk 3*. Een industriële MgSO<sub>4</sub> oplossing met een concentratiebereik van 16 tot 22 wt% en een temperatuursbereik van 10 tot -5 °C is onderzocht. Geleidbaarheidsmetingen zijn gecorreleerd aan concentraties en temperatuur met de empirische Casteel-Amis vergelijking terwijl brekingsindexmetingen gecorreleerd zijn aan concentraties en temperatuur met een ontwikkeld empirisch model. De metastabiele lijnen voor ijs en zout van het MgSO<sub>4</sub> systeem zijn bepaald op basis van metingen op het begin van kristallisatie gedurende koeling van oplossingen met verscheidene concentraties. Binnen het werkbereik van EFC is de relatieve oververzadiging berekend als σ<sub>ijsmax</sub>=0.2 en σ<sub>zoutmax</sub>=0.23. De fout in geleidbaarheid met betrekking tot de breedte van de metastabiele zone is ongeveer 20% en in brekingsindexmetingen 3%.

Hoofdstuk 4 presenteert de derde generatie Cooled Disc Column Crystallizer (CDCC-3) en Skid Mounted Unit, ontworpen en geconstrueerd voor productiecapaciteiten van 130 ton/jaar MgSO<sub>4</sub>·7H<sub>2</sub>O en water. De volledig mobiele Skid Mounted Unit bestaat uit de CDCC-3, een bandfilter, een waskolom, voorraadvaten en speciale meetinstrumenten te weten beeldanalyse, data-acquisitie en een besturingssysteem gebaseerd op Fieldbus. De praktische prestaties van CDCC-3, met een capaciteit van 220 liter, 7 compartimenten en 7,7 m²/m³ koeloppervlak, is geëvalueerd in termen van eigenschappen voor warmteoverdracht en productkwaliteit. Voor een verblijftijd van 30 min en variërende logaritmisch gemiddelde temperatuursverschillen tussen bulk en de koelvloeistof van de CDCC-3 is de warmteflux berekend en zijn de gemiddelde kristalgroottes en onzuiverheden voor het MgSO<sub>4</sub> systeem gemeten. De experimentele data is gebruikt om de parameters voor kinetische relaties voor nucleatie- en groeisnelheden te schatten voor ijs en het MgSO<sub>4</sub> 11H<sub>2</sub>O zout.

Zoals voorafgaand reeds een aantal malen genoemd is, is in dit promotiewerk een waterige MgSO<sub>4</sub> oplossing gebruikt als modelsysteem om de fysische fenomenen van EFC te begrijpen en om de technologie te ontwikkelen. Voor uitgebreider onderzoek is de kristalstructuur van het MgSO<sub>4</sub> zout nabij eutectische condities bestudeerd en gerapporteerd in *Hoofdstuk 5*. Het MgSO<sub>4</sub> zouthydraat gevormd onder ongeveer 0°C is bewezen MgSO<sub>4</sub>11H<sub>2</sub>O (undecahydraat) te zijn in plaats van het gebruikelijk gerapporteerde MgSO<sub>4</sub>·12H<sub>2</sub>O (dodecahydraat). De kristallen zijn gegroeid vanuit oplossing door eutectische vrieskristallisatie en koelingkristallisatie. De analyse van de kristalstructuur en de moleculaire rankschikking van deze kristallen zijn bepaald door gebruik te maken van röntgendiffractie aan éénkristallen. Raman spectroscopie is gebruikt voor het karakteriseren van MgSO<sub>4</sub>·11H<sub>2</sub>O en voor het vergelijken van de trillingsspectra met het MgSO<sub>4</sub>·7H<sub>2</sub>O zout. Tussen de twee zouten zijn belangrijke verschillen gevonden voornamelijk in het type interactie van water met sulfaatgroepen in het rooster, gezien de verschillende trillingen van uitrekking van O-H, alsmede sulfaat, O-H...O (sulfaat) en O-Mg-O bands vibrational modes. Thermogravimetrische analyse bevestigt de stoichiometrie van het MgSO<sub>4</sub>·11H<sub>2</sub>O zout. Bovendien zijn de Miller indexen van de belangrijkste facetten van MgSO<sub>4</sub>·11H<sub>2</sub>O kristallen gedefinieerd.

Het oplossen van de formule voor MgSO<sub>4</sub>·11H<sub>2</sub>O bracht het idee naar boven om het gerelateerde molecuul in de natuur te vinden en het te deponeren als een nieuwe mineraalsoort. *Hoofdstuk 6* omvat de ontdekking van het natuurlijke voorkomen van het nieuwe mineraal MgSO<sub>4</sub>·11H<sub>2</sub>O –Meridianiite- als zoutinsluiting in pakijs uit het Saroma meer in Japan en in Antarctisch ijs. Het bestaan van meridianiite is bevestigd door gebruik te maken van Raman spectroscopie door vergelijking met en presentatie van de excellente overeenkomst tussen de Raman spectra van synthetisch MgSO<sub>4</sub>·11H<sub>2</sub>O en de insluitingen. Epsomite en mirabilite Raman spectra zijn ook gepresenteerd om te vergelijken met meridianiite. Zowel meridianiite insluitingen in pakijs als Antarctisch ijs vertonen een overeenstemmende morfologie met de synthetische MgSO<sub>4</sub>·11H<sub>2</sub>O kristallen.

In Hoofdstuk 7 zijn nucleatie en kristalgroei vanuit waterige MgSO<sub>4</sub> oplossing op een gekoeld oppervlak theoretisch en experimenteel bestudeerd. Een beter begrip van deze fenomenen is erg belangrijk voor het voorkomen van aankorsting op gekoelde oppervlakken zodat de operationele kosten van industriële kristallisatoren verlaagd kunnen worden. De productiesnelheid van exces entropie van warmte- en stofoverdracht in, uit en over het grensvlak is gebruikt om de fluxen en krachten van het systeem te definiëren. De methode beschrijft het grensvlak als een aparte (tweedimensionale) fase in lokaal evenwicht. Gekoppelde vergelijkingen voor warmte- en massaflux vanuit de nietevenwichtsthermodynamica (Onsager theorie met reciproque relaties) zijn gedefinieerd voor kristalgroei en de temperatuursprong op het grensvlak van het groeiende kristal. Alle overdrachtsweerstanden op het grensvlak zijn bepaald door MgSO<sub>4</sub>·7H<sub>2</sub>O kristallisatie op een gekoeld oppervlak te gebruiken als voorbeeld. De koppelingscoëfficiënt liet de verdelingsratio van kristallisatiewarmte tussen het zout en de vloeistoffases zien.

Vanuit een economisch en milieutechnisch oogpunt gezien, is snelle implementatie van eutectische vrieskristallisatie gewenst. Gedurende de afgelopen tien jaar heeft een succesvolle samenwerking tussen de kennisinstituten, een apparatenbouwer en de gebruikers (procesindustrie) EFC ontwikkeld tot aan proeffabriekschaal. Suggesties voor de snelste implementatie van EFC-technologie in de markt zijn gemaakt gebaseerd op het Cyclic Innovation Model (CIM). Dit model beschouwt het innovatieproces als gekoppelde cyclussen van verandering, waar ontwikkelingen in alle cyclussen tegelijkertijd plaatsvinden en gedreven worden door een ondernemer. Traditioneel gezien worden innovaties beschouwd als lineaire kettingen van onafhankelijke acties, waarbij iedere fase een aanzienlijke hoeveelheid tijd vereist wat de volgende fase vertraagd. Dit is een belangrijke oorzaak voor het traditioneel lange implementatietraject. CIM overwint de belemmeringen die lineaire kettinginnovatie met zich meebrengt door ontwikkelingen in alle cyclussen te stimuleren en het laten samenwerken van alle betrokken actoren in gekoppelde netwerken. Hoofdstuk 8 tracht het cyclische innovatiemodel te beschrijven en een pad uit te zetten voor commercialisering van de eutectische vrieskristallisatie technologie.

## Özet (Turkish summary)

# Ötektik Donma Kristalizayonunda Boyut Büyütme

Ekonomik sebepler, global rekabet ve katılaşan çevre yönetmelikleri, (bio)-kimyasal tesis sahipleri ve buna bağlı olarak teknoloji geliştiricilerini daha temiz, enerji dostu ve ucuz proses donanımlarını üretmeye ve kullanmaya zorlamaktadır. Proses endüstrisinde ekipman ve enerji masraflarının yarıdan çoğunun, teorik gereksinimden 10 ila 100 katı fazlasını harcayan ayırma teknolojilerine kullanıldığı bilinmektedir. Daha verimli ayırma sistemleri kullanıldığında yılda yaklasik  $10^{20}$  J enerji tasarruf edilebilir. Ne yazık ki günümüzde büyük miktarlarda değerli endüstriyel çözelti, kullanılan arıtma metodlarının fazla enerji gereksinimi ya da uygun teknolojilerin henüz gelişmemesi nedeniyle hiç işlenemeden elden çıkarılmaktadır. Halbuki ekonomik arıtma teknolojilerinin geliştirilmesi sayesinde bu çözeltiler kolaylıkla değerli hammaddelere dönüştürülebilirler.

Bu tez çalışması süresinde, yenilikçi bir kristalizasyon metodu olan Ötektik Dondurma Kristalizasyonu (Eutectic Freeze Crystallization-EFC), araştırılıp geliştirilmiştir. Çözeltilerin ötektik sıcaklık ve bileşimi civarında çalıştırılan EFC, (değerli)-çözünmüş tuzları (ve/veya asitleri) ve suyu pek çok proses akımından geri kazanmak için kullanılır. %100 teorik verim ve evaporatif kristalizasyonla karşılaştırıldığında %90' a ulaşan enerji tasarrufu özellikleri EFC teknolojisini cazip kılmaktadır. EFC kullanımı ile büyük miktarlarda tuzlu çözelti üreten proseslerin ekolojik ve ekonomik olarak yürütülmesi cazip hale gelecektir. Bu teknoloji son derece yüksek saflıkta ürünler sunarken, yüksek sıcaklıklarda çalışan metodların istenmeyen yan etkilerini önler (örneğin nitrik asitle çalışmada zehirli duman çıkışı). Ayrıca suyun arıtılması sırasında ekstra kimyasalların eklenmesini de engeller. Ayrıca ürün kalitesinin korunması için, yüksek sıcaklık çalışma şartlarının uygun olmadığı gıda ve ilac endüstrisinde de kullanılabilir. Besleme çözeltisi EFC işlemi öncesinde ters osmosis (reverse osmosis) methoduyla konsantre edilecek

kadar temiz ve seyreltik ise, EFC ve ters osmosis metotları mükemmel bir kombinasyon oluşturur.

EFC yeni bir ünit operasyon olmasının yanı sıra, atıktan hammadde üreterek onu değere çeviren yeni bir düşünce sistemini de beraberinde getirmektedir.

Giriş ve bu konudaki geçmiş çalışmalara yönelik kısa bir özet, *Bölümde 1*' de sunulmaktadır.

#### Özetle tezin amaçları:

- Ötektik donma kristalizasyonu ekipman ve teknolojisinin endüstriyel ölçeğe geçirilmesi.
- Ötektik donma kristalizasyonu fiziksel olgusunun deneysel analizler ve hibrit ötektik tip kristalizör optimizasyonu açısından anlaşılması.
- MgSO<sub>4</sub> model çözeltisinin keşfedilmemiş temel özelliklerinin araştırılması.
- MgSO<sub>4</sub> çözeltisinin soğuk yüzeylerde nükleasyon ve büyümesinin kabuk oluşumu (scale formation) ile ilişki; ve bu oluşumun önlenmesinin teorik ve deneysel olarak anlaşılması.
- Ötektik donma kristalizasyonun endüstriye hızla uyarlanmasını sağlıyacak bir model önerilerek, bilim ile sanayinin bağdaştırılması.

EFC operasyonları için tasarlanan pilot ölçekli Soğutmalı Disk Kolon Kristalizorü (Cooled Disc Column Crystallizer- CDCC-2) ile ilgili deneysel çalışma *Bölüm 2*' de sunulmaktadır. 150 litre kapasiteye ve 5.6 m²/m³ soğutma yüzeyine sahip kristalizör, endüstriyel MgSO<sub>4</sub> solüsyonu kullanılarak test edilmiştir. CDCC-2 performansı daha önceki EFC kristalizör tasarımlarına kıyasla ısı transferi, buz-tuz kristal boyutları, üretim ve kristal büyüme hızları açısından değerlendirilmiştir.

Çözelti konsantrasyonunun ve aşırı doygunluğunun anında (inline) belirlenmesi, ötektik dondurma kristalizasyonu deneylerinin değerlendirilmesi ve aynı anda buz ve tuz üreten sistemin proses kontrolünün sağlanması açısından önemlidir. *Bölüm 3*' de anında (inline) iletkenlik (conductivity) ve refraktif indeks (refractive index) tekniklerinin, MgSO<sub>4</sub>

çözeltisinin konsantrasyon ve süper doygunluk ölçümlerinde kullanılması anlatılmıştır. Endüstriyel MgSO<sub>4</sub> çözeltisi, %16 ve 22 konsantrasyonları ve 10 ila -5 °C sıcaklıkları arasında incelenmiştir. İletkenlik (conductivity) konsantrasyon ve sıcaklıkla emperik Casteel-Amis denklemi (Casteel-Amis equation) ile; refraktif indeks (refractivity index) ise konsantrasyon ve sıcaklık ile geliştirilen emperik bir model kullanılarak ilişkilendirilmiştir. MgSO<sub>4</sub> sisteminde buz ve tuz metastabilite limitleri (metastable lines), değişik konstantrasyonlarda yapılan onlarca soğutma deney sonuçlarına dayandırılarak çizilmiştir. EFC çalışma aralığında,  $\sigma_{buz-max}$ =0.2 and  $\sigma_{tuz-max}$ =0.23 relatif doygunlukları (relative supersaturations) hesaplanmıştır. İletkenlik ölçümleri yaklaşık %20, refraktif indeks ölçümlerinin ise %3 hata içerdigi tespit edilmiştir.

Bölüm 4' de üçüncü jenerasyon Soğutmalı Disk Kolon Kristalizörü (Cooled Disc Column Crystallizer- CDCC-2) ve 130 ton/yıl MgSO<sub>4</sub>·7H<sub>2</sub>O ve su üretme kapasitesine sahip Skid Mounted Ünite (Skid Mounted Unit) tasarımları sunulmaktadır. Tamamen mobil olan Skid Mounted Ünite, CDDC-3, bir bant filtre (band filter), bir yıkama kolonu (wash column) ve depolama tanklarının (storage tanks) yanısıra, görüntü analizi (image analysis), bilgi toplama (data acquisition) ve field-bus kontrol sistemi (field bus based control system) gibi özel ölçüm cihazlarından oluşmuştur. 220 litre kapasite, 7 kompartman ve 7.7 m²/m³ sogutma yüzeyine sahip CDCC-3' ün performansı, ısı iletim özellikleri ve ürün kalitesi açısından değerlendirilmiştir. MgSO<sub>4</sub> çözelti sistemi için, CDCC-3 içerisinde sabit 30 dakikalik kalma süresi (residence time) ve değişken çözelti (bulk)-soğutucu (coolant) logaritmik ortalama sıcaklık farkları kullanılarak ısı akısı, ortalama kristal boyları ve kristallerin safsızlık içerikleri ölçülmüştür. Deneysel veriler, buz ve MgSO<sub>4</sub>·11H<sub>2</sub>O tuzu için nükleasyon ve büyüme hız kinetik parametrelerinin tespitinde kullanılmıştır.

Daha önceden de söz edildiği gibi bu tez çalışmasında, EFC fiziksel olgusunun anlaşılması ve teknolojinin geliştirilmesi için MgSO<sub>4</sub> çözeltisi model sistem olarak kullanılmıştır. Daha detaylı bir araştırma için ötektik şartlarda MgSO<sub>4</sub> tuz yapısı üstüne yapılan çalışma *Bölüm 5*' de raporlandırılmıştır. Yaklaşık 0 °C sıcaklığın altında oluşan

MgSO<sub>4</sub> kristal hidrat yapısının genel olarak bilinen MgSO<sub>4</sub>·12H<sub>2</sub>O (dodecahydrate) yerine MgSO<sub>4</sub>·11H<sub>2</sub>O (undecahydrate) olduğu ispatlanmıştır. Kristaller, çözeltiden ötektik donma (eutectic freeze) ve soğuma kristalizasyonu (cooling crystallization) yöntemleriyle büyütülmüştür. Kristallerin yapısı ve molekül düzeni tek kristal X-Ray difraktif (single crystal X-Ray diffraction) tekniği ile tespit edilmiştir. Raman Spektrospik yöntemi (Raman Spectroscopy), MgSO<sub>4</sub>·11H<sub>2</sub>O tuzunun karakterizasyonu ve MgSO<sub>4</sub>·7H<sub>2</sub>O tuzu ile kıyaslanması amacıyla kullanılmıştır. İki tuz arasında suyla sulfat gruplarının etkileşimleri, O-H stretching vibrasyonları, O-H...O (sulfat) ve O-Mg-O bant vibrasyonları başta olmak üzere önemli farklar mevcuttur. Termogravimetrik analizler (thermo gravimetric analysis) MgSO<sub>4</sub>·11H<sub>2</sub>O tuzundaki su molekül sayısını stokiometrik olarak onaylamaktadır. Ayrıca MgSO<sub>4</sub>·11H<sub>2</sub>O kristalinin temel yüzeyleri icin Miller indeksi (Miller indices) tanımlanmıştır.

MgSO<sub>4</sub>·11H<sub>2</sub>O formulünün çözülmesi, bahsi geçen molekülün doğada bulunabilme olasılığını ve mineral olarak kayıtlandırılabileceği fikrini doğurmuştur. *Bölüm 6*, MgSO<sub>4</sub>·11H<sub>2</sub>O yapısındaki yeni mineral -Meridianiite-' in doğada Japonya-Saroma Gölü'nde ve Antarktika buzulundaki keşfini anlatmaktadır. Micro Raman Spektroskopik (Micro Raman Spectroscopy) yöntemi, Meridianiite' in varlığını sentetik MgSO<sub>4</sub>·11H<sub>2</sub>O kristalleri ile deniz ve Antarktika buzullarındaki safsızlıkların (inclusions) arasındaki mükemmel çakısmayı göstererek kanıtlamıştır. Ayrıca Epsomit (epsomite) ve Mirabilit (mirabilite) Raman spektraları da Meridianiite ile karşılaştırılmıştır. Hem deniz hem de Antarktika buzullarında Meridianiite safsızlıklarının (inclusions) sentetik MgSO<sub>4</sub>·11H<sub>2</sub>O kristalleri ile benzer morfolojiye sahip olduğu gözlemlenmiştir.

Bölüm 7' de MgSO<sub>4</sub> çözeltisi kullanılarak soğuk yüzey üzerinde kristallerin nükleasyonu ve büyümesi teorik ve deneysel olarak araştırılmıştır. Bu fenomenin daha iyi anlaşılması, soğuk yüzeylerde kabuk oluşumunun engellenmesi ve endüstriyel kristalizörlerdeki operasyon maliyetinin düşürülmesi açısından büyük önem taşır. Kristalizasyon arayüzeyine (interface) giren, çıkan ve içinden geçen ısı ve kütle iletimi excess entropi üretim hızları (excess entropy production rate for heat and mass transport) sistemin akı ve kuvvetlerini tanımlamakta kullanılmıştır. Bu metot, kristalizasyon arayüzeyini (interface)

lokal olarak dengede ayri bir faz (iki boyutlu) gibi tanımlamaktadır. Denge durumunda olmayan sistem (non-equilibrium) termodinamiğinin (karşılıklı ilişkili Onsager teorisi-Onsager theory with reciprocal relations) sunduğu çift (coupled) ısı ve kütle akısı denklemleri, kristal büyümesi ve büyüyen kristalin arayüzeyindeki (interface) sıcaklık artışını (temperature jump) tanımlamaktadır. Tüm taşıma dirençleri, soğuk yüzeyde MgSO<sub>4</sub>·7H<sub>2</sub>O kristallendirilerek tayin edilmiştir. Çiftleştirilen katsayı (coupling coefficient), kristalizasyon entalpisinin (heat of crystallization) tuz ve sıvı fazlar arasındaki dağılım katsayısını göstermektedir.

Ekonomik ve ekolojik açıdan, ötektik dondurma kristalizasyon teknolojisinin sanayiye hızla uygulanması istenmektedir. Son on yıl boyunca bilim enstitüleri, bir ekipman üreticisi ve kullanıcılarının başarılı (proses endustrisi) ortaklığı EFC' yi pilot ölçek boyutuna kadar geliştirmiştir. EFC teknolojisinin en hızlı şekilde sanayiye uygulanması için yenilikleri 'değişim çevrimleri' esasıyla tanımlayan Çevrimsel Yenilikçi Model (Cyclic Innovation Model-CIM) sunulmuştur. Bu modelde gelişmeler, aynı anda tüm alt çevrimlerinde bir girişimcinin yönetiminde gerçekleşir. Geleneksel olarak yeniliklerde her etap birbirinden bağımsız yol alır (lineer model-linear chain). Bir sonraki etap bir öncekinin sonlanmasıyla başlar bu da dogal olarak sonuca ulasmada hatrı sayılır bir zaman kaybıdır. Oysa CIM, tüm çevrimlerde gelişmeyi tetikliyerek ve tüm aktörleri birbiriyle kaynaştırıp beraber çalışmaya yönlendirerek lineer modelin maruz kaldığı engellerin üstesinden gelmeyi onerir. *Bölüm 8*' de Çevrimsel Yenilikçi Model kullanılarak ötektik dondurma kristalizasyon teknolojisinin sanayilesmesi için bir yol çizilmektedir.

### Acknowledgements

A journey is made easier when you travel together with colleagues, collaborators, friends, family and loved ones. It is now the opportunity to express my gratitude to all those wonderful people who contributed, either directly or indirectly, in making my PhD thesis possible.

Firstly, I would like to thank my promoter and supervisor Prof. dr. Geert-Jan Witkamp for his support and encouragement during this thesis's work. Dear Geert-Jan, thank you sincerely for giving me the opportunity to work on the EFC project as well as allowing me the freedom in carrying out this research and entrusting me with great responsibilities; even on the subjects that were beyond my educational background. Working with you was a great pleasure. A heartfelt thank you for everything...

The EFC project would not have been successful without the cooperation of each superb team member. I am very grateful to have had the opportunity to work with all my EFC team friends: Robert (excellent scientist), Daniela, Jaap, Marcos, Chrismono, Ad van de Vijver (great management with lots of experience), Hans Evers (superman with endless energy!) and Stefan ten Hagen (my hero! everything is possible with his creative hands). I wish to express my sincere gratitude to all of you who helped whenever I was in need.

Dear Prof. dr. Signe Kjelstrup, I would like to express my sincere appreciation to you for the high quality scientific discussions, the attention, the care and importance you gave to our work. Thank you very much for all your support, and hospitality in Norway.

Prof. Hondoh, you welcomed me in your lab in Japan and provided me with all the help that I required. I would like to express my deep gratitude to you and your group for your hospitality, friendliness and for all your scientific input. Meridianite would not have been discovered without your cooperation. I hope this is just a start between two groups.

I am deeply indebted to Dr. Ernst Burke (Chairman of International Mineralogical Association-Commission on New Minerals and Mineral Names) for your interest,

constant support, advice and patience during my adventure of a new mineral discovery. I was very lucky in meeting you at the right moment. Without Dr. Burke's help and experience, my signature under Meridianiite would not be possible. Thank you very much Dr. Burke, you opened a new door in my career...

It is my pleasure to thank Prof. dr. ir. Berkhout and Dr. Dap Hartmann for their attention, care and the importance they showed to my last chapter. Thank you very much for this excellent effort in such a limited time frame. I wish to further express my sincere appreciation to Dap for his beautiful article called "Meridianiite bestaat" on the NRC Handelsblad. You made Meridianiite and myself famous in The Netherlands!

Dear Prof. van Rosmalen, many many thanks for spending your precious time with me. Listening to *crystallization* from you is always a source of great enthusiasm. I am very grateful to hear your fruitful comments and criticisms. It is also a great honour to have you present on my examining committee.

My Holland adventure started 5 years ago, when I met with Prof. dr. ir. Peter Jansens and Giljam Bierman at a seminar in İstanbul. I would like to express my sincere appreciation to both of them and to my first supervisor Marcello Seckler for all the efforts they put in to bringing me to The Netherlands and all their kindness during my PhD research.

EFC research has been funded and supported by the Ministry of Economic Affairs, the Ministry of Housing, Spatial Planning, and Environment, the Ministry of Education and Science in The Netherlands through the EET program, Kemira Agro Ventures, Larox-Pannevis B.V., Nedmag Industries Mining & Manufacturing B.V., TNO, AVR B.V. and DSM Research. It was always extremely helpful to me to get feed-back from the industry people and to have good discussions and different points of views shared on the project development. I would like to thank them all for their confidence in me. Dear Mees Hasselaar, I would like to thank for your valuable contribution to my last chapter.

My dear colleague-friend-brother Marcos! My special thanks to you, for all the fruitful discussions about science and life and for all your help. Sharing the same faith, you are

almost the only one who understands me perfectly! It was always immense fun working with you. Also, my thanks to Sally for her patience when I kept you at the office during weekends and late in the evenings for the experiments or for calculations! You are almost done friend, I wish you lots of success... Muchas gracias!

I had the pleasure to supervise and work with several students who did their graduation work in the EFC project. My dear students Vincent, Donny, Haci, Rafa, Rachid and Fatih, you contributed greatly to this thesis. Thank you very much for helping me, conduct all the experiments in order to understand the fundamentals of this research. I am very grateful for your cooperation and patience in the stressful moments. It was fun working with you, thank you very much for your help. I wish all of you a successful life.

My special thanks to the great technical staff that were always very kind and helpful during my PhD period. Thank you very much Jan (who always welcomed me with a smile on his face), Michel (who is always patient with my urgent(!) many-many ICP samples), André, Paul Durville, Martijn, Gerard, Theo, Jan, Duco (special thanks for helping with the TGA), Rob, Bert, Daniël, Jasper, Johan and all the others...

My gratitude goes to our dear secretaries and managerial support Helma, Leslie, Toine, Aris, Carol, Maltie, Brenda, Petra, Anne Marie, Loes, Judith, Caroline and Marloes. Thank you very much for being always kind and helpful. Hennie, ook bedankt voor de Nederlandse lessen!

I also would like to express my gratitude towards some people from P&E who spent their precious time to discuss my scientific work: Herman Kramer, Joop ter Horst, Joachim Gross and Infante Ferreira. Thank you very much...

Dear Prof. dr. Jack Dillon, I would like to thank you for your politeness and interest in my research. I always praised and appreciated your aristocracy and kindness in sharing your precious time with me during our short-conversations in the corridors. Thank you very much, you are so kind...

I am one of the few lucky-PhD's having the chance of working both in previous-API and in new-P&E organisation. I tasted the colourful, multi-cultural, cosy atmosphere in both groups. Sincere thanks to all of those nice and friendly colleagues for sharing their time with me. From API: Abhilash (dear smiley-fast speaking friend, do you really speak English?!?), Andréanne, Aris, Cristiana (3C: Carzy-Cute-Clever Italianini), Christof, Ferize (İyiliklerin-tatlı sohbetin herşeyden önemlisi dostluğun için sonsuz teşekkür ediyorum canım arkadaşım. Hayat sana umarım herzaman güzellikler sunar), Frans, Maaike R. Marcel, Mark, Martijn, Paulo, Pieter, Raymond, Takuya (9.00 till 24.00 working colleague-Takuya go home!), Vanesa, Yohanna and from P&E: Ali, Albert, Aravind, Aylin, Bart, Christian, Elenora, Erika, Ernesto, Fatemeha, Gianluca, Hélène (friendly, lately joined roommate), Jacopo, Jelan, Jeroen, John, Kamarza, Kedar, Maakie K., Magdalena, Mahsa, Marco, Marcin, Marta L., Marta K., Mattia (cheerful morning welcomer), Richard, Ryan, Savad (cold-evening & weekend's, next-office-warm friend), Shangfeng (sweet hardworking roommate), Stijn, Traci (dear pretty English corrector), Tomasz, Widya, Xiaohua... It was tremendous fun, a great honour and pleasure to work with all of you all and learning your wonderful cultures. I wish all you the best for your future!

Jelan, I would like to thank you for helping me to design this wonderful cover and being so patient with me in doing that. Impossible is never possible with your magic penmousepad-computer and your creativity. Thank you very much!

Richard, you are a great Dutch translator! Besides translating my summary and propositions, you also gave corrections and suggestions. Luckily(!) they only ask the Dutch version of the summary not the whole thesis. Thank you very much dear friend...

My dear 'paranimf' Yorgo, you are the first person that I met in Delft. I really enjoyed much our time spend as a flat mate and as a friend with so many great memories!

I am also very thankful to all the friends that I had the pleasure to meet during my PhD in Delft. My PhD would not have been much fun without any of you...

Canım kardeşim-paranimf'im Begüm'cüğüm. Arkadaşlığımız üniversite ve asistanlık yıllarımıza dayansa da dostluğumuz şans eseri girdiğimiz bir sunumla başlayan Hollanda maceramız esnasında pekişti. Beraber başvurduk, kabul edildik ve Delft'e geldik. Senin varlığın Hollanda'daki yeni yaşamıma alışmamı kolaylaştıran en onemli etkendi. Acemiliğimizi, evimizi, şahitliğimizi paylaştık. Sonra Şenol katıldı aramıza. Başım her sıkıştığında fikirleriniz, ilginiz ve desteğinizle hep yanımdaydınız. Siz benim Hollanda'daki ailem oldunuz. Dostluğunuz ve tüm yardımlarınız için her ikinize de çok teşekkür ediyorum.

Sevgili ev arkadaşım Gülay'cığım, kısa bir süreyi paylaşmış olsak da seninle çok güzel ve zarif günler geçirdik. Hayat karşısındaki dik duruşunu, planlı yaşamını hep takdir ettim. Hatta özendim. Paylaştıkların için paylaştıklarımız için çok teşekkür ediyorum.

Bıcırık-çılgın 'Aylin kardeş'! Son yılda gitgide artan yoğunluğumda sabahları güne senin şarkıların ve güler yüzünle başlamak çok güzeldi. Bitmek bilmeyen komik maceraların, hayatıma bu zor günlerde renk kattı. Sana hayatında ve tezinde başarılar dilerken sabah şarkıların için teşekkür ediyorum.

Canim arkadaşlarım Şafak ve Muammer, Delft'e gelmenize benden daha fazla kimse sevinmemiştir herhalde. Her ikinize de desteğiniz, dostluğunuz ve yardımlarınız için çok çok tesekkür ediyorum.

Moral desteklerini hiçbir zaman esirgemeyen sevgili Ayça, Banu, Burcu, Çiğdem, Duygu, Gökhan ve Zorbay başta olmak üzere Türkiye ve Hollanda'daki tüm arkadaşlarıma çok çok teşekkur ediyorum. Hepiniz harikasınız...

Doktora çalışmam için beni destekleyen ve yönlendiren İstanbul Teknik Üniversitesindeki tüm değerli hocalarıma candan teşekkür ediyorum.

Sevgili Mahir Amca'cığım, Amsterdam'da beni karşılamaya geldiginiz gün sanki dün gibi, o günü hiç bir zaman unutmayacağım. Sizin ve ailenizin Hollanda'ki varlığı bana burada kendimi hep huzurlu ve güven içinde hissetmemi sağladı. Tüm yardımlarınız için çok teşekkür ediyorum.

...ve değerli ailem...

Sonsuz sevgi, ilgi ve desteğini her an bana ve ablama veren; kendini, bizi iyi ve faydali

bireyler olarak yetiştirmeye adayan, beni en iyi anlayan, fedakar cefakar ve emekleri

yadsınamaz, çok iyi kalpli, eşsiz insan ve bügüne gelmemin en onemli sebebi biricik

Anne'ciğime,

İlk yol göstericim, her zaman gurur duyduğum, gerçek bir bilim adamı, yeteneklerimi en

doğru ve en faydalı şekilde nasıl kullanabileceğimi öğreten, fedakar, çok iyi bir insan,

bugünü görmeyi en cok arzu eden ancak malesef şu an hayatta olmayan fakat her an beni

izlediğini bildiğim canım Baba'cığıma,

Doktora çalışmam süresince beni kayıtsız şartsız destekleyen, sabırla bekleyen, seven,

yönlendiren, güçlendiren, onurlandıran, en imkansıza ulaşmayı hedeflediğimde bile bunu

başaracağıma inanan ve ulaştığım başarımı büyük bir heyecanla kutlayan sevgili

Senlav'ım ve ailesine,

Sevgi, destek ve varlığını her an yanımda hissettiğim, sahip olmaktan onur duyduğum

melek kalpli ablam-arkadaşım Çağla'm, sevgili ağabeyim Mete ve bir tanecik yeğenim

yaşama sevincim Yiğit'e,

Hayatımın her kilometre tasında sevgi, ilgi ve dualarıyla yanımda olan ve olacaklarını

bildiğim, haklarını hiçbir zaman ödeyemiyeceğim canım anneannem, sevgili halam,

biricik dayım ve tatlı Gül ablama,

Sıkıntı, üzüntü ve mutlu günlerimde hep yanımda olan, en zayıf düştüğüm anlarda bana

ışığı gösteren, fedakar, dünya iyisi, her an sevgi ve ilgi dolu, canim arkadaşım, sırdaşım,

örnek aldığım, hakkı ödenemez harika teyzeciğim Zuhal'ime,

Ve tabii ki Maviş'e...

çok teşekkür ediyorum... İyi ki varsınız...

F. Elif Genceli

Delft, 14 December 2007

€ WI Penceli.

220

### **Curriculum vitae**

#### Fatma Elif Genceli

born March 11<sup>th</sup>, 1976 in Istanbul, Turkey



1987-1994	High school, Istanbul Moda Collage (honor degree), Turkey
1994-1998	Undergraduate, Bachelor of Science in Chemical Engineering,
	Istanbul Technical University, Istanbul, Turkey
1998-2000	Postgraduate, Master of Science in Chemical Engineering (honor degree),
	Istanbul Technical University, Istanbul, Turkey
2000-2002	PhD research and Assistant in Chemical Engineering,
	Istanbul Technical University, Istanbul, Turkey
2002-2007	PhD research in Process Equipment, Process & Energy Department
	Delft University of Technology, Delft, The Netherlands
2007-	Post Doc research in Process Equipment, Process & Energy Department
	Delft University of Technology, Delft, The Netherlands

#### **Awards & Successes**

- October 2004 Best Poster Presentation, Netherlands Process Technology Symposium (NPS4)
- 1998-2000 Scholarship of TUBITAK for MSc Program on the basis of BSc education results
- 1 June 2007 Genceli F.E.; Peterson R.C., *Meridianiite* (*MgSO*<sub>4</sub> •11*H*<sub>2</sub>*O*) approval as a valid mineral species (IMA 2007-011) by the Commission on New Mineral Names and Mineral Nomenclature of the International Mineral Association

### List of publications

- Genceli E.; Apak E.; Razvigorova M.; Minkova V.; Ekinci E.; Preparation, modification, and characterization of pitches from apricot stones, *Fuel Processing Technology*. Volume 75, Issue 2, 2002, pp. 97-107.
- Genceli F.E.; Yenigün M.B.; Changing career plans of Turkish women towards technical arena, *International Symposium Engineer Of The 21<sup>st</sup> Century*. ISBN 5-94211-073-5, pp. 316–323, 16-19 Sept 2002, Saint Petersburg Russia.
- Genceli F.E.; Himawan C.; Seckler M.M.; Witkamp G.J.; Inline determination of supersaturation in Eutectic Freeze Crystallization of MgSO<sub>4</sub> 12H<sub>2</sub>O, WASIC-Workshop on Advance in Sensoring in Industrial Crystallization. ISBN 975-561-254-8, pp. 18-25, 18-20 June 2003, Istanbul, Turkey.
- Gärtner R.S.; Genceli F.E.; Trambitas D.O.; Witkamp G.J.; Impurity gradients in solution-grown ice and MgSO<sub>4</sub> 12H<sub>2</sub>O crystals measured by cryo-laser ablation and high-resolution-induced-coupled plasma mass spectrograph, *Journal of Crystal Growth*. Volume 275, Issues 1-2, 2005, pp.e1773-e1778.
- Genceli F.E.; Himawan C.; Witkamp G.J.; Inline determination of supersaturation and metastable zone width of MgSO<sub>4</sub> 12H<sub>2</sub>O with conductivity and refractive index measurement techniques, *Journal of Crystal Growth*. Volume 275, Issues 1-2, 2005, pp. e1757-e1762.
- Genceli F.E.; Gärtner R.; Witkamp G.J.; Eutectic freeze crystallization in a 2nd generation cooled disk column crystallizer for MgSO<sub>4</sub>-H<sub>2</sub>O system, *Journal of Crystal Growth.* Volume 275, Issues 1-2, 2005, pp. e1369-e1372.

- Gärtner R.S.; Genceli F.E.; Rodriguez M.; Trambitas D.O.; Witkamp G.J.; Impurity Incorporation in Solution-Grown Ice and MgSO<sub>4</sub> 12H<sub>2</sub>O crystals during Eutectic Freeze Crystallization, *Netherlands Process Technology Symposium (NPS4)*. 26-27 October 2004, Veldhoven, The Netherlands.
- Genceli F.E.; Gärtner R.; Witkamp G.J.; Eutectic Freeze Crystallization in a 3rd Generation Cooled Disk Column Crystallizer, *Netherlands Process Technology Symposium (NPS4)*. 26-27 October 2004, Veldhoven, The Netherlands.
- Genceli, F.E.; Eutectic Freeze Crystallization, *NPT Processtechnologie*, Augustus 2005, No.4, 19-20.
- Genceli F.E.; Trambitas D.; Gärtner R.S.; Rodriguez M.; Witkamp G.J.;
   3<sup>rd</sup> generation cooled disk column crystallizer and a skid mounted unit for eutectic freeze crystallization, VDI Berichte (1901 II), art. no. D-15, pp. 855-860, 16<sup>th</sup> International Symposium on Industrial Crystallization. 11-14 Sept 2005, Dresden, Germany.
- Genceli F.E.; Gärtner R.S.; Trambitas D.; Rodriguez M.; Witkamp G.J.;
   A sustainable technology: Eutectic freeze crystallization From batch laboratory to continuous industry applications, Sustainable (Bio)Chemical Process Technology Incorporating the 6th International Conference on Process Intensification. pp. 235-242, 27-29 September 2005, Delft, The Netherlands.
- Evers H.; Gärtner R.S.; Genceli F.E.; Kruse J.H.J.; Rodriguez M.; ten Hagen S.; Trambitas D.O.; van der Vijver A.S.; Witkamp, G.J.; Industrial Application of Eutectic Freeze Crystallization (EFC)-The Skid-Mounted Pilot Plant, *Netherlands Process Technology Symposium (NPS5)*, 25-26 October 2005, Veldhoven, The Netherlands.

- Genceli F.E.; Lutz M.; Spek A.L.; Witkamp G.J.; Crystallization and Characterization of a New Magnesium Sulfate Hydrate MgSO<sub>4</sub>·11H<sub>2</sub>O -, Crystal Growth & Design. 7 (12), 2460–2466.
- Genceli F.E.; Witkamp G.J.; MgSO<sub>4</sub> 11H<sub>2</sub>O-From Crystallization to Characterization-2<sup>nd</sup> International Workshop on Physics of Ice Core Records (PICR-2). ILTS, 2-6 February 2007, Sapporo, Japan.
- Genceli F.E.; Peterson R.C., Meridianiite (MgSO<sub>4</sub>·11H<sub>2</sub>O) approval as a valid mineral species by the Commission on New Mineral Names and Mineral Nomenclature of the International Mineral Association (IMA 2007-011), 1 June 2007.
- Genceli F. E.; Horikawa S.; Iizuka Y.; Sakurai T.; Hondoh T.; Kawamura T.;
   Witkamp G.J; Meridianiite: detected in ice, submitted for publication to *Journal of Glaciology*.
- Genceli F.E.; Rodriguez Pascual M.; Kjelstrup S.; Witkamp G.J.; Coupled heat and mass transfer during crystallization of MgSO<sub>4</sub>·7H<sub>2</sub>O on a cooled surface, submitted for publication to *Crystal Growth & Design*.
- Genceli F.E.; Hartmann D.; Witkamp G.J.; Berkhout G.; Cyclic Innovation Model Application: Eutectic Freeze Crystallization, prepared for publication in Separation and Purification Journal.